The molecular basis of mouse adaptation and virulence by human enterovirus 71

Zainun Zaini

DECLARATION

I declare that the research presented here is my own original work and has not been submitted to any other institution for the award of a degree

……..

Zainun Zaini

ACKNOWLEDGEMENTS

There are so many important people who have contributed academically, emotionally and financially during the development and completion of this thesis. I am eternally indebted to my supervisor, Professor Peter McMinn, whose support, advice, encouragement and invaluable guidance has made this project possible. Your confidence in me has made the past four years of my PhD a less painful experience.

Special thanks to the members of the Molecular Virology Unit, Patchara, Belinda, Chee Choy, Emily and Sara for their expert technical assistance, support and friendship. My sincere thanks also goes to the staff of Infectious Disease and Immunology Department; Catherine, Rebecca, Jason, Becky, Jean as well the staff of Laboratory Animal Services.

My gratitude also goes to the Government of Brunei Darussalam for providing the scholarship that enables me to undertake this course as well as the personnel at the Brunei High Commission in Canberra for ensuring my welfare.

Of course, this PhD is only possible because of my parents and family who since my birth and throughout the years of my education, have raised me, supported me and provided me with the best advice. Lastly but not least, I thank my husband Asmawi, my two children Iffah and Izzat whose support and never ending love has given me strength throughout this trying ordeal.

ABSTRACT

Human enterovirus 71 (HEV71), a member of the human enterovirus A species of the family *Picornaviridae*, is an emerging pathogen that has recently become a serious health threat in the Asia-Pacific region. Although infection normally causes mild illness that is often undiagnosed, HEV71 has emerged as the dominant cause of large outbreaks of hand, foot and mouth disease (HFMD) in the Asia-Pacific region and can cause serious central nervous system infections leading to aseptic meningitis and encephalitis with a very high mortality. A mouse model is currently the most convenient small animal model for studies of HEV71 pathogenesis and for the primary assessment of potential vaccines against HEV71. Since most HEV71 field isolates do not naturally infect mice, a mouse-adapted strain of HEV71 is required for infection of mice. The primary aim of this project was to produce mouse virulent strains of HEV71 isolated from different outbreaks of HFMD in the Asia-Pacific Region and to elucidate the molecular basis of their mouse virulence.

Infectious cDNA clones of HEV71 were initially generated and used as tools to investigate the molecular basis of HEV71 virulence and pathogenesis in mice. Two infectious cDNA clones of HEV71 clinical isolates, HEV71-C2 (genogroup C2) and HEV71-C4 (genogroup C4) were successfully constructed using a low copy-number plasmid vector and an appropriate bacterial host. Transfection of cells with cDNA clones or RNA transcripts derived from these clones produced infectious viruses. Phenotypic characterisation of the clone-derived viruses was performed and they were found to have indistinguishable cell culture growth

phenotypes compared to their respective wild-type viruses. However, attempts to generate infectious cDNA clones of another clinical isolate, HEV71-B5 (genogroup B5) were unsuccessful.

Our previous work has shown that prior Chinese hamster ovary (CHO) cell-adaptation of HEV71 was a necessary first step in the adaptation of HEV71 to growth in murine hosts. Consequently, we selected CHO cell-adapted strains of HEV71-B5 and HEV71-C2 by serial passage in CHO cells at high multiplicities of infection. During the course of CHO cell passage, virus growth improved significantly, with increasing virus titres and the presence of cytopathic effect observed. A study of virus growth kinetics revealed that the CHO cell-adapted strains of HEV71-B5 (CHO-B5) and HEV71-C2 (CHO-C2) grew efficiently in CHO cells with maximum titres >100-fold higher than unadapted parental virus. Both CHO-B5 and CHO-C2 harboured single amino acid mutations within the VP2 capsid protein gene. CHO-B5 has an amino acid substitution of K^{149}→I in VP2 and CHO-C2 has an amino acid substitution of K^{149}→M in VP2. The isolate HEV71-C4 failed to adapt to CHO cells during serial passage. Infectious cDNA clone-derived populations of HEV71-C4 containing the mutations K^{149}→I or K^{149}→M in VP2 were generated by site-directed mutagenesis. Both mutations resulted in the ability of the virus to replicate efficiently in CHO cells, indicating that amino acid position 149 in VP2 is critical for the adaptation of HEV71 to growth in CHO cells.

A mouse-virulent strain of HEV71-B5 (MP-B5) was further selected by serial passage of CHO-B5 in newborn BALB/c mice. MP-B5 induces severe disease of high mortality in newborn mice in a dose-dependent manner. Skeletal muscle is

the primary site of virus replication and results in severe myositis. MP-B5 has five additional nucleotide sequence changes, two of which are located in the 5′ UTR and the three within the open reading frame (ORF). Two of the ORF mutations resulted in deduced amino acid changes in the capsid protein VP1: S^{241}→L and K^{244}→E; the third ORF mutation was a synonymous C→T change at nucleotide position 6072 within the 3D polymerase gene. Infectious cDNA clone-derived mutant virus populations of HEV71-26M (genogroup B3) (CHO-26M) containing the VP1 mutations identified in MP-B5 were generated in order to determine the mutation(s) responsible for mouse virulence. Only viruses expressing the VP1 (K^{244}→E) mutation were virulent in 5-day-old BALB/c mice, indicating that the VP1 (K^{244}→E) change is the critical genetic determinant of mouse adaptation and virulence in this model.

We also modified the capsid protein of HEV71-C4 to generate a mouse virulent strain, based on the genetic information derived from our previous genogroup B3 mouse-adapted virus (MP-26M). Infectious clone-derived mutant virus populations containing the capsid protein mutations VP1: Q^{145}→E and Q^{145}→G were generated by site-directed mutagenesis of a full-length clone of HEV71-C4 containing CHO cell-adaptation marker, VP2 (K^{149}→I). Viruses expressing the VP1 (Q^{145}→E) were virulent in 5-day-old BALB/c mice with 100% mortality rate observed. Skeletal muscle appears to be the primary site of replication of this virus with limb muscle showing severe myositis. Virus was also isolated from spleen, liver, heart and brain of infected mice.

The infectious cDNA clones constructed in this study have provided a valuable technical vehicle by which to dissect HEV71 virulence determinants and can be further used to study the translation and replication processes of HEV71. The mouse model of HEV71 infection has provided a fundamental basis to study the pathogenesis of HEV71. Additionally, potential HEV71 vaccine candidates can be evaluated in this more cost effective animal model. As more information emerges regarding the molecular processes of HEV71 infection, further advances may lead to the development of effective antiviral treatments and, ultimately, a vaccine-protection strategy for prevention and control of this important human pathogen.

TABLE OF CONTENTS

DECLARATION i

ACKNOWLEDGEMENTS ii

ABSTRACT iii

TABLE OF CONTENTS vii

LIST OF FIGURES xiii

LIST OF TABLES xvii

PUBLICATIONS, PRESENTATIONS AND AWARDS xx

ABBREVIATIONS xxii

CHAPTER ONE: LITERATURE REVIEW

1.1. Classification of the Family *Picornaviridae* 1

1.2. Human enterovirus 71 (HEV71) 1

1.3. HEV71 structure and organisation 5

1.3.1. Virion structure 5

1.3.2. Genome structure 6

1.4. HEV71 molecular biology 10

1.4.1. Virus entry into cells 10

1.4.2. Viral protein translation 11

1.4.3. Viral genome replication 14

1.4.4. Release of virus from cells 17

1.5. HEV71 genogroup 18

1.6. Molecular epidemiology of HEV71 20

1.7. HEV71 entry and spread in the host 23

1.8. Clinical features of HEV71 23

1.8.1. HFMD and herpangina 23

1.8.2. Neurological disease 24

1.8.3. Neurogenic pulmonary oedema 25

1.8.4. Other HEV71 associated disease 26

1.9. Pathogenesis of HEV71 26

1.10. Molecular determinants of HEV71 virulence 29

1.11. Cell culture and animal models of HEV71 infection 32

1.11.1. Cell culture 32

1.11.2. Non-human primate models 32

1.11.3. Mouse models 33

1.12. Aims of this study 36

CHAPTER TWO: MATERIALS AND METHODS

2.1. Cells and Viruses 37

2.1.1. Cell lines 37

2.1.2. Viruses 37

2.2. Virus assays 38

2.2.1. Virus infection 38

2.2.2. Harvesting virus 38

2.2.3. Plaque purification 39

2.2.4. Median tissue culture infectious dose ($TCID_{50}$) assays 39

2.2.5. Single-step growth analysis 40

2.3. Molecular biological techniques 40

2.3.1. Plasmids 40

2.3.2. Bacterial strains 40

2.3.3. Restriction endonuclease digestion 41

2.3.4. Agarose gel electrophoresis 41

2.3.5. Purification of DNA from agarose gels 41

2.3.6. Preparation of plasmid DNA 42

2.3.7. DNA ligation 42

2.3.8. Transformation of DNA into *E.coli* 42

2.3.9. Isolation of viral RNA 43

2.3.10. Reverse transcription of viral RNA 43

2.3.11. Polymerase chain reaction (PCR) 44

2.3.12. DNA sequencing 49

2.3.13. Construction of full-length cDNA clones of HEV71 52

2.3.14. Construction of HEV71 variants by site-directed mutagenesis 64

2.3.15. Transfection 67

2.4. Mouse experiments 67

2.4.1. Humane endpoint (HD_{50}) determination 68

2.4.2. Mouse virulence assay 70

2.4.3. Tissue distribution and viral load determination 70

2.4.4. Histological studies 70

2.5. Bioinformatics 71

2.5.1. Sequence analysis 71

2.5.2. Phylogenetic analysis 71

2.5.3. RNA structure prediction 72

2.5.4. Protein homology modelling 72

2.6. Statistical analysis 72

CHAPTER THREE: SEQUENCE ANALYSIS AND CONSTRUCTION OF GENOME LENGTH INFECTIOUS cDNA CLONES OF HEV71 GENOGROUPS B5, C2 AND C4

3.1. Introduction 73

3.2. Result 74

3.2.1. Complete genome sequencing of HEV71 strains 74

3.2.2. Sequence comparison to the HEV71 prototype strain 77

3.2.3. Evolutionary and genetic relationships to other HEV71 genogroups 79

3.2.4. Viral RNA secondary structure analysis 82

3.2.5. Design, construction and recovery of infectious cloned-derived viruses 89

3.2.6. Genotypic characterisation of infectious clones 93

3.2.7. Phenotypic characterisation of the clone-derived viruses 95

3.3. Discussion 98

CHAPTER FOUR: A REVERSE GENETIC STUDY OF THE ADAPTATION OF HUMAN ENTEROVIRUS 71 TO GROWTH IN CHINESE HAMSTER OVARY CELL CULTURES

4.1. Introduction 105

4.2. Results 106

4.2.1. CHO cell-adaption of HEV71 106

4.2.2. Phenotypic characterisation of CHO cell-adapted HEV71 109

4.2.3. Comparison of nucleotide and amino acid sequences of the wild-type and CHO cell-adapted HEV71 112

4.2.4. Construction of mutant virus and phenotypic characterisation of

clone-derived virus 115

4.2.5. Homology modeling 120

4.2.6. Infectivity of CHO cell-adapted variants and clone-derived viruses containing the CHO cell-adaptation marker in BALB/c mice 122

4.3. Discussion 124

CHAPTER FIVE: MOUSE ADAPTATION OF A SUB-GENOGROUP B5 STRAIN OF HUMAN ENTEROVIRUS 71 IS ASSOCIATED WITH A NOVEL LYSINE TO GLUTAMIC ACID SUBSTITUTION AT POSITION 244 IN PROTEIN VP1

5.1. Introduction 128

5.2. Results 130

5.2.1. MP-B5 has increased virulence in newborn BALB/c mice 130

5.2.2. Susceptibility of infant BALB/c mice to infection with MP-B5 134

5.2.3. Tissue distribution and histopathological changes in mice infected with MP-B5 136

5.2.4. Sequence comparison of HEV71-B5, CHO-B5 and MP-B5 141

5.2.5. Phenotypic characterisation of CHO-B5 and MP-B5 143

5.2.6. Construction of full-length infectious cDNA clone containing the VP1 protein mutations identified in MP-B5 146

5.2.7. An amino acid substitution in VP1 (K^{244}→E) is solely responsible for mouse adaptation and virulence 152

5.2.8. Tissue distribution and histopathologic changes in mice infected with CHO-26M-VP1-K244E-CDV 155

5.2.9. The VP1 (K^{244}→E) mouse virulent marker is located in the HI loop 160

5.3. Discussion 162

CHAPTER SIX: A SINGLE MUTATION IN CAPSID PROTEIN VP1 (Q^{145}→E) OF A GENOGROUP C4 STRAIN OF HUMAN ENTEROVIRUS 71 GENERATES A MOUSE VIRULENT PHENOTYPE

6.1. Introduction 169

6.2. Results 170

6.2.1. Construction of a full-length sub-genogroup C4 infectious cDNA clone containing the VP1 protein mutations identified in MP-26M 170

6.2.2. An amino acid substitution in VP1 (Q^{145}→E) is solely responsible for mouse adaptation and virulence 175

6.2.3. Phenotypic characterisation of C4-VP2I-VP1E-CDV 178

6.2.4. Homology modeling 184

6.3. Discussion 186

CHAPTER SEVEN: GENERAL DISCUSSION 189

REFERENCES 200

APPENDICES 219

LIST OF FIGURES

PAGE

CHAPTER ONE

Figure 1.1 Molecular surfaces of five icosahedral asymmetric units of HEV71 8

Figure 1.2 HEV71 structure of the virion 8

Figure 1.3 Schematic diagram representing the core structural eight-stranded β-sandwich shared by VP1, VP2 and VP3 9

Figure 1.4 Genome structure of HEV71 13

Figure 1.5 VPg and *cis*-active RNA sequences and structures required for PV RNA replication 16

Figure 1.6 Geographic distribution of HEV71 genogroups and sub-genogroups between 1960 and 2011 22

CHAPTER TWO

Figure 2.1 The schematic diagram of the construction of the sub-genomic and full length cDNA clones of HEV71-B5 61

Figure 2.2 The schematic diagram of the construction of the sub-genomic and full length cDNA clones of HEV71-C2 62

Figure 2.3 The schematic diagram of the construction of the sub-genomic and full length cDNA clones of HEV71-C4 63

CHAPTER THREE

Figure 3.1 A phylogenetic tree showing the full-length sequence analysis of the three representative strains of HEV71 81

Figure 3.2 Sequence alignments of the cloverleaf and IRES elements of HEV71-B5, HEV71-C2, HEV71-C4 84

Figure 3.3 Predicted 5′ UTR secondary structures of HEV71-B5, HEV71-C2 and HEV71-C4 85

Figure 3.4 Predicted 3′ UTR secondary structures of HEV71-B5, HEV71-C2 and HEV71-C4 86

Figure 3.5 Predicted *cre* structures of HEV71-B5, HEV71-C2 and HEV71-C4 88

Figure 3.6 Replication kinetics of the parental and clone-derived HEV71-C2 on RD cells 96

Figure 3.7 Replication kinetics of the parental and clone-derived HEV71-C4 on RD cells 97

CHAPTER FOUR

Figure 4.1 CHO cell-adaptation of HEV71-B5, HEV71-C2 and HEV71-C4 108

Figure 4.2 Replication kinetics of CHO cell-adapted viruses in CHO cells 110

Figure 4.3 Nucleotide and amino acid sequence alignment of CHO cell-adapted viruses 114

Figure 4.4 Schematic representation of the infectious cDNA clones of HEV71-C4 and cDNA clones containing the VP2 mutations constructed by site-directed mutagenesis 117

Figure 4.5 Stability of introduced VP2 mutations, K^{149}→I and K^{149}→M, during CHO cell culture passage 118

Figure 4.6 Replication kinetics of C4-VP2I-CDV and C4-VP2M-CDV in CHO cells 119

Figure 4.7 Predicted three-dimensional structure of VP2 protein 121

CHAPTER FIVE

Figure 5.1 MP-B5-infected BALB/c mice 133

Figure 5.2 Survival of BALB/c mice infected with MP-B5 135

Figure 5.3 Viral loads in selected tissues of BALB/c mice after challenge with MP-B5 138

Figure 5.4 Histological analysis of MP-B5 infection in BALB/c mice 140

Figure 5.5 Replication kinetics of MP-B5 in RD and CHO cells 144

Figure 5.6 Schematic representation of the infectious cDNA clones of CHO-26M and cDNA clones containing VP1 mutations constructed by site-directed mutagenesis 149

Figure 5.7 The predicted 5′ UTR SLDs IV and VI of MP-B5 150

Figure 5.8 Stability of introduced VP1 mutations, S^{241}→L and K^{244}→E, during cell culture passage 151

Figure 5.9 Survival of BALB/c mice after challenge with CHO-26M-VP1-S241L-CDV, CHO-26M-VP1-K244E-CDV or CHO-26M-VP1-CDV 153

Figure 5.10 Viral loads in selected tissues of BALB/c mice after challenge with CHO-26M-VP1-K244E-CDV 157

Figure 5.11 Stability of VP2-149I and VP1-244E mutation after passage of CHO-26M-VP1-K244E-CDV in BALB/c mice 158

Figure 5.12 Histological analysis of CHO-26M-VP1-K244E-CDV infection in BALB/c mice 159

Figure 5.13 Predicted three-dimensional structure of VP1 protein 161

CHAPTER SIX

Figure 6.1 Amino acid sequence alignment of the VP2 and VP1 regions of HEV71-C4, HEV71-26M, CHO-26M and MP-26M strains 173

Figure 6.2 Schematic representation of the infectious cDNA clones of C4-VP2I and cDNA clones containing VP1 mutations constructed by site-directed mutagenesis 173

Figure 6.3 Stability of introduced VP1 mutation, Q^{145}→E and Q^{145}→G, during cell culture passage 174

Figure 6.4 Survival of BALB/c mice infected with C4-VP2I-VP1E-CDV or C4-VP2I-VP1G-CDV 177

Figure 6.5 Viral loads in selected tissues of BALB/c mice after challenge with C4-VP2I-VP1E-CDV 180

Figure 6.6 Stability of VP2-149I and VP1-145E mutation after passage of C4-VP2I-VP1E-CDV in BALB/c mice 181

Figure 6.7 Histological analysis of C4-VP2I-VP1E-CDV-infected mice 182

Figure 6.8 Replication kinetics of C4-VP2I-VP1E-CDV in Vero cells 183

Figure 6.9 Predicted three-dimensional structure of HEV71 VP1 protein with three alternative amino acid residue 145 185

LIST OF TABLES

PAGE

CHAPTER ONE

Table 1.1 Current *Picornaviridae* classification scheme 3

Table 1.2 Current classification of Genus *Enterovirus* (human) 4

CHAPTER TWO

Table 2.1 Primers used to sequence the complete genome of HEV71-B5, CHO-B5 and MP-B5 45

Table 2.2 Primers used to sequence the complete genome of HEV71-C2, CHO-C2 and clone-derived virus of strain HEV71-C2 46

Table 2.3 Primers used to sequence the complete genome of HEV71-C4 and clone-derived virus of strain HEV71-C4 47

Table 2.4 Primers used for amplification and sequencing of VP1 gene of HEV71-C4 variants 48

Table 2.5 Primers used for amplification and sequencing of VP1 gene of CHO-26M variants 48

Table 2.6 Primers used for amplification and sequencing of VP2 gene of HEV71 48

Table 2.7 5′ RACE primers used to sequence the 5′ terminus sequences of all HEV71 51

Table 2.8 Full length cDNA clones of HEV71-B5, HEV71-C2 and HEV71-C4 57

Table 2.9 Primers used for the construction of full-length cDNA clones of HEV71-B5 58

Table 2.10 Primers used for the construction of full-length cDNA clones of HEV71-C2 59

Table 2.11 Primers used for the construction of full-length cDNA clones of HEV71-C4 60

Table 2.12 List of HEV71 variants constructed by site-directed mutagenesis 65

Table 2.13 Primers used for the construction of full-length cDNA clones of HEV71-C4 containing mutations in the VP2 coding region 66

Table 2.14 Primers used for the construction of full-length cDNA clones of HEV71-C4 containing mutations in the VP1 coding region 66

Table 2.15 Primers used for the construction of full-length cDNA clones of CHO-26M containing mutations in the VP1 coding region 66

Table 2.16 Clinical grading scale of the severity of HEV71 infection in mice 69

CHAPTER THREE

Table 3.1 Gene region of BRU-2006-35334, 0964-SYD-98 and 540V-VNM-05 76

Table 3.2 Percentage nucleotide and amino acid sequence identities of BRU-2006-35334, 0964-SYD-98 and 540V-VNM-05 compared to prototype HEV71-BrCr 78

Table 3.3 Virus isolates retrieved from the NCBI GenBank used in the construction of phylogenetic tree 80

Table 3.4 Summary of the construction of full-length HEV71 cDNA clones and the infectivity of clone-derived virus 92

Table 3.5 Sequence comparison of parental HEV71-C2 and clone-derived virus HEV71-C2-CDV 94

Table 3.6 Sequence comparison of parental HEV71-C4 and clone-derived virus HEV71-C4-CDV 94

CHAPTER FOUR

Table 4.1 Nucleotide and amino acid differences identified in the genomes of wild-type HEV71-B5, HEV71-C2 and their CHO cell-adapted variants 113

Table 4.2 Infectivity of CHO cell-adapted variants and mutant CDVs population in newborn BALB/c mice 123

CHAPTER FIVE

Table 5.1 Mouse-adaptation of CHO-B5 132

Table 5.2 Percentage mortality in BALB/c mice after MP-B5 infection 132

Table 5.3 Nucleotide and amino acid changes identified in the genomes of wild-type HEV71-B5, CHO-B5 and MP-B5 142

Table 5.4 Mortality profile, mean survival time and HD_{50} values after challenge with serial 10-fold dilutions of the parental or mutant CHO-26M viruses 154

CHAPTER SIX

Table 6.1 Mortality profile, mean survival time and HD_{50} values after challenge with serial 10-fold dilutions of the parental or mutant C4-VP2I viruses 177

PUBLICATIONS, PRESENTATIONS AND AWARDS

PUBLICATIONS

1. **Zaini, Z.** and McMinn, P. (2012). A single mutation in capsid protein VP1 (Q145E) of a genogroup C4 strain of human enterovirus 71 generates a mouse virulent phenotype. Journal of General Virology 93 (9): 1935-1940.
2. **Zaini, Z.**, Phuektes, P. and McMinn, P. (2012). Mouse adaptation of a sub-genogroup B5 strain of human enterovirus 71 is associated with a novel lysine to glutamic acid substitution at position 244 in protein VP1. Virus Research 167 (1): 86-96.
3. **Zaini, Z.**, Phuektes, P. and McMinn, P. (2012). A reverse genetic study of the adaptation of human enterovirus 71 to growth in Chinese hamster ovary cell cultures. Virus Research 165 (2): 151-156.

PRESENTATIONS

1. **Zaini, Z.** and McMinn, P. (2012). A single mutation in capsid protein VP1 (Q145E) of a genogroup C4 strain of human enterovirus 71 generates a mouse virulent phenotype. 15th Annual Meeting of the European Society for Clinical Virology, Madrid, Spain.
2. **Zaini, Z.**, Phuektes, P. and McMinn, P. (2012). Mouse adaptation of a sub-genogroup B5 strain of human enterovirus 71 is associated with a novel lysine to glutamic acid substitution at position 244 in protein VP1. 9th Asia-Pacific Congress of Medical Virology, Adelaide, Australia.
3. **Zaini, Z.**, Phuektes, P. and McMinn, P. (2011). A reverse genetic study of the adaptation of human enterovirus 71 to growth in Chinese hamster ovary cell cultures. Australasian Virology Society Meeting, Kingscliff, NSW, Australia.

AWARDS

1. 2012 Asia-Pacific Congress of Medical Virology Young Investigator Scholarship
2. 2012 Daphne Goulston Scholarship

ABBREVIATIONS

>	greater than
%	percent
×g	times gravity
°C	degree Celsius
µg	microgram
$3D^{pol}$	RNA-dependent RNA polymerase
ATCC	American Type Culture Collection
ATP	adenosine triphosphate
BEV	bovine enterovirus
bp	base pairs
CD	cluster of differentiation
cDNA	complementary deoxyribonucleic acid
CDV	clone-derived virus
CHO	Chinese hamster ovary
cm	centimetre
CNS	central nervous system
CO_2	carbon dioxide
COPI	coat protein complex I
COS-7	SV40 transformed African green monkey kidney cells
CPE	cytopathic effect
cre	*cis*-acting replication element
CstF	cellular cleavage stimulation factor
CVA16	coxsackievirus A16
CVB3	coxsackievirus B3
dCTP	deoxycytidine triphosphate
DMEM	Dulbecco's Modified Eagles Medium
DNA	deoxyribonucleic acid
dNTP	deoxynucleotide triphosphate
DTT	dithiothreitol
E. coli	*Escherichia coli*

EDTA	ethylenediamine tetra-acetic acid
eIF4G	eukaryotic initiation factor 4G
et al.	and others
FBP	far upstream element binding protein
FBS	foetal bovine serum
g	gram
GFP	green fluorescent protein
h	hour
HBSS	Hank's balance salt solution
HD_{50}	50% humane endpoint
HEV71	human enterovirus 71
HEVA	human enterovirus group A
HFMD	hand, foot and mouth disease
HLA	human leucocyte antigen
hnRNP	heterogeneous nuclear ribonucleoprotein
i.c.	intracerebral
i.p.	intraperitoneal
IBDV	infectious bursal disease virus
IFN	interferon
IL	interleukin
IRES	internal ribosome entry site
kb	kilobase pairs
KCl	potassium chloride
kDa	kiloDalton
kV	kilovolt
LB	lysogeny broth
LD_{50}	50% lethal dose
$MgCl_2$	magnesium chloride
$MgSO_4$	magnesium sulphate
MHC	major histocompatibility complex
min	minute
mL	millilitre
mM	millimolar

MOI	multiplicity of infection
mRNA	messenger ribonucleic acid
MVE	Murray Valley encephalitis virus
NaCl	sodium chloride
ng	nanogram
NK	natural killer cells
nm	nanometre
nt	nucleotide
ORF	open reading frame
p.i.	post-infection
PABP	poly (A) binding protein
PBS	phosphate buffered saline
PCR	polymerase chain reaction
PDB	protein databank file
pmol	picomole
Poly (A)	polyadenylated
PSGL-1	P-selectin glycoprotein ligand-1
PV	poliovirus
PV1M	poliovirus type I Mahoney
RD	rhabdomyosarcoma cells
RdRp	RNA-dependent RNA polymerase
RNA	ribonucleic acid
RNAse	ribonuclease
RT	reverse transcription
s	second
SCARB2	scavenger receptor class B, member 2
SEM	standard error of the mean
SLD	stem loop domain
TAE	tris acetate EDTA buffer
$TCID_{50}$	median tissue culture infectious dose
TdT	terminal deoxynucleotidyl transferase
U	unit
UTR	untranslated region

UV	ultraviolet
Vero	African green monkey kidney cells
VP	virus protein
VPg	viral protein genome-linked
w/v	weight for volume
µF	microfarad
µg	microgram
µL	microlitre
µm	micrometre
µM	micromolar
Ω	ohm

1. CHAPTER ONE

LITERATURE REVIEW

1.1. Classification of the Family *Picornaviridae*

Members of *Picornaviridae* family are non-enveloped viruses with a single-stranded RNA genome of positive polarity. The family *Picornaviridae* is one of the largest RNA virus families composed of 12 genera based on biological and genetic properties: *enterovirus*, *cardiovirus*, *aphthovirus*, *hepatovirus*, *parechovirus*, *erbovirus*, *kobuvirus*, *teschovirus*, *sapelovirus*, *senecavirus*, *tremovirus* and *avihepatovirus* (Knowles *et al.*, 2012) (http://www.picornaviridae.com), which all contain viruses that infect vertebrates. Table 1.1 describes the current *Picornaviridae* classification scheme. Human enterovirus 71 (HEV71), the subject of this thesis, is classified as a member of Human enterovirus A (HEVA) species (Table 1.2) within the genus *Enterovirus*.

1.2. Human enterovirus 71 (HEV71)

HEV71 was first isolated from the stool of an infant with encephalitis in California in 1969 (Schmidt *et al.,* 1974). Since then, HEV71 infections have been found to be associated with a wide range of diseases. It is most often associated with outbreaks of hand, foot and mouth disease (HFMD), a self-limiting childhood disease characterised by a brief febrile illness and vesicular lesions on the hands, feet and mouth. In addition to HFMD, HEV71 often causes herpangina, a disease characterised by an abrupt onset of fever and sore throat, associated with small vesicular or ulcerative lesions on the posterior oropharynx. Other

members of HEVA, particularly coxsackievirus A16 (CVA16) and coxsackievirus A10 (CVA10) also cause HFMD and herpangina (Pallansch & Roos, 2007). HFMD and herpangina caused by HEV71 is clinically indistinguishable from HFMD caused by other members of HEVA (Pallansch & Roos, 2007). However, HEV71 epidemics are the greatest cause for public health concern because children younger than 5 years old infected with HEV71 are at risk of developing neurological complications similar to those associated with poliovirus (PV) (McMinn, 2002). A pattern of increased epidemic activity and endemic circulation of HEV71 has been observed in the region since 1997 and is associated with the regular emergence of new genetic lineages of HEV71. However, the reason for this increase in HEV71 circulation remains unknown.

Table 1.1 Current *Picornaviridae* classification scheme (Knowles *et al.*, 2012)

Genus	Species
Enterovirus	Human enterovirus A
	Human enterovirus B
	Human enterovirus C
	Human enterovirus D
	Simian enterovirus A
	Bovine enterovirus
	Porcine enterovirus B
	Human rhinovirus A
	Human rhinovirus B
	Human rhinovirus C
Cardiovirus	Encephalomyocarditis virus
	Theilovirus
Apthovirus	Foot-and-mouth disease virus
	Bovine rhinitis A virus
	Bovine rhinitis B virus
	Equine rhinitis A virus
Hepatovirus	Hepatitis A virus
Parechovirus	Human parechovirus
	Ljungan virus
Erbovirus	Equine rhinitis B virus
Kobuvirus	Aichi virus
	Bovine kobuvirus
Teschovirus	Porcine teschovirus
Sapelovirus	Porcine sapelovirus
	Simian sapelovirus
	Avian sapelovirus
Senecavirus	Seneca Valley virus
Tremovirus	Avian encephalomyelitis virus
Avihepatovirus	Duck hepatitis A virus

Table 1.2 Current classification of Genus *Enterovirus* (human)

Species	Name of members
Human enterovirus A	Coxsackieviruses A2-A8, A10, A12, A14, A16, Human enteroviruses 71, 76, 89-92, 114, 119
Human enterovirus B	Coxsackieviruses A9, A23, Coxsackieviruses B1-B6, Echovirus 1-9, 11-21, 24-27, 29-33, Human enteroviruses 69, 73-75, 77-88, 93, 97,98, 100, 101, 106, 107
Human enterovirus C	Polioviruses 1-3, Coxsackieviruses A1, A11, A13, A17, A19, A20-A22, A24, Human enteroviruses 95, 96, 99, 102, 104, 105, 109, 113, 116, 117 and 118
Human enterovirus D	Human enteroviruses EV68, EV70, EV94, EV111 and EV120
Human rhinovirus A	Human rhinovirus A1, A2, A7-A13, A15, A16, A18-A25, A28-A34, A36, A38-A41, A43-A47, A49-A51, A53-A68, A71, A73-A78, A80-A82, A85, A88-A90, A94-A96, A98, A100-A103
Human rhinovirus B	Human rhinovirus B3-B6, B14, B17, B26, B27, B35, B37, B42, B48, B52, B69, B70, B72, B79, B83, B84, B86, B91-B93, B97 and B99
Human rhinovirus C	Human rhinovirus C1-C49

1.3. HEV71 structure and organisation

1.3.1. Virion structure

HEV71 is a non-enveloped, positive-sense RNA virus with an icosahedral capsid, usually 27-20 nm in diameter. Virions consist of a protein shell (capsid) with no lipid envelope surrounding the genome. The crystal structure of HEV71 has been recently determined (Plevka *et al.*, 2012) (Figure 1.1). The capsid is composed of 60 identical units (protomers), each consisting of three surface proteins (VP1, VP2 and VP3) and an internal protein VP4 (Figure 1.2). The lack of a lipid envelope confers stability in host environments, including upon exposure to human gastric acid. Virions can also survive at room temperature for several days (Racaniello, 2007).

The VP1, VP2 and VP3 polypeptides have no sequence homology, yet all three proteins share similar topology i.e. they form an eight-stranded, anti-parallel β-barrel (Figure 1.3). This domain is a wedge-shaped structure made up of two anti-parallel β-sheets. One β-sheet forms the wall of the wedge, and the second, which has a bend in the centre, forms both a wall and the floor. The wedge shape facilitates the packing of structural units to form a dense, rigid protein shell. Packing of the β-barrel domains is strengthened by a network of protein-protein contacts on the interior of the capsid, which is formed by the N-terminal extensions of VP1 to VP3 as well as VP4. This is essential for the stability of the virion (Racaniello, 2007). The VP4 polypeptide differs significantly from the other 3 structural proteins in that it has an extended conformation. This protein is similar in position and conformation to the NH2-terminal sequences of VP1 and VP3 and functions as a detached NH2-terminal extension of VP2 rather than

as an independent capsid protein. The main structural differences between VP1, VP2 and VP3 lie in the loops that connect the β-strands and in the N- and C-terminal sequences that extend from the β-barrel domain. Picornavirus genera differ in these external loops and this accounts for the observed differences in surface relief of each genus and in the thickness of the capsid wall, which gives each picornavirus its distinct morphology and antigenicity (Racaniello, 2007).

1.3.2. Genome structure

The genome of HEV71 is a single-stranded, polyadenylated, positive-sense RNA of approximately 7.5 kb in size. Genomic RNA is infectious and the positive-sense RNA directly encodes the viral proteins necessary for RNA replication. The RNA genome is covalently linked to a virally encoded 22-amino acid polypeptide, VPg (viral protein genome-linked), at the 5′ terminus of the genome (Figure 1.4). The viral genome contains a single open reading frame (ORF), encoding a polyprotein of 2,194 amino acids. The polyprotein is divided into three regions, P1, P2 and P3. The P1 region encodes four viral structural proteins, VP1-VP4. The P2 and P3 regions encode seven non-structural proteins, 2A-C and 3A-D, respectively, involved in RNA replication, polyprotein processing and in the shut-down of host cell protein synthesis.

The ORF is flanked by 5′ and 3′ untranslated regions (UTR), with a poly (A) tail at the 3′ terminus of the 3′ UTR (McMinn, 2002). The 5′ UTR of HEV71 is predicted to fold into six stem-loop domains (SLDs), where SLD I is a cloverleaf structure and SLD II through VI constitute the internal ribosome entry site (IRES) (Thompson & Sarnow, 2003). The HEV71 5′ UTR contains a type I IRES, which is

common to all members of the genus *Enterovirus* (Thompson & Sarnow, 2003). The primary roles of the cloverleaf domain and IRES are in the control of replication and translation, respectively (Hellen & Sarnow, 2001; Hunziker *et al.*, 2007; Kauder *et al.*, 2006; Lyons *et al.*, 2001).

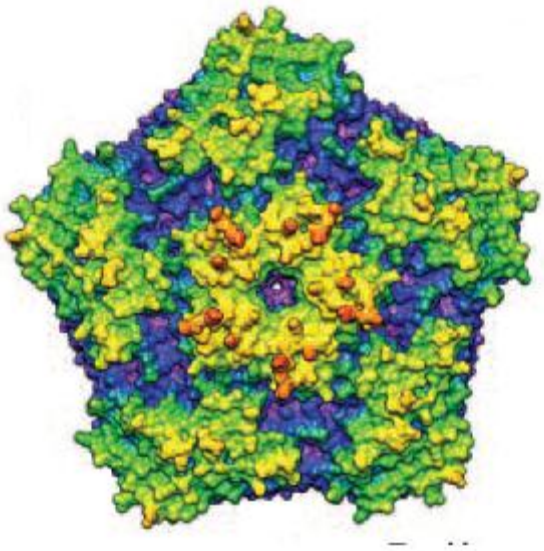

Figure 1.1 Molecular surfaces of five icosahedral asymmetric units of HEV71 viewed down a fivefold axis. Taken from Plevka *et al.* (2012).

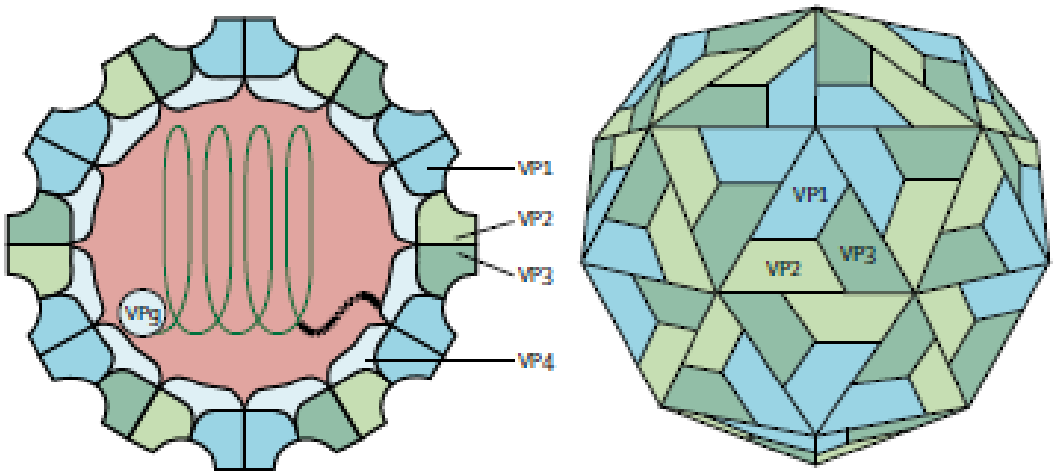

Figure 1.2 HEV71 structure of the virion. Each protomer in the virus capsid contains a copy of the four structural viral proteins (VP1-VP4). Taken from Solomon *et al.* (2010).

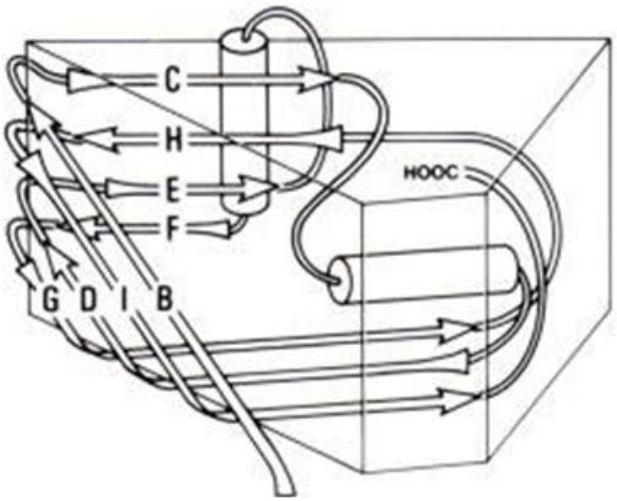

Figure 1.3 Schematic diagram representing the core structural eight-stranded β-sandwich shared by VP1, VP2 and VP3. Taken from Racaniello, (2007).

1.4. HEV71 molecular biology

At a molecular level, picornavirus infections are comprised of four processes: virus entry into cells, viral protein synthesis, viral RNA replication and virion assembly and release (reviewed by Bek & McMinn, 2012).

1.4.1. Virus entry into cells

The first stage of picornavirus infection of susceptible cells is mediated by the interaction of the viral capsid with specific receptors on the cell membrane. Receptors are host cell molecules (usually membrane-associated) that bind virus attachment proteins and are required for entry. Virus receptors have essential roles in the early steps of viral infection. They are therefore a primary determinant of host range and tissue tropism. Different types of cell surface molecules serve as cellular receptors for picornaviruses and some are shared among picornaviruses and members of other virus families.

HEV71 uses several different receptors to attach to cells (Patel & Bergelson, 2009), the most important being scavenger receptor class B, member 2 (SCARB2) (Yamayoshi *et al.*, 2012; Yamayoshi & Koike, 2011; Yamayoshi *et al.*, 2009). The residue Q172 of the HEV71 VP1 protein, located adjacent to the capsid canyon, interacts with a region of SCARB2 that includes the critical residues I144-F151 (Chen *et al.*, 2012; Yamayoshi & Koike, 2011). Following endocytosis of receptor-bound HEV71, SCARB2 facilitates virus uncoating within the acidified endosome (Chen *et al.*, 2012; Lin *et al.*, 2012). A high-resolution analysis that provides a model for the early stages of HEV71 uncoating was recently elucidated (Wang *et al.*, 2012c). Here the VP1 GH loop acts as an

adaptor-sensor for attachment to the cellular receptor.

1.4.2. Viral protein translation

Following HEV71 virion uncoating within the acidified endosome, viral protein synthesis commences and the non-structural proteins required to support viral replication are translated directly from input viral RNA. The HEV71 genome is uncapped and the 5′ UTR enables translation of the viral polyprotein in a cap-independent manner (Thompson & Sarnow, 2003). This involves internal ribosome binding, followed by ribosome scanning of the mRNA to identify an appropriate downstream start site AUG codon. Heterogeneous nuclear ribonucleoprotein (hnRNP) A1 interacts with the IRES; and either hnRNP A1 or hnRNP A2 are essential for the IRES-directed translation (Lin *et al.*, 2008). The linker region between the IRES and the ORF interacts with two far upstream element binding proteins (FBPs). Binding of FBP2 inhibits translation (Lin *et al.*, 2009b); however, FBP1 can out-compete FBP2 binding (Huang *et al.*, 2011a; Shih *et al.*, 2011), which allows translation to continue. Several other cellular factors have been shown to associate with the HEV71 IRES, but their role in HEV71 protein translation has not been confirmed (Shih *et al.*, 2011).

Following viral protein translation, proteolytic processing of the viral polyprotein into precursor and mature viral proteins occurs via the viral-encoded proteinases (Bedard & Semler, 2004). The primary cleavage event occurs at the junction between the P1 and P2 precursor proteins and is mediated by the viral proteinase 2A, leading to the rapid separation of capsid precursor P1 from the non-structural proteins (Figure 1.4). The HEV71 2A protease is capable

of cleaving several host proteins, including the translation initiation factor eIF4G, which is involved in cap-dependent translation. The secondary cleavage events within the viral protein precursors are carried out by the 3C protease, which produces crucial factors in protein processing and RNA replication. The HEV71 3C protease cleaves the cellular cleavage stimulation factor, 39 pre-RNA, subunit 2, 64 kDa (CstF-64), which is required for polyadenylation of cellular pre-mRNA (Weng *et al.*, 2009). This enhances translation of the HEV71 genome by shutting down host cell protein synthesis and directing resources to viral protein synthesis (Thompson & Sarnow, 2003).

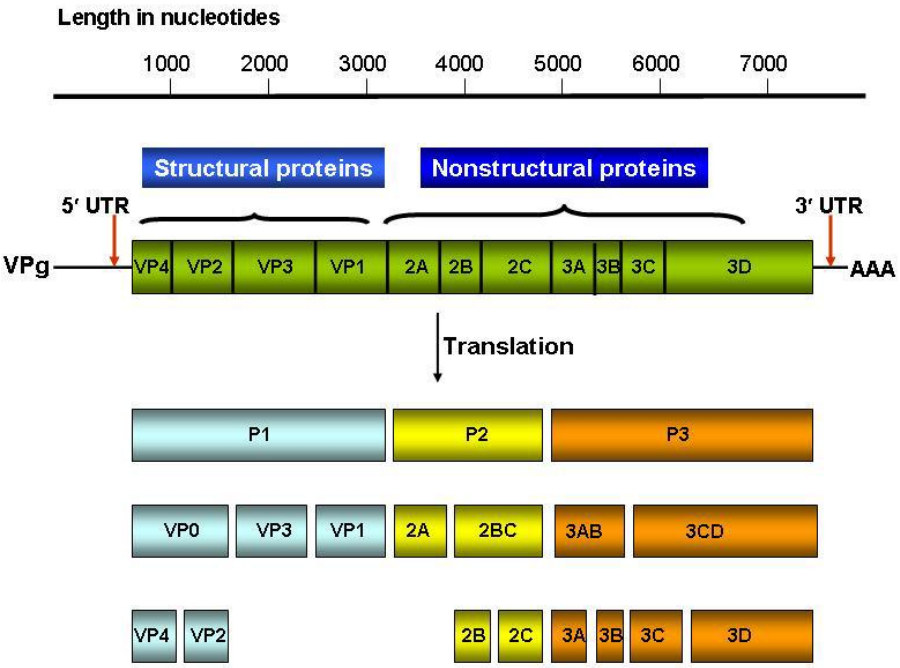

Figure 1.4 Genome structure of HEV71. The VPg is covalently linked to the 5′ end. A single ORF is preceded by a 5′ UTR, and followed by a 3′ UTR, and a poly (A) tail. Following translation into a single polyprotein, the coding region is cleaved into P1, P2 and P3 regions. Intermediate and final cleavage products are shown. Taken from Racaniello, (2007).

1.4.3. Viral genome replication

Picornaviruses utilise a unique replication mechanism to generate new viral progeny via their ability to synthesise RNA from an RNA template. It is generally accepted that picornaviral RNA replication proceeds via the following pathway:

+ strand RNA ----> - strand RNA synthesis ----> replicative form (RF) ---->

+ strand RNA synthesis ----> replicative intermediate (RI) ----> + strand RNA

The newly synthesised viral proteins associate together and with cellular proteins to form the replication complex and initiate viral RNA replication. The viral gene 3B encodes a 22 amino acid polypeptide known as VPg. In PV, two adenosine nucleotides on an RNA stem-loop structure, known as the *cis*-acting replication element (*cre*), form the template for the addition of two uracil residues to VPg by the viral RNA-dependent RNA polymerase (RdRp) $3D^{pol}$, a process known as uridylylation (Paul *et al.*, 2003). The putative HEV71 *cre* stem-loop structure is located within the 2C gene (Chen *et al.*, 2009). VPg and uridylylated VPg (VPGpUpUOH) function as primers for PV RNA replication.

There are four *cis*-active RNA elements required for viral RNA replication in the PV genome; the cloverleaf domain, the *cre*, the 3′ UTR and the 3′ poly (A) tail (Figure 1.5). Negative-sense HEV71 template RNA is copied from the 3′ terminus of positive-sense genomic RNA. The 3′ UTR of HEV71 contains three putative SLDs (X, Y and Z) (Kok *et al.,* 2012), followed by a poly (A) tail, which associates with the host protein poly (A) binding protein (PABP) (Lin *et al.*, 2009a) and recruits the $3D^{pol}$-VPgpUpUOH primer complex, where two uracil residues bind as a primer for elongation of negative-strand RNA (Lin *et al.*, 2009a). PABP

interacts with a replication complex of viral and host proteins assembled at the cloverleaf domain within the 5′ UTR. The resulting double-stranded RNA duplex, known as the replicative form (Bedard *et al.*, 2007), switches off viral protein translation.

The HEV71 positive-sense genomic RNA has two 5′ terminal uracils that are essential for replication (Bek & McMinn, 2010). Following synthesis of the negative strand, a second $3D^{pol}$-VPgpUpUOH is recruited to the 3′ end of the negative strand, where the complementary adenosines are recognised by the VPgpUpUOH primer. $3D^{pol}$ then extends a new positive strand RNA molecule. This two-stage replication process takes place in replication complexes that assemble on lipid membrane-associated lattices on autophagosome-like structures (Huang *et al.*, 2009a). A recent study has demonstrated that HEV71 viral RNA replication is dependent on a host protein, coat protein complex I (COPI), vesicle which is an essential component of the trafficking machinery cycling between the endoplasmic reticulum and Golgi complex (Wang *et al.*, 2012a).

Picornavirus RdRps are known to have high misincorporation rates (Castro *et al.*, 2005) resulting in the formation of a high quasispecies diversity during genomic RNA replication, which is thought to influence the adaptation of picornaviruses during infection of the host (Pfeiffer & Kirkegaard, 2005).

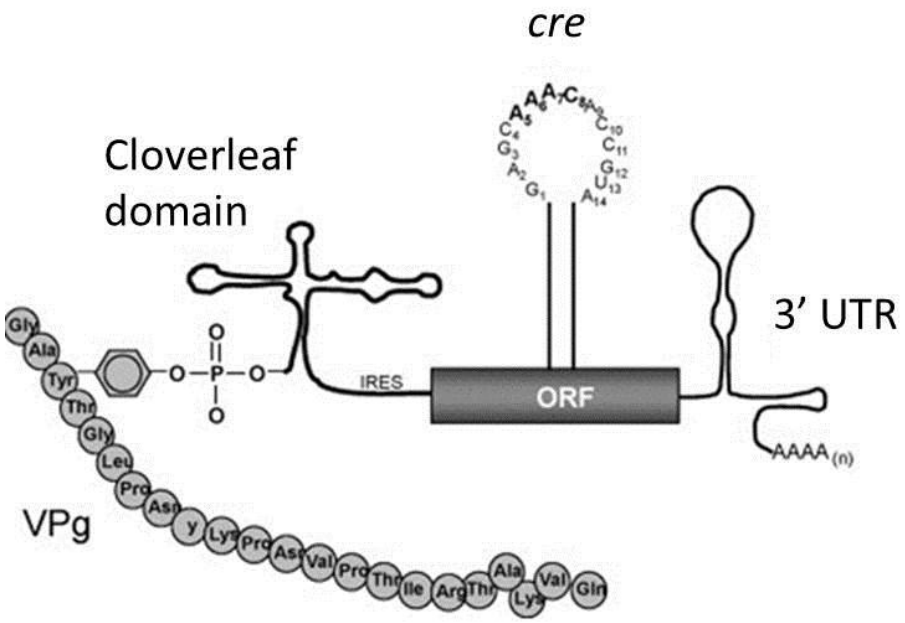

Figure 1.5 VPg and *cis*-active RNA sequences and structures required for PV RNA replication. There are four distinct *cis*-active RNA sequences and structures required for RNA replication: the cloverleaf domain, the *cre*, a 3′ UTR and 3′ poly (A) tail. Taken from Steil & Barton (2009).

1.4.4. Release of virus from cells

According to the current model of picornavirus virion assembly, capsid proteins organise into protomers containing one copy each of VP1-VP4 (Yi *et al.*, 2011). Five protomers then assemble via VP1 self-association at an interaction domain spanning amino acids 66-297 (Lal *et al.*, 2006) to form a pentamer. The pentamers have been shown to bind the viral genome. Twelve pentamers, with bound RNA, assemble to form the viral capsid.

Evidence from various picornavirus models suggest that these viruses tightly regulate apoptosis in the host cell, blocking apoposis during virion production and promoting apoptosis to assist with the release of progeny virus. HEV71 induces apoptosis in infected cells after approximately 24 h (Kuo *et al.*, 2002; Shih *et al.*, 2008). Transient expression of either the HEV71 2A protease (Kuo *et al.*, 2002) or the 3C protease (Li *et al.*, 2002) can induce apoptosis in infected cells. The cleavage of eIF4G by protease 2A (Kuo *et al.*, 2002) and the activation of caspase-3 by protease 3C (Li *et al.*, 2002; Shih *et al.*, 2008) are possible mechanisms by which HEV71 triggers apoptosis. *In vitro* analysis suggests that the oxidising environment within glucose-6-phosphate dehydrogenase-deficient cells enhances virus replication and cytopathic effect (Ho *et al.*, 2008).

1.5. HEV71 genogroup

Genotyping of HEV71 has not yet been standardised. Many researchers studying the molecular epidemiology of HEV71 have used different methods to designate genogroup and sub-genogroup. The most widely used genes for genotyping HEV71 for molecular epidemiological investigations are VP1 (AbuBakar *et al.*, 2009; Brown *et al.*, 1999; McMinn *et al.*, 2001a; Sanders *et al.*, 2006) and VP4 (Cardosa *et al.*, 2003; Munemura *et al.*, 2003; Shimizu *et al.*, 2004; Tu *et al.*, 2007). The gene sequence of VP1 capsid is commonly used for molecular typing of enteroviruses because VP1 capsid binds to the cellular receptor and is subjected to immune selection. On the other hand, VP4 is only 207 nucleotides in length, making it relatively straightforward to amplify and sequence. A drawback of VP4 is that it is the most conserved capsid protein and hence nucleotide changes are fewer compared to VP1. VP1 and VP4 gene sequences both provide similar phylogenetic information, but the higher bootstrap values observed in VP1 dendograms provide greater statistical confidence, particularly when elucidating new genogroups. Thus the use of the shorter VP4 gene may be helpful for HEV71 surveillance but the VP1 gene should still be used for molecular epidemiologic research and for confirming data obtained with VP4-based analyses (Cardosa *et al.*, 2003).

Based on the VP1 sequence, HEV71 is divided into four genogroups: A, B, C and D; genogroups B and C are further divided into sub-genogroups B1-B5 and C1-C5, respectively (Brown *et al.*, 1999; Deshpande *et al.*, 2003; Yip *et al.*, 2010). Virus isolates belonging to the same genogroup have more than 92% nucleotide sequence identity, compared to 78-83% identity between HEV71 strains from

different genogroups. By contrast, VP4 sequence data cannot discriminate some isolates at the sub-genogroup level but can still be used to designate isolates into different genotype (Chan *et al.*, 2010). Classification of HEV71 genogroups using complete genome sequences has been proposed (Chan *et al.*, 2010). HEV71 classification using complete genomes showed the presence of four genogroups (A-D) with sub-genogroup B1-B4 and C1-C3 and C5; in this study, sub-genogroup C4 was re-classified as genogroup D. Phylogenetic trees based on full genome sequences are highly robust, as they take into consideration changes in the sequences of both the structural and non-structural genes. However it is not always possible or practical to sequence the complete genome for epidemiological studies.

Non-structural genomic regions are not commonly used for molecular epidemiological studies. A non-structural protein gene was found to be a recombination hot-spot in HEV71 and also other HEVA viruses (Huang *et al.*, 2008). A recent study of publicly available HEV71 sequences found that most recombination breakpoints were located in the 3D polymerase protein (Chen *et al.*, 2010). In other studies, recombination breakpoints have been identified in the 5′ UTR (McWilliam Leitch *et al.*, 2012; van der Sanden *et al.*, 2011), at amino acid position 145 in VP1 (Chen *et al.*, 2010) and at the 2A-2B junction (Yip *et al.*, 2010; Yoke-Fun & AbuBakar, 2006; Zhang *et al.*, 2011b). Recombinant strains have frequently predominated in epidemics, suggesting that recombination events in HEV71 may lead to viral re-emergence (Chen *et al.*, 2010; Huang *et al.*, 2011b; McWilliam Leitch *et al.*, 2012; Yoke-Fun & AbuBakar, 2006)

1.6. Molecular epidemiology of HEV71

HEV71 was first identified in California in 1969 (Schmidt *et al.*, 1974). Despite causing severe epidemics in Bulgaria in 1975 and Hungary in 1978, HEV71 was generally associated with relatively minor and infrequent epidemics until 1997, when 41 children died of acute HEV71 infection in Malaysia (Chua & Kasri, 2011), followed shortly afterward by a large HFMD epidemic associated with 78 fatal cases in Taiwan in 1998 (Wang *et al.*, 2012b).

The molecular epidemiology of specific HEV71 genetic lineages was recently reviewed (McMinn, 2012). Genogroup A is represented by a single virus strain, the prototype HEV71 isolate BrCr, isolated in the USA in 1969 (Schmidt *et al.*, 1974). A small outbreak of HFMD due to HEV71 belonging to genogroup A was recently reported in China (Yu *et al.*, 2010), however, the source of virus in this outbreak is unclear. Genogroup B lineages: B1 and B2, circulated between 1970 and 1990 (McMinn, 2002); and B3-B5 have emerged in Southeast Asia since 1997 (Huang *et al.*, 2009b); a progenitor lineage, B0, has recently been proposed to describe isolates that circulated in Europe between 1963 and 1967 (van der Sanden *et al.*, 2009). Genogroup C lineages: C1 replaced B as the dominant genotype in Europe and America from 1987; C2 emerged in 1995; and C3-C5 have been involved in epidemic activity in Southeast Asia since 1997 (Cardosa *et al.*, 2003; Solomon *et al.*, 2010). Genogroup D emerged as a single virus strain isolated in India in 2002 (Deshpande *et al.*, 2003).

The circulation of HEV71 genetic lineages in different geographic regions since 1960 have been presented in numerous publications (AbuBakar *et al.*, 2009;

Cardosa *et al.*, 2003; De *et al.*, 2011; Fujimoto *et al.*, 2002; Herrero *et al.*, 2003; Lin *et al.*, 2006; Mao *et al.*, 2010; McMinn *et al.*, 2001a; Puenpa *et al.*, 2011; Sanders *et al.*, 2006; Schuffenecker *et al.*, 2011; Shimizu *et al.*, 2004; Solomon & Willison, 2003; Tee *et al.*, 2010; Tu *et al.*, 2007; van der Sanden *et al.*, 2009; Yu *et al.*, 2010; Zhang *et al.*, 2009) and is summarised in Figure 1.6.

It is evident that a diverse population of HEV71 strains can circulate widely and a temporal change in the relative prevalence of particular genogroups of HEV71 is possible. The pattern of changes in viral lineages suggested global spread with regular introduction of new strains that replaced previous strains. Interestingly, recent studies have identified several sub-genogroup-specific recombination events (McWilliam Leitch *et al.*, 2012; van der Sanden *et al.*, 2011) that appear to act as founding events in sub-genogroup emergence and global expansion (McWilliam Leitch *et al.*, 2012), suggesting that recombination has played a crucial role in HEV71 evolution.

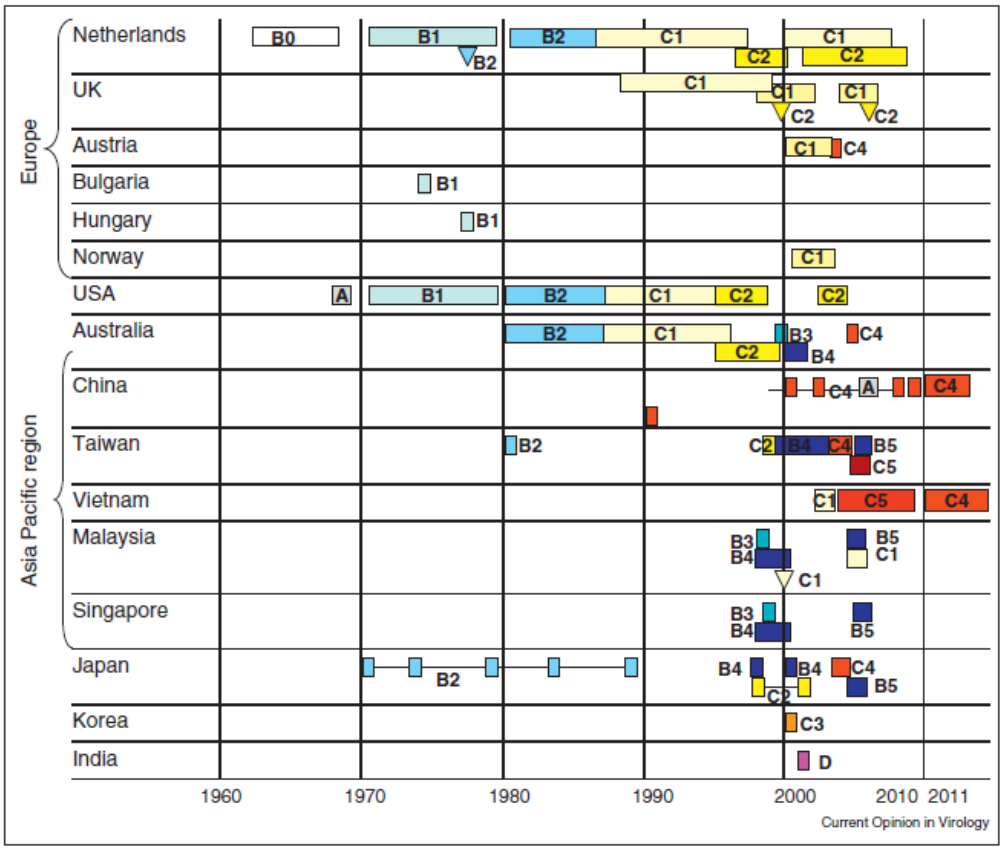

Figure 1.6 Geographic distribution of HEV71 genogroups and sub-genogroups between 1960 and 2011. Triangles represent the isolation of a single strain. Taken from McMinn, (2012).

1.7. HEV71 entry and spread in the host

HEV71 is transmitted predominantly via the faecal-oral route, but can also spread through contact with virus-contaminated oral secretions, vesicular fluid, surfaces or fomites and in respiratory droplets (Chung *et al.*, 2001). As with other enteroviruses, initial viral replication is presumed to occur in the lymphoid tissues of the oropharyngeal cavity (tonsils) and small bowel (Peyer's patches), with further multiplication in the regional lymph nodes (deep cervical and mesenteric nodes), giving rise to a viraemia. Most infections are controlled by host responses at this point and remain asymptomatic. Further dissemination of enteroviruses to the reticuloendothelial system (liver, spleen, bone marrow, and lymph nodes), heart, lung, pancreas, skin, mucous membranes and central nervous system (CNS) coincides with the onset of clinical features. For HEV71, viral shedding from the throat can occur up to 2 weeks after an acute HEV71 infection and virus can be isolated from the stool for up to 11 weeks. Epidemiological and experimental studies suggest that PV can invade the CNS system through a disrupted blood–brain barrier or by retrograde axonal spread along cranial or peripheral nerves. For HEV71, studies in mice and assessments of the distribution of virus and inflammation in fatal human cases implicate the latter route (Chen *et al.*, 2007a; Chung *et al.*, 2001; Ong *et al.*, 2008; Wong *et al.*, 2008).

1.8. Clinical features of HEV71

1.8.1. HFMD and herpangina

Epidemics of HFMD have been associated most frequently with CVA16, although HEV71 has been increasingly recognised as another cause of the disease. The

illness is characterised by 3 to 4 days of fever and the development of a vesicular exanthem on the buccal mucosa, tongue, gum and palate and a papulovesicular exanthem on the hands, feet and buttocks. Clinical observations from HEV71 epidemics in Japan (Komatsu *et al.*, 1999) and Western Australia (McMinn *et al.*, 2001a) indicate that the HFMD rashes due to CVA16 and HEV71 may differ. The rash associated with CVA16 infection is characterised by the formation of larger vesicles than the HEV71 infection, where the rash is more frequently papular and/or petechial often with areas of diffuse erythema on the trunk and limbs. HFMD in a healthy adult has been reported (Tai *et al.*, 2009) caused by intrafamilial transmission of HEV71.

Herpangina is a febrile illness of relatively sudden onset with complaints of fever and sore throat. Characteristic lesions are found on the anterior tonsillar pillars, soft palate, uvula and tonsils and on the posterior pharynx (Pallansch & Roos, 2007). Patients may report anorexia, malaise, irritability, headache, backache and diarrhea. The illness is usually self-limited and disappears within a few days.

1.8.2. Neurological disease

HEV71 has been recognised as highly neurotropic and associated with a diverse range of neurological disease such as aseptic meningitis (non-bacterial inflammation of the meninges), brainstem and/or cerebellar encephalitis, acute flaccid paralysis (AFP) and several post-infectious neurological syndromes. AFP associated with HEV71 infection appears to be milder and associated with higher rates of complete recovery than occurs after PV infection. HEV71 may induce AFP by several mechanisms in addition to virus-mediated destruction of anterior

horn motor neurons and this is reflected in the more varied clinical presentation of HEV71-associated AFP than seen during PV infection. In a study conducted by Chen *et al*. (2007b) on the surveillance of HEV71 in Taiwan, AFP was defined as acute onset of paresis or paralysis of one or more skeletal muscle groups, usually of one or more limbs. The most severe neurological manifestation of HEV71 infection is brainstem encephalitis. Children with this infection usually present with myoclonus, tremor, ataxia, nystagmus and cranial nerve palsies (McMinn, 2002). Hamaguchi *et al.* (2008) also described an acute encephalitis that was caused by intrafamilial transmission of HEV71 in an adult. Encephalitis was characterised by a disturbance in the level of consciousness such as lethargy, drowsiness or coma (Chen *et al.*, 2007b). Aseptic meningitis is characterised by headache, meningeal signs and mononuclear pleocytosis (>5×10^6 leukocytes per L if the patient was older than 1 month or > 25×10^6 leukocytes per L if the patient was a newborn) in addition to a negative bacterial culture (Chen *et al.*, 2007b).

1.8.3. Neurogenic pulmonary oedema

Several post mortem studies of neurogenic pulmonary oedema due to HEV71 infection have been described (Lum *et al.*, 1998a; Lum *et al.*, 1998b; Shekhar *et al.*, 2005). Neurogenic pulmonary oedema is characterised by respiratory distress, tachypnea, tachycardia, pink frothy sputum and rapidly progressing, patchy, diffuse pulmonary infiltrates and congestion on a chest x-ray (Chen *et al.*, 2007b). Lum *et al*. (1998b) described four cases of fatal encephalomyelitis associated with neurogenic pulmonary oedema during an outbreak of HFMD. In all cases there was sudden and rapid progression of pulmonary and

cardiovascular decompensation leading to death. HEV71 involvement of the medullary vasomotor centres resulted in neurogenic pulmonary oedema. Radiologic or clinical evidence of pulmonary oedema was present in all cases. These observations were supported by increased lung weight and histologic evidence of pulmonary oedema. The authors postulated that there is a causative link between HEV71 and the histologic changes in the brainstem as the cause of neurogenic pulmonary oedema and cardiac dysfunction leading to death.

1.8.4. Other HEV71 associated disease

Acute respiratory disease (other than neurogenic pulmonary oedema) has been linked to the HEV71 infection. Respiratory diseases associated with HEV71 infection include pharyngitis, croup, broncholitis and pneumonia (Gilbert *et al.*, 1988; Merovitz *et al.*, 2000; Tsai *et al.*, 2001). Most respiratory infections occur in children 1-3 years of age and are often of sufficient severity to require hospitalisation. A single case of intrauterine infection with HEV71 leading to symptomatic foetal infection (hydrocephalus, hepatosplenomegaly) and stillbirth has been reported (Chow *et al.*, 2000). In this case antigen was detected within neurons of foetal brainstem structures and HEV71 RNA was detected in several maternal and foetal tissues providing direct evidence of foetal infection.

1.9. Pathogenesis of HEV71

The wide variety of clinical manifestations resulting from HEV71 infection, ranging from mild HFMD to fatal encephalitis, has demonstrated the complexity of HEV71 pathogenesis. HEV71 causes neurological disorders in virus-infected patients mainly through the induction of inflammation in the CNS. Although the

pathogenesis of HEV71 associated with neurological diseases has been studied intensively, the mechanisms of HEV71 disease progression remain unclear. Initial viral replication probably occurs in the intestine, since virus can be detected in stool for several weeks after infection (Chung *et al.*, 2001). The ability of HEV71 to infiltrate, infect and replicate in cells of the CNS has been clearly demonstrated, as viral antigen was detected in the cytoplasm of neurons (Wong *et al.*, 2008). The major targets of HEV71 in the CNS are the spinal cord and brainstem (Wong *et al.*, 2008). The distribution of viral lesions in the CNS is wider than PV infection, involving both the pyramidal and extrapyramidal tracts of the CNS (Wong *et al.*, 2008).

The mechanisms of viral entry into the CNS after replication in peripheral tissues are currently unknown. Several studies have shown that viraemia is necessary for the spread of virus to the CNS, for example, monkeys inoculated intravenously, intracerebally or orally with HEV71 developed neurological syndromes clinically and pathologically similar to human cases of encephalitis (Nagata *et al.*, 2004; Zhang *et al.*, 2011a). Neuroinvasion is most likely preceded by virus replication in extraneural tissues. Wong *et al*. (2008) examined the distribution of inflammatory responses in the CNS of human HEV71 encephalitis cases. Based on distinct inflammatory responses found in the CNS (spinal cord gray matter, brainstem, hypothalamus, and subthalamic and dentate nuclei), the authors speculated that virus spreads into the CNS via the peripheral nervous system, most likely via motor pathways. However, spread of virus into the CNS via the haematogenous route and subsequent crossing of the blood-brain barrier has not been ruled out.

Both viral factors such as virulence and tropism and host factors such as the distribution of host cell receptors and the immune system may contribute to the pathogenesis of HEV71 encephalitis and be responsible for the observed differences in the clinical manifestations of HEV71 infection. One genetic study in Taiwan reported that HLA-A33 is associated with increased susceptibility to HEV71 infection, although the role of the MHC remains unknown (Chang *et al.*, 2008). The researchers noted that HLA-A33 is more frequent in Asian populations than in caucasian populations, which might explain the high prevalence of HEV71 epidemics in Asia. They also suggested that HLA-A2 could be linked to the risk of cardiopulmonary failure in patients with HEV71 infection.

The role of host factors in HEV71 encephalitis has been suggested by several findings (reviewed by Weng *et al.* 2010). Children that developed neurogenic pulmonary oedema had abnormal cytokine activation that produced severe systemic inflammatory responses (Wang *et al.*, 2003). Patients with neurogenic pulmonary oedema were found to have significantly higher levels of plasma interleukin-6 (IL-6), IL-10, IL-13, IL-1β and interferon (IFN)-γ lower levels of circulating CD4+ T cells, CD8+ T cells and natural killer (NK) cells than the other HEV71 cases (Wang *et al.*, 2003). It was also found that children with meningoencephalitis had an altered cellular immune response associated with a high frequency of the G/G genotype of the cytotoxic T lymphocyte antigen-4 polymorphism (Yang *et al.*, 2001). Significant elevation of B cell counts was also associated with the development of neurological manifestations in HEV71-infected children (Xie *et al.*, 2010). More studies need to be carried out to clarify the role of viral and host factors in the pathogenesis of HEV71 infection.

1.10. Molecular determinants of HEV71 virulence

Similar to PV, HEV71 is a neurotropic enterovirus. Molecular genetic analyses of PV virulence have shown that minor sequence variations in the 5′ UTR are sufficient to account for large differences in neurovirulence (Evans *et al.*, 1985; Kawamura *et al.*, 1989; Macadam *et al.*, 1991). CVA16 is known as the most common causative agent of HFMD and only rarely causes severe or fatal CNS infections. Numerous clinical and epidemiological studies have established that HEV71 possesses an intrinsic neurovirulence that distinguishes it from CVA16, however, the genetic determinants of HEV71 neurovirulence remain elusive.

In an attempt to identify HEV71 neurovirulence determinants, several studies have compared genomic regions known to influence the neurovirulence of PV, in particular, the 5′ UTR (AbuBakar *et al.*, 1999; Shih *et al.*, 2000; Singh *et al.*, 2002) and the VP1 gene (Brown *et al.*, 1999; Singh *et al.*, 2002) of HEV71 strains isolated from well characterised mild and severe clinical cases. These studies have all failed to identify neurovirulence determinants. A recent study has compared the complete genomes of HEV71 strains derived from mild cases and severe cases (Chang *et al.*, 2012). Nucleotide differences in HEV71 strains isolated from severe cases were observed primarily in the IRES of the 5′ UTR. In the protein-coding region, an E to Q substitution at amino acid position 145 of structural protein VP1 occurred in several of the virulent strains (Chang *et al.*, 2012). There was also a report of a fatal case of HEV71 infection with a single nucleotide variation in domain V of the 5′ UTR (Tong *et al.*, 2011). Although it seems likely that the HEV71 IRES is an important neurovirulence determinant, nucleotide variation linked to neurovirulence in the HEV71 IRES has not been

identified to date, and so the role of this structure in the control of HEV71 neurovirulence remains unclear.

There also appears to be no correlation between severity of disease and genetic lineage, as viruses of all genotypes are capable of causing severe disease, as are viruses of multiple lineages within each genotype (Brown *et al.*, 1999; Shimizu *et al.*, 1999; Wang *et al.*, 2012d). During the Perth HEV71 epidemic in 1999, it was noted that genogroup C2 viruses were exclusively isolated from cases of severe neurological disease and that only one case of uncomplicated HFMD was caused by a C2 genogroup virus (McMinn, 2002). Comparison of the VP1 deduced amino acid sequences with VP1 consensus amino acid sequences for HEV71 genogroups A, B, C and CVA16 revealed the presence of an alanine to valine mutation at position 170 of VP1 in all five strains isolated from children with severe neurological disease. By contrast, the earliest virus isolate in this lineage obtained from a case of uncomplicated HFMD had alanine at position 170 in VP1. These data suggest that the VP1 (A170 to V) mutation may have been associated with increased neurovirulence of HEV71 during the Perth epidemic. However, the effect of this amino substitution on neurovirulence has not been reported to date.

HEV71 neurovirulence is a complex phenotypic characteristic that is likely to be determined by more than one region of the virus genome. Since outbreaks usually involve closely related genetic variants of HEV71 with a varying spectrum and outcome of disease severity, this raises the possibility that other environmental and host factors, such as age-related resistance and cross-

protective immunity, are likely to play significant role in the case outcome. Differing viral loads or inoculation doses during the acquisition of infection, as well as variable host immune status and responses, are other critical factors that can potentially influence clinical outcome and mortality (McMinn, 2002).

Quasispecies arise from rapid genomic evolution powered by the high mutation rate of RNA viral replication (Domingo & Holland, 1997; Domingo *et al.*, 1997). For viruses, the term quasispecies refers to a mutant swarm of related but genetically distinct population members. While a high mutation rate is dangerous for a virus as it results in non-viable individuals, it has been hypothesised that high mutation rates create a "cloud" of potentially beneficial mutations at the population level, which afford the viral quasispecies a greater probability to evolve and adapt to new environments and challenges during infection. Increasing evidence indicates that quasispecies evolution may lead to the selection of virulent viruses and to the emergence of new viral pathogens (Domingo & Holland, 1997). However, viral factors and host barriers influence virally induced disease, and asymptomatic versus symptomatic infection is governed by a 'virulence threshold' (Lancaster & Pfeiffer, 2012). Incorporating virulence thresholds into predictions of viral population behaviours can provide an additional dimension to quasispecies dynamics in that virulent viruses must be present above certain proportion in order to cause disease. Therefore understanding modulation of virulence thresholds could lend insight into disease outcome and aid in rational therapeutic and vaccine design.

1.11. Cell culture and animal models of HEV71 infection

1.11.1. Cell culture

HEV71 infection has been studied most frequently in human rhabdomyosarcoma (RD) cells (Kok *et al.*, 2012; Leong & Chow, 2006), where HEV71 infection suppresses the expression of cellular transcription and translation regulators and anti-apoptotic genes (Lee *et al.*, 2011; Leong & Chow, 2006). Neuronal cell lines SK-N-SH (human neuro-epithelioma) cells (Tung *et al.*, 2010) and SH-SY5Y (human neuroblastoma) cells (Kok *et al.*, 2012) have also been used to study changes in mRNA expression during HEV71 infection. *In vitro* techniques continue to advance methods for visualising HEV71 infection of cells, including a fluorophore (Ghukasyan *et al.*, 2007), luciferase (Kok *et al.*, 2012) and green fluorescent protein (GFP) (Chen *et al.*, 2012) reporter systems.

1.11.2. Non-human primate models

Similar to the related PV, HEV71 has a limited host range, with humans the only known natural host. Old World monkeys such as cynomolgus, rhesus and African green monkeys can be infected experimentally with HEV71 (Arita *et al.*, 2005; Chumakov *et al.*, 1979; Hagiwara *et al.*, 1982; Hashimoto & Hagiwara, 1982; Nagata *et al.*, 2002). The susceptibility of cynomolgus monkeys to HEV71 oral infection was previously investigated (Hashimoto & Hagiwara, 1982). CNS lesions were observed in all monkeys from 7-12 days after infection and HEV71 was recovered from the CNS and other tissues. Specific immunofluorescence was detected in degenerating nerve cells, in associated inflammatory reactive cells and in macrophages of the parenchyma of the CNS. Serum neutralising antibody titres rose between 14 and 21 days post-infection (p.i.). Thus, orally infected

monkeys appear to provide an excellent model for infection in man. Unfortunately, the high cost of monkeys and their maintenance precludes their widespread use for studies of viral pathogenesis.

1.11.3. Mouse models

A small animal model would provide a more cost-effective and practical tool for studies of HEV71 pathogenesis and for vaccine development. However, HEV71 field isolates do not naturally infect mice, although a few mouse-virulent wild-type strains have been identified (Chang *et al.*, 2010). Laboratory mice are only susceptible to HEV71 infection in the first four days of life and become completely resistant by six days of age (Roberts & Boyd, 1987).

Most of the mouse models developed to date have required prior mouse adaptation of virus populations. Several groups have reported the development of a mouse-adapted HEV71 strain by serial passage in mice (Arita *et al.*, 2008; Chen *et al.*, 2004; Chua *et al.*, 2008; Ong *et al.*, 2008; Wang *et al.*, 2004) and the mouse-adaptation of HEV71 was recently reviewed (McMinn, 2012). A mouse model of HEV71 infection developed by Chua *et al.* (2008), involved the selection of a mouse-adapted strain (MP-26M) by six passages of the HEV71 clinical isolate HEV71-26M (sub-genogroup B3) in BALB/c mice. Two mutations in the capsid protein genes VP1 (G145E) and VP2 (K149I) were found to act cooperatively to generate the mouse-adapted phenotype. MP-26M causes acute flaccid paralysis in newborn BALB/c mice owing to the development of severe skeletal muscle myositis (Chua *et al.*, 2008).

A similar mouse model was developed by four passages of the Taiwanese HEV71 strain 4643 (sub-genogroup C2) in one-day-old ICR mice to generate the mouse-adapted strain MP4 (Chen *et al.*, 2004; Wang *et al.*, 2004). Histopathological examination of tissues from MP4-infected mice also revealed the presence of skeletal muscle myositis plus evidence of neuronal loss and apoptosis in the spinal cord and brain stem (Wang *et al.*, 2004). Recently, the two mutations responsible for mouse adaptation of MP4, located in the structural protein genes VP1 (G145E) and in VP2 (K149M), have been reported (Huang *et al.*, 2012). Interestingly, the mutations are located at identical positions to those responsible for the mouse-adapted phenotype of MP-26M (Chua *et al.*, 2008).

A mouse model of HEV71 infection developed by Arita *et al*. (2008) included the serial passage of virus in adult non-obese, diabetic, severe combined immunodeficient (NOD/SCID) mice. The Nagoya strain of HEV71 (sub-genogroup B1) was mouse-adapted by three serial passages in the brains of 16-day-old NOD/SCID mice, resulting in a single amino acid substitution in VP1 (G145K). This mutation was found to be essential for the mouse adapted phenotype, which is at the same site in VP1 responsible for mouse adaptation in the Chua *et al.* (2008) and Huang *et al*. (2012) models.

Ong *et al*. (2008) mouse-adapted a sub-genogroup B3 clinical isolate of HEV71 by serial passage in one-day-old ICR mice. Histopathological examination of tissues from two-week-old ICR mice infected with mouse-adapted virus revealed the presence of CNS disease with features similar to human disease, although skeletal muscle myositis was also observed. The mutations responsible for the

phenotype of this mouse adapted strain have not been reported to date. Wang *et al*. (2011) mouse-adapted a HEV71 strain 0805 (sub-genogroup C4) by serial passages of the virus in the muscle of one-day-old ICR mice. Mice infected with the mouse-adapted virus showed increased muscle virus load resulting in severe necrotising myositis in the skeletal and cardiac muscles and enteritis. Further analysis revealed many mutations in different regions of the genome of the mouse muscle-adapted virus population. However, the contribution of each mutation on virulence was not investigated. Khong *et al*. (2012) recently reported a mouse model of HEV71 infection in which two-week-old immunodeficient AG129 mice were shown to be susceptible to oral infection with non-mouse-adapted strain of HEV71 (5865/SIN/00009; sub-genogroup B4). Mice infected with this virus developed flaccid limb paralysis owing to a combination of skeletal muscle myositis and infection of the brainstem and anterior horns of the spinal cord.

Despite their restriction to infection of mice in the first two weeks of life and the predominance of myositis as the cause of morbidity and mortality, mouse models of HEV71 infection using mouse-adapted strains have proven useful in determining the protective efficacy of candidate HEV71 vaccines. Wu *et al.* (2001) developed a passive protection assay based on the immunisation of pregnant female mice and challenge of their offspring within the first week of life and were able to demonstrate 80% survival of five-day-old pups born to mothers immunised with a heat-inactivated strain of HEV71 and challenged with a lethal dose of virus. This model has been reproduced widely in the assessment of candidate HEV71 vaccine efficacy.

1.12. Aims of this study

HEV71 has recently become an important human pathogen, causing epidemics of HFMD associated with severe neurological complications. However, little is known about the biology and pathogenesis of this virus. Research investigating positive-sense RNA viruses has been considerably advanced by the development of reverse genetic systems. With the introduction of defined genetic changes into full-length infectious-clone constructs, the role of viral specific genetic elements in viral replication and virulence can be determined.

The specific objectives of this study are:

1. To construct genome length infectious cDNA clones of HEV71 belonging to different genogroups isolated from different HEV71 outbreaks.
2. To study the molecular determinants of HEV71 growth in Chinese hamster ovary cell cultures.
3. To determine the molecular basis of mouse adaptation by HEV71.
4. To generate a mouse virulent HEV71 strain by reverse genetic manipulation of the capsid protein.

2. CHAPTER TWO

MATERIALS AND METHODS

2.1. Cells and Viruses

2.1.1. Cell lines

African green monkey kidney (Vero) cells (ATCC CCL-81), human rhabdomyosarcoma (RD) cells (ATCC CCL-136), SV40 transformed African green monkey kidney (COS-7) cells (ATCC CRL-1651) and Chinese hamster ovary (CHO) cells (ATCC CCL-61) were used in this study. All cell lines were grown at 37°C in an atmosphere containing 5% CO_2/95% air. Growth medium consisted of Dulbecco's modified Eagle's medium (DMEM) (*In Vitro* Technologies) supplemented with 5% foetal bovine serum (FBS) (Bovogen Biologicals) and 2mM L-glutamine.

2.1.2. Viruses

HEV71 strains BRU/2006/35334 (sub-genogroup B5, HEV71-B5, VP1 gene GenBank Accession Number: FM201342), 0964/SYD/98 (sub-genogroup C2, HEV71-C2, VP1 gene GenBank Accession Number: AY940113) and 540V/VNM/05 (sub-genogroup C4, HEV71-C4, VP1 gene GenBank Accession Number: AM490151) were isolated from patients with HFMD in Brunei in 2006, Sydney in 1998 and Vietnam in 2005, respectively. Viruses were plaque purified as described in section 2.2.3 and propagated on RD cells to increase the titre for use in subsequent assays. HEV71-B5 and HEV71-C2 were then passaged in CHO cells for four passages and eight passages, respectively, to select CHO cell-adapted HEV71-B5 (CHO-B5) and CHO cell-adapted HEV71-C2 (CHO-C2). CHO-

B5 was then passaged five times by intracerebral (i.c) inoculation in newborn BALB/c mice to select mouse-adapted virus. Mouse-adapted virus derived from the fifth mouse passage was passaged a further two times in Vero cells and designated as MP-B5.

2.2. Virus assays

2.2.1. Virus infection

Confluent cell monolayers (Vero, RD or CHO) in a tissue culture flask (Cellstar) or plate (Costar) were initially examined under the microscope to ensure cells are healthy and confluent. Growth medium was then removed from the flask/plate, followed by the addition of virus suspension. Generally the volume of virus suspension added into cells was 50-100 µL in 24-well format, 100-200 µL in 12-well format, 200-400 µL in 6-well format, 0.5 mL in T25 flask, 1 mL in T75 flask, 2 mL in T175 flask, or virus was added at a specific multiplicity of infection (MOI). The flask/plate was then rocked gently every 10-15 min to ensure all cells were in contact with the virus suspension. After 1 h incubation, the virus suspension was removed from the flask/plate and washed once with phosphate buffered saline (PBS) followed by the addition of maintenance medium consisting of DMEM supplemented with 2% FBS and 2 mM L-glutamine. The flask/plate was incubated in 37°C in an atmosphere containing 5% CO_2/95% air until cytopathic effect (CPE) was observed.

2.2.2. Harvesting virus

Cells were examined daily for the presence of CPE. Once approximately 80% CPE had developed, the cells were then frozen and thawed three times and

transferred to centrifuge tubes before centrifugation at 1,000×g for 10 min at 4°C to sediment cell debris. The virus supernatant was then collected into cryotubes and stored at -80°C until required.

2.2.3. Plaque purification

Vero cell monolayers in 12-well tissue culture plates (Costar) at a density of 2.2×10^5 cells per well was used for plaque assays. Ten-fold serial dilutions of virus were inoculated at 100 µL per well. After incubation for 30 min at 37°C, virus was removed and the cells washed with PBS. Cells were then overlaid with 1 mL of 0.5% agarose (ICN) in DMEM supplemented with 2% FBS and 2 mM L-glutamine. After incubation for four days, 0.5% agarose in 2% FBS/2mM L-glutamine/DMEM was overlaid onto the first layer of agarose gel and further incubated for three days. Plaques (separate group of cells showing CPE) were selected and picked up using pipette tips. The cells and agar were then dissolved in 300 µL of DMEM supplemented with 5% FBS and 2mM L-glutamine at 4°C overnight. The procedure was repeated three times to select a plaque-purified virus populations. The plaque-purified virus was then expanded in RD cells in a tissue culture flask or plate, as described in section 2.2.1.

2.2.4. Median tissue culture infectious dose ($TCID_{50}$) assays

Vero cell monolayers (1×10^4 cells per well) in 96-well tissue culture plates (Costar) were inoculated with 10-fold serial dilutions (100 µL) of each virus stock and incubated at 37°C with 5% CO_2 for five days prior to observation for the presence of CPE. Virus titres were then calculated following method of Reed & Muench (1938). The limit of detection of virus titration by $TCID_{50}$ assay was

found to be $\log_{10}$ 2.2 $TCID_{50}$.

2.2.5. Single-step growth analysis

Monolayers of RD and CHO cells, grown overnight in 48-well tissue culture plates (Costar) at a seeding density of 1×10^5 and 5×10^4 cells per well, respectively, were infected with the virus at indicated MOI for 1 h at 37°C. Infected cells were washed three times with PBS and overlaid with 300 µL DMEM supplemented with 2% FBS and 2mM L-glutamine. Cells and supernatants were collected every 4 h for 24 h, with the first time point (time=0) collected immediately after the addition of DMEM. Samples at each time point were frozen and thawed three times and clarified by centrifugation at 1,000×g for 10 min prior to the determination of the virus titre by $TCID_{50}$ assay.

2.3. Molecular biological techniques

2.3.1. Plasmids

The plasmid vector used for the construction of sub-genomic and/or full length clones of HEV71 in this study was pMC18 (a derivative of pWSK29 kindly provided by Dr. Andrew Davidson, Monash University, Melbourne, Australia). The plasmid construct pCMV-T7Pol expressing T7 RNA polymerase was provided by Dr. Rob Hurrelbrink, Division of Virology, Telethon Institute for Child Health Research, Perth, Australia. Plasmid pCMV-T7Pol was used for co-transfection to rescue clone-derived virus.

2.3.2. Bacterial strains

Escherichia coli (*E.coli*) strain XL10-gold (Stratagene) was used for all

transformations in this study.

2.3.3. Restriction endonuclease digestion

DNA was digested with appropriate restriction enzymes (Promega or New England Biolabs) according to the manufacturer's instructions. Generally, restriction endonuclease digestions were performed with an excess of enzyme at 37°C for 1-4 h or overnight when the complete digestion of vector and insert DNA was required for cloning purposes.

2.3.4. Agarose gel electrophoresis

DNA samples for electrophoresis were mixed with dye loading buffer and loaded into wells of set agarose gel (AppliChem). DNA samples were separated by electrophoresis through 0.6-2% agarose gels, depending on the estimated product size. Electrophoresis was run at approximately 6 V/cm in 1×TAE buffer (1×TAE = 40 mM Tris acetate, 1 mM EDTA). A 1 kb ladder (Geneworks) or 100 kb ladder (Geneworks) were used as molecular weight markers. DNA was visualised by exposure to UV light on a transilluminator (Bio-Rad) after staining in 10 μg/mL of ethidium bromide solution (Bio-Rad).

2.3.5. Purification of DNA from agarose gels

For cloning or sequencing purposes, DNA samples were mixed with dye loading buffer and SYBR green (Molecular Probes) before electrophoresis. DNA was visualised by exposure to visible light on a Dark Reader Transilluminator (Clare Chemical Research) and the expected DNA band was excised from the gel. Purification of DNA from agarose gels was performed using a Gel Extraction Kit

(Qiagen) according to the manufacturer's instructions.

2.3.6. Preparation of plasmid DNA

Small scale preparations of plasmid DNA were performed using the Spin Miniprep kit (Qiagen), according to the manufacturer's instructions.

2.3.7. DNA ligation

The plasmid vectors and insert DNA were digested with the appropriate enzymes (Promega or New England Biolabs) according to the manufacturer's instructions. Ligation reactions were performed for 30 min at room temperature. Generally, insert to vector molar ratios of 1:1 or 3:1 were used. Standard ligation reactions contained either 50 or 100 ng of vector DNA, an appropriate amount of insert DNA, 30 mM Tris-HCL pH7.8, 10 mM $MgCl_2$, 10 mM dithiothreitol (DTT), 1 mM ATP and 1 unit of T4 DNA ligase (New England Biolabs).

2.3.8. Transformation of DNA into *E.coli*

Electro-competent cells were prepared by the method of Siguret *et al.* (1994) and were stored in 15% glycerol at -80°C until use. A 40 µL volume of cells was thawed on ice and approximately 1-5 µL of the DNA ligation mix was added to the cells. The mixture was then added to a 0.1 cm electroporation tube (Astral Scientific), previously cooled on ice, and cells were electroporated using a BioRad GenePulsor apparatus (Bio-Rad) set at 1.25 kV, 200 Ω resistance and 25 µF capacitance. 500 µL of pre-warmed SOC medium (2% tryptone (w/v), 1% yeast extract (w/v), 8.5 mM NaCl, 20 mM glucose, 2.5 mM KCl, 10 mM $MgCl_2$) was immediately added to each cuvette and the mixture transferred to a 1.5 mL

eppendorf tube prior to incubation at 37°C for 1 h with continuous shaking. The transformation mixture was subsequently plated onto LB agar (LB medium plus 1.5% agar) containing appropriate antibiotics (high copy ampicillin at 100 µg/mL, low copy ampicillin at 1 µg/mL or kanamycin at 50 µg/mL).

2.3.9. Isolation of viral RNA

Virus was propagated in cell culture until required. Cells were subjected to freeze-thaw for three times and cell debris was separated by centrifugation at 1,000×g for 10 min at 4°C leaving virus in the supernatant. Viral RNA was then extracted using the QIAamp® Viral RNA mini kit (Qiagen) according to the manufacturer's instructions and eluted in 60 µL of AVE buffer.

2.3.10. Reverse transcription of viral RNA

First strand cDNAs of viruses for subsequent cloning and sequencing were synthesised using SuperScript™ III reverse transcriptase (Invitrogen). Reverse transcription (RT) reactions were carried out in 0.2 mL tubes in a reaction volume of 20 µL. A sample of 8 µL of viral RNA prepared as described in section 2.3.9; 3 µL of an appropriate primer (30 pmol) and 500 µM of dNTP were mixed and heated at 65°C for 5 min before chilling on ice for 5 min. 1× concentration of enzyme buffer as supplied by the manufacturer, 10 mM DTT, 40 U of RNAsin (New England Biolabs) and 200 U of SuperScript™ III reverse transcriptase were then added. The mixture was incubated at 42°C for 1 h before inactivation of the enzyme at 70°C for 15 min. One microliter of RnaseH (New England Biolabs) was added and the mixture incubated at 37°C for 20 min. RT products were stored at -20°C until required.

2.3.11. Polymerase chain reaction (PCR)

(a) PCR for cloning

Viral DNA fragments used for cloning were amplified by PCR using platinum *Taq* DNA polymerase High Fidelity (Invitrogen). The PCR was carried out in 0.2 mL tubes in a reaction volume of 25 µL. PCR reactions contained 10 pmol each of appropriate forward and reverse primer, 400 µM of dNTPs, 1.5 or 2 mM MgSO4, 1 U of platinum *Taq* DNA polymerase High Fidelity, template first-strand cDNA and 1× concentration of enzyme buffer as supplied by the manufacturer. The amplifications were performed in an automated thermocycler, with an initial denaturation at 94°C for 2 min, followed by 40 cycles of 94°C for 30 s, 55°C for 30 s and 68°C for 1 min per 1000 bp, then a final incubation at 68°C for 10 min.

(b) PCR for sequencing

Viral DNA fragments used for sequencing were amplified using PCR supermix (Invitrogen). The PCR was carried out in 0.2 mL tubes in a reaction volume of 25 µL. PCR reactions contained 10 pmol each of appropriate forward and reverse primers, 22 µL of PCR supermix and 1 µL of template first-strand cDNA. Reactions were incubated for 2 min at 94°C, then 40 cycles of 94°C for 30 s, 50°C for 30 s and 72°C for 2 min and finally incubated at 72°C for 2 min. Primers used for whole genome sequencing in this study are listed in Tables 2.1, 2.2 and 2.3. Primers used for sequencing of VP1 (HEV71-C4 variants), VP1 (CHO-26M variants) and VP2 genes in this study are listed in Tables 2.4, 2.5 and 2.6, respectively.

Table 2.1 Primers used to sequence the complete genome of HEV71-B5, CHO-B5 and MP-B5

Primer name *	Nucleotide position †	Sequence (5′ to 3′) #
EV71-1F	1-24	TTA AAA CAG CCT GTG GGT TGC ACC
CHO-533F	536-557	CAG CGG AAC CGA CTA CTT TGG G
EV71-1R	624-644	CGG ATG GCC AAT CCA ATA GCT
EV71-3F	958-977	**CCA TCY GCY GAR GCD TGT GG**
EV71-2R	1114-1136	**TTC ACB GAM ACA TCY GGG CGC GT**
EV71-4F	1564-1580	**GAY TCH GCY YTG AAC CA**
EV71-3R	1792-1811	**GGR GTG GGR TGR AAR TTT GG**
B5_2057F	2057-2079	CAC TGG AGG TCA CTT TCA TGT TC
EV71-4R	2368-2387	**AAR TTC TTY TGG GCY GCC GC**
B5_2778F	2778-2802	CAT AAC TGG TTA TGC GCA AAT GCG C
B5_3034R	3012-3034	CGG GTG ACA TGA ACG GAA CTG AG
B5_3496F	3496-3519	CGT TGT GAC TGT CAA ACA GGA GTG
B5_3682R	3660-3682	GGC ACC TTA AGA TGC CTC CGC AG
B5_4333F	4333-4355	CAT TTC TGT CGC AAG TTC CAA CC
B5_4556R	4531-4556	GGT GGC AGT GAG TAC ACA CTA GAG TG
B5_5166F	5166-5185	GCG CCA ATA CTG TAG GGA GC
B5_5336R	5315-5336	GAA TAC GCG CCT TGA AAC CCC G
B5_5658F	5658-5681	CAT TCC AGA GAC CAT TAG TGG CGC
B5_6027R	6008-6027	CAC ACT AGG CTC CAG CTT AG
B5-6661F	6661-6681	CTC AGC CCA GTA TGG TTC AGG
B5_6825R	6804-6825	GGA AGT ACC AGA ACA CCC TGA G
B5_7294R	7273-7294	CAT AAT TGG GAA TGG CCA ACG C
6F-MLV		<u>CCG CGG GAA TTC ACG CGT</u> TTT TTT TTT TTT TTT TTT TTT TTT GCT ATT CTG GTT

* Forward primers are suffixed with "F" and reverse primers are suffixed with "R". 6F-MLV primer is a universal reverse primer with 25 nt poly (T) that will anneal to all HEV71 3′ poly (A) tail followed by *EcoRI* and *MluI* sites (underlined) and was provided by Dr Patchara Phuektes

Degenerate primers are emboldened. Mixed bases codes: D (ATG); B (TCG); H (ATC); M (AC); Y (CT); R (AG)

† Nucleotide position is based on HEV71-B5

Table 2.2 Primers used to sequence the complete genome of HEV71-C2, CHO-C2 and clone-derived virus of strain HEV71-C2

Primer name *	Nucleotide position †	Sequence (5′ to 3′) #
EV71-1F	1-24	TTA AAA CAG CCT GTG GGT TGC ACC
CHO-533F	533-554	CAG CGG AAC CGA CTA CTT TGG G
EV71-1R	621-641	CGG ATG GCC AAT CCA ATA GCT
EV71-3F	955-974	**CCA TCY GCY GAR GCD TGT GG**
EV71-2R	1111-1133	**TTC ACB GAM ACA TCY GGG CGC GT**
EV71-4F	1561-1577	**GAY TCH GCY YTG AAC CA**
EV71-3R	1789-1808	**GGR GTG GGR TGR AAR TTT GG**
EV71-5F	2326-2342	**GTY CCA ATW GGR GCR CCC AA**
EV71-4R	2365-2384	**AAR TTC TTY TGG GCY GCC GC**
EV71-6F	3010-3029	**TCH GTN CCR TTY ATG TCA CC**
EV71-5R	3121-3145	**CYG ARA AHG TRC CCA TCA TGT T**
EV71-7F	3547-3566	**CCD GTC AGY TTY TCD AAA CC**
EV71-6R	3967-3986	**GTN GCB GTN ARD GTR ACC AT**
EV71-8F	4327-4343	**GCY CAY TTY TGY CGC AA**
EV71-7R	4555-4574	**CCR TCR AAD TGR TCH GGG TC**
EV71-9F	4846-4865	**GAB YTR GGY AGR YTD GAT GC**
EV71-8R	5059-5081	**CTR AAY TTR GGB GGN CCT TGG AA**
C2-5991F	5995-6011	TTT CTG CGC TGC CCT GA
EV71-9R	6001-6023	**ACR CTD GGY TCN ARY TTD GTG CG**
EV71-11F	6646-6665	**TAT GAY GCY AGY CTY AGC CC**
C2-6844R	6820-6840	CCC TTC TAT GAG AGA CAG TGC
6F-MLV		CCG CGG GAA TTC ACG CGT TTT TTT TTT TTT TTT TTT TTT TTT GCT ATT CTG GTT

* Forward primers are suffixed with "F" and reverse primers are suffixed with "R". 6F-MLV primer is a universal reverse primer with 25 nt poly (T) that will anneal to all HEV71 3′ poly (A) tail followed by *EcoRI* and *MluI* sites (underlined) and was provided by Dr Patchara Phuektes

Degenerate primers are emboldened. Mixed bases codes: N (ACGT); D (ATG); B (TCG); H (ATC); W (AT); M (AC); Y (CT); R (AG)

† Nucleotide position is based on HEV71-C2

Table 2.3 Primers used to sequence the complete genome of HEV71-C4 and clone-derived virus of strain HEV71-C4

Primer name *	Nucleotide position †	Sequence (5′ to 3′) #
EV71-1F	1-24	TTA AAA CAG CCT GTG GGT TGC ACC
CHO-533F	531-552	CAG CGG AAC CGA CTA CTT TGG G
EV71-1R	619-639	CGG ATG GCC AAT CCA ATA GCT
EV71-3F	953-972	**CCA TCY GCY GAR GCD TGT GG**
EV71-2R	1109-1131	**TTC ACB GAM ACA TCY GGG CGC GT**
EV71-4F	1559-1575	**GAY TCH GCY YTG AAC CA**
EV71-3R	1787-1806	**GGR GTG GGR TGR AAR TTT GG**
EV71-5F	2324-2340	**GTY CCA ATW GGR GCR CCC AA**
EV71-4R	2363-2382	**AAR TTC TTY TGG GCY GCC GC**
C4-2537R	2522-2537	CCT GTG TGT TCT GGC C
EV71-6F	3008-3027	**TCH GTN CCR TTY ATG TCA CC**
EV71-5R	3119-3143	**CYG ARA AHG TRC CCA TCA TGT T**
C4-3206F	3206-3225	CAC GTC AGG GCG TGG ATA CC
EV71-7F	3545-3564	**CCD GTC AGY TTY TCD AAA CC**
C4-3661R	3642-3660	CCA CAA TCA CCA GGT TCT G
EV71-6R	3965-3984	**GTN GCB GTN ARD GTR ACC AT**
EV71-8F	4325-4341	**GCY CAY TTY TGY CGC AA**
EV71-7R	4553-4572	**CCR TCR AAD TGR TCH GGG TC**
EV71-9F	4844-4863	**GAB YTR GGY AGR YTD GAT GC**
EV71-8R	5057-5079	**CTR AAY TTR GGB GGN CCT TGG AA**
C4-5109F	5108-5125	CCA GCC CCA GAC GCT ATT
EV71-10F	5693-5715	**GKK ATM AAY ACD GAR CAY ATG CC**
C4-5756R	5738-5755	GCC ATA CTG CAC AAC GTC
C4-5768F	5767-5787	CAG TGG TAA GCC TAC TCA TCG
EV71-9R	5999-6021	**ACR CTD GGY TCN ARY TTD GTG CG**
EV71-11F	6644-6663	**TAT GAY GCY AGY CTY AGC CC**
C4-6797R	6770-6793	CCC ACC AAG CAC ACA ATA GGT CTT
EV71-10R	6795-6810	**GAR CAV CCW GAG GGC AT**
6F-MLV		CCG CGG GAA TTC ACG CGT TTT TTT TTT TTT TTT TTT TTT TTT GCT ATT CTG GTT

* Forward primers are suffixed with "F" and reverse primers are suffixed with "R". 6F-MLV primer is a universal reverse primer with 25 nt poly (T) that will anneal to all HEV71 3′ poly (A) tail followed by *EcoRI* and *MluI* sites (underlined) and was provided by Dr Patchara Phuektes

Degenerate primers are emboldened. Mixed bases codes: V (ACG); N (ACGT); D (ATG); B (TCG);

H (ATC); W (AT); K (TG); M (AC); Y (CT); R (AG)

† Nucleotide position is based on HEV71-C4

Table 2.4 Primers used for amplification and sequencing of VP1 gene of HEV71-C4 variants

Primer name *	Nucleotide position†	Sequence (5′ to 3′)
C4-2538F	2538-2557	TGA GCA GTC ATC GAC TGG AT
C4-3148R	3130-3148	AGT CCG CAC TGA GAA TGT G

* Forward primers are suffixed with "F" and reverse primers are suffixed with "R"

† Nucleotide position is based on HEV71-C4

Table 2.5 Primers used for amplification and sequencing of VP1 gene of CHO-26M variants

Primer name *	Nucleotide position†	Sequence (5′ to 3′)
CHO-2806F	2809-2831	GTG GAG TTG TTC ACC TAC ATG CG
CHO-3519R	3496-3522	GTA CAC TCC TGT TTG ACA GTC ACA ACG

* Forward primers are suffixed with "F" and reverse primers are suffixed with "R"

† Nucleotide position is based on HEV71-26M

Table 2.6 Primers used for amplification and sequencing of VP2 gene of HEV71

Primer name *	Nucleotide position†	Sequence (5′ to 3′) #
EV71-3F	953-972	CCA TCY GCY GAR GCD TGT GG
EV71-3R	1787-1806	GGR GTG GGR TGR AAR TTT GG

* Forward primers are suffixed with "F" and reverse primers are suffixed with "R"

† Nucleotide position is based on HEV71-C4

Y=C or T, R=A or G, D=A or T or G

(c) 5′ rapid amplification of cDNA ends (5′ RACE)

First-strand cDNA was generated as described in section 2.3.10, with 20 pmol of appropriate BR primer (Table 2.7) and was purified using a PCR extraction kit (Qiagen). Purifed first-strand cDNA was then subjected to terminal deoxynucleotidyl transferase (TdT) poly (C) tailing reaction. Reactions were carried out in 0.2 mL tubes in a reaction volume of 20 µL. A sample of 10 µL of purified cDNA, 250 µM of dCTP and 1× concentration of enzyme buffer as supplied by manufacturer were mixed and heated at 94°C for 2 min. 1 U of TdT (Promega) was then added to the mixture and further incubated at 37°C for 20 min before inactivation of enzyme at 70°C for 10 min. dc-tailed cDNA was then used for PCR amplification using PCR supermix (Invitrogen) with Anchor primer and appropriate AR primer (Table 2.7). Reactions were carried out in 0.2 mL tubes in a reaction volume of 25 µL. PCR reactions contained 10 pmol of Anchor primer, 10 pmol of appropriate AR primer, 21 µL of PCR supermix and 2 µL of dC-tailed cDNA. Reactions were incubated for 2 min at 94°C, then 40 cycles of 94°C for 30 s, 55°C for 30 s and 72°C for 45 s and finally incubated at 72°C for 3 min. Gel-purified PCR products were then sequenced with the appropriate AR primer as described in section 2.3.12.

2.3.12. DNA sequencing

The nucleotide sequences of the PCR products or cloned DNA fragments were determined by automated DNA sequencing using Capillary Electrophoresis sequencing technology. Sequencing was performed by Australian Genome Research Facility Ltd. (AGRF) of Westmead Millenium Institute, Sydney, New South Wales, Australia. Analysis of DNA chromatograms were performed using

the program Chromas™ version 2.33 (Technelysium Pty. Ltd. Australia) and Sequencher version 4.7 (Gene Codes Corporation).

Table 2.7 5′ RACE primers used to sequence the 5′ terminus sequences of all HEV71

Primer name*	Nucleotide position #	Sequence (5′ to 3′) †
	Universal Forward Primer	
Anchor primer		GGC CAC GCG TCG ACT AGT ACG GGI IGG GII GGG IIG
	HEV71-B5	
B5-AR	416-439	GCT CAA TAG ACT CTT CGC ACC ATG
EV71-BR	617-638	GGC CAA TCC AAT AGC TAT ATG G
	HEV71-C2	
C2-AR	425-448	GGA CTA CCA GCT AGC TCA ATA GGC
EV71-BR	615-636	GGC CAA TCC AAT AGC TAT ATG G
	HEV71-C4	
C4-AR	411-434	GCT CAG TAG ACT CTT CGC ACC ATG
EV71-BR	613-634	GGC CAA TCC AAT AGC TAT ATG G

* Reverse primers are suffixed with "R"

Nucleotide position is based on their respective viruses

† I: Inositol

2.3.13. Construction of full-length cDNA clones of HEV71

The strategy for construction of all full-length infectious cDNA clones of HEV71 in this study was similar. Generally, first-strand cDNA fragments covering the full-length genome of HEV71 virus were synthesised from genomic viral RNA with SuperScript™ III reverse transcriptase (Invitrogen), as described in section 2.3.10. cDNA fragments were then used for PCR amplifications to amplify the 5′ terminal and 3′ terminal fragments of the viral genome. The amplified products were then cloned into plasmid vectors to construct sub-genomic 5′ and 3′ half clones. With the use of unique restriction sites, the 5′ terminal and 3′ terminal fragments from two sub-genomic clones were assembled into a genome-length cDNA clone. Construction procedures of each full-length cDNA clone are described in the following section. A list of HEV71 full-length clones constructed during this study is provided in Table 2.8. The nucleotide numbering in sub-genomic or full-length clones in this study is presented in the form of X^{Y}. X represents restriction enzyme sites and superscript Y represents the nucleotide position in the viral genome. For example, *Eco*RI^{1400} corresponds to the *Eco*RI restriction enzyme digestion site at nucleotide position 1400 of the viral genome.

2.3.13.1 Construction of a full-length cDNA clone of HEV71-B5

The steps involved in the construction of sub-genomic and full-length cDNA clones of HEV71-B5 in pMC18 are shown in Figure 2.1.

(a) Construction of the 5′ half clone, pMC18/5′-B5

A 5′ terminal fragment of the viral genome, spanning nucleotide 1-2874, was generated by PCR as described in section 2.3.11. Forward primer, C2-EV71-5′-F

and reverse primer, B5-EV71-5′-R, were used in the PCR reaction (Table 2.9). A *Sal*I restriction site, T7 RNA polymerase promoter and two additional G residues were incorporated into the forward primer upstream of the viral genome, and a *Not*I site was added into the reverse primer downstream of nucleotide 2874. The PCR product was digested with *Sal*I and *Not*I and the fragment cloned into pMC18 at the *Sal*I and *Not*I sites. The resultant clone, pMC/5′-B5, is 8234 nucleotides in length.

(b) Construction of the 3′ half clone, pMC18/3′-B5

A 3′ terminus, covering nucleotides 2836-7412 of the viral genome and a 25 nucleotide poly (A) tail was amplified using primers B5-EV71-3′-F and C4-EV71-3′-R, with *Sal*I and *Not*I sites incorporated into the forward and reverse primers, respectively (Table 2.9). PCR conditions were as described in section 2.3.11. The PCR product was digested with *Sal*I and *Not*I, and the excised fragment was then cloned into *Sal*I- and *Not*I-predigested pMC18. The resultant clone, pMC/3′-B5, is 9943 nucleotides in length.

(c) Construction of the full-length clone, pHEV71-B5

The full length cDNA clone, pHEV71-B5 was constructed by excising a *Eco*RI^{2842} – *Not*I fragment from clone pMC18/3′-B5 and then re-cloning it into the *Eco*RI^{2842} – *Not*I sites of cloned pMC18/5′-B5. The resultant clone was 12,797 nucleotides in length and contained a T7 RNA polymerase promoter and two additional G residues upstream of the viral cDNA.

2.3.13.2 Construction of a full-length cDNA clone of HEV71-C2

The steps involved in the construction of sub-genomic and full-length cDNA clones of HEV71-C2 in pMC18 are shown in Figure 2.2.

(a) Construction of the 5′ half clone, pMC18/5′-C2

A 5′ terminal fragment of the viral genome, spanning nucleotide 1-4580, was generated by PCR as described in section 2.3.11. The forward primer C2-EV71-5′-F and reverse primer C2-EV71-5′-R were used in the PCR reaction (Table 2.10). A *Sal*I restriction site, T7 RNA polymerase promoter and two additional G residues were incorporated into the forward primer upstream of the viral genome, and a *Not*I site was added into the reverse primer downstream of nucleotide 4580. The PCR product was digested with *Sal*I and *Not*I and the fragment re-cloned into pMC18 at the *Sal*I and *Not*I sites. The resultant clone, pMC/5′-C2, is 9940 nucleotides in length.

(b) Construction of the 3′ half clone, pMC18/3′-C2

A 3′ terminal fragment covering nucleotides 4521-7409 of the viral genome and a 25 nucleotide poly (A) tail was amplified using primers C2-EV71-3′-F and C4-EV71-3′-R, with *Sal*I and *Not*I sites incorporated into forward and reverse primers, respectively (Table 2.10). PCR conditions were as described in section 2.3.11. The PCR product was digested with *Sal*I and *Not*I, and the excised fragment was then re-cloned into *Sal*I- and *Not*I-predigested pMC18. The resultant clone, pMC/3′-C2, is 8261 nucleotides in length.

(c) Construction of the full-length clone, pHEV71-C2

The full length cDNA clone, pHEV71-C2 was constructed by excising *Acc*III^{4551} – *Not*I fragment from clone pMC18/3′-C2 and then re-cloning it into the *Acc*III^{4551} – *Not*I sites of cloned pMC18/5′-C2. The resultant clone was 12,800 nucleotides in length and contained a T7 RNA polymerase promoter and two additional G residues upstream of the viral cDNA.

2.3.13.3 Construction of a full-length cDNA clone of HEV71-C4

The steps involved in the construction of sub-genomic and full-length cDNA clones of HEV71-C4 in pMC18 are shown in Figure 2.3.

(a) Construction of the 5′ half clone, pMC18/5′-C4

A 5′ terminal fragment of the viral genome, spanning nucleotide 1-4224, was generated by PCR as described in section 2.3.11. The forward primer C2-EV71-5′-F and reverse primer C4-EV71-5′-R were used in the PCR reaction (Table 2.11). A *Sal*I restriction site, T7 RNA polymerase promoter and two additional G residues were incorporated into the forward primer upstream of the viral genome, and a *Not*I site was added into the reverse primer downstream of nucleotide 4224. The PCR product was digested with *Sal*I and *Not*I and the fragment re-cloned into pMC18 at the *Sal*I and *Not*I sites. The resultant clone, pMC/5′-C4, is 9583 nucleotides in length.

(b) Construction of the 3′ half clone, pMC/3′-C4

A 3′ terminal fragment covering nucleotides 4074-7405 of the viral genome and a 25 nucleotide poly (A) tail was amplified using primers C4-EV71-3′-F and C4-

EV71-3′-R, with *Sal*I and *Not*I sites incorporated into the forward and reverse primers, respectively (Table 2.11). PCR conditions were as described in section 2.3.11. The PCR product was digested with *Sal*I and *Not*I, and the excised fragment was re-cloned into *Sal*I- and *Not*I-predigested pMC18. The resultant clone, pMC/3′-C4, is 8698 nucleotides in length.

(c) Construction of the full-length clone, pHEV71-C4

The full length cDNA clone, pHEV71-C2 was constructed by excising *EcoR*I^{4208} – *Not*I fragment from clone pMC18/3′-C4 and then re-cloning it into the *EcoR*I^{4208} – *Not*I sites of cloned pMC18/5′-C4. The resultant clone was 12,790 nucleotides in length and contained a T7 RNA polymerase promoter and two additional G residues upstream of the viral cDNA.

Table 2.8 Full length cDNA clones of HEV71 strains HEV71-B5, HEV71-C2 and HEV71-C4

Plasmid clone	Derived virus	Description
pHEV71-B5	Not obtained	Contains a T7 RNA polymerase promoter, GG residues, viral cDNA of the HEV71-B5 genome and 25 poly (A); cloned into plasmid vector pMC18
pHEV71-C2	C2-CDV	Contains a T7 RNA polymerase promoter, GG residues, viral cDNA of the HEV71-C2 genome and 25 poly (A); cloned into plasmid vector pMC18
pHEV71-C4	C4-CDV	a T7 RNA polymerase promoter, GG residues, viral cDNA of the HEV71-C4 genome and 25 poly (A); cloned into plasmid vector pMC18

Table 2.9 Primers used for the construction of full-length cDNA clones of HEV71-B5

Primer name*	Nucleotide sequence 5′ to 3′	Special features
C2-EV71-5′-F	AAGCTTGCATGCGTCGACTAATACGACTCACTATAGGTTAAAACAGCCTGTGG	Contains a *Sal*I site (GTCGAC), a T7 RNA polymerase promoter and two additional G residues immediately upstream of the 5′ terminus of the viral sequence
B5-EV71-5′-R	GGATCCGCGGCCGCACCAGTAGGAGTGCA	Contains a *Not*I site (GCGGCCGC) adjacent to the viral sequence
B5-EV71-3′-F	AAGCTTGCATGCGTCGACGATGCGGAATTCACTTTCGT	Contains a *Sal*I site (GTCGAC) adjacent to the viral sequence
C4-EV71-3′-R	GGATCCGCGGCCGCTTTTTTTTTTTTTTTTTTTTTTTTTTTGCTATTCTGG	Contains a *Not*I site (GCGGCCGC), 25 poly (A) at the 3′ terminus of the viral sequence

* Forward primers are suffixed with “F” and reverse primers are suffixed with “R”

Table 2.10 Primers used for the construction of full-length cDNA clones of HEV71-C2

Primer name*	Nucleotide sequence 5′ to 3′	Special features
C2-EV71-5′-F	AAGCTTGCATGCGTCGACTAATACGACTCACTATAGGTTAAAACAGCCTGTGG	Contains a *Sal*I site (GTCGAC), a T7 RNA polymerase promoter and two additional G residues immediately upstream of the 5′ terminus of the viral sequence
C2-EV71-5′-R	GGATCCGCGGCCGCTTGTATCCGTCAAAGTGGTC	Contains a *Not*I site (GCGGCCGC) adjacent to the viral sequence
C2-EV71-3′-F	AAGCTTGCATGCGTCGACCAAGTACCGCTCCAGTGTGTATTCCTT	Contains a *Sal*I site (GTCGAC) adjacent to the viral sequence
C4-EV71-3′-R	GGATCCGCGGCCGCTTTTTTTTTTTTTTTTTTTTTTTTTTGCTATTCTGG	Contains a *Not*I site (GCGGCCGC), 25 poly (A) at the 3′ terminus of the viral sequence

* Forward primers are suffixed with “F” and reverse primers are suffixed with “R”

Table 2.11 Primers used for the construction of full-length cDNA clones of HEV71-C4

Primer name*	Nucleotide sequence 5′ to 3′	Special features
C2-EV71-5′-F	AAGCTTGCATGCGTCGACTAATACGACTCACTATAGGTTAAAACAGCCTGTGG	Contains a *Sal*I site (GTCGAC), a T7 RNA polymerase promoter two additional G residues immediately upstream of the 5′ terminus of the viral sequence
C4-EV71-5′-R	GGATCCGCGGCCGCAGTTATTTAGGAATTCAACC	Contains a *Not*I site (GCGGCCGC) adjacent to the viral sequence
C4-EV71-3′-F	AAGCTTGCATGCGTCGACAAAGTGCTTCCTGGCTCAAGAAGTTC	Contains a *Sal*I site (GTCGAC) adjacent to the viral sequence
C4-EV71-3′-R	GGATCCGCGGCCGCTTTTTTTTTTTTTTTTTTTTTTTTTTTGCTATTCTGG	Contains a *Not*I site (GCGGCCGC), 25 poly (A) at the 3′ terminus of the viral sequence

* Forward primers are suffixed with “F” and reverse primers are suffixed with “R”

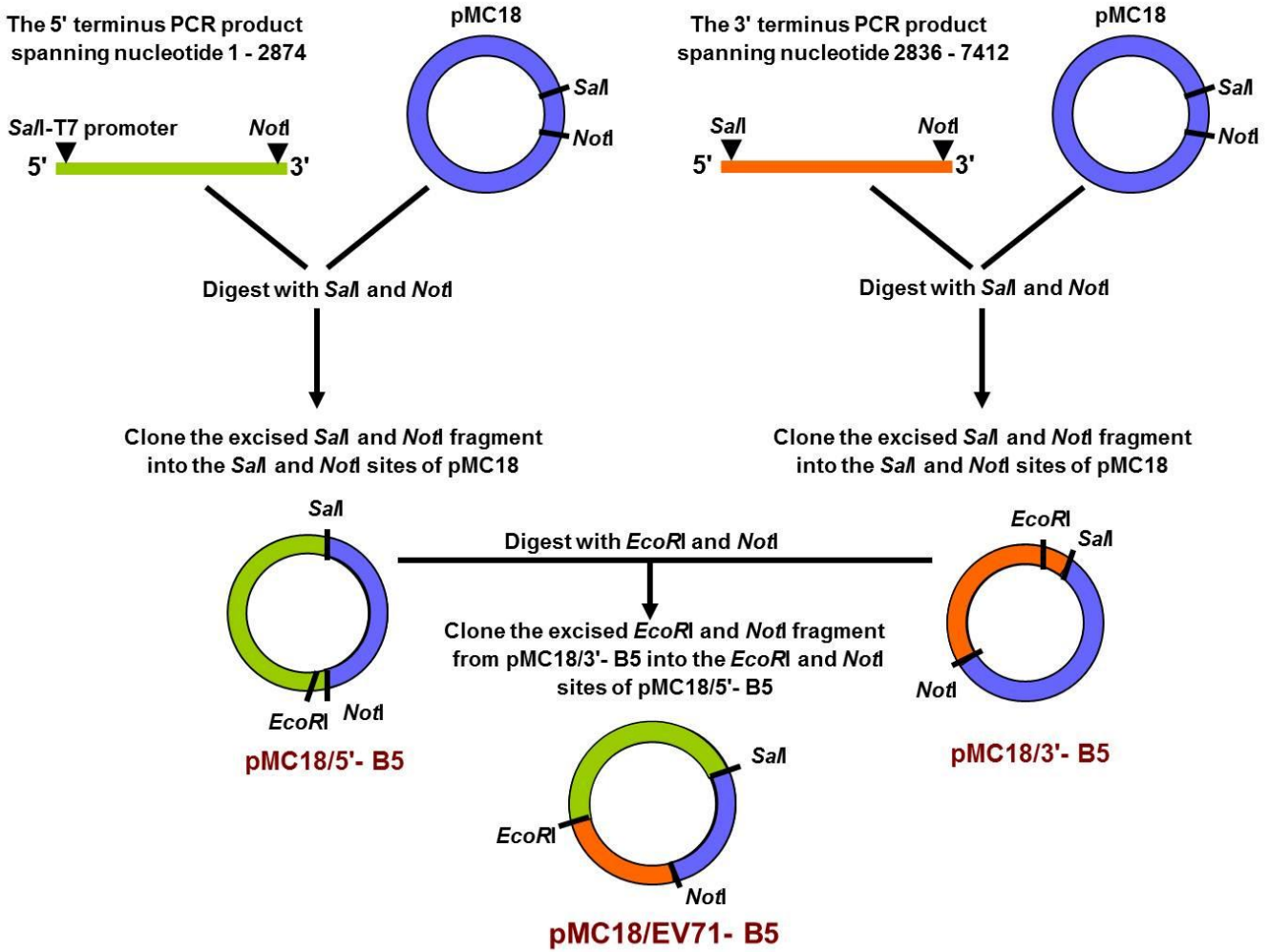

Figure 2.1 The schematic diagram of the construction of the sub-genomic and full length cDNA clones of HEV71-B5 in pMC18.

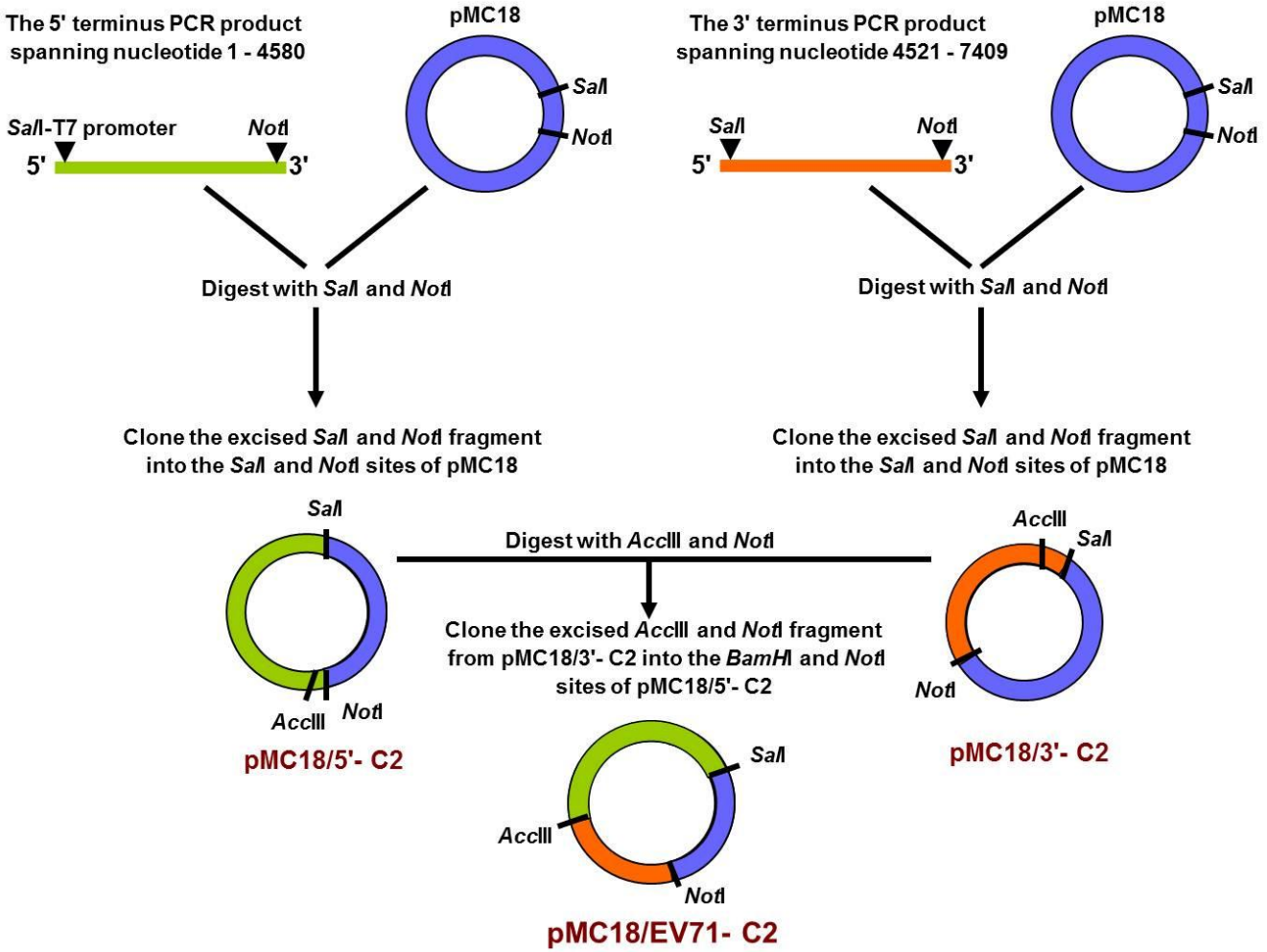

Figure 2.2 The schematic diagram of the construction of the sub-genomic and full length cDNA clones of HEV71-C2 in pMC18.

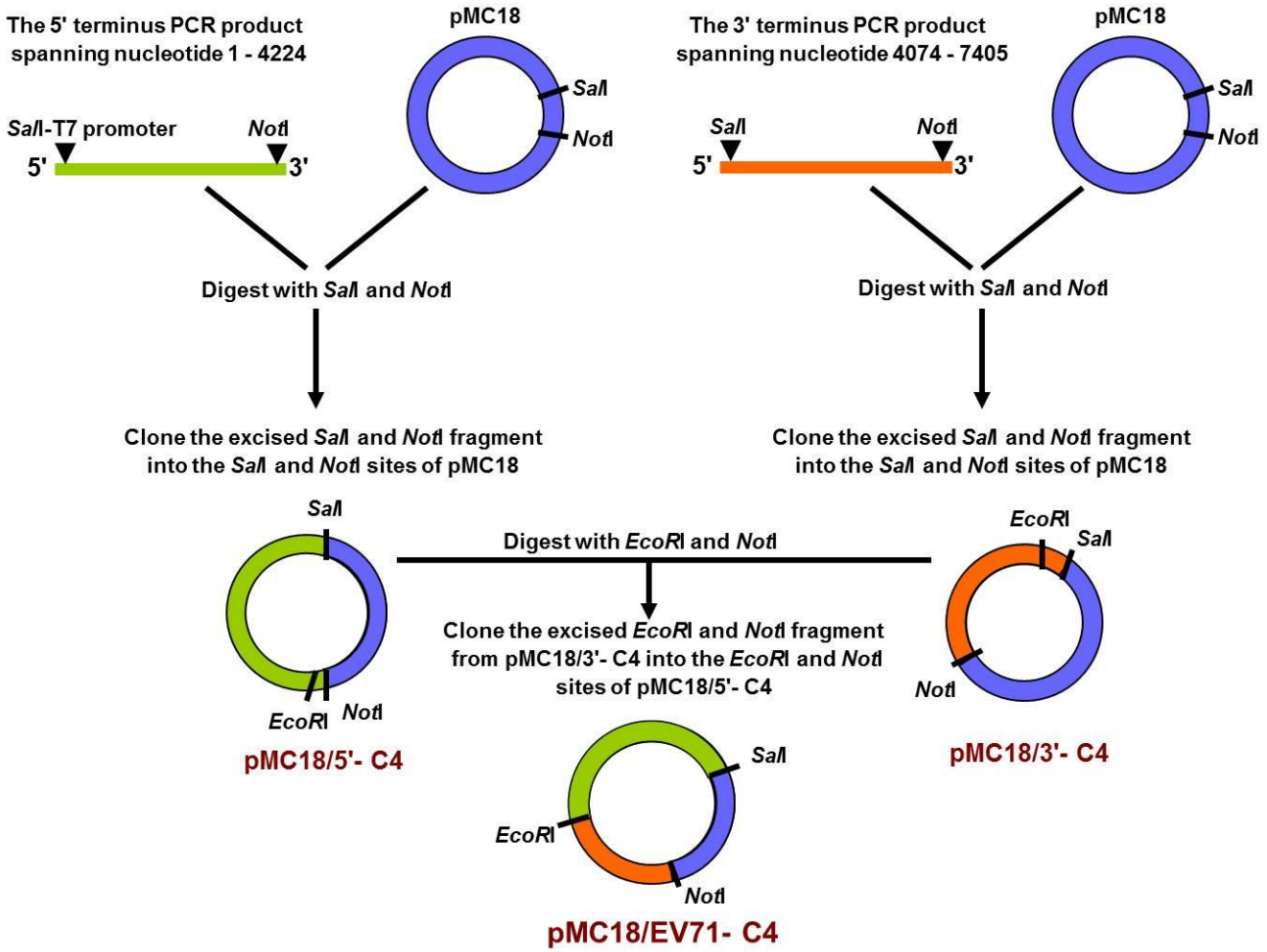

Figure 2.3 The schematic diagram of the construction of the sub-genomic and full length cDNA clones of HEV71-C4 in pMC18.

2.3.14. Construction of HEV71 variants by site-directed mutagenesis

In order to identify the molecular determinants that affect the phenotypic differences between the HEV71 strains selected in these studies, full-length infectious cDNA clones of HEV71 containing the mutations of interest were constructed by site-directed mutagenesis. The QuikChange Lightning Site-Directed Mutagenesis kit (Stratagene) was used to generate point mutations according to the manufacturer's instructions. The collection of HEV71 variants generated in this manner are shown in Table 2.12. All mutagenic primers were designed using the QuikChange Primer Design Program available on the Agilent Technologies website (https://www.genomics.agilent.com/). Primers used for construction of HEV71-C4 containing VP2 and VP1 mutations are listed in Table 2.13 and 2.14, respectively. Primers used for construction of CHO-26M containing VP1 mutations are listed in Table 2.15. All mutagenesis reactions were performed without sub-cloning and a single clone of each mutant was selected and purified plasmid DNA prepared for sequence analysis. VP2 and/or VP1 gene RT-PCR and nucleotide sequencing was undertaken to ensure that the site-specific changes were present in the mutated plasmid clones.

Table 2.12 List of HEV71 variants constructed by site-directed mutagenesis

Plasmid clone	Parental clone	Derived virus	Description
C4-VP2I	HEV71-C4	C4-VP2I-CDV	Contains viral cDNA of the C4 genome with a mutation at VP2-K^{149}→I
C4-VP2M	HEV71-C4	C4-VP2M-CDV	Contains viral cDNA of the C4 genome with a mutation at VP2-K^{149}→M
C4-VP2I-VP1E	C4-VP2I	C4-VP2I-VP1E-CDV	Contains viral cDNA of the C4 genome with mutations at VP2-K^{149}→I and VP1-Q^{145}→E
C4-VP2I-VP1G	C4-VP2I	C4-VP2I-VP1G-CDV	Contains viral cDNA of the C4 genome with mutations at VP2-K^{149}→I and VP1-Q^{145}→G
CHO-26M-VP1-S241L	CHO-26M	CHO-26M-VP1-S241L-CDV	Contains viral cDNA of the 26M genome with mutations at VP2-K^{149}→I and VP1-S^{241}→L
CHO-26M-VP1-K244E	CHO-26M	CHO-26M-VP1-K244E-CDV	Contains viral cDNA of the 26M genome with mutations at VP2-K^{149}→I and VP1-K^{244}→E
CHO-26M-VP1	CHO-26M	CHO-26M-VP1-CDV	Contains viral cDNA of the 26M genome with mutations at VP2-K149→I, VP1-S^{241}→L and VP1-K^{244}→E

Table 2.13 Primers used for the construction of full-length cDNA clones of HEV71-C4 containing mutations in the VP2 coding region

Primer name*	Nucleotide position#	Nucleotide sequence 5′ to 3′
C4-VP2-K149I-F	1380-1411	GTCACCCCCCTTACATACAGACTCAACCCGGC
C4-VP2-K149I-R	1380-1411	GCCGGGTTGAGTCTGTATGTAAGGGGGGTGAC
C4-VP2-K149M-F	1377-1407	ACAGTCACCCCCCTTACATGCAGACTCAACC
C4-VP2-K149M-R	1377-1407	GGTTGAGTCTGCATGTAAGGGGGGTGACTGT

* Forward primers are suffixed with "F" and reverse primers are suffixed with "R"

Nucleotide position is based on HEV71-C4

Table 2.14 Primers used for the construction of full-length cDNA clones of HEV71-C4 containing mutations in the VP1 coding region

Primer name*	Nucleotide position#	Nucleotide sequence 5′ to 3′
C4-VP1-Q145E-F	2855-2887	TGCACACCCACCGGAGAGGTTGTCCCACAGTTG
C4-VP1-Q145E-R	2855-2887	CAACTGTGGGACAACCTCTCCGGTGGGTGTGCA
C4-VP1-Q145G-F	2854-2884	GTGCACACCCACCGGAGGAGTTGTCCCACAG
C4-VP1-Q145G-R	2854-2884	CTGTGGGACAACTCCTCCGGTGGGTGTGCAC

* Forward primers are suffixed with "F" and reverse primers are suffixed with "R"

Nucleotide position is based on HEV71-C4

Table 2.15 Primers used for the construction of full-length cDNA clones of CHO-26M containing mutations in the VP1 coding region

Primer name*	Nucleotide position#	Nucleotide sequence 5′ to 3′
CHO-26M-S241L-F	3147-3181	GCGAAATGTGGGGTCATTAAAGTCCAAGTACCCTC
CHO-26M-S241L-R	3147-3181	GAGGGTACTTGGACTTTAATGACCCCACATTTCGC
CHO-26M-K244E-F	3156-3188	GGGGTCATCAAAGTCCGAGTACCCTCTGGTTGT
CHO-26M-K244E-R	3156-3188	ACAACCAGAGGGTACTCGGACTTTGATGACCCC
CHO-26M-VP1-F	3156-3188	GGGGTCATTAAAGTCCGAGTACCCTCTGGTTGT
CHO-26M-VP1-R	3156-3188	ACAACCAGAGGGTACTCGGACTTTAATGACCCC

* Forward primers are suffixed with "F" and reverse primers are suffixed with "R"

Nucleotide position is based on HEV71-26M

2.3.15. Transfection

Transfection of plasmid full-length cDNA clones and variants was performed on COS-7 cells using Lipofectamine™ 2000 (Invitrogen) according to the manufacturer's protocol. Briefly, COS-7 cells were seeded into 12-well tissue culture trays (Costar) at a density of 3×10^5 cells/well. Cells were grown in DMEM supplemented with 5% FBS and 2 mM L-glutamine. After incubation for 18-24 h, cells were washed once with PBS and replaced with serum-free medium, OptiMEM (Invitrogen), prior to transfection. The lipid-nucleic acid complex containing 1.6 μg of each full-length cDNA construct, 1.6 μg pCMV-T7Pol expressing the T7 RNA polymerase and 4 μL of Lipofectamine™ 2000 was added to the cells and incubated for 4 h. The transfection medium was then removed and replaced with DMEM supplemented with 2% FBS and 2 mM L-glutamine and the cells incubated for a further 48 h. Transfected cells were then subjected to three cycles of freezing-thawing and the virus supernatant clarified by centrifugation at 1,000×g for 10 min at 4°C. Clone-derived virus stocks are designated by the suffix "CDV" to distinguish them from their respective parental viruses. The recovered CDVs were then passaged in specific cell lines to increase their titres for subsequent assays or were stored at -80 °C until required.

2.4. Mouse experiments

Specific-pathogen-free pregnant BALB/c mice were obtained from the Animal Resources Centre, Perth, Australia. Mice were housed in filter-topped cages on a deep litter of sawdust and were provided with food and water *ad libitum*. All mouse studies were approved by the University of Sydney Animal Ethics Committee.

2.4.1. Humane endpoint (HD_{50}) determination

In order to minimise distress, 50% humane endpoints (HD_{50}) were used instead of 50% lethal endpoints (LD_{50}). HD_{50} values were calculated from the time of onset of lethal infection rather than waiting until death ensued. HD_{50} assays have been found to be almost identical to LD_{50} virulence assays (Wright & Phillpotts, 1998). Groups of six 5-day-old BALB/c mice were infected by intraperitoneal (i.p.) inoculation with 50 μL of ten-fold serial dilutions of virus or infectious CDV populations to be tested and observed for 14 days for clinical signs of HEV71 infection. Mice born on the same day were randomly divided between mothers. Control mice were inoculated with PBS diluent. Clinical signs were graded according to the scale shown in Table 2.16. Mice that developed grade 3 paralysis (inability to move all limbs; no movement) were euthanased. The HD_{50} value in 5-day-old BALB/c mice was calculated by the method of Reed & Muench (1938).

Table 2.16 Clinical grading scale of the severity of HEV71 infection in mice

Grade	Clinical signs
0	Normal
1	Limb weakness; some movement possible
2	Paralysis of affected limbs; minimal movement
3	Quadriplegia (inability to move all limbs; no movement)
Other signs	Failure to thrive, lethargy, stomach empty of milk, atonic bladder, hunched posture, ruffled fur, head tilt

Adapted from published guidelines for animal monitoring (Davis, 1999/2000; Foltz & Ullman-Cullere, 1999)

2.4.2. Mouse virulence assay

Specific groups of 5-day-old BALB/c mice were infected via the i.p. route at a dose of approximately $10^4 \times TCID_{50}$ of each infectious CDV populations to be tested. Control mice were inoculated with PBS. Mice were observed twice daily for 14 days p.i. and the percentage survival calculated for each group; mice showing grade 3 paralysis or higher were euthanased. All animals were sacrificed by CO_2 narcosis at the end of the experiment.

2.4.3. Tissue distribution and viral load determination

Groups of twelve 5-day-old BALB/c mice were infected i.p. at a dose of $10^2 \times HD_{50}$. At one, three and five days p.i. or once grade 3 paralysis was observed, three mice from each group were anaesthetised by i.p. injection with a mixture of ketamine and xylazine (Troy Laboratories) in PBS at 5 μL per gram body weight. The thoracic cavity was opened to expose the heart and whole blood collected by intracardiac puncture. After perfusion with PBS, spleen, liver, heart, skeletal muscle and brain were collected, weighed, snap-frozen in liquid nitrogen and stored at -80°C. Tissues were homogenised manually with a Dounce homogeniser, prepared as 10% (w/v) suspensions in Hank's balanced salt solution (HBSS) and clarified twice by centrifugation at 1,000×g for 10 min at 4°C. Virus titres in each tissue homogenate were determined by $TCID_{50}$ assay on Vero cells. Viral titres in blood were determined as $TCID_{50}$ mL^{-1}. Viral titres in tissue homogenates were determined as $TCID_{50}$ g^{-1}.

2.4.4. Histological studies

Tissues for histological analysis (skeletal muscle, spinal cord and brain) were

collected from three infected mice at clinical grade 3 or higher and were fixed in 10% buffered formalin overnight, dehydrated in 70% ethanol and embedded in paraffin. For each tissue specimen, several sections (4-5 μm) were cut in a microtome, mounted on glass slides and stained with haematoxylin and eosin (Fronine).

2.5. Bioinformatics

2.5.1. Sequence analysis

Sequence data for cloning purposes was manipulated using Clone Manager 5.2/Align Plus 4.0 software (SciEd Central). Multiple sequence alignments were performed using Clustal X (2.1). Pairwise alignments were performed using the pairwise sequence alignment tool available online at http://www.ebi.ac.uk/Tools/psa/. Full-length sequence assembly was performed using Sequencher version 4.7 (Gene Codes Corporation). Homology searches were conducted using the BLAST server at the National Center for Biotechnology Information (National Library of Medicine, Bethesda, MD, USA). Multiple sequence alignments of the cloverleaf and IRES elements of HEV71 were edited in Jalview web server (http://www.jalview.org/). All sequencing chromatograms were viewed using Chromas™ version 2.33 (Technelysium Pty Ltd).

2.5.2. Phylogenetic analysis

Phylogenetic analyses were conducted in MEGA5 software (Tamura *et al.*, 2011). The evolutionary history was inferred by using the Maximum Likelihood method based on the Kimura 2-parameter model. Bootstrap verification of the resulting

phylogenetic tree was performed by analysis of 1,000 bootstrapped pseudo-replicates.

2.5.3. RNA structure prediction

All secondary structures were predicted using the RNA folding form in the MFOLD web server (http://mfold.rna.albany.edu/) (Zuker, 2003). The parameters used are as follows; folding temperature at 37°C, linear RNA sequence, percent sub-optimality number of 5, upper bound on the number of computed foldings of 50, default window parameter, maximum interior/bulge loop size of 30, maximum asymmetry of an interior/bulge loop of 30 and no limit to the maximum distance between paired bases.

2.5.4. Protein homology modelling

The complete amino acid sequences of the capsid protein VP2 and VP1 genes were individually submitted to an online fully automated protein homology modeling program, SWISS-MODEL (http://swissmodel.expasy.org/) and the predicted three-dimensional structure of each of the proteins were viewed in Deepview/Swiss-Pdb Viewer v4.0.4 (http://www.expasy.org/spdbv/).

2.6. Statistical analysis

Kaplan-Meier survival plots and statistical analyses were performed using GraphPad Prism version 5.04 Software, San Diego California USA, www.graphpad.com. A p value of <0.05 was considered statistically significant.

3. CHAPTER THREE

SEQUENCE ANALYSIS AND CONSTRUCTION OF GENOME LENGTH INFECTIOUS cDNA CLONES OF HEV71 GENOGROUPS B5, C2 AND C4

3.1. Introduction

The ability to produce cDNA clone-derived virus is a powerful tool in studying the molecular determinants of virulence and other phenotypic properties of RNA viruses. Such clones facilitate genetic manipulation of RNA viral genomes and thus the role of specific viral genetic elements in viral replication, transcription, translation or virulence can be investigated. The methods of producing genome-length cDNA clones of RNA viruses have improved greatly since the first animal virus infectious clone was constructed by Racaniello & Baltimore (1981). Nonetheless, construction of infectious cDNA clones is still considered technically difficult and laborious. In general, the first step is reverse transcription of the viral RNA into a single-stranded cDNA. A double-stranded cDNA copy of the viral genome is generated by PCR amplification using a single-stranded cDNA as a template, and the double-stranded copy cloned into a plasmid vector followed by transformation into a bacterial host to multiply. The full-length cDNA clone is then *in vitro* transcribed into RNA, and the RNA transcript is transfected into cells to rescue clone-derived virus. Alternatively, the plasmid cDNA clone is transfected into cells directly.

HEV71 has emerged as an important cause of viral encephalitis in Southeast Asia over the past 15 years (Solomon *et al.*, 2010). A pattern of increased epidemic activity and endemic circulation of HEV71 has been observed in the region since

1997 and is associated with the regular emergence of new genetic lineages of HEV71. However, the reason for this increase in HEV71 circulation remains unknown. In order to develop effective vaccines and control strategies, it is essential to understand the biology of this virus. The aim of the work described in this chapter was to sequence the complete genome of three selected HEV71 strains from outbreaks of HFMD. These three HEV71 strains were fully sequenced and their genomes analysed so that each individual genomic sequence could be used to construct infectious cDNA clones. The construction and characterisation of these infectious cDNA clones is also reported in this chapter.

3.2. Result

3.2.1. Complete genome sequencing of HEV71 strains

In this study, we performed complete genome sequencing of several HEV71 clinical isolates: HEV71 strains BRU-2006-35334; 0964-SYD-98; and 540V-VNM-05. These strains were isolated from patients with HFMD in Brunei in 2006 (AbuBakar *et al.*, 1999), Sydney in 1998 (Sanders *et al.*, 2006) and southern Vietnam in 2005 (Tu *et al.*, 2007), respectively. Only the VP1 gene of these strains had previously been sequenced. Therefore the complete genomic sequence of these viruses were determined and analysed.

The clinical isolates were initially plaque purified and propagated in RD cells up to at least five passages for amplification and sequencing. Up to a total of 15 synthetic oligonucleotide primer pairs were designed to amplify overlapping fragments (sizes between 500 and 800 bp) that span the whole genome of HEV71, based on the alignment of available full-length sequences of different

HEV71 genogroups. The 5′ end terminal sequences of all three viruses was obtained using the 5′ RACE method. BRU-2006-35334, 0964-SYD-98 and 540V-VNM-05 genomes were found to be 7412 nt, 7409 nt and 7405 nt, respectively excluding the poly (A) tail.

The 5′ UTR of BRU-2006-35334, 0964-SYD-98 and 540V-VNM-05 was found to be 747 nt, 744 nt and 742 nt respectively, followed by an ORF that encoded a viral polyprotein consisting of 2194 codons, between a start codon (ATG) located at position 748/745/743 nt and a stop codon (TAA/TAG) located at position 7327/7324/7322 nt of the genome. The virus strains had 3′ UTRs which were 83 nt, 83 nt and 81 nt, respectively. Table 3.1 summarises the specific data on the major gene regions of the three viruses. The complete genomic sequences of all the three viruses are included in Appendix A of this thesis and the annotated complete genome sequences of these viruses have been deposited to GenBank sequence database. The GenBank accession numbers for BRU-2006-35334, 0964-SYD-98 and 540V-VNM-05 are JN992282, JN992283 and JQ965759, respectively.

Table 3.1 Gene region of BRU-2006-35334, 0964-SYD-98 and 540V-VNM-05

Gene region		Nucleotide position		
		BRU-2006-35334	**0964-SYD-98**	**540V-VNM-05**
Genome		1-7412	1-7409	1-7405
5′ UTR		1-747	1-744	1-742
P1				
	VP4	748-954	745-951	743-949
	VP2	955-1716	952-1713	950-1711
	VP3	1717-2442	1714-2439	1712-2437
	VP1	2443-3333	2440-3330	2438-3328
P2				
	2A	3334-3783	3331-3780	3329-3778
	2B	3784-4080	3781-4077	3779-4075
	2C	4081-5067	4078-5064	4076-5062
P3				
	3A	5068-5325	5065-5322	5063-5320
	3B	5326-5391	5323-5388	5321-5386
	3C	5392-5940	5389-5937	5387-5935
	3D	5941-7326	5938-7323	5936-7321
3′ UTR		7330-7412	7327-7409	7325-7405

3.2.2. Sequence comparison to the HEV71 prototype strain

The HEV71 strain BRU-2006-35334, 0964-SYD-98 and 540V-VNM-05 complete genome sequences were then individually aligned with the prototype strain HEV71-BrCr (GenBank accession no. U22521) (Brown & Pallansch, 1995). All alignments were performed using a pairwise sequence alignment tool available online at http://www.ebi.ac.uk/Tools/psa/. The pairwise alignment was created using the Needle-Wunsch algorithm with a gap-penalty of 10.0 and an extend penalty of 0.5. The nucleotide and amino acid identities between the three HEV71 strains and the prototype EV71-BrCr are summarised in Table 3.2.

All the three HEV71 strains have different genome lengths compared to the prototype, with BRU-2006-35334 being four nucleotides longer, 0964-SYD-98 being one nucleotide longer and 540V-VNM-05 being three nucleotides longer, respectively. Comparison of the ORF revealed that all of the strains had a similar degree of nucleotide (80%) and amino acid (95%) sequence identity with the prototype. The viruses had the highest amino acid sequence identity with the prototype in the VP4 capsid protein (99-100%). Both BRU-2006-35334 and 540V-VNM-05 had the lowest amino acid identity in 3B (91% and 86% respectively) whereas 0964-SYD-98 had the lowest identity in 3C (89%).

Table 3.2 Percentage nucleotide and amino acid sequence identities of BRU-2006-35334, 0964-SYD-98 and 540V-VNM-05 compared to prototype HEV71-BrCr ^

Gene region	Length (nt)*	BRU- 2006-35334		096-SYD-98		540V-VNM-05	
		nt	aa	nt	aa	nt	aa
Genome	7412/7409/7405	80	95	80	95	80	95
5′ UTR	747/744/742	86	-	83	-	85	-
P1							
VP4	207	83	99	84	100	83	100
VP2	762	81	98	81	97	81	98
VP3	726	81	98	82	98	82	98
VP1	891	81	94	83	95	83	95
P2							
2A	450	76	95	78	95	79	96
2B	297	78	94	79	97	76	94
2C	987	78	95	80	96	78	97
P3							
3A	258	84	99	77	93	83	99
3B	66	71	91	70	91	70	86
3C	549	74	92	76	89	77	92
3D	1386	80	94	78	93	78	92
3′ UTR	83/83/81	92	-	92	-	77	-

^ Prototype HEV71-BrCr complete genome is 7408 nt in length, the 5′ UTR is 743 nt in length and the 3′ UTR is 83 nt in length (Brown & Pallansch, 1995)

* Where three figures are given, the first refers to BRU-2006-35334, the second to 0964-SYD-98 and the third to 540V-VNM-05

3.2.3. Evolutionary and genetic relationships to other HEV71 genogroups

In this study, 31 complete HEV71 genomes from all previously established genogroups were retrieved from GenBank (Table 3.3) and phylogenetic analysis was performed. All of the available complete genome sequences including BRU-2006-35334, 0964-SYD-98 and 540V-VNM-05 VP1 were then aligned using Clustal X (2.0) (Thompson *et al.*, 1997). Phylogenetic trees were constructed in MEGA5 software (Tamura *et al.*, 2011) and the evolutionary history was inferred by using the Maximum Likelihood method based on the Kimura 2-parameter model. Bootstrap verification of the resulting phylogenetic tree was performed by analysis of 1000 bootstrapped pseudo-replicates. CVA16 prototype strain CVA16-G10 (Poyry *et al.*, 1994) was included as an outgroup. The phylogenetic analysis of complete genome sequences of HEV71 clustered BRU-2006-35334, 0964-SYD-98 and 540V-VNM-05 into sub-genogroups B5, C2 and C4, respectively (Figure 3.1). Based on the phylogenetic analysis of VP1 nucleotide sequences, BRU-2006-35334, 0964-SYD-98 and 540V-VNM-05 also belong to sub-genogroups B5, C2 and C4 (AbuBakar *et al.*, 2009; Sanders *et al.*, 2006; Tu *et al.*, 2007), respectively, showing that the phylogenetic tree constructed with the VP1 gene generally reflected the genogroup assignments determined using the complete genome sequences.

Table 3.3 Virus isolates retrieved from the NCBI GenBank used in the construction of phylogenetic tree

Strains	Year	Country	GenBank accession no.
Human coxsackievirus A16 (CVA16-G10)	1951	Africa	U05876
BrCr	1970	USA	U22521
266-TW86	1986	Taiwan	FJ357384
244-TW86	1986	Taiwan	FJ357381
236-TW86	1986	Taiwan	FJ357379
7423-MS-87	1987	USA	ETU22522
MY104-9-SAR-97	1997	Malaysia	DQ341368
26M-AUS-4-99	1999	Australia	EU364841
N7008-TW99	1999	Taiwan	FJ357375
SB2864-SAR-00	2000	Malaysia	DQ341366
PP37-MAL-01	2001	Malaysia	DQ341365
5865-sin-98	1998	Singapore	AF316321
M0380-TW08	2008	Taiwan	FJ357385
NUH0083-SIN-08	2008	Singapore	FJ461781
SB12736-SAR-03	2003	Malaysia	DQ341362
N2838-TW03	2003	Taiwan	FJ357378
5511-SIN-00	2000	Singapore	DQ341364
1M-AUS-12-00	2000	Australia	DQ341361
S40221-SAR-00	2000	Malaysia	DQ341358
J115-MAL-01	2001	Malaysia	DQ341360
7F-AUS-6-99	1999	Australia	DQ341357
TW-2086-98	1998	Taiwan	AF119796
Tainan-6092-98	1998	Taiwan	AF304459
NCKU9822	1998	Taiwan	AF136379
03-KOR-00	2000	South Korea	DQ341356
06-KOR-00	2000	South Korea	DQ341355
Fuyang-0805	2008	China	FJ439769
GZ-08-01	2008	China	FJ360544
Anhui1-09-China	2009	China	GQ994988
BJ08	2008	China	FJ828519
N3340-TW-02	2002	Taiwan	EU131776
2007-07364	2007	Taiwan	EU527983

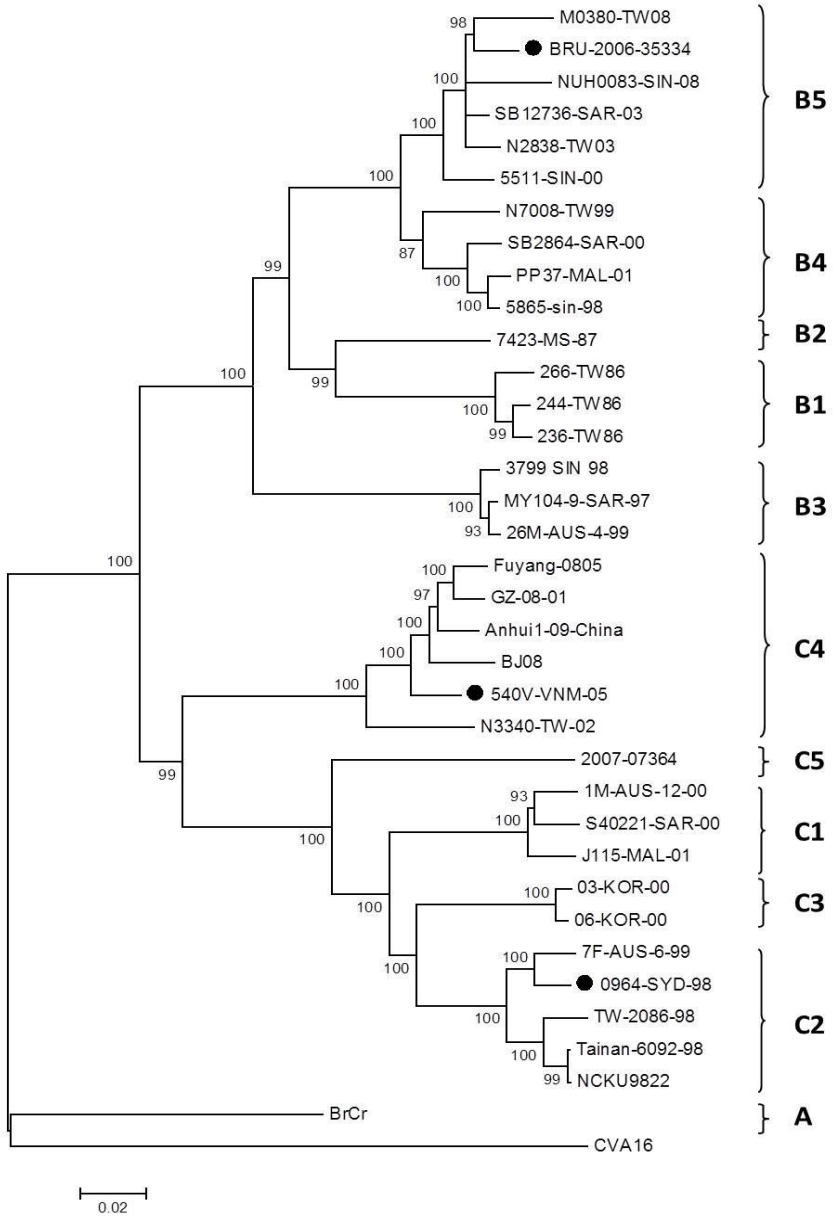

Figure 3.1 A phylogenetic tree showing the full-length sequence analysis of the three representative strains of HEV71 (shown as black circles) and other HEV71 strains and with CVA16 as the outgroup. Evolutionary analyses were conducted in MEGA5. The evolutionary history was inferred by using the Maximum Likelihood method based on the Kimura 2-parameter model. The percentage of replicate trees in which the associated taxa clustered together in the bootstrap test (1000 replicates) are shown next to the branches. The tree is drawn to scale, with branch lengths measured in the number of substitutions per site.

3.2.4. Viral RNA secondary structure analysis

Complex RNA secondary structures have been identified both in the non-coding and coding regions of the enterovirus genome (Goodfellow *et al.*, 2000; Pilipenko *et al.*, 1989; Pilipenko *et al.*, 1992a). The non-coding regions, 5′ and 3′ UTRs, contain RNA secondary structural motifs that are important for viral replication and/or translation (Andino *et al.*, 1993; Andino *et al.*, 1990; Pilipenko *et al.*, 1989; Pilipenko *et al.*, 1992a). An internal structural element, *cre* has been identified within the 2C coding region of several enteroviruses (Goodfellow *et al.*, 2000; Paul *et al.*, 2000; van Ooij *et al.*, 2006). Enteroviruses employ both stem-loops and bulges within these RNA secondary structures as contact points for cellular and viral protein binding (Andino *et al.*, 1993; Andino *et al.*, 1990; Paul *et al.*, 2000). The protein-RNA interactions on the secondary structures are required during RNA replication and translation processes. In this study, we have performed secondary structure analysis of our three selected HEV71 strains.

3.2.4.1 5′ UTR and 3′ UTR

The 5′ UTR of HEV71 is predicted to fold into six SLDs, where SLD I is a cloverleaf structure and SLD II through VI constitute IRES (Thompson & Sarnow, 2003). Computer predictions of 5′ UTR secondary structures of HEV71 strain BRU-2006-35334 (HEV71-B5), 0964-SYD-98 (HEV71-C2) and 540V-VNM-05 (HEV71-C4) were performed based on the cognate structures of poliovirus type 1 Mahoney strain (PV1M, GenBank accession no. V01149). The predicted secondary structures of PV1M have been validated by chemical and enzymatic probing for nucleotides involved in base pairing and mutagenesis analysis (Pilipenko *et al.*, 1992a). The 5′ UTR sequences of HEV71-B5, HEV71-C2, HEV71-

C4 and PV1M were aligned, and the nucleotide sequence and boundary of each domain of HEV71 5′ UTR identified (Figure 3.2). The structure of each SLD of HEV71 5′ UTR was then predicted using MFOLD web server (http://mfold.rna.albany.edu/) (Zuker, 2003). The predicted SLD structures of each virus are shown in Figure 3.3. The 5′ UTR SLD secondary structures of HEV71-B5, HEV71-C2 and HEV71-C4 were found to be generally similar to one another, except for the SLD II structure of HEV71-B5, which was predicted to differ from both HEV71-C2 and HEV71-C4 (Figure 3.3).

Similar to the 5′ UTR, the 3′ UTR also contains secondary structural elements. The enterovirus 3′ UTR folds into two common SLDs, SLD X and Y, as in PV1M (Pilipenko *et al.*, 1992b). The 3′ UTR of coxsackievirus B3 (CVB3) and other members of the HEV-B species possess an additional stem-loop structure, SLD Z (Merkle *et al.*, 2002). We aligned the 3′ UTR sequences of HEV71-B5, HEV71-C2, HEV71-C4, PV1M and CVB3 Nancy strain (GenBank accession no. JN048468), and secondary structure predicted using Mfold web server. The 3′ UTR secondary structure of HEV71-C4 was predicted to fold into stem-loop X and Y (Figure 3.4). Similar to the 3′ UTR of CVB3, the 3′ UTR secondary structures of HEV71-B5 and HEV71-C2 on the other hand were predicted to contain three stem-loops X, Y and Z (Figure 3.4). SLD Z RNA secondary structure was also previously reported in HEVA species viruses including CVA16 and HEV71 (Chan & AbuBakar, 2005; Kok *et al.*, 2012).

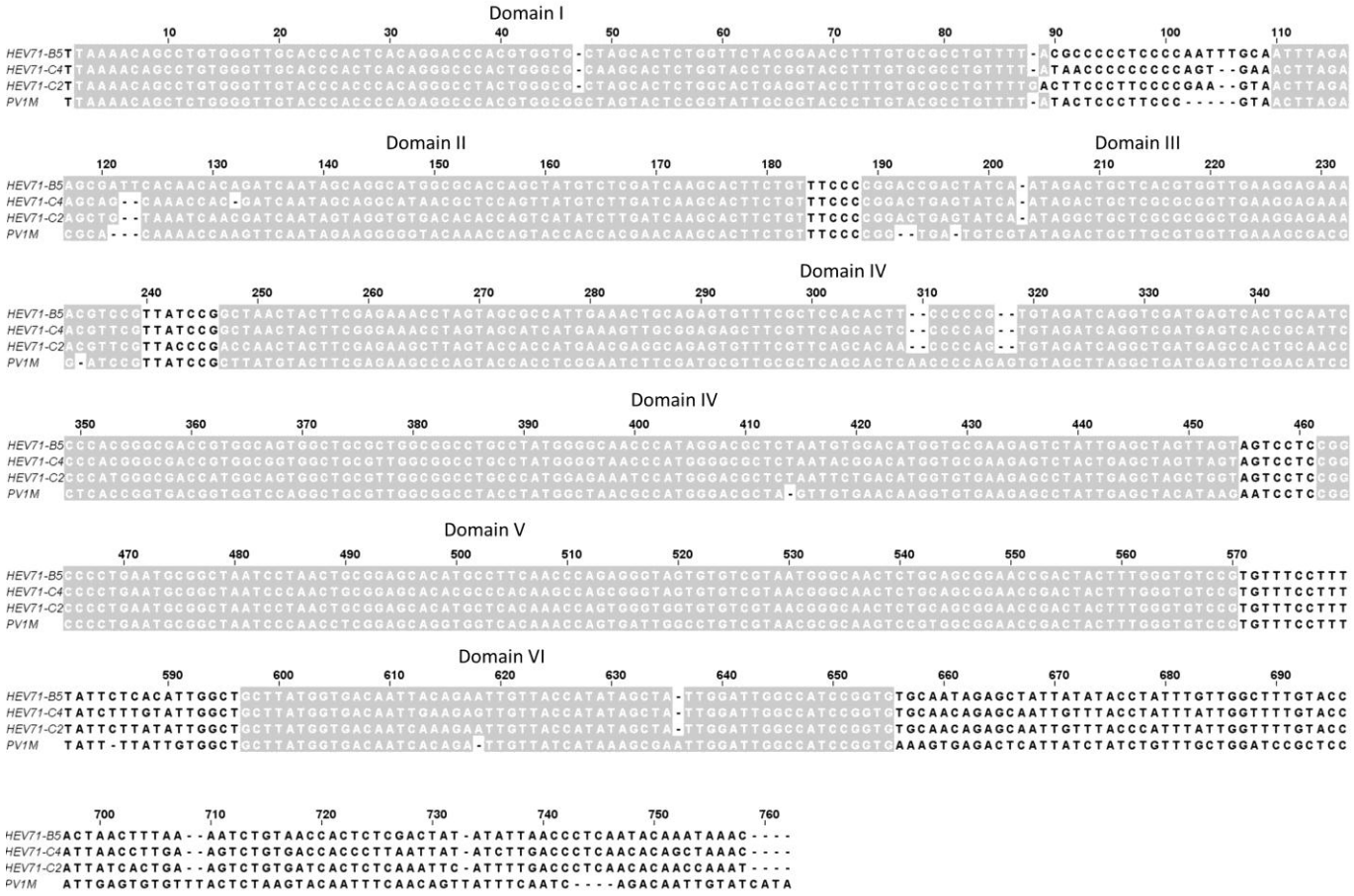

Figure 3.2 Sequence alignments of the cloverleaf and IRES elements of HEV71-B5, HEV71-C2, HEV71-C4 and PV1M based on known PV1M 5′ secondary structure sequences. Corresponding domains are indicated. Gap sequence is represented as (-).

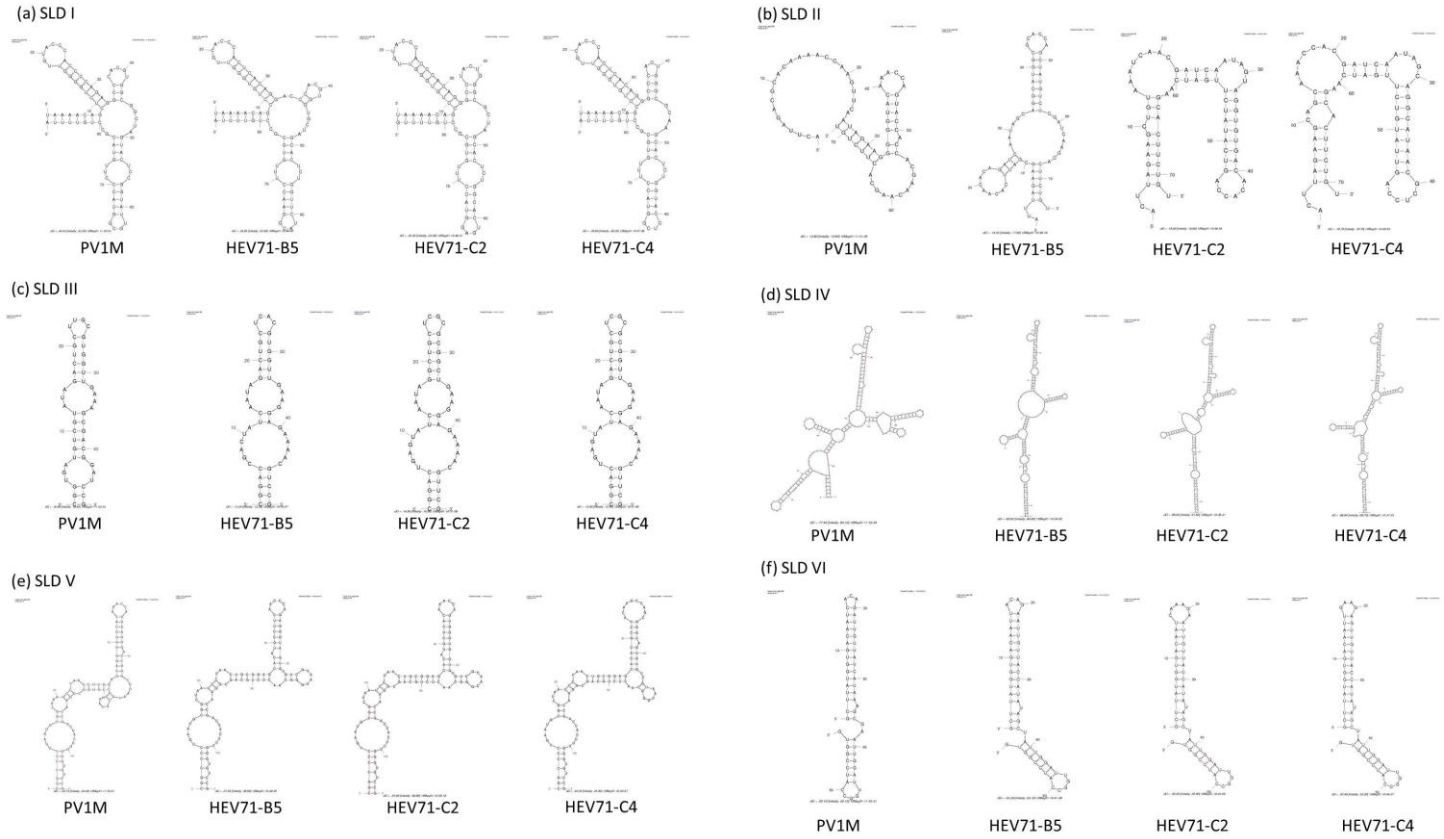

Figure 3.3 The predicted 5′ UTR SLDs; (a) SLD I, (b) SLD II, (c) SLD III, (d) SLD IV, (e) SLD V and (F) SLD VI of HEV71-B5, HEV71-C2 and HEV71-C4 based on the 5′ UTR sequences and structures of PV1M. The structure of each domain was predicted using MFOLD web server.

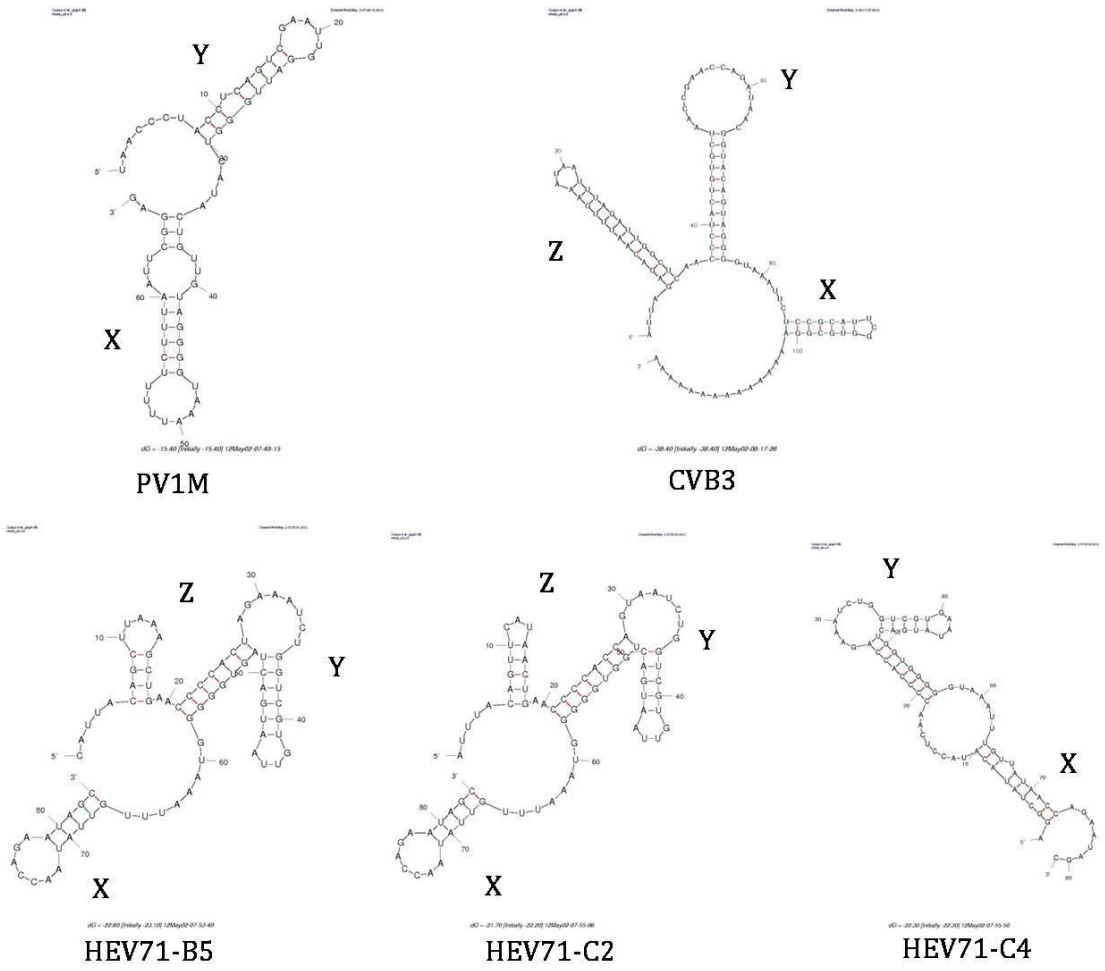

Figure 3.4 The predicted 3′ UTR secondary structures of HEV71-B5, HEV71-C2 and HEV71-C4 based on the 3′ UTR sequences and structures of PV1M and CVB3. The 3′ UTR secondary structures of each virus were predicted using MFOLD web server. SLD structures X, Y and Z of the 3′ UTR are indicated.

3.2.4.2 cis-acting replication element (*cre*)

Cre functions as a template for $3D^{pol}$ during the uridylylation of VPg in RNA synthesis (Paul *et al.*, 2000). *Cre* elements have been identified within the 2C protein gene of PV (Goodfellow *et al.*, 2000; Paul *et al.*, 2000) and CVB3 (van Ooij *et al.*, 2006). The *cre* sequences of HEV71-B5, HEV71-C2 and HEV71-C4 were identified by nucleotide sequence comparison with the *cre* sequences of PV1M and CVB3, and the *cre* structures predicted by the MFOLD web server. The nucleotide position of the *cre* region within the genomes of HEV71-B5, HEV71-C2 and HEV71-C4 were found to be at position 4401-4461 nt, 4398-4458 nt and 4396-4456 nt, respectively. The predicted *cre* structures are shown in Figure 3.5.

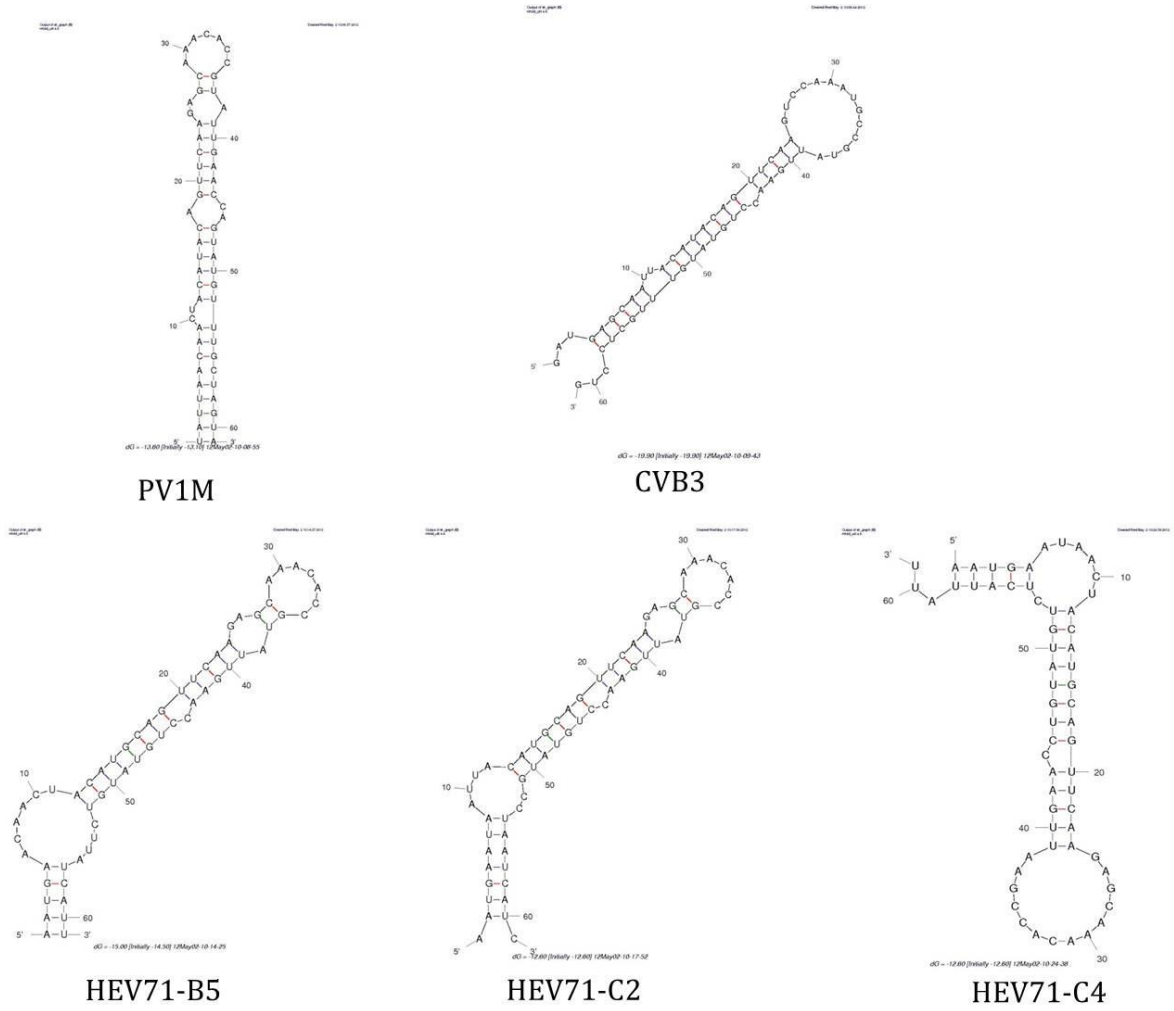

Figure 3.5 Predicted *cre* structures of HEV71-B5, HEV71-C2 and HEV71-C4 based on the *cre* sequences and structures of PV1M and CVB3. The *cre* secondary structures of each virus were predicted using the MFOLD web server.

3.2.5. Design, construction and recovery of infectious cloned-derived viruses

HEV71 strains BRU-2006-35334 (HEV71-B5), 0964-SYD-98 (HEV71-C2) and 540V-VNM-05 (HEV71-C4), were used as a parental strains for developing a reverse genetic system for HEV71. In order to produce infectious RNA from full-length cDNA clones *in vitro* or *in vivo*, the RNA polymerase promoter of bacteriophage T7 and an additional two G residues were positioned immediately upstream of the 5′ terminus of the viral cDNA in order to facilitate transcription and to improve transcription efficiency, respectively (Chua *et al.*, 2008). A poly (A) tail of 25 nucleotides was incorporated immediately downstream of the viral cDNA in order to generate synthetic virus with an authentic 3′ terminus (Chua *et al.*, 2007; Phuektes *et al.*, 2011).

Selection of appropriate plasmid vectors and bacterial host strains has been found to be critical for construction of infectious cDNA clones of several RNA viruses (Hurrelbrink *et al.*, 1999; Lai *et al.*, 1991). Previously, the full-length cDNA clone of two other HEV71 strains (HEV71-26M and HEV71-6F) were successfully constructed (Chua *et al.*, 2008; Phuektes *et al.*, 2011). The full-length cDNA clone of HEV71-26M and HEV71-6F were constructed in two sub-genomic clones, using plasmid pMC18 and *E. coli* strain XL10-gold as the bacterial host. Given this, we used a similar construction strategy to generate infectious cDNA clones of HEV71-B5, HEV71-C2 and HEV71-C4.

Sub-genomic (pMC18/5′-B5 and pMC18/3′-B5) and full-length cDNA clones of HEV71-B5; sub-genomic clones (pMC18/5′-C2 and pMC18/3′-C2) and full-length

cDNA clones of HEV71-C2; sub-genomic clones (pMC18/5′-C4 and pMC18/3′-C4) and full-length cDNA clones of HEV71-C4, were successfully constructed in pMC18 using different restriction sites for cloning, according to the unique restriction sites identified in the viral genome and in the pMC18 vector. All sub-genomic and full-length clones were propagated in *E. coli* strain XL10-gold at 30°C. Cloning and assembly of sub-genomic and full-length clones was assisted by the use of the Clone Manager 5.2/Align Plus 4.0 software (SciEd Central). The cloning procedures for each strain are described in section 2.2.13 and the schematic diagram of the construction of the sub-genomic and full-length cDNA clones is shown in Figures 2.1-2.3. All sub-genomic and full-length clones were randomly selected and screened for anticipated band size by restriction endonuclease digestion.

We further transfected COS-7 cells with the full-length cDNA clones using Lipofectamine™ 2000 in order to rescue clone-derived viruses. The full-length cDNA clone was co-transfected with plasmid pCMV-T7Pol. pCMV-T7Pol, which expresses T7 RNA polymerase, provides the T7 RNA polymerase for transcription of full-length viral cDNA within the cells. Transfection of cells was undertaken by mixing 1.6 μg of full-length viral cDNA and 1.6 μg of pCMV-T7Pol with 4 μL of Lipofectamine™ 2000, and the mixture added to the cells. Transfection protocols are described in section 2.2.15. CPE was observed from secondary infected Vero and RD cells within 24-48 h. Cloned-derived virus HEV71-C2-CDV was recovered from 1 of 10 clones screened and clone-derived HEV71-C4-CDV was recovered from 1 of 6 clones screened, respectively. However, we were unable to recover infectious virus from our full-length

HEV71-B5 cDNA clones despite several repeated cloning attempts. Table 3.4 summarises the construction of our full-length HEV71 cDNA clones and the infectivity of cloned-derived virus. The clone-derived viruses, HEV71-C2-CDV and HEV71-C4-CDV were further passaged in RD cells four times to increase the titre for use in subsequent experiments.

Table 3.4 Summary of the construction of full-length HEV71 cDNA clones and the infectivity of clone-derived virus

Virus strain	Plasmid vector	Bacterial host strain	Number of G residues	Recovery of clone-derived virus
HEV71-B5	pMC18	XL10-Gold	2G	No
HEV71-C2	pMC18	XL10-Gold	2G	Yes
HEV71-C4	pMC18	XL10-Gold	2G	Yes

3.2.6. Genotypic characterisation of infectious clones

Mutations can be introduced during any of the steps undertaken to construct full-length cDNA clones, including, reverse transcription, PCR and ligation reactions. Furthermore, mutations can also occasionally occur during propagation of the full-length cDNA clone in bacterial hosts. Therefore, sequence and phenotypic comparisons with wild-type virus is required to authenticate the cDNA clones and clone-derived viruses. The clone-derived viruses, HEV71-C2-CDV and HEV71-C4-CDV, at RD passage 4, were fully sequenced and compared to their respective parental virus sequences. A total of eight nucleotide differences were identified within the ORF of HEV71-C2-CDV: VP2 (A1359T), VP3 (C2277T), VP1 (T2550C), 2A (A3513G), 2C (A4641G and A4921G) and 3D (T6402C and A6900G). Only one of the mutations, 2C (A4921G), resulted in a change in the deduced amino acid sequence S282G; the others were all synonymous nucleotide changes (Table 3.5). Comparison of the HEV71-C4-CDV nucleotide sequence with that of its parental virus, HEV71-C4, revealed three nucleotide differences, all of which were within the ORF: VP1 (C2988T), 2C (A4507G) and 3C (A5511G). Two of the mutations, VP1 (C2988T) and 3C (A5511G), resulted in deduced amino acid sequence changes, S184L and Q42R, respectively (Table 3.6).

Table 3.5 Sequence comparison of parental HEV71-C2 and clone-derived virus HEV71-C2-CDV

Region	Nucleotide position	Nucleotide		Amino acid position	Amino acid	
		HEV71-C2	HEV71-C2-CDV		HEV71-C2	HEV71-C2-CDV
VP2	1359	A	T	136	A	A
VP3	2277	C	T	188	Y	Y
VP1	2550	T	C	37	H	H
2A	3513	A	G	61	G	G
2C	4641	A	G	188	S	S
	4921	A	G	282	S	G
3D	6402	T	C	155	S	S
	6900	A	G	321	E	E

Table 3.6 Sequence comparison of parental HEV71-C4 and clone-derived virus HEV71-C4-CDV

Region	Nucleotide position	Nucleotide		Amino acid position	Amino acid	
		HEV71-C4	HEV71-C4-CDV		HEV71-C4	HEV71-C4-CDV
VP1	2988	C	T	184	S	L
2C	4507	A	G	144	R	R
3C	5511	A	G	42	Q	R

3.2.7. Phenotypic characterisation of the clone-derived viruses

The clone-derived viruses, HEV71-C2-CDV and HEV71-C4-CDV, were then compared phenotypically to their respective parental viruses by determining growth kinetics in RD cells. RD cell monolayers in 24-well tissue culture trays were infected with HEV71-C2-CDV or with HEV71-C4-CDV and their respective parental viruses at a MOI of 1. Cell culture supernatants were collected at 4 h intervals for 24 h and the virus yields quantified by $TCID_{50}$ assay on Vero cells. As shown in Figure 3.6, the growth kinetics of HEV71-C2-CDV and its parental virus, HEV71-C2, were nearly identical (p>0.05), with titres rising from 4 h p.i. and both peaking at $>10^6$ $TCID_{50}$ mL^{-1} at 20 h p.i. HEV71-C4-CDV also displayed a growth phenotype similar to its parental virus HEV71-C4 (p>0.05), both with peak titre > 10^6 $TCID_{50}$ mL^{-1} at 24 h p.i. (Fig. 3.7). These data suggest that the parental and clone-derived viruses of both HEV71 strains are indistinguishable in their replication in RD cells.

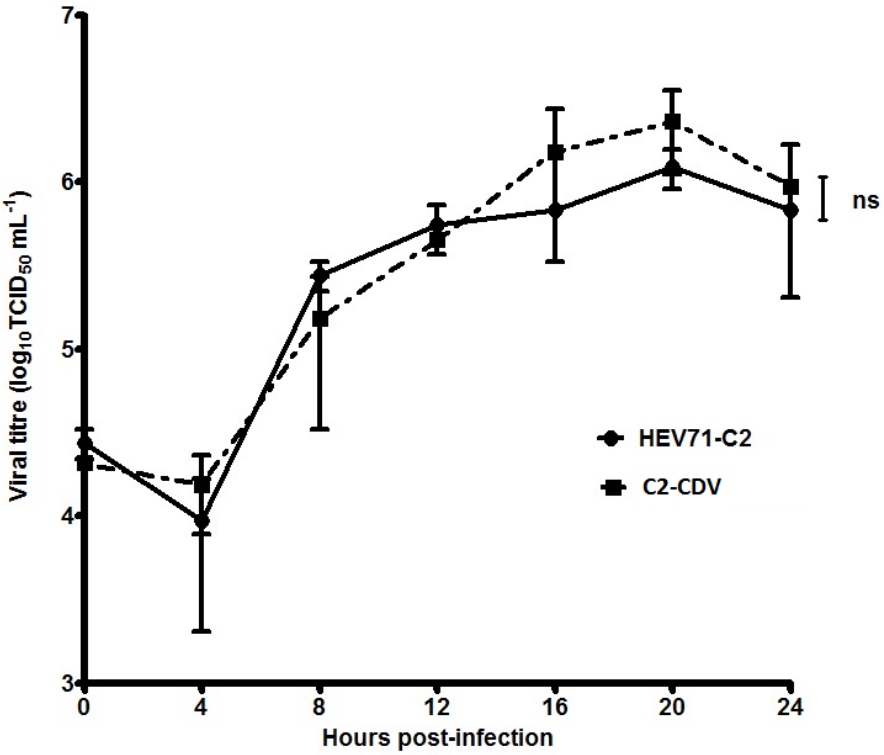

Figure 3.6 Replication kinetics of the parental and clone-derived HEV71-C2 on RD cells. Cell monolayers were infected at MOI of 1. Cell culture supernatants were collected at the times indicated. Samples at each time point were freeze-thawed three times and clarified by centrifugation prior to determination of virus titre by $TCID_{50}$ assay. All assays were performed in duplicate. At each time point, the titres are means of two samples; error bars represent SEM. The Mann-Whitney test was used to compare the titres between the two growth curves; ns denotes significance value of $p>0.05$.

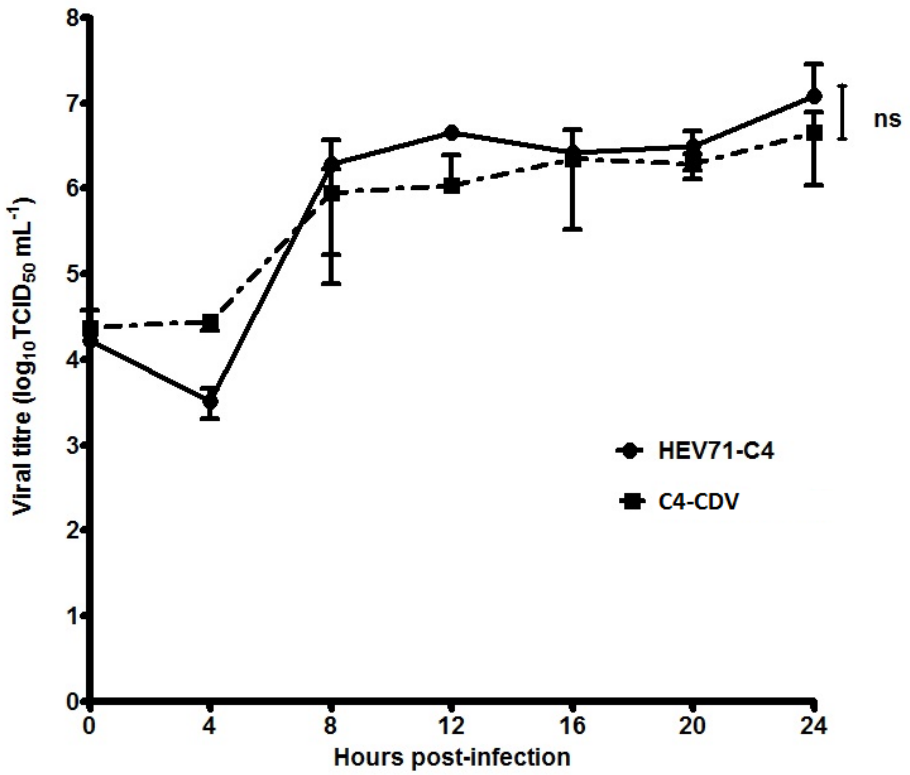

Figure 3.7 Replication kinetics of the parental and clone-derived HEV71-C4 on RD cells. Cell monolayers were infected at MOI of 1. Cell culture supernatants were collected at the times indicated. Samples at each time point were freeze-thawed three times and clarified by centrifugation prior to determination of virus titre by $TCID_{50}$ assay. All assays were performed in duplicate. At each time point, the titres are means of two samples; error bars represent SEM. The Mann-Whitney test was used to compare the titres between the two growth curves; ns denotes significance value of $p>0.05$.

3.3. Discussion

HEV71 is a genetically diverse virus that is capable of rapid evolution (Tee *et al.*, 2010). With the exception of the prototype strain, HEV71-BrCr (genogroup A), all known HEV71 isolates belong to one of the two genogroups, B and C. In this study, we selected and analysed three HEV71 clinical isolates: HEV71 strains BRU-2006-35334 (HEV71-B5); 0964-SYD-98 (HEV71-C2); and 540V-VNM-05 (HEV71-C4). The selected virus strains were isolated from geographically and temporally different outbreaks of HFMD and belong to three distinct lineages: B5, C2 and C4, respectively. They have different genome lengths compared to the prototype strain HEV71-BrCr, but the ORF length for each virus is identical to the prototype strain. Predicted RNA secondary structures were also identified in all of the HEV71 strains studied, using PV1M and CVB3 as reference strains for secondary structure identification.

Strain BRU-2006-35334 was isolated in Brunei in 2006 from a patient diagnosed with HFMD (AbuBakar *et al.*, 2009). In 2006, Brunei reported its first major outbreak of HEV71 infection, associated with fatalities from neurologic complications. More than 1,681 children were affected, with 3 deaths resulting from severe neurologic disease (AbuBakar *et al.*, 2009). The Brunei 2006 HEV71 outbreak was caused predominantly by sub-genogroup B5 virus. Brunei is surrounded entirely by the East Malaysian state of Sarawak. Sarawak has experienced HEV71 outbreaks every three years (1997, 2000 and 2003), caused by B3, B4 and B5 sub-genogroups, respectively (Ooi *et al.*, 2007). All B5 sub-genogroup isolates reported seem to have diverged from an ancestral strain 5511-SIN-00, isolated in Singapore as early as 2000 (Ooi *et al.*, 2007).

Subsequently, sub-genogroup B5 emerged in Japan (Mizuta *et al.*, 2005) and Sarawak (Ooi *et al.*, 2007), before appearing in Peninsular Malaysia and Brunei in 2006.

Strain 0964-SYD-98 isolated from a nasopharyngeal aspirate sample in Sydney in 1998 belongs to sub-genogroup C2 (Sanders *et al.*, 2006). At this time, strains of sub-genogroup C2 were also causing a large outbreak in Taiwan (Shih *et al.*, 2000). Sub-genogroup C2 strains have been isolated in Australia since 1995 (Brown *et al.*, 1999), but prior to 1999 no epidemics with this sub-genogroup had been reported in Australia. A second outbreak involving strains of sub-genogroup C2 occurred in Perth in 1999, where over a six month period approximately 6000 cases of HFMD were reported (McMinn *et al.*, 2001b). The C2 viruses isolated in Sydney are closely related to the 1999 Perth C2 viruses. Sub-genogroup C2 also has a global distribution. Since the 1998 HFMD outbreak in Taiwan, C2 had also been frequently reported in many Asian, European and American countries (Huang *et al.*, 2010; Tao *et al.*, 2012; van der Sanden *et al.*, 2009; Wang *et al.*, 2002).

Strain 540V-VNM-05 was isolated in Southern Vietnam in 2005 and belongs to sub-genogroup C4 (Tu *et al.*, 2007). Viruses belonging to sub-genogroup C4 were first identified in the People's Republic of China in 1998 and again in 2000 (Shimizu *et al.*, 2004) before their identification in Southern Vietnam during 2005. The most recent and largest HEV71 epidemics reported to date have occurred in China between 2008 and 2011 and are owing to the widespread circulation of virus belonging to the C4 sub-genogroup (De *et al.*, 2011; Mao *et*

al., 2010; Zhang *et al.*, 2009). Therefore it was of interest to select genetically distinct and predominant strains isolated from different HEV71 outbreaks in the Asia – Pacific region for the generation of infectious cDNA clones as well as the other studies described in this thesis.

Infectious cDNA clones provide a valuable tool for studying the molecular biology of RNA viruses. This approach is based on the infectious nature of positive stranded viral RNA genomes in permissive host cells. In this study, full-length infectious cDNA clones of the HEV71 clinical isolates, HEV71-C2 and HEV71-C4 were successfully generated using a protocol generated from previous members of our group (Chua *et al.*, 2008; Phuektes *et al.*, 2011). Sub-genomic and full-length cDNA clones of HEV71-C2 and HEV71-C4 were successfully constructed in the low copy number plasmid, pMC18 (approximately 6 copies per cell), and using the bacterial host *E. coli* XL10-gold. This plasmid has previously been used successfully for the construction of an MVE virus infectious cDNA clone (Hurrelbrink *et al.*, 1999) and also for two other strains of HEV71 (Chua *et al.*, 2008; Phuektes *et al.*, 2011). It has also been shown previously that full-length HEV71 clones amplified in bacterial strain, *E. coli* XL10-gold, are infectious, in contrast to full length clones amplified in the DH10B bacterial strain (Phuektes *et al.*, personal communication). These findings clearly demonstrate that a fortuitous combination of plasmid vector and bacterial host is critical for generating infectious cDNA clones of HEV71. It remains unclear why *E. coli* XL10-gold is more suitable for propagating cDNA clones of HEV71 than DH10B.

Previous work showed that only HEV71 clones containing 2 G residues

immediately upstream of the 5′ terminus of viral cDNA were found to be infectious (Phuektes *et al*., personal communication). Most enterovirus infectious cDNA clones contain an additional 1, 2 or 3 G residues at the 5′ end of the viral cDNA and these non-viral nucleotides have not been shown to alter the specific infectivity of *in vitro* transcribed RNA (Arita *et al.*, 2005; Kraus *et al.*, 1995; Martino *et al.*, 1999). It has also been shown that one additional G residue at the end of the T7 promoter sequence is important for *in vitro* transcription efficiency (Janda *et al.*, 1987). In this study, HEV71-C2 and HEV71-C4 containing two G residues at the 5′ terminus were found to be infectious, similar to the previously constructed full length infectious cDNA clones of HEV71 (Chua *et al.*, 2008; Phuektes *et al.*, 2011). The earlier report of HEV71 infectious clone of strain BrCr also contains two G residues. It is possible that the inclusion of two G residues in HEV71 clones provide the optimal conditions for efficient transcription and RNA synthesis.

The poly (A) tail at the 3′ end may play an important role in the infectivity of enterovirus cDNA clones. It has been reported that PV RNAs with poly (A) tails of less than 8 A nucleotides in length were much less efficient in negative-strand RNA synthesis than those with 80 A nucleotides (Herold & Andino, 2001). Silvestri *et al.* (2006) showed that PV RNAs with 3′ terminal poly (A)11 and poly(A)12 had negative-strand RNA synthesis at 1-3% of the level observed for PV RNAs with 3′ terminal poly (A)80 RNA, and increasing the length of the poly (A) tail from 12 to 20 residues resulted in an increase in negative strand synthesis by 30-fold or greater. PV RNA with poly (A)20 had a similar level of negative-strand RNA synthesis to poly (A)80. These results indicate that the length of poly

(A) tail plays an important role in viral RNA replication and infectivity, possibly by assisting the binding of poly (A) binding protein. The HEV71 clones reported in this study and by Chua *et al*. (2008) and Phuektes *et al*. (2011) were designed to contain a 25-mer poly (A) tail.

Either the cDNA clone or RNA transcripts have been used in transfection to recover clone-derived virus populations in most infectious clone systems (Boot *et al.*, 1999; Hurrelbrink *et al.*, 1999; Yun *et al.*, 2003). Transfection of plasmid cDNA has been reported to have several advantages (Boot *et al.*, 2001). *In vitro* transcription, which is an expensive and laborious process, is not required and infectivity is less affected by RNA degradation. In addition, Boot *et al*. (2001) compared RNA and cDNA transfection methods for rescue of infectious bursal disease virus (IBDV) and found that cDNA transfection gave rise to a much higher level of viral protein expression than RNA transfection and was more efficient in recovering a crippled variant of IBDV. In a previous study, clone-derived HEV71 was obtained by transfection of either plasmid cDNA or RNA transcripts into susceptible cells (Phuektes *et al*., personal communication). However, the recovery efficiencies between these two transfection methods were not compared. Since transfection of cDNA is simpler and less expensive, this method is preferable for recovering of clone-derived HEV71 populations. Therefore in this study, our clone-derived HEV71 populations were obtained by transfection of plasmid cDNA into COS-7 cells.

In this study, we failed to generate a full-length infectious cDNA clone of HEV71-B5. To achieve successful infection, viral transcripts must interact with viral-

encoded proteins, most particularly with the viral replicase and with host cell components that formthe translation machinery; therefore the structure of viral transcripts need to mimic that of virion RNA as closely as possible (Boyer & Haenni, 1994). Several parameters have a dramatic influence on the infectivity of viral transcripts: (1) the heterogeneity of transcript population, (2) the presence of point mutations , and (3) the sequence at the 5′ and 3′ ends (number and sequence of non-viral nucleotides, presence of a cap structure at the 5′ end or a poly (A) tail at the 3′ end) (Boyer & Haenni, 1994). The non-infectious HEV71-B5 full-length clones were not sequenced to identify the mutation/s that caused the non-infectious phenotype. Therefore, a genetic analysis could not be made on this non-infectious full-length cDNA clones.

Genotypic and phenotypic characterisation of clone-derived virus populations in comparison with parental virus is required to confirm the authenticity of the clone-derived virus. Full-length sequencing was performed for the newly generated clone-derived viruses. HEV71-C2-CDV contain eight nucleotide mutations compared to its parental virus, but only one of the mutations resulted in a change in the deduced amino acid sequence in gene 2C (S282G). This mutation is not located within the *cre* region of HEV71-C2 and therefore is unlikely to play a significant role in the overall fitness of the virus. Comparison of HEV71-C4-CDV to its parental virus, HEV71-C4, revealed three nucleotide differences, all located within the ORF. Two of the mutations resulted in changes to the deduced amino acid sequence, in VP1 (S184L) and 3C (Q42R). These mutations may have been introduced either during RT-PCR amplification or during cloning. Alternatively, these mutations may reflect the quasispecies nature

of the parental virus. The quasispecies theory states that an RNA virus population does not consist of a single wild-type genotype but instead is an ensemble of related genotypes (Domingo & Holland, 1997; Holland *et al.*, 1982). The growth kinetics of clone-derived HEV71-C2-CDV and HEV71-C4-CDV were compared to their respective parental viruses in cell-culture. The clone-derived viruses showed *in vitro* growth properties indistinguishable to that of their respective parental viruses.

In conclusion, we have successfully constructed full-length infectious cDNA clones of two HEV71 clinical isolates that belong to different genogroups. These infectious clones were used throughout the studies described in subsequent chapters. Furthermore, the availability of these infectious cDNA clones will make a significant contribution to the future study of viral replication, disease pathogenesis and virulence.

4. CHAPTER FOUR

A REVERSE GENETIC STUDY OF THE ADAPTATION OF HUMAN ENTEROVIRUS 71 TO GROWTH IN CHINESE HAMSTER OVARY CELL CULTURES

4.1. Introduction

One of the major ongoing challenges in studying the pathogenesis of HEV71 infection is the lack of a suitable animal model. The most authentic animal model for HEV71 infection is the cynomolgus macaque model (Arita *et al.*, 2007; Arita *et al.*, 2005; Nagata *et al.*, 2002), which mimics human disease closely. However, owing to financial and ethical constraints, this model has not been used extensively. Therefore, several mouse models have been developed to allow investigations of pathogenesis and to perform efficacy studies of vaccines. Most of the mouse models developed to date have required prior mouse adaptation of HEV71 populations.

Our initial studies have shown that infection of newborn mice by i.p. or i.c. inoculation of HEV71 does not cause a clinically overt disease. A previous study conducted using HEV71 sub-genogroup B3 (Chua *et al.*, 2008) showed that prior adaptation to growth in CHO cells was an essential first step in the selection of a mouse-adapted strain of HEV71. In this study, we adapted the three selected HEV71 isolates (described in Chapter 3) to growth in CHO cells. We also examined several phenotypic and molecular characteristics of the CHO cell-adapted virus and identified the molecular determinants of CHO cell-adaptation.

This work was recently published (Zaini *et al.*, 2012b) and a copy of the manuscript reprint is included in Appendix B.

4.2. Results

4.2.1. CHO cell-adaption of HEV71

To generate CHO cell-adapted virus, confluent CHO cells in 12-well tissue culture plates, at a seeding density of 2 .2×10^5 cells per well, were infected with HEV71-B5, HEV71-C2 or HEV71-C4, respectively, at a MOI of 10 for 1 h at 37°C. The cells were then washed with PBS and overlaid with 1.0 mL DMEM supplemented with 2% FBS and 2mM L-glutamine and cultured for three days at 37°C. No CPE was observed in infected CHO cells at passage one. Thus, the viruses were blind passaged in CHO cells with 500 μL of clarified virus supernatant from the previous passage. Virus titres from each of the passages were quantified by $TCID_{50}$ assay on Vero cells. CHO cell adaptations were considered complete when the titres reached approximately 10^7 $TCID_{50}$ mL^{-1}.

During the course of CHO cell-adaptation, the growth of both HEV71-B5 and HEV71-C2 improved significantly, with increasing virus titres observed at each passage and the final titre reaching similar levels to that observed for unadapted virus in primate cells, including Vero cells and RD cells. CHO cell-adapted HEV71-B5 (CHO-B5) reached a titre of 4.2×10^7 $TCID_{50}$ mL^{-1} at passage four and CPE was observed by passage two. On the other hand, CHO cell-adapted HEV71-C2 (CHO-C2) reached a titre of 1.5×10^7 $TCID_{50}$ mL^{-1} at passage eight and CPE was observed by passage five. By contrast, HEV71-C4 failed to adapt to CHO cells, with no virus detected at passage four (Figure 4.1). This finding was consistent

with another attempt in our laboratory to adapt a different strain of HEV71 belonging to sub-genogroup C4 using a similar adaptation procedure (Phuektes, personal communication). Both CHO cell-adapted CHO-B5 and CHO-C2 strains were then plaque purified and isolated plaques passaged on CHO cells three times to increase the titre for use in subsequent assays.

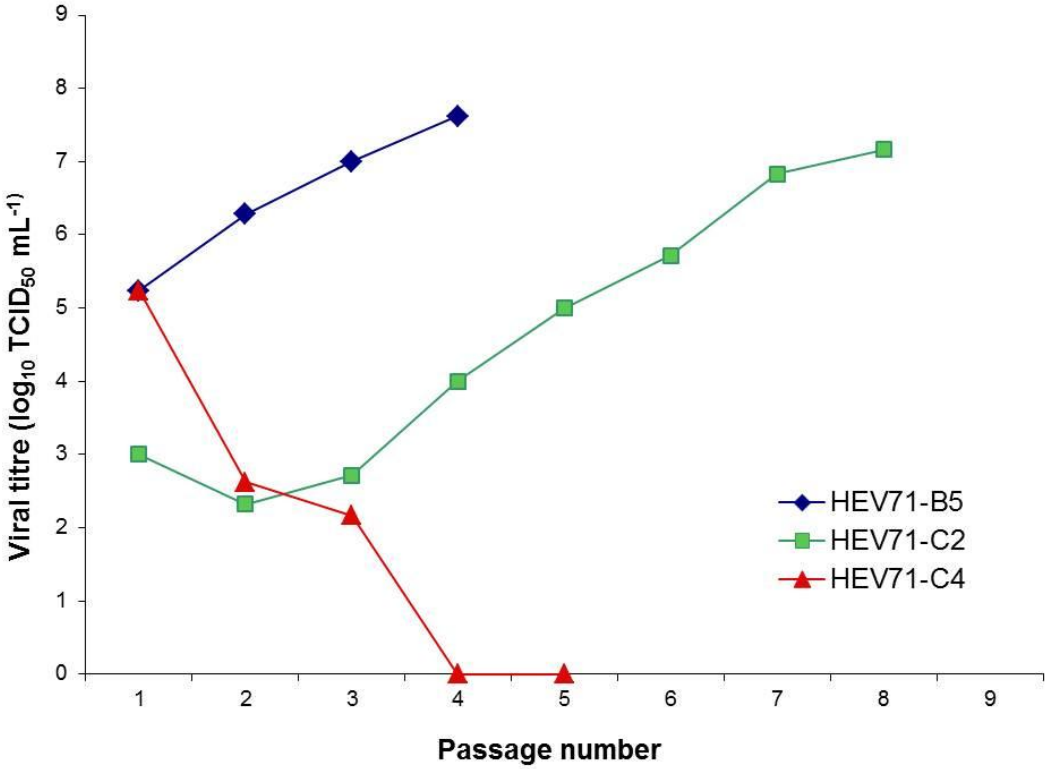

Figure 4.1 CHO cell-adaptation of HEV71-B5, HEV71-C2 and HEV71-C4. Confluent CHO cells were infected with HEV71-B5, HEV71-C2 or HEV71-C4 at a MOI of 10 to create the first passage in CHO cells; all subsequent passages were infected with 500 µL of clarified virus supernatant from the previous passage and virus titres from each of the passages were quantified by $TCID_{50}$ assay on Vero cells.

4.2.2. Phenotypic characterisation of CHO cell-adapted HEV71

The replication kinetics of the unadapted parental and CHO cell-adapted virus were examined in CHO cells over a 24 h time period. Due to the difference in virus titres between the plaque-purified CHO-B5 and CHO-C2, we decided to infect the CHO cells at MOIs of 5 and 0.5, respectively; the same MOIs were used for their respective parental viruses. Both parental viruses, HEV71-B5 and HEV71-C2, replicated poorly in CHO cells (Figure 4.2). By contrast, CHO-B5 and CHO-C2 grew efficiently in CHO cells, with maximum titres >100-fold higher than that of parental virus.

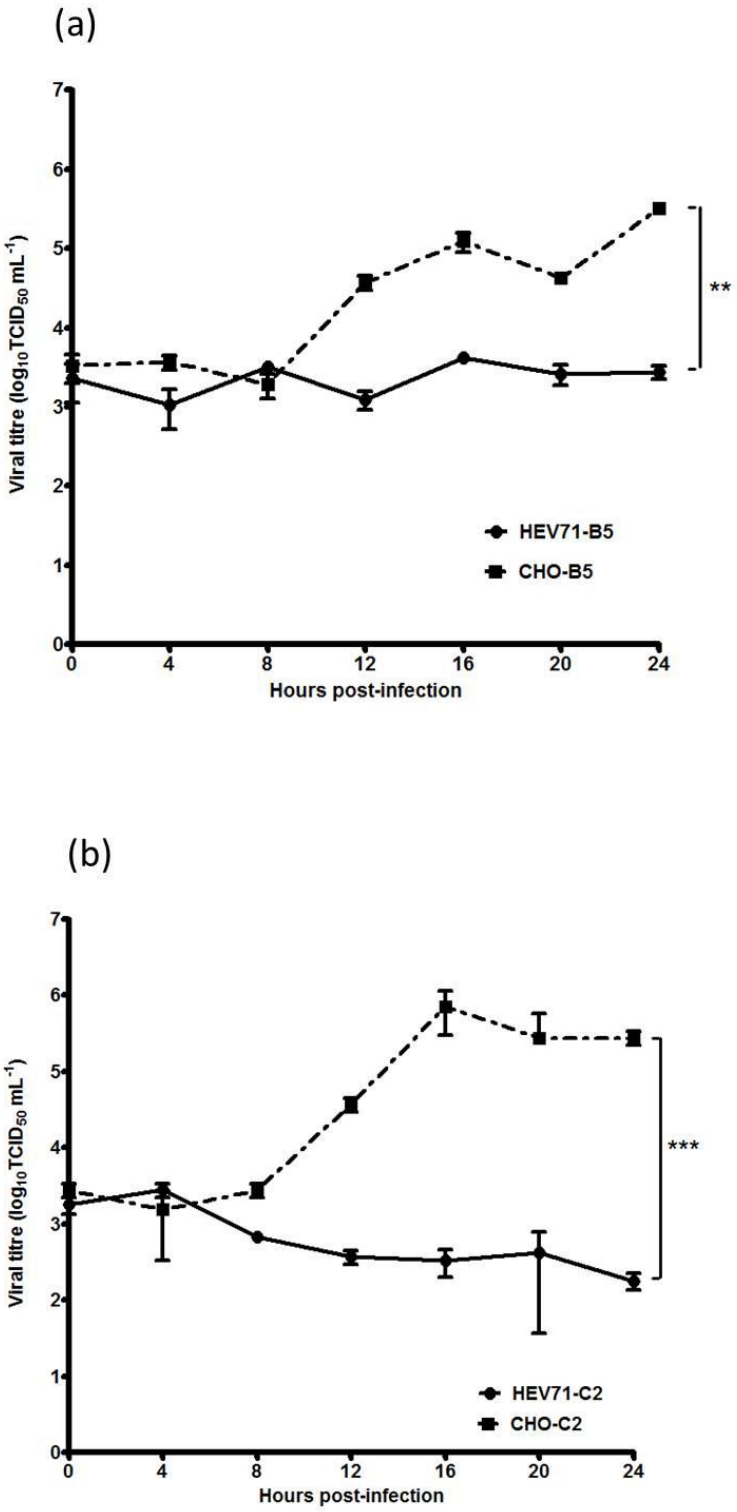

Figure 4.2 Replication kinetics in CHO cells of (a) HEV71-B5 and CHO-B5 (MOI=5), (b) HEV71-C2 and CHO-C2 (MOI=0.5). Cell monolayers were infected at the indicated MOI. Cell culture supernatants were then collected at the times

indicated. Samples at each time point were freeze-thawed three times and clarified by centrifugation prior to determination of virus titre by $TCID_{50}$ assay. All assays were performed in duplicate. At each time point, the titres are the means of two samples; error bars represent SEM. The Mann-Whitney test was used to compare the titres between the two growth curves. ** denotes significance value $p<0.01$, *** denotes significance value $p<0.001$.

4.2.3. Comparison of nucleotide and amino acid sequences of the wild-type and CHO cell-adapted HEV71

To identify the cause of the altered CHO cell phenotype, whole genome sequencing of the CHO cell-adapted strains were performed using synthetic oligonucleotide primers designed to amplify overlapping fragments of the genome. The complete genomic sequences of CHO-B5 and CHO-C2 are included in Appendix A of this thesis and the annotated complete genome sequences of these viruses have been deposited to GenBank sequence database. The GenBank accession numbers for CHO-B5 and CHO-C2 are JN992284 and JN992285, respectively. The complete nucleotide and deduced amino acid sequences of HEV71-B5, HEV71-C2, CHO-B5 and CHO-C2 were then compared in order to identify mutations associated with adaptation of virus to growth in CHO cells (Table 4.1). Comparison of the HEV71-B5 and CHO-B5 sequences revealed two nucleotide differences, both of which are located in the virus polyprotein ORF. Only one of these mutations resulted in a change in the deduced amino acid sequence, VP2 (K^{149}→I). On the other hand, comparison of HEV71-C2 and CHO-C2 sequences revealed a single nucleotide difference that resulted in a change in the deduced amino acid sequence, VP2 (K^{149}→M). The nucleotide and deduced amino acid sequences around the VP2 mutation region were aligned to clearly demonstrate these changes (Figure 4.3). In a previous study (Chua *et al*., 2008), CHO cell-adapted HEV71 of sub-genogroup B3 was also shown to harbor the K^{149}→I mutation in the VP2 capsid protein gene. They demonstrated that the VP2 K^{149}→I change was solely responsible for improved growth in CHO cells.

Table 4.1 Nucleotide and amino acid differences identified in the genomes of wild-type HEV71-B5, HEV71-C2 and their CHO cell-adapted variants

HEV71 sub-genogroup	Viral protein	Nucleotide position	Nucleotide		Amino acid position	Amino acid	
			Wild-type	CHO-adapted		Wild-type	CHO-adapted
B5	VP2	1400	A	T	149	K	I
	3C	5574	A	G	61	E	E
C2	VP2	1397	A	T	149	K	M

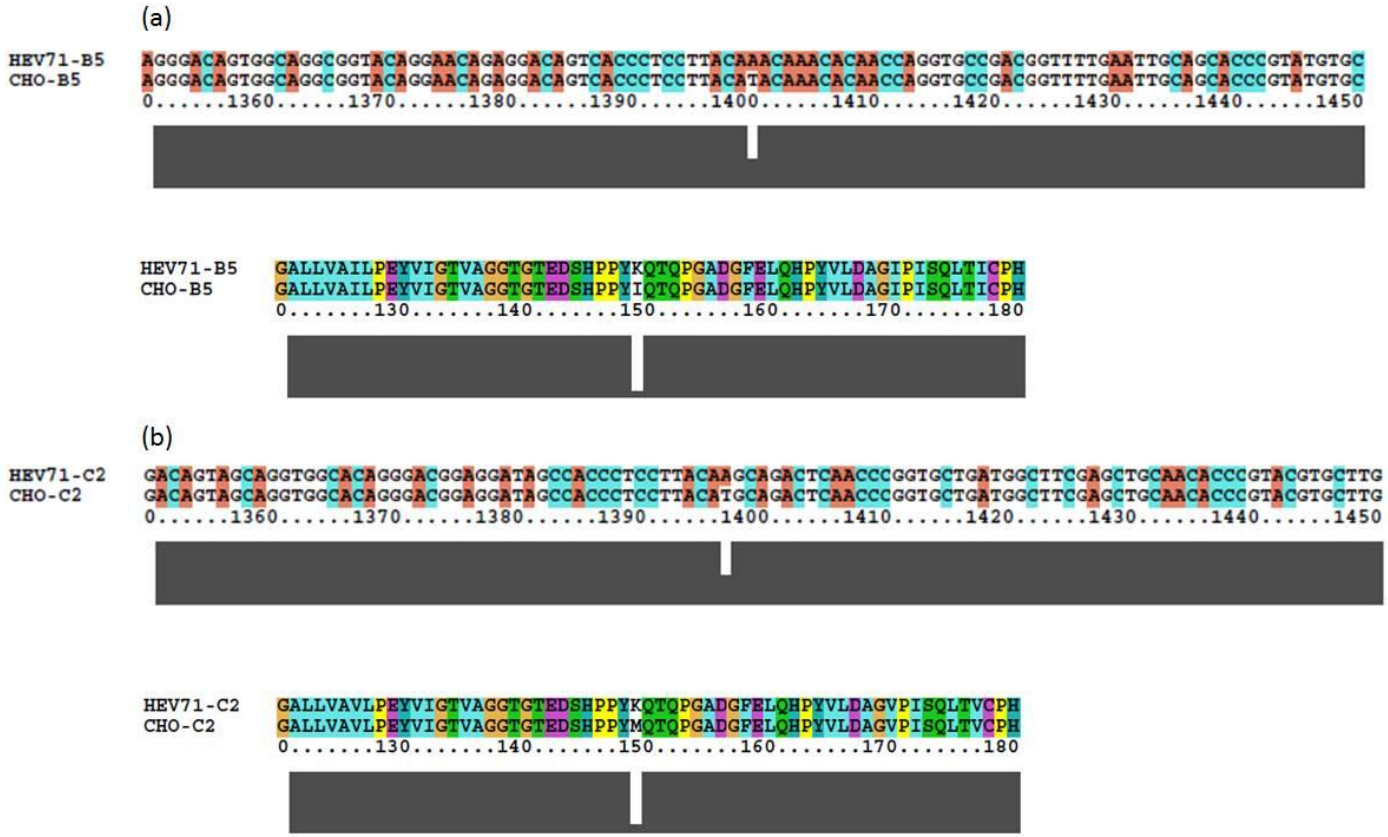

Figure 4.3 Nucleotide and amino acid sequence alignment of (a) HEV71-B5 and CHO-B5, (b) HEV71-C2 and CHO-C2, showing the single nucleotide and deduced amino acid mutation at position 149 within the VP2 capsid protein gene. The grey shaded region indicates consensus sequence.

4.2.4. Construction of mutant virus and phenotypic characterisation of clone-derived virus

Further analysis of the CHO cell-adaptation process by HEV71 was undertaken using infectious cDNA clones of HEV71 (constructed as in Chapter 3). We were particularly interested to determine if CHO cell-adaptation of HEV71-C4, which is refractory to CHO cell-adaptation during serial passage, could be forced by a reverse genetic approach. We determined the HEV71-C4 capsid protein deduced amino acid residue to be lysine (K) at position 149 in VP2. The VP2 capsid protein K^{149}→I and K^{149}→M mutation was then introduced into the full-length HEV71-C4 cDNA clone by site-directed mutagenesis (Figure 4.4). A single clone of each mutant was selected and purified plasmid DNA was prepared for sequencing analysis. Partial VP2 genes were sequenced to confirm the presence of the appropriate mutations. Infectious CDVs were recovered from transfected COS-7 cells at two days post-transfection and were passaged three times on CHO cells in order to generate working stocks for cell culture characterisation. VP2 gene RT-PCR and nucleotide sequencing was also undertaken to ensure that the site-specific change remained present in the rescued virus populations. Nucleotide sequencing showed that all mutant viruses had retained the introduced mutations at CHO cell passage three (Figure 4.5).

The replication kinetics of both C4-VP2I-CDV and C4-VP2M-CDV were then examined in CHO cells (MOI = 2) and compared to parental C4-CDV. The CHO cell replication kinetics and virus yields of both mutants were similar, with a lag phase of approximately 8 h p.i. and virus titres increasing thereafter (Figure 4.6). Both C4-VP2I-CDV and C4-VP2M-CDV grew efficiently in CHO cells, with titres

rising from 8 h p.i. and peaking at 24 h p.i. The maximum titres for both mutant viruses were >100-fold higher than that of their parental virus. No significant increase in viral titre was observed for the C4-CDV at 24 h p.i. These data demonstrate clearly that both amino acid substitutions VP2-K^{149}→I or M conferred the CHO cell-adapted phenotype on HEV71-C4.

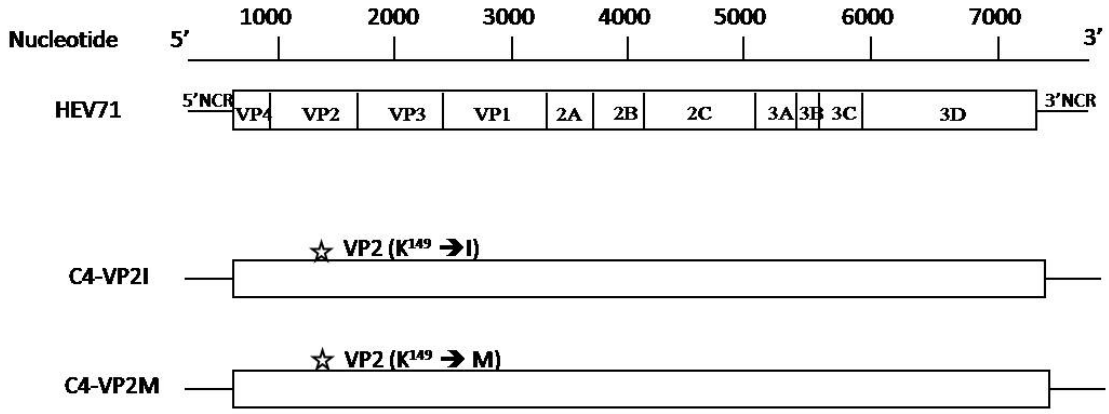

Figure 4.4 Schematic representation of the infectious cDNA clones of HEV71-C4 and cDNA clones containing the VP2 mutations constructed by site-directed mutagenesis. Genome maps of HEV71-C4 and its mutants are represented as an open box with individual genes and non-coding regions indicated for HEV71-C4. Amino acid mutations introduced in C4-VP2I (VP2, K^{149}→I) and C4-VP2M (VP2, K^{149}→M) are shown as open stars.

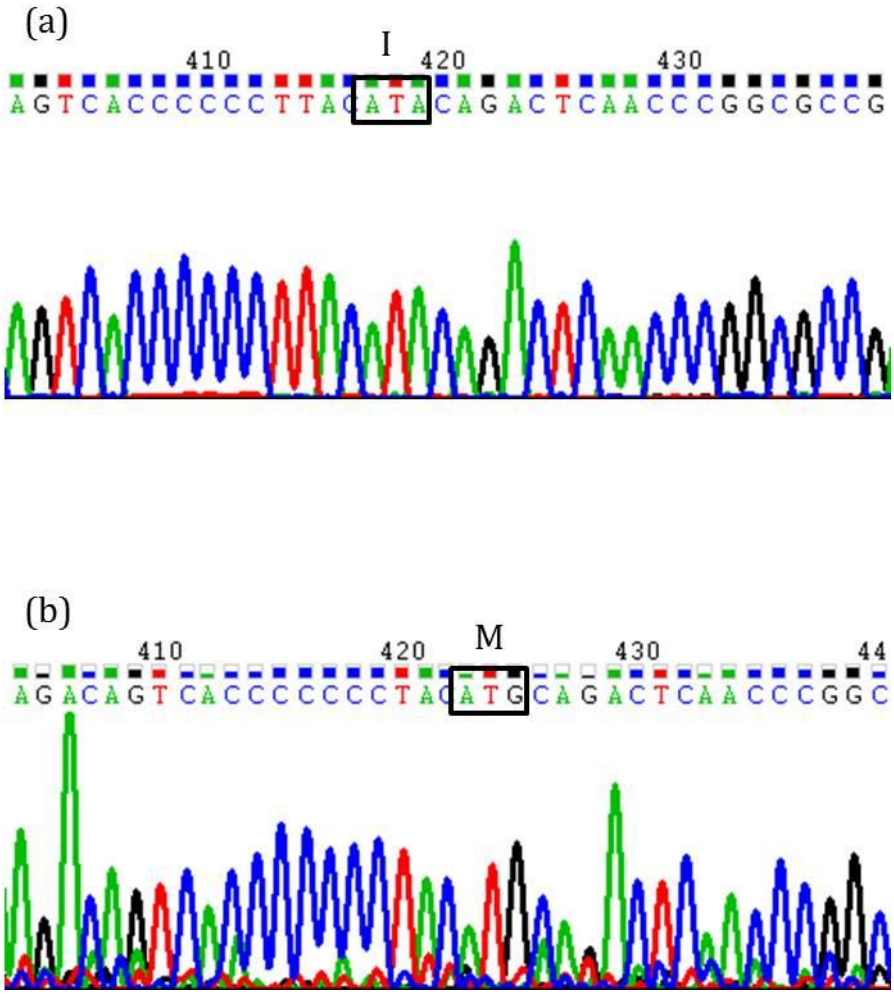

Figure 4.5 Stability of introduced VP2 mutations (a) K^{149}→I and (b) K^{149}→M during CHO cell culture passage. Clone-derived virus populations were passaged three times in CHO cells and viral RNA was extracted from culture supernatants collected at passage three. The VP2 genes were amplified by RT-PCR and their nucleotide sequences determined. The open box indicates the nucleotide sequence of the site-specific change and the deduced amino acid residue is indicated above the box.

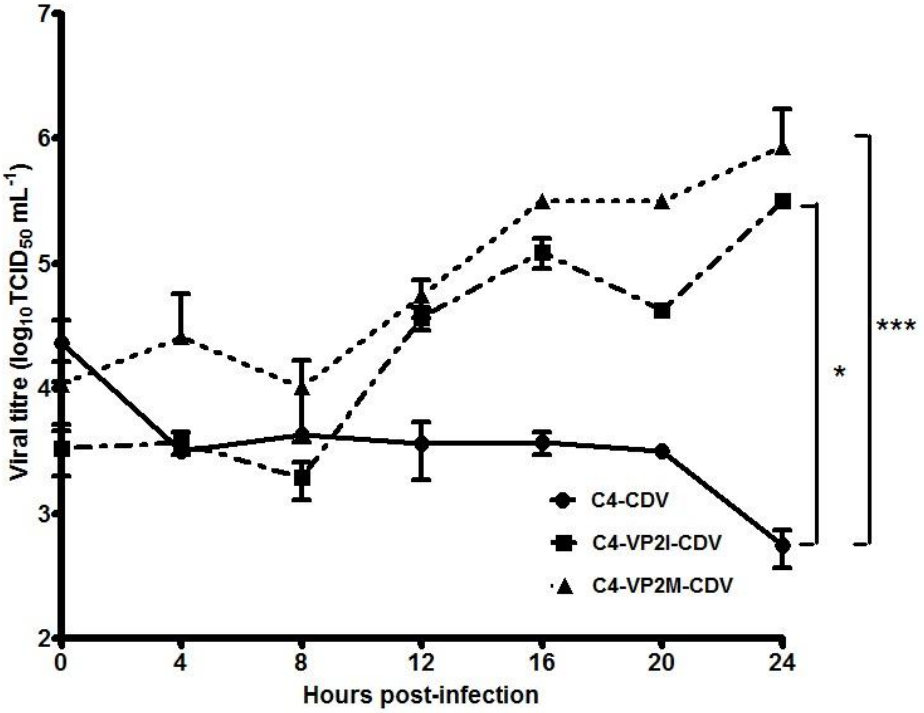

Figure 4.6 Replication kinetics in CHO cells of C4-CDV, C4-VP2I-CDV and C4-VP2M-CDV. Cell monolayers were infected at an MOI of 2. Cell culture supernatants were then collected at the times indicated. Samples at each time point were freeze-thawed three times and clarified by centrifugation prior to determination of virus titres by $TCID_{50}$ assay. All assays were performed in duplicate. At each time point, the titres are the means of two samples; error bars represent SEM. The Mann-Whitney test was used to compare the titres between C4-CDV vs C4-VP2I-CDV and C4-CDV vs C4-VP2M-CDV. * denotes significance value $p<0.05$, *** denotes significance value $p<0.001$.

4.2.5. Homology modeling

In order to the locate position of the amino acid substitutions within the three-dimensional structures of the VP2 capsid protein of the CHO-adapted variants, three-dimensional structural models of the VP2 protein were predicted by homology modeling. The virus most closely related to HEV71 by primary sequence, for which there is VP2 protein x-ray crystallographic data, is bovine enterovirus (BEV). The amino acid identity between HEV71-B5/C2 and BEV VP2 protein is 58%. The known x-ray crystallographic structure of BEV capsid protein (PDB number: 1BEV_2) was thus used to predict the location of mutations found in the VP2 capsid protein of CHO cell-adapted variants. The VP2-149K was predicted to be located in the surfaced-exposed region of the EF loop (Figure 4.7a). The basic polar lysine found in HEV71-B5 and HEV71-C2 (Figure 4.7b) was substituted with neutral non-polar isoleucine and neutral non-polar methionine in CHO-B5 (Figure 4.7c) and CHO-C2 (Figure 4.7d), respectively.

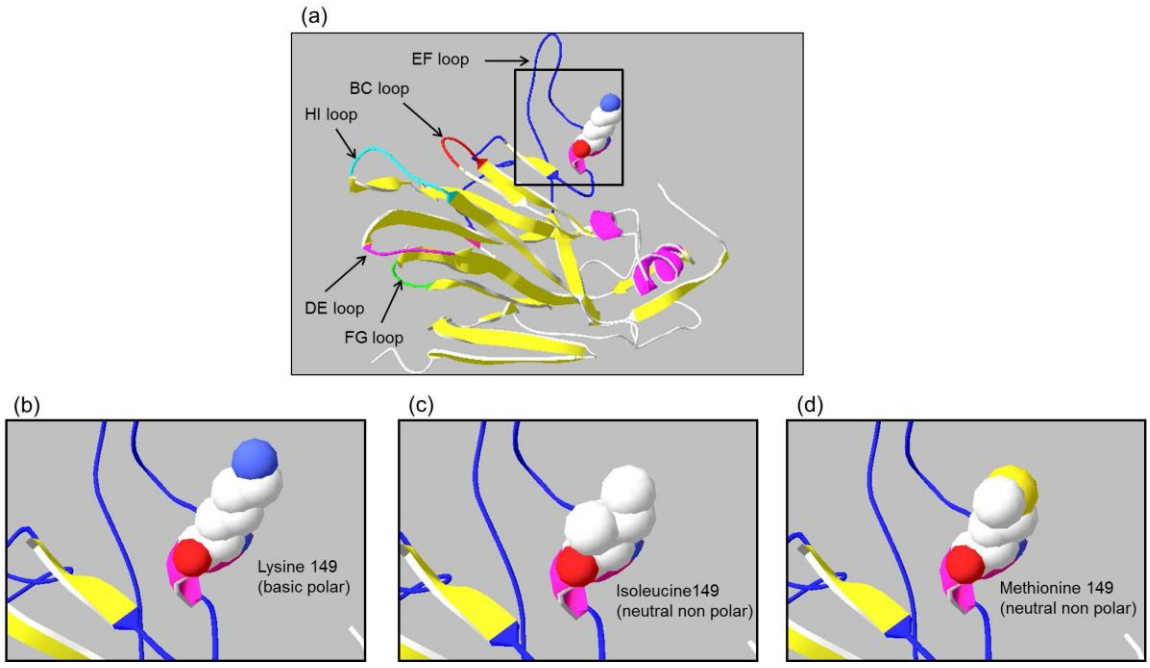

Figure 4.7 Homology models showing the predicated three-dimensional structure of (a) the HEV71 VP2 protein with amino acid residue 149 located on the surface-exposed EF loop, (b) the HEV71-B5 and HEV71-C2 VP2 protein with lysine (basic polar) at amino acid position 149, (c) CHO-B5 VP2 protein with isoleucine (neutral and non-polar) at amino acid residue 149, (d) CHO-C2 VP2 protein with methionine (neutral and non-polar) at amino acid residue 149, based on the known three-dimensional crystallographic structure of bovine enterovirus (BEV) VP2 capsid protein (PDB number: 1BEV_2). Amino acid residue 149 of VP2 is displayed as a space-fill model and each individual loop shown by arrows.

4.2.6. Infectivity of CHO cell-adapted variants and clone-derived viruses containing the CHO cell-adaptation marker in BALB/c mice

We next determined the infectivity of the CHO cell-adapted virus and CDVs containing the CHO cell-adaptation marker in a litter of 1 day-old BALB/c mice. In our laboratory, BALB/c mice have been shown to be susceptible to the prototype EV71-BrCr infection and showed early onset of disease and death (Chua *et al*., unpublished data). Thus, BALB/c mice were selected for all our animal experiments. Groups of five to nine 1 day-old BALB/c mice were inoculated with approximately $10^5 \times TCID_{50}$ of each CHO cell-adapted virus (CHO-B5 and CHO-C2) or CDVs containing the CHO cell-adaptation marker (C4-VP2I-CDV and C4-VP2M-CDV) and were then observed for 14 days p.i. Two mice infected with CHO-B5 showed weakness in both hindlimbs at 6 days p.i. These mice were euthanased for brain and skeletal muscle tissue collection and subsequent mouse adaptation was further described in Chapter 5. Mice inoculated with other virus populations remained healthy with no observable clinical signs of infection or mortality up to 14 days p.i. (Table 4.2).

Table 4.2 Infectivity of CHO cell-adapted variants and mutant CDVs population in newborn BALB/c mice

Virus	Mortality (%)
CHO-B5	22
CHO-C2	0
C4-VP2I-CDV	0
C4-VP2M-CDV	0

4.3. Discussion

In this study, the molecular basis of CHO cell-adaptation by HEV71 strains belonging to different sub-genogroups was identified by the use of a reverse genetic approach. Unadapted HEV71-B5, HEV71-C2 and HEV71-C4 are unable to replicate in CHO cells. CHO cell-adapted variants of HEV71-B5 and HEV71-C2, CHO-B5 and CHO-C2, respectively, were selected after serial passage in CHO cells at a high MOI. HEV71-C4 was not able to adapt to growth in CHO cells after three passages. The replication kinetics of the HEV71-C4 clone-derived virus containing the CHO cell-adaptation marker, C4-VP2I (VP2, K^{149}→I) and C4-VP2M (VP2, K^{149}→M) clearly demonstrated that amino acid substitutions at amino acid position VP2-149K are solely responsible for the adaptation of virus to growth in CHO cells. Mutations at this site were also observed during *in-vivo* adaptation of HEV71 (MP-4643) in random-bred ICR mice (Chen *et al.*, 2004), in which a basic polar lysine residue was substituted by neutral non-polar leucine (Wang *et al.*, 2004).

Previous studies have shown that the expression of specific receptors for human enteroviruses on the cell surface of rodent cells allows effective viral replication similar to that seen in susceptible human cells expressing the corresponding viral receptors, including human poliovirus receptor (Mendelsohn *et al.*, 1989) and human intercellular adhesion molecule-1 (Shafren *et al.*, 1997). Human SCARB2 (Yamayoshi *et al.*, 2009) and human P-selectin glycoprotein ligand-1 (PSGL-1) (Nishimura *et al.*, 2009) have been identified as cellular receptors for HEV71. Expression of human SCARB2 enables mouse L929 cells to support HEV71 replication and develop CPE (Yamayoshi *et al.*, 2009). These findings

suggest that the efficacy of replication of enteroviruses is dependent upon the expression of specific receptors on the cell surface, including rodent cell lines that are naturally non-permissive for enterovirus infection. However, most PSGL-1-binding strains of HEV71 replicate poorly in mouse L929 cells expressing human PSGL-1 (Miyamura *et al.*, 2011). Possible adaptive mutations were identified during serial passage in L929 cells expressing human PSGL-1, which included an amino acid change at VP2-149K (Miyamura *et al.*, 2011) also identified in association with CHO cell-adaptation in this study. This shows that an adaptive mutation in the capsid proteins was required for efficient viral replication of PSGL-1 binding strains of HEV71 in mouse L929 cells expressing human PSGL-1.

The VP2-149 mutations identified in our CHO-adapted virus are located in the EF loop, a known major antigenic region for the related PV (Burke *et al.*, 1991). VP2 forms part of a deep cleft on the virion surface of poliovirus that functions as a site of virion attachment to the cellular receptor (Hogle *et al.*, 1985). In the related PV, amino acid residue Thr-31 of VP2 have been associated with mouse adaptation (Couderc *et al.*, 1996; Couderc *et al.*, 1993). This residue is located in the EF loop of VP2 which is thought to be important to the stability of the infectious virion (Couderc *et al.*, 1993). This determinant confers a mouse-adapted phenotype on PV by possibly allowing more efficient receptor-mediated conformational changes during viral uncoating and internalisation (Couderc *et al.*, 1996). From our mouse infectivity study, however, the VP2-149K mutation was not sufficient to confer a mouse virulent phenotype, but only conferred an adaptation to improved growth in CHO cells.

The EF loop forms part of the interface between capsid subunits and regulation of the stability of this interface is important in controlling assembly and disassembly of the virus (Colston & Racaniello, 1994). Other than changes in the efficacy of viral uncoating, a change in the specificity of receptor binding may be responsible for binding to unidentified mouse cell receptors and may explain the observed phenotype (Murray *et al.*, 1988). It remains unclear whether the VP2-K^{149}→I or M mutations observed in our study are responsible for receptor switching to a CHO cell surface protein that is not expressed on either human or primate cells. It is possible that the VP2-K^{149}→I or M mutations alter the conformation of the EF loop, thus allowing recognition of a wider range of receptor molecules.

In our study, HEV71-C4 failed to adapt to CHO cells by natural selection. Adaptation has been described as the modification of an organism to make it more fit for existence within a certain environment (Domingo & Holland, 1997; Domingo *et al.*, 1997). RNA virus populations are complex and contain heterogeneous mixtures of related viral genomes called quasispecies (Domingo & Holland, 1997; Domingo *et al.*, 1997). Viral quasispecies evolution is decisively influenced by high mutation rates (rate of nucleotide misincorporation per nucleotide copied) during viral replication and in some cases also by molecular recombination and genome segment reassortment (Domingo *et al.*, 2012). During viral infections, viral quasispecies play a key role in the adaptability of viruses to changing environments and the fate of the population as a whole. Viruses with beneficial mutations are able to survive and adapt to a new environment, thus generating new quasispecies. Adaptability is linked to four

closely related parameters: replication rate, viral load, genetic heterogeneity and viral fitness (Domingo *et al.*, 2012). This explains why some strains of HEV71 may rapidly adapt to growth under strong selective pressure of CHO cell passage whereas other strains do not.

In conclusion, the molecular basis of CHO cell-adaptation of HEV71 was investigated and characterised. Amino acid substitutions K^{149}→I or K^{149}→M located on the surface-exposed EF loop of VP2 were associated with CHO cell-adaptation. The CHO cell-adapted viruses and CDVs containing the CHO cell-adaptation markers enabled us to further select and construct viruses with increased virulence in mice, as reported in subsequent chapters of this thesis.

5. CHAPTER FIVE

MOUSE ADAPTATION OF A SUB-GENOGROUP B5 STRAIN OF HUMAN ENTEROVIRUS 71 IS ASSOCIATED WITH A NOVEL LYSINE TO GLUTAMIC ACID SUBSTITUTION AT POSITION 244 IN PROTEIN VP1

5.1. Introduction

A suitable animal model is required in order to perform clinically relevant pathogenesis investigations and HEV71 vaccine and therapeutic efficacy studies. Most HEV71 field isolates do not naturally infect mice, although a few mouse-virulent wild-type strains have been identified (Chang *et al.*, 2010). The mouse-virulence of one such mouse-virulent strain has been shown to depend on a single residue (C158) in the 5′ UTR IRES (Yeh *et al.*, 2011). However, the pathogenicity of mouse-virulent wild-type strains in mice does not correlate with their human pathogenicity (Chang *et al.*, 2010). A transgenic mouse expressing the human receptor for HEV71, SCARB2, has not yet been reported. IFNRI/II knockout mice have recently been shown to support infection of unadapted strains of HEV71 (Khong *et al.*, 2012). However, the use of immune knockout mice is of limited practical value for vaccine efficacy studies (Bek & McMinn, 2010).

Since humans are the only natural host of HEV71, it is necessary to adapt virus to growth in other species. Several studies have reported the development and pathologic characterisation of mouse-adapted HEV71 strains belonging to various sub-genogroups (Chen *et al.*, 2004; Chua *et al.*, 2008; Ong *et al.*, 2008; Wang *et al.*, 2011; Wang *et al.*, 2004). Molecular determinants of HEV71 mouse

virulence have been reported from several mouse-adapted viral models. A glycine (G) to glutamic acid (E) change at amino acid 145 in the VP1 capsid protein has been identified as the genetic determinant of mouse adaptation and virulence in two models (Arita *et al.*, 2008; Chua *et al.*, 2008). However, as the genetic determinants of mouse virulence have not been identified in several other reported mouse-adaptation models (Chen *et al.*, 2004; Ong *et al.*, 2008; Wang *et al.*, 2011; Wang *et al.*, 2004), the possibility remains that novel determinants of mouse adaptation and virulence are yet to be identified.

HEV71 strains belonging to sub-genogroup B5 have been isolated from recent HFMD outbreaks reported in Brunei and Malaysia (AbuBakar *et al.*, 2009; Chua *et al.*, 2007). In Chapter 4, we selected a CHO cell-adapted variant of a HEV71 strain belonging to sub-genogroup B5 by serial passages in CHO cells (Zaini *et al.*, 2012b). In this study, we further generated a mouse-virulent strain from the sub-genogroup B5 CHO cell-adapted strain, which is genetically distinct from previously published mouse-adapted HEV71 strains. We also determined the cell culture growth and mouse virulence phenotypes of this mouse-adapted virus and have rigorously identified the molecular determinants of mouse adaptation. Here we report the identification of a unique molecular determinant of HEV71 mouse adaptation and virulence. This work was recently published (Zaini *et al.*, 2012a) and a copy of the manuscript reprint is included in Appendix C.

5.2. Results

5.2.1. MP-B5 has increased virulence in newborn BALB/c mice

Previous work by Chua *et al*. (2008) demonstrated that prior CHO cell-adaptation of HEV71 was a necessary first step in the adaptation of HEV71 to growth in murine hosts. Consequently, in order to generate mouse-adapted HEV71-B5, we initially adapted parental HEV71-B5 to growth in CHO cells by serial passage (×4), as described in Chapter 4, to generate CHO-B5 (Zaini *et al.*, 2012b). Mouse-adaptation was initiated by inoculating two litters of 1-day-old BALB/c mice (n=9) by i.c. inoculation with 10 µL of CHO-B5 (10^5 $TCID_{50}$/dose). Two infected mice showed weakness in both hindlimbs at 6 days p.i. These mice were euthanased for brain and skeletal muscle tissue collection; the other seven infected mice remained healthy up to 14 days p.i. Subsequent mouse passages were carried out by i.c. inoculation with 10 µL of 10% (w/v) skeletal muscle homogenates from one of the symptomatic mice. Skeletal muscle homogenates were used for the subsequent mouse passages due to the presence of much higher viral titres compared to brain homogenates (data not shown). The mortality in mice increased rapidly from 22% to 100% between mouse passages 1 and 2, respectively, without a significant increase in the viral titre observed (Table 5.1). Virus from the fifth mouse passage was cultured twice on Vero cells to generate virus stocks , which were designated as MP-B5.

Our prior study of the mouse-adaptation of HEV71 (sub-genogroup B3) showed that mice infected with a lethal dose of mouse-adapted virus at 5-7 days of age survived until day 5 p.i. and mortality reached 100% by day 8 p.i. Mice at 14 days of age and older were completely resistant to mouse-adapted HEV71 infection

(Chua *et al.*, 2008). We also have previously investigated oral infection of mice with mouse-adapted HEV71 and found that BALB/c mice are susceptible to infection via the oral route in an age- and dose-dependent manner, although the HD_{50} values after oral infection are $>10^3$-fold higher than infection via i.p. inoculation. Thus, for practical reasons, mice were inoculated at five-days-of-age via the i.p. route of infection in all of our subsequent experiments.

We next determined the HD_{50} value of MP-B5 by i.p. inoculation of serial dilutions of virus in six groups of 5-day-old BALB/c mice. After infecting or mock-infecting mice with serial dilutions of MP-B5, the mice were observed twice daily for clinical signs of illness for 14 days p.i. The majority of mice infected with the highest virus dose (8.7×10^4 $TCID_{50}$) developed forelimb and/or hindlimb flaccid paralysis, atonic bladder, ruffled fur, weight loss and severe lethargy after three days p.i. (Figure 5.1). Several infected mice also showed erythematous lesions on the soles of the paws, which are in a similar position to HFMD lesions observed in humans. Infected mice were euthanased upon reaching clinical grade 3 paralysis (refer to Table 2.16 for clinical grading scale). A mortality rate of 100% was observed at virus doses greater than 8.7×10^1 $TCID_{50}$ (Table 5.2). All mock-infected mice survived beyond 14 days p.i. The HD_{50} value of MP-B5 was determined as 2.4×10^1 $TCID_{50}$.

Table 5.1 Mouse-adaptation of CHO-B5 by serial passage in 1-day-old BALB/c mice

Mouse passage number	Skeletal muscle viral titre ($TCID_{50}$ g^{-1})	Mortality (%)
1	5.2×10^{4}	22
2	1.2×10^{4}	100
3	3.2×10^{5}	100
4	2.7×10^{4}	100
5	3.0×10^{4}	100

Table 5.2 Percentage (%) mortality in 5-day-old BALB/c mice after MP-B5 infection

Mortality (%) at the indicated virus dose ($TCID_{50}$)						HD_{50} ($TCID_{50}$)*
8.7×10^{-1}	8.7×10^{0}	8.7×10^{1}	8.7×10^{2}	8.7×10^{3}	8.7×10^{4}	
0	25	83.3	100	100	100	2.4×10^{1}

* HD_{50} values were determined by the method of Reed & Muench (1938)

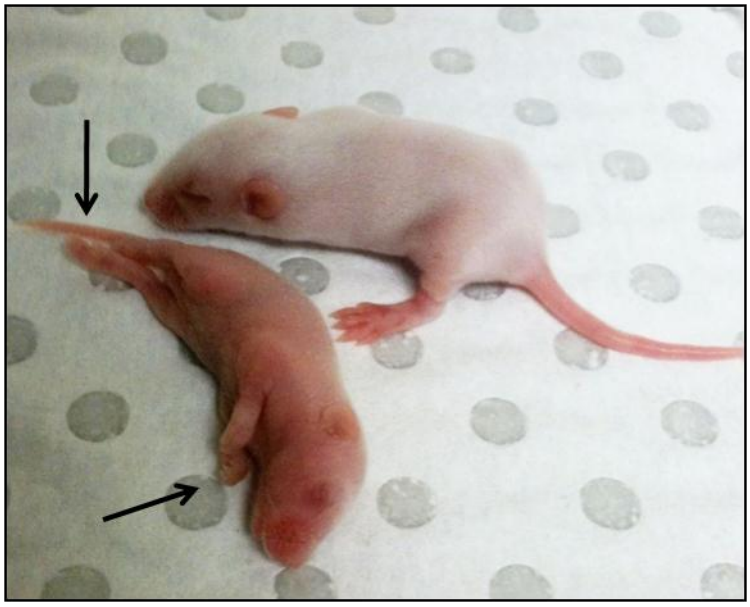

Figure 5.1 MP-B5-infected (left) and mock-infected (right) BALB/c mice four days after i.p. infection with a lethal dose of MP-B5. Hindlimb and forelimb flaccid paralysis (arrows) were observed only in the MP-B5 infected mice; mock-infected mice remained healthy throughout the 14 day observation period.

5.2.2. Susceptibility of infant BALB/c mice to infection with MP-B5

To further characterise the virulence of MP-B5, we next performed a survival analysis study in order to determine if host susceptibility to MP-B5 was dose-dependent. We infected groups of twelve to fifteen 5-day-old BALB/c mice i.p. with $10\times HD_{50}$, $10^2\times HD_{50}$ or $10^3\times HD_{50}$ MP-B5, respectively. Mice were observed twice daily for 14 days p.i. and the percentage (%) survival was calculated for each group. Mice infected at a dose of $10^3\times HD_{50}$ showed 100% mortality, with death commencing at four days p.i. and reaching 100% by five days p.i. Death of mice infected at a dose of $10^2\times HD_{50}$ commenced at five days p.i. and reached 100% mortality by seven days p.i. Mice infected at a dose of $10\times HD_{50}$ reached 80% mortality with death commencing at six days p.i. (Figure 5.2). All mock-infected mice survived beyond 14 days p.i., with no clinically-apparent disease observed. All MP-B5-infected mice showed similar clinical signs of infection (forelimb and/or hindlimb flaccid paralysis, ruffled fur, weight loss and severe lethargy) irrespective of the virus inoculation dose. These data indicate that MP-B5 induces fatal disease in five-day-old BALB/c mice in a dose-dependent manner when infected via the i.p. route.

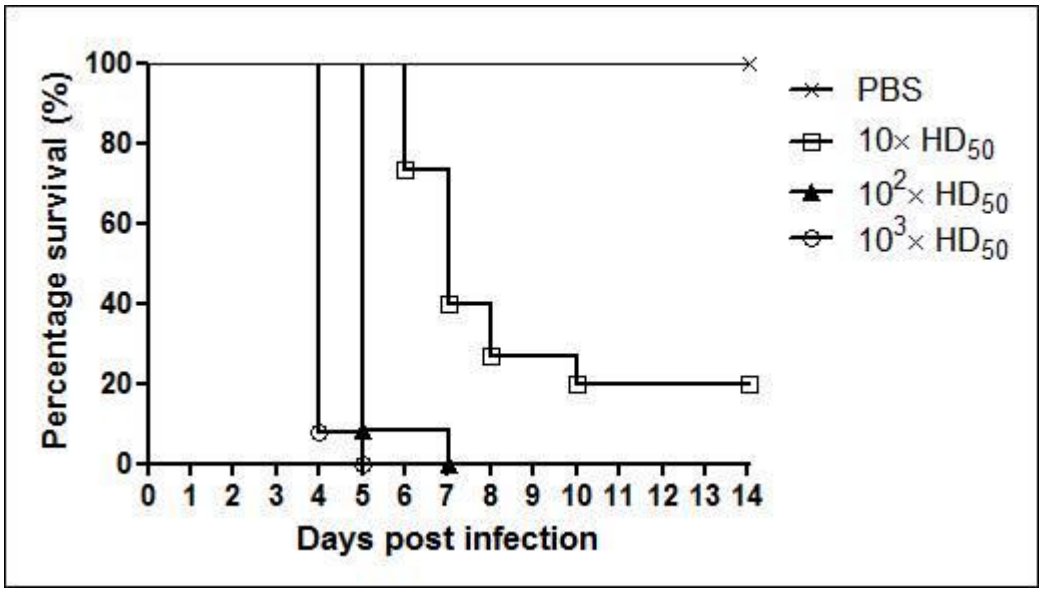

Figure 5.2 Survival of 5-day-old BALB/c mice infected with MP-B5 by i.p. inoculation. Kaplan-Meier plots show survival after challenge with 10×, 10^2× and 10^3× HD_{50} of MP-B5, respectively.

5.2.3. Tissue distribution and histopathological changes in mice infected with MP-B5

In order to investigate the tissue tropism of MP-B5, the tissue distribution of virus in infected host tissues was examined. Groups of twelve 5-day-old BALB/c mice were inoculated i.p. with $10^2 \times HD_{50}$ of MP-B5. Whole blood and tissue samples including heart, liver, spleen, skeletal muscle and brain from three infected mice were collected at one, three and five days p.i. and virus titres determined by $TCID_{50}$ assay on Vero cells. Virus infectivity was detected in the spleen, liver and skeletal muscle at one day p.i. (Figure 5.3). Virus first appeared in heart muscle at three days p.i. and was consistently detected in high titre in skeletal muscle, peaking at $>10^4$ $TCID_{50}$ g^{-1} at five days p.i., indicating that muscle and/or connective tissue is the primary site of MP-B5 infection in mice. All MP-B5-infected mice developed flaccid limb paralysis by four days p.i. Viraemia was not observed at any time point and virus was not detected in the brain in any of the mice examined.

We next examined the histopathological changes occurring in the tissues of MP-B5-infected mice. Groups of twelve 5-day-old BALB/c mice were inoculated i.p. with $10^2 \times HD_{50}$ of MP-B5. Brain, spinal cord and skeletal muscle tissue was collected from three infected mice showing clinical grade 3 paralysis (5-6 days p.i.). The spinal cord sections spanned cervical, thoracic and lumbar sections. The most notable histopathological changes observed in the MP-B5-infected mice were in skeletal muscle tissue sections (Figure 5.4). Neutrophil infiltration and myocyte necrosis, indicating the presence of severe myositis, was observed in all skeletal muscle sections examined. This finding is consistent with that of the

tissue distribution analysis (Figure 5.3), in which high viral titres were observed in skeletal muscle tissues of MP-B5-infected mice. Although myositis was observed in the muscle tissue surrounding the spinal cord sections, no significant foci of inflammation were observed in the brain and spinal cord sections of any MP-B5-infected mice (Figure 5.4). Furthermore, no histological abnormalities were detected in the tissues of any mock-infected mice (Figure 5.4).

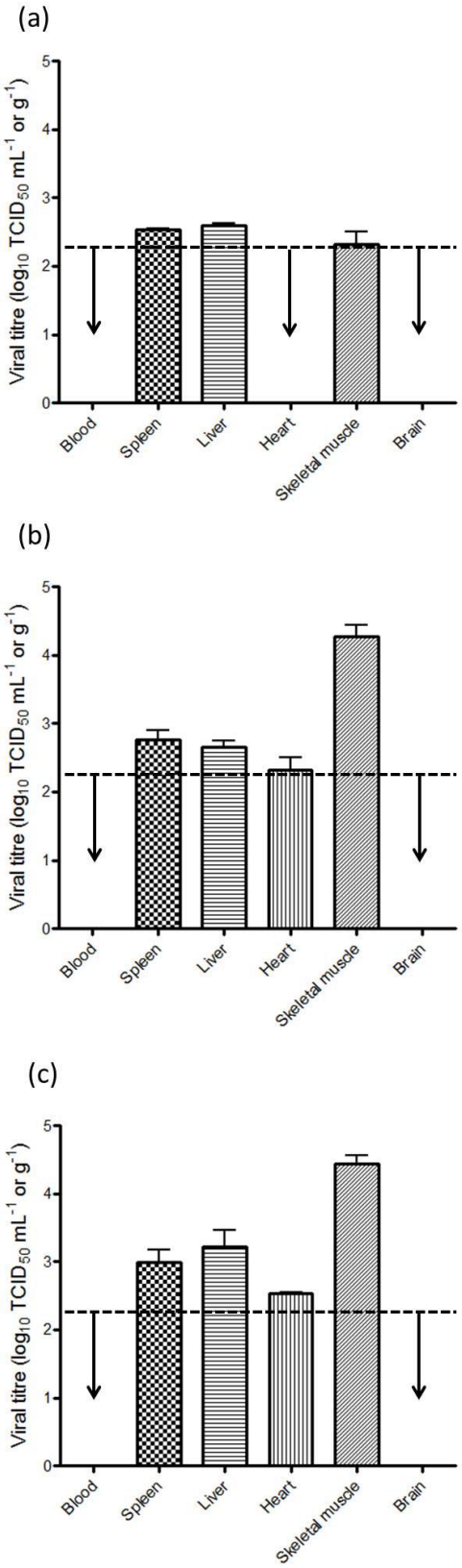

Figure 5.3 Viral loads in selected tissues of 5-day-old BALB/c mice at (a) 1 day, (b) 3 days, (c) 5 days p.i. after i.p. challenge with $10^2 \times HD_{50}$ of MP-B5. Viral titres

in blood were determined as $TCID_{50}$ mL^{-1}. Viral titres in tissue homogenates were determined as $TCID_{50}$ g^{-1}. Each time point represents the mean tissue titre of three mice; error bars represent SEM. Dashed line indicates the detection limit of virus titration by $TCID_{50}$ assay (log_{10} 2.2 $TCID_{50}$) and arrows indicates samples with titres below the limit of detection.

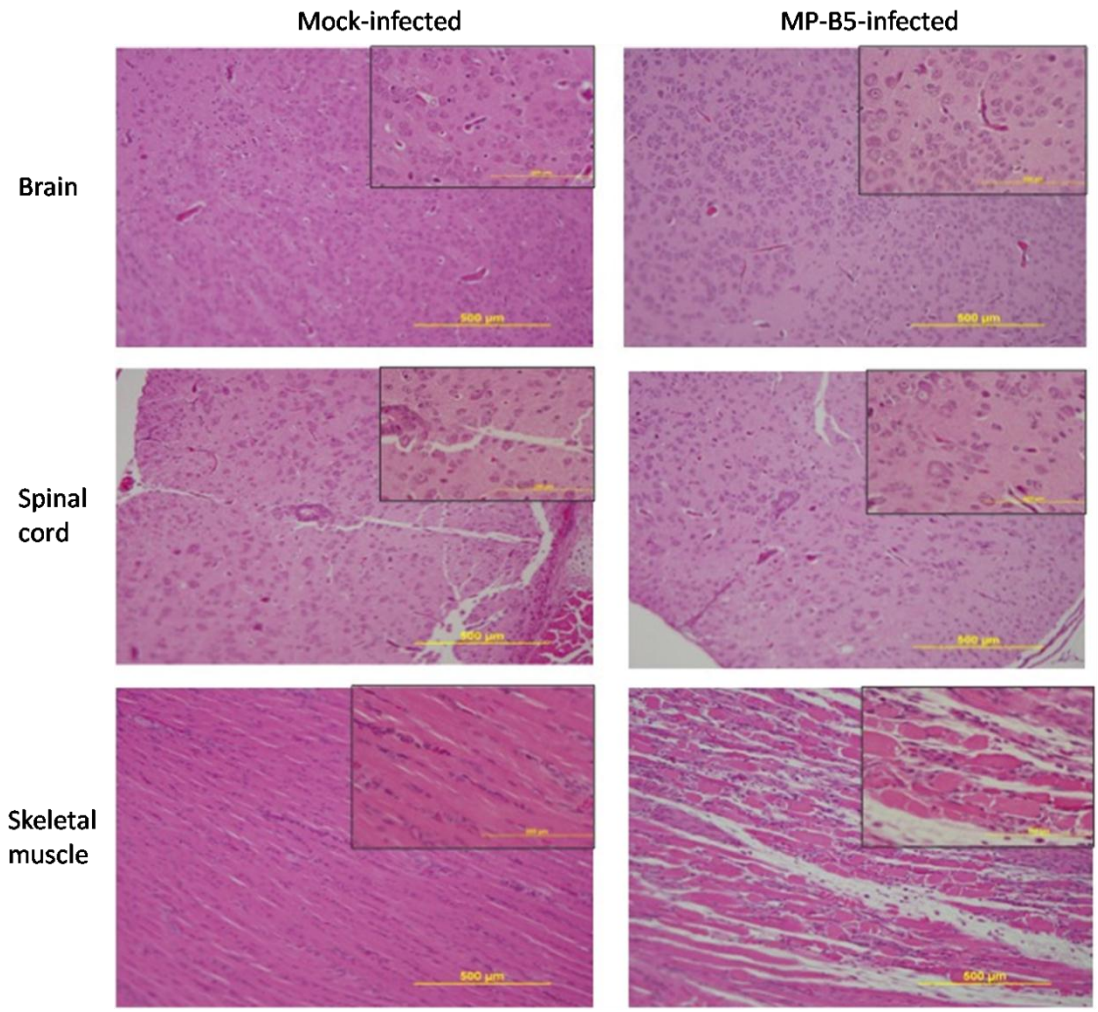

Figure 5.4 Histological analysis of MP-B5 infection in 5-day-old BALB/c mice. Groups of twelve 5-day-old BALB/c mice were inoculated i.p. with $10^2 \times HD_{50}$ of MP-B5. Three mice showing clinical grade 3 paralysis (5-6 days p.i.) were sacrificed and tissues collected. In MP-B5-infected tissues (right column), severe myositis is present in all skeletal muscle tissues examined. No histological abnormalities were observed in any brain or spinal cord sections of B5-MP-infected mice. Mock-infected tissues are shown in the left column. Observations were made at a magnification of ×10. Insets at the top right corners are observations made at ×40 magnification.

5.2.4. Sequence comparison of HEV71-B5, CHO-B5 and MP-B5

In order to identify the genetic changes associated with the virulent phenotype of MP-B5 in BALB/c mice, the complete genome nucleotide and deduced amino acid sequences of MP-B5 was determined and compared to HEV71-B5 and CHO-B5 (Table 5.3). The complete genomic sequence of MP-B5 is included in Appendix A of this thesis and the annotated complete genome sequences of this strain have been deposited to GenBank sequence database (GenBank ID: JQ724182). Both CHO-B5 and MP-B5 shared more than 99% nucleotide and amino acid identity to wild-type HEV71-B5, indicating a close genetic relationship between these variants, consistent with the limited mouse passaging undertaken during the selection of MP-B5. Comparison of the HEV71-B5 and CHO-B5 sequences revealed one nucleotide difference located in the virus ORF, resulting in a change in the deduced amino acid sequence in VP2 (K^{149}→I) (Zaini *et al.*, 2012b). Mutation in VP2 at amino acid position 149 has previously been shown to be the sole genetic determinant of the CHO cell growth-adapted phenotype (Chapter 4) (Zaini *et al.*, 2012b). Five additional nucleotide sequence changes were identified in MP-B5, two of which are located in the 5′ UTR and the three within the ORF. Two of the ORF mutations resulted in deduced amino acid changes in the capsid protein VP1: S^{241}→L and K^{244}→E; the third ORF mutation was a synonymous C→T change at nucleotide position 6072 within the 3D polymerase gene (Table 5.3).

Table 5.3 Nucleotide and amino acid changes identified in the genomes of wild-type HEV71-B5, CHO-B5 and MP-B5

Region	Nucleotide sequence				Deduced amino acid sequence			
	Position	HEV71-B5	CHO-B5	MP-B5	Position	HEV71-B5	CHO-B5	MP-B5
5′ UTR	345	A	A	G				
	601	C	C	T				
VP2	1400	A	T	T	149	K	I	I
VP1	3164	C	C	T	241	S	S	L
	3172	A	A	G	244	K	K	E
3D	7062	C	C	T	374	F	F	F

5.2.5. Phenotypic characterisation of CHO-B5 and MP-B5

In order to determine whether a more efficient replication phenotype contributed to the increased virulence of MP-B5 in mice, the growth kinetics of both viruses were investigated in both RD and CHO cells. RD and CHO cell monolayers in 24-well tissue culture trays were infected with CHO-B5 or MP-B5 (MOI = 5). Viruses were harvested at 4 h intervals for 24 h and the yields quantified by $TCID_{50}$ assay on Vero cells. Both CHO-B5 and MP-B5 showed similar growth kinetics in RD and CHO cells (p>0.05). In RD cells both CHO-B5 and MP-B5 had a lag phase of approximately 4 h p.i., with titres rising thereafter and peaking at 12 h p.i. (Figure 5.5a). In CHO cells, both viruses had a longer lag phase of up to 8 h p.i. and virus titre reached plateau at 24 h p.i. (Figure 5.5b). Both CHO-B5 and MP-B5 appeared to replicate efficiently in both RD and CHO cells indicating that their efficient growth in cell culture is not a contributing factor to the greater virulence of MP-B5 in mice.

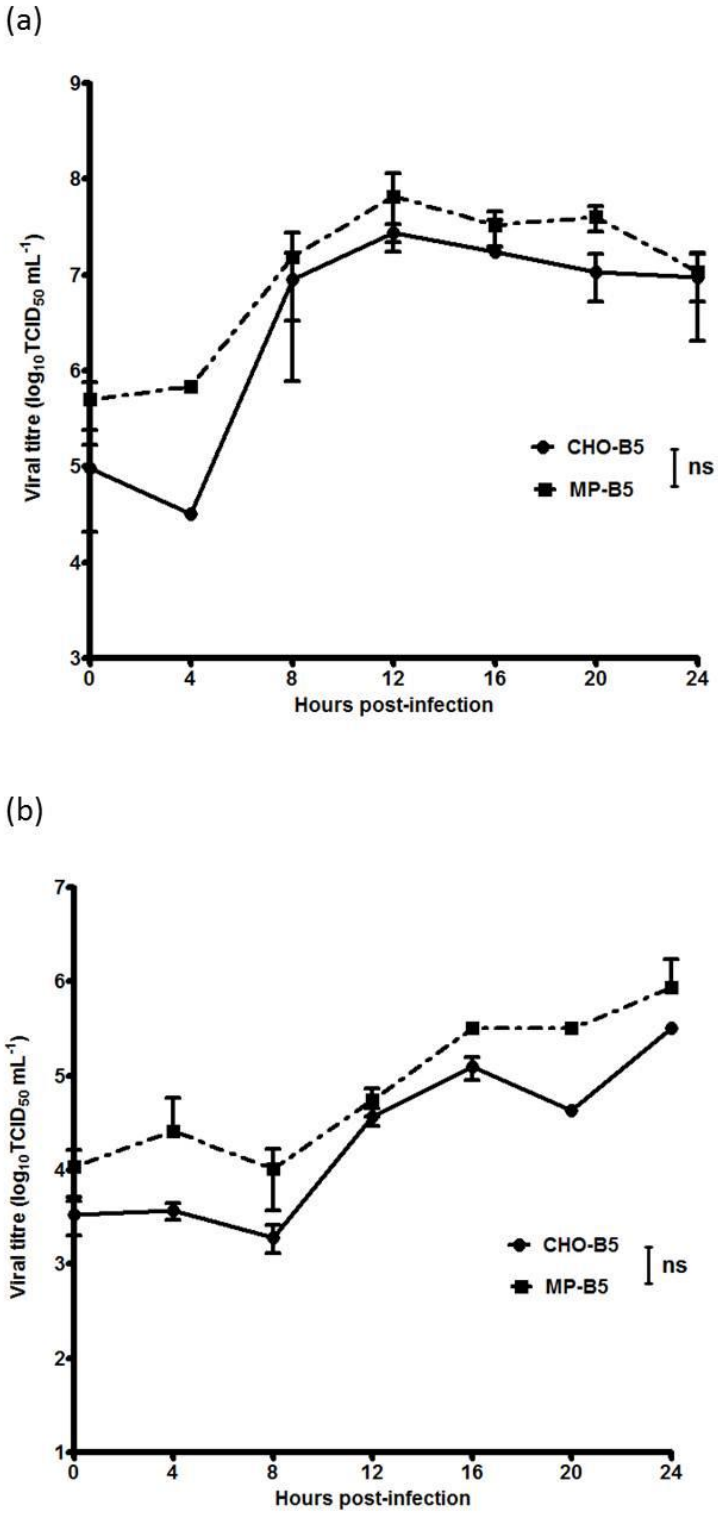

Figure 5.5 Replication kinetics of the CHO-B5 and MP-B5 in (a) RD, (b) CHO cells. Cell monolayers were infected at a MOI of 5×$TCID_{50}$/cell. Cell culture supernatants were collected at the times indicated. Samples at each time point

were freeze-thawed three times and clarified by centrifugation prior to determination of virus titres by $TCID_{50}$ assay. All assays were performed in duplicate. At each time point, the titres are means of two samples; error bars represent SEM. The Mann-Whitney test was used to compare the titres between the two growth curves; ns denotes significance value of $p>0.05$.

5.2.6. Construction of full-length infectious cDNA clone containing the VP1 protein mutations identified in MP-B5

In order to identify which of the mutations identified in MP-B5 were associated with the increased mouse virulence of MP-B5, we attempted to construct a full-length infectious cDNA clone of the parental virus, HEV71-B5 (Chapter 3). However, despite several attempts, we were unable to recover infectious virus from several full-length cDNA clones. However, we have previously constructed a full-length infectious cDNA clone of a sub-genogroup B3 strain of HEV71 (HEV71-26M) (Chua *et al.*, 2008). We have also previously constructed a full-length infectious cDNA clone of HEV71-26M containing the CHO cell growth marker, VP2-K^{149}→I (CHO-26M) (Chua *et al.*, 2008). The genomes of HEV71-26M and HEV71-B5 share 87.2% nucleotide and 97.7% amino acid identity and both belong to genogroup B. From previous work, we know that it is not possible to obtain stable CDV populations that contain only the VP1 mouse adaptation mutations and that the CHO-adaptation mutation, VP2-K^{149}→I, appears to increase the stability of the VP1 mouse adaptation mutations (Chua *et al.*, 2008). Sequence analysis also revealed that CHO-26M has the same amino acid residues as CHO-B5 at positions 241 and 244 of the VP1 gene. Consequently, we decided to use the full-length infectious cDNA clone of CHO-26M as the parental clone for further genetic manipulation.

In order to determine if one or both of the two amino acid mutations in VP1 was responsible for the mouse adaptation and virulence of MP-B5, we investigated the effects of the two ORF mutations by constructing three variants containing either a single or both mutations in the VP1 gene. The VP1 mutations S^{241}→L,

K^{244}→E and a combination of both mutations were introduced into the CHO-26M full-length clone by site-directed mutagenesis of the CHO-26M VP1 gene, generating variants CHO-26M-VP1-S241L, CHO-26M-VP1-K244E and CHO-26M-VP1 (containing both VP1 mutations), respectively (Figure 5.6).

A single clone of each mutant was selected and purified plasmid DNA prepared for sequence analysis. VP1 gene RT-PCR and nucleotide sequencing was undertaken to ensure that the site-specific changes were present in the mutated clones. MP-B5 also contains two mutations in the 5′ UTR, at nucleotide positions 345 and 601 of SLD IV and VI, respectively. Nucleotides at these positions are conserved amongst HEV71 strains, including HEV71-26M and HEV71-B5. We determined that the 5′ UTR mutations observed in MP-B5 do not cause alterations in predicted RNA secondary structures (Figure 5.7). Furthermore, although both nucleotide changes in the 5′ UTR are located within the IRES, they are not located within known 5′ UTR mutation "hotspots" that may influence the virulence of HEV71 (Wang *et al.*, 2004; Yeh *et al.*, 2011). Given this, the 5′ UTR mutations in MP-B5 were not investigated further.

We successfully recovered CDVs from transfected cells at two days post-transfection. The CDVs were passaged twice on Vero cells in order to generate high titre working stocks. CDV stocks were found to have viral titres of $>10^6$ $TCID_{50}$ mL^{-1}. It is possible that the amino acid substitutions introduced during mouse-adaptation may revert to that of parental virus during primate or human cell culture passage, as was observed by Chua *et al.* (2008) and Jia *et al.* (2001). Consequently, we investigated the stability of the introduced mutations during

Vero cell culture passage by examining the VP1 (S^{241}→L) and VP1 (K^{244}→E) nucleotide sequences of the CDVs at Vero cell passage levels 1 and 2. The VP1 gene of the CDV stocks was amplified by RT-PCR and their nucleotide sequences determined. The VP1 (S^{241}→L) mutation was retained during the two passages in Vero cells for both CHO-26M-VP1-S241L-CDV and CHO-26M-VP1-CDV (Figure 5.8). By contrast, the VP1 (K^{244}→E) mutation reverted to the wild-type sequence by the second Vero cell passage in both CHO-26M-VP1-K244E-CDV and CHO-26M-VP1-CDV. Therefore, we chose to use CDV only from Vero cell passage one for our mouse virulence studies, as the VP1 (K^{244}→E) mutation was retained in the mutant CDVs at this passage level.

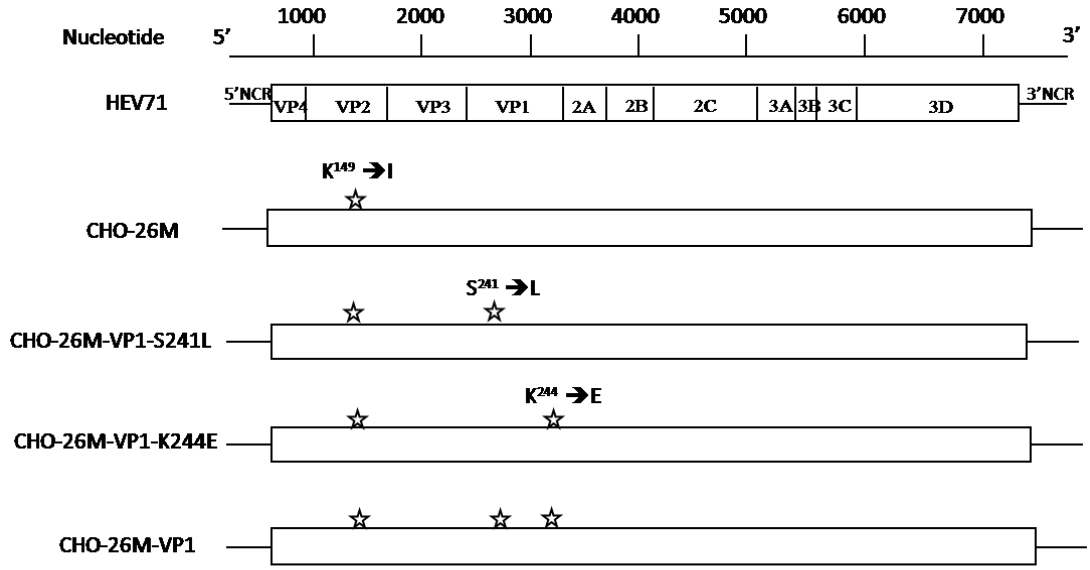

Figure 5.6 Schematic representation of the infectious cDNA clones of CHO-26M and cDNA clones containing VP1 mutations constructed by site-directed mutagenesis. Genome maps of parental and mutant CHO-26M are represented as an open box, with individual genes and non-coding regions indicated for HEV71. Amino acid mutations introduced in CHO-26M-VP1-S241L (VP1, S^{241}→L), CHO-26M-VP1-K244E (VP1, K^{244}→E) and CHO-26M-VP1 (double mutant VP1, S^{241}→L and K^{244}→E) are shown as open stars.

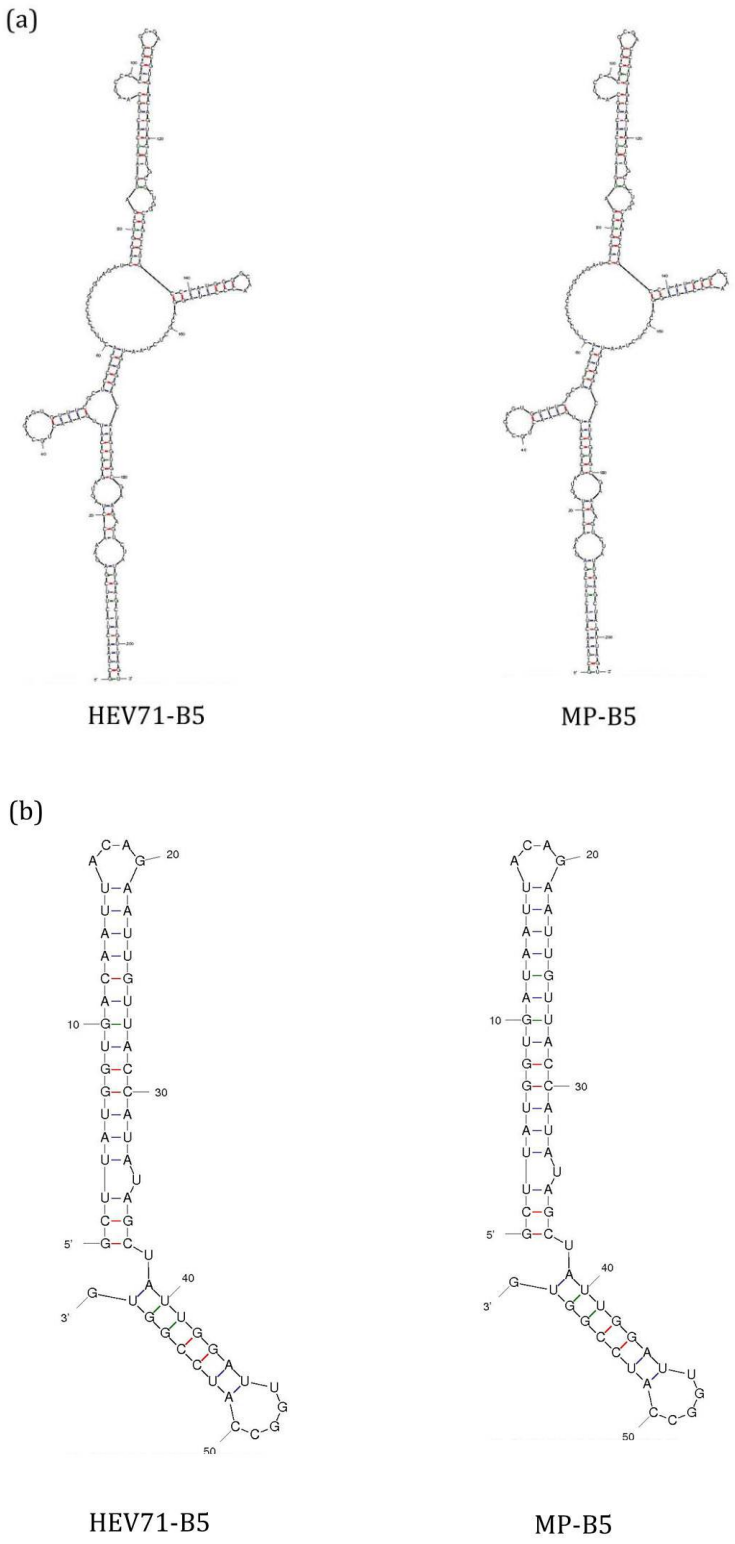

Figure 5.7 The predicted 5′ UTR SLDs; (a) SLD IV and (b) SLD VI of HEV71-B5 and MP-B5. The structure of each SLD was predicted using MFOLD web server.

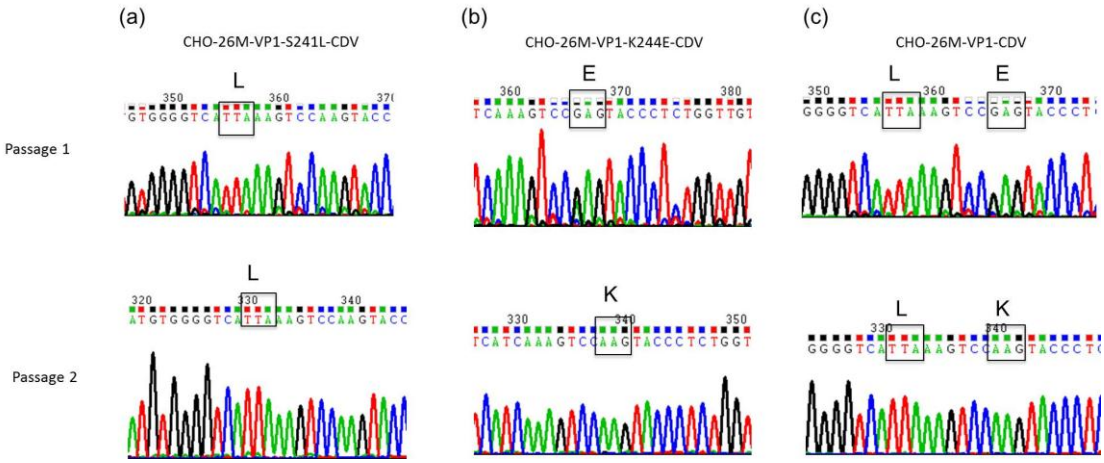

Figure 5.8 Stability of introduced VP1 mutations during cell culture passage: (a) S^{241}→L, (b) K^{244}→E, (c) double mutant S^{241}→L and K^{244}→E. Infectious cDNA clone-derived virus populations were passaged twice in Vero cells and viral RNA was extracted from culture supernatants collected at each passage level. The VP1 gene was amplified by RT-PCR and their nucleotide sequences determined. The open box indicates the nucleotide sequence of the site-specific change and the deduced amino acid residue is indicated above the box.

5.2.7. An amino acid substitution in VP1 (K^{244}→E) is solely responsible for mouse adaptation and virulence

We next performed mouse virulence assays to compare the survival of 5 day-old BALB/c mice after i.p. inoculation with the parental or mutant CDVs. Groups of twelve to fifteen 5 day-old BALB/c mice were infected with approximately 10^4 $TCID_{50}$ of each CDV population and were then observed for 14 days p.i. As expected, the parental CHO-26M-CDV virus population caused no observable morbidity or mortality in infected mice (Figure 5.9). CHO-26M-VP1-S241L-CDV also exhibited a non-virulent phenotype in mice, with no observable clinical signs of infection or mortality up to 14 days p.i., similar to the parental virus (p>0.05). By contrast, the two mutant CDV populations that contained either the VP1 alone or in combination with the VP1 (S^{241}→L) change, CHO-26M-VP1-K244E-CDV and CHO-26M-VP1-CDV, caused 100% mortality in infected mice with a mean survival time of 3.1 (± 0.3) and 3.0 (± 0.0) days p.i., respectively.

We next determined HD_{50} values of the parental and mutant viruses by infecting groups of six 5-day-old BALB/c mice i.p. with serial 10-fold dilutions of virus. The HD_{50} values of CHO-26M-VP1-K244E-CDV and CHO-26M-VP1-CDV were determined to be 7.5×10^{-1} $TCID_{50}$ and 4.8×10^{-1} $TCID_{50,}$ respectively (Table 5.4). This demonstrates that an amino acid substitution in VP1 (K^{244}→E) is alone sufficient to confer the mouse virulent phenotype upon clone-derived CHO-26M and thus is likely to be the critical molecular determinant of mouse virulence in our mouse-adapted virus MP-B5.

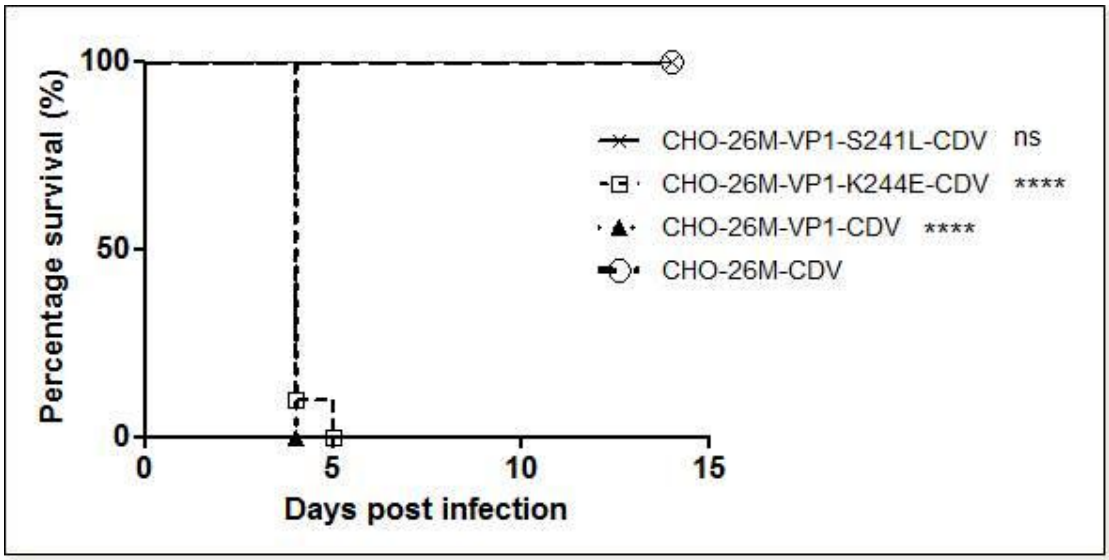

Figure 5.9 Survival of 5-day-old BALB/c mice infected i.p. with parental and mutant viruses. Kaplan-Meier plots show survival after challenge with CHO-26M-VP1-S241L-CDV, CHO-26M-VP1-K244E-CDV, CHO-26M-VP1-CDV or parental CHO-26M-CDV. The Mantel-Cox Log-rank test was used to compare the survival of mutant virus-infected pups to parental CHO-26M-CDV-infected pups at 14 days p.i. **** denotes significance value $p<0.0001$ and ns denotes significance value $p>0.05$.

Table 5.4 Mortality profile, mean survival time and HD_{50} values after challenge with serial 10-fold dilutions of the parental or mutant viruses

Virus	Mortality (%)	Mean survival time (days ± SEM)	HD_{50} ($TCID_{50}$)*
CHO-26M-CDV	0	>14	$> 10^4$
CHO-26M-VP1-S241L-CDV	0	>14	$> 10^4$
CHO-26M-VP1-K244E-CDV	100	3.1 ± 0.3	7.5×10^{-1}
CHO-26M-VP1-CDV	100	3.0 ± 0.0	4.8×10^{-1}

* HD_{50} values were determined by the method of Reed & Muench (1938)

5.2.8. Tissue distribution and histopathologic changes in mice infected with CHO-26M-VP1-K244E-CDV

Since our HEV71 sub-genogroup B5 marker of mouse virulence, VP1-244E, was investigated on the background of HEV71 sub-genogroup B3 clone, it was of interest to further analyse the infectivity pattern of CHO-26M-VP1-K244E-CDV in mice and compare it to that of MP-B5. We investigated the tissue distribution of CHO-26M-VP1-K244E-CDV in infected mouse tissues. Groups of twelve 5-day-old BALB/c mice were inoculated i.p. with $10^2 \times HD_{50}$ of CHO-26M-VP1-K244E-CDV. Three infected mice showing clinical grade 3 paralysis (at five days p.i.) were sacrificed, perfused, tissues collected and viral titres determined. Virus infectivity was detected in the spleen, liver, heart and skeletal muscle (Figure 5.10). The virus was detected in high titre in skeletal muscle, with a titre $>10^4$ $TCID_{50}$ g^{-1}, indicating that muscle and/or connective tissue is the primary site of CHO-26M-VP1-K244E-CDV in mice, similar to that observed for MP-B5 virus. The lack of viraemia and absence of virus in the brain was also similar to our earlier finding for MP-B5 virus. We also recovered viral genomic RNA from the skeletal muscle homogenate, which was amplified by RT-PCR using primers specific for the VP2 and VP1 genes and the amplicons sequenced. We confirmed that the VP2-149I and VP1-244E mutations persisted after passage in BALB/c mice (Figure 5.11).

We next examined the histopathological changes occurring in the tissues of CHO-26M-VP1-K244E-CDV-infected mice. Groups of twelve 5-day-old BALB/c mice were inoculated i.p. with $10^2 \times HD_{50}$ of CHO-26M-VP1-K244E-CDV. Brain, spinal cord and skeletal muscle tissue was collected from three infected mice showing

clinical grade 3 paralysis (5-6 days p.i.) The most notable histopathological changes observed in the infected mice were in skeletal muscle tissue sections (Figure 5.12). As with MP-B5, severe inflammatory myositis was observed in all skeletal muscle sections examined and no significant foci of inflammation were observed in the brain and spinal cord sections (cervical and lumbar) of any CHO-26M-VP1-K244E-CDV-infected mice.

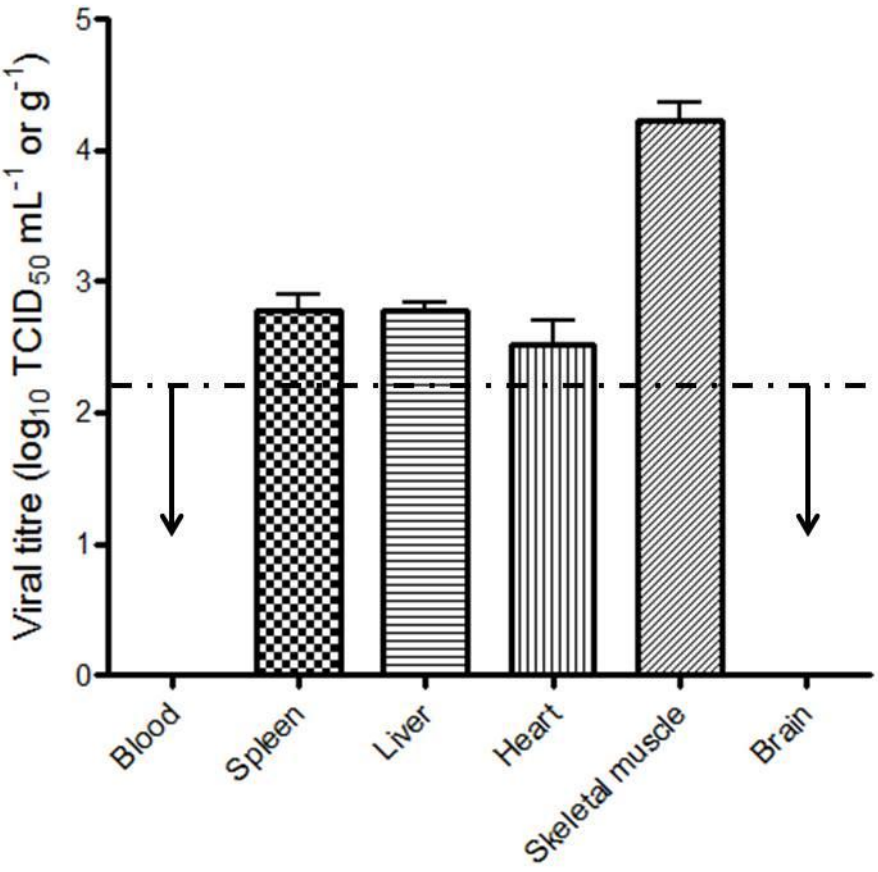

Figure 5.10 Viral loads in selected tissues of 5-day-old BALB/c mice at 5 days p.i. after i.p. challenge with $10^2 \times HD_{50}$ of CHO-26M-VP1-K244E-CDV. Viral titres in blood were determined as $TCID_{50}$ mL^{-1} and viral titres in tissue homogenates were determined as $TCID_{50}$ g^{-1}. Each time point represents the mean tissue titre of three mice; error bars represent SEM. Dashed line indicates the detection limit of virus titration by $TCID_{50}$ assay (log_{10} 2.2 $TCID_{50}$) and arrows indicates samples with titres below the limit of detection.

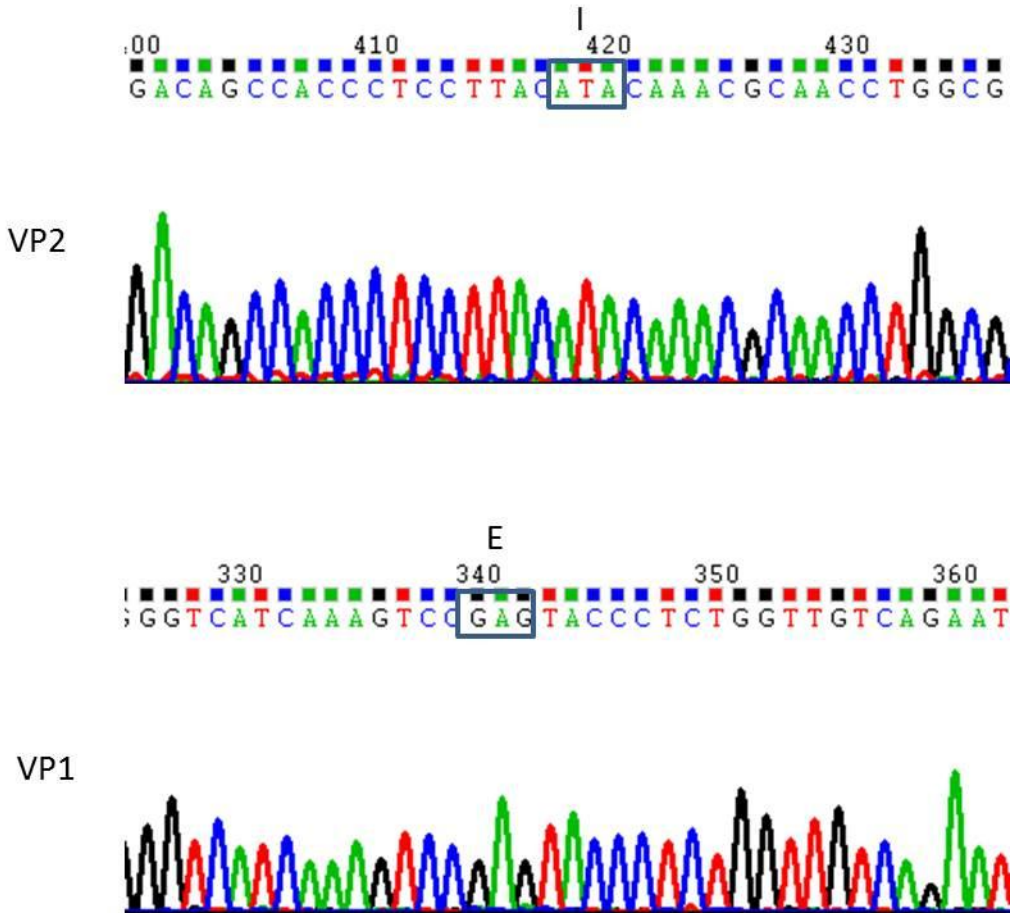

Figure 5.11 Stability of VP2-149I and VP1-244E mutation after passage of CHO-26M-VP1-K244E-CDV in BALB/c mice. Viral RNA was extracted from skeletal muscle homogenates. The VP2 and VP1 gene was amplified by RT-PCR and their nucleotide sequences determined. The open box indicates the nucleotide sequence of the mutation site and the deduced amino acid residue is indicated above the box.

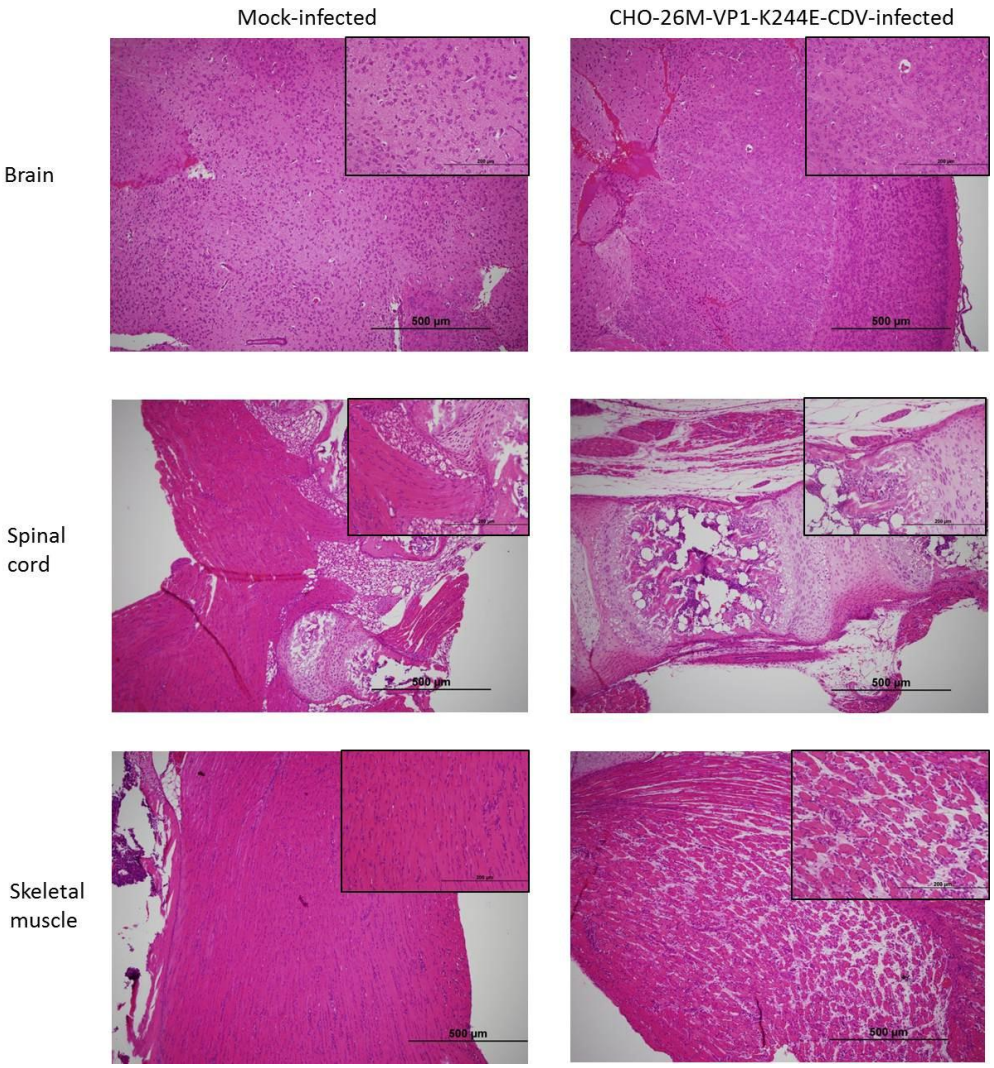

Figure 5.12 Histological analysis of CHO-26M-VP1-K244E-CDV infection in 5-day-old BALB/c mice. Groups of twelve 5-day-old BALB/c mice were inoculated i.p. with $10^2 \times HD_{50}$ of CHO-26M-VP1-K244E-CDV. Three mice showing clinical grade 3 paralysis (at 5-6 days p.i.) were sacrificed and tissues collected. In MP-B5-infected tissues (right column), myositis is present in all skeletal muscle tissues examined. No histological abnormalities were observed in any brain or spinal cord sections of CHO-26M-VP1-K244E-CDV-infected mice. Mock-infected tissues are shown in the left column. Observations were made at a magnification of ×10. Insets at the top right corners are observations made at ×40 magnification.

5.2.9. The VP1 (K^{244}→E) mouse virulent marker is located in the HI loop

In order to identify the location of the VP1 (K^{244}→E) mouse virulence marker on the VP1 protein, the three-dimensional structure of the VP1 protein of HEV71-B5 was predicted by homology modeling. The most closely related VP1 gene to that of HEV71 by primary sequence and for which there is structural data is BEV. The amino acid sequence identity between the HEV71-B5 and BEV VP1 proteins is 41%. The known crystallographic structure of the BEV VP1 capsid protein (PDB number: 1BEV_1) was thus used to predict the location of amino acid 244 on the three-dimensional structure of the HEV71 VP1 capsid protein. Amino acid 244 is predicted to be located in the surface-exposed HI loop of the VP1 protein (Figure 5.13a). The basic polar lysine found in HEV71-B5 (Figure 5.13b) was substituted with an acidic polar glutamic acid in MP-B5 (Figure 5.13c). Another reported molecular determinant for HEV71 mouse virulence, VP1-G^{145}→E, was predicted to be located on the surface-exposed DE loop of VP1 (Chua *et al.*, 2008). We mapped both amino acid residue 244 and 145 on our homology model to determine if these two residues are in close proximity on the VP1 three-dimensional structure. Both mouse virulent markers are located on the loop at the outward-facing end of the β sheet and are closely adjacent to one another (Figure 5.13d).

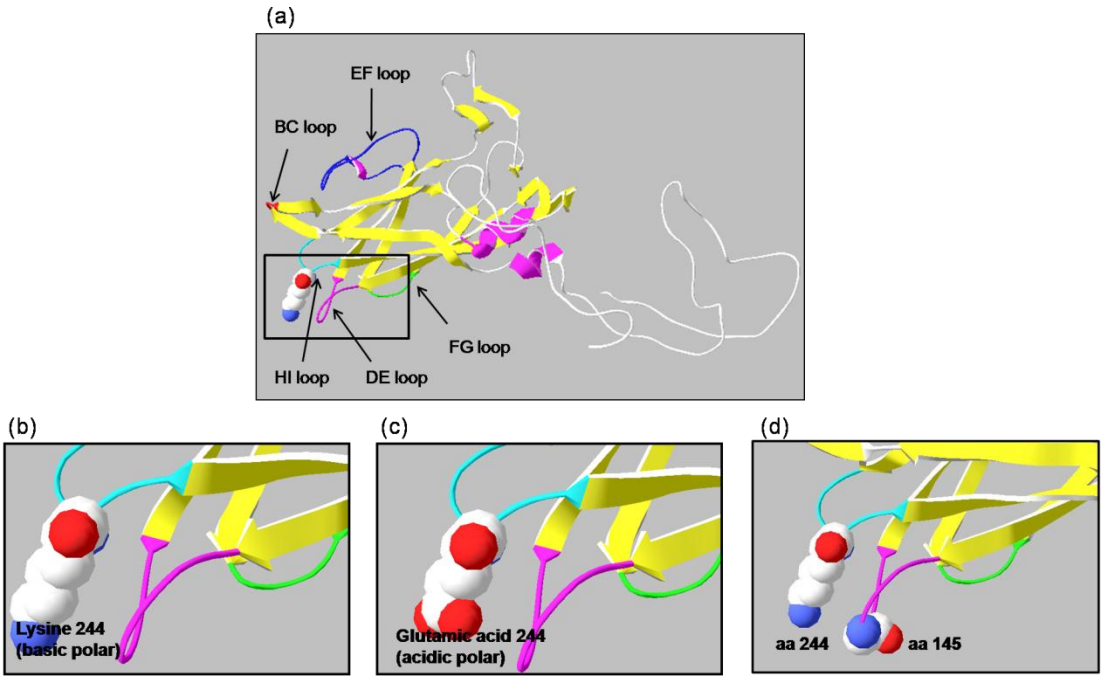

Figure 5.13 Homology models showing the predicted three-dimensional structure of (a) the HEV71-B5 VP1 protein, with amino acid residue 244 located on the surface-exposed HI loop; (b) the HEV71-B5 VP1 protein (enlarged image), with lysine at amino acid position 244; (c) the MP-B5 VP1 protein (enlarged image), with glutamic acid (acidic polar) at amino acid residue 244;(d) the HEV71-B5 VP1 protein (enlarged image), with amino acid residue 244 and 145 located on the surface-exposed HI and DE loop of VP1, respectively. The HEV71 VP1 homology model is based on the known three-dimensional crystallographic structure of bovine enterovirus (BEV) VP1 capsid protein (PDB number: 1BEV_1). Amino acid residues 244 and 145 of VP1 are displayed as a space-fill models and each individual loop is shown by arrows.

5.3. Discussion

In this study, we have selected a mouse-adapted HEV71 strain (MP-B5) belonging to sub-genogroup B5. The mouse-adapted strain was selected by serial passage of parental virus in CHO cells and in newborn BALB/c mice. Newborn BALB/c mice infected i.p. with MP-B5 developed severe disease in a dose-dependent manner. Skeletal muscle is the primary site of MP-B5 replication in mice. Histological analysis of skeletal muscle showed that infection with the mouse-adapted virus induced severe inflammatory myositis. No histological abnormalities were observed in the brain or spinal cords of any MP-B5-infected mice. The presence of myositis in MP-B5-infected mice and a lack of evidence of CNS disease suggest that the observed limb flaccid paralysis was due primarily to severe inflammatory myositis. In a related study, Chua *et al*. (2008) found that the primary site of infection by mouse-adapted HEV71 in mice was skeletal muscle and that the cause of death was severe inflammatory myositis, regardless of route of virus inoculation. Chua *et al*. (2008) also showed that viral titres in the muscle tissue of mouse-adapted virus-infected mice were $>10^3$-fold higher than in any other tissues examined (including viraemia). The lack of viraemia observed in our study may be due to the lower sensitivity of the $TCID_{50}$ assay compared to that of Chua *et al*. (2008), such that any virus present in blood is below the limit of detection ($\log_{10}$ 2.2 $TCID_{50}$) of our assay.

Whilst HEV71 infection-mediated neurological disease is the major cause of morbidity and mortality in people, it was observed as early as 1979 that HEV71 clinical isolates displayed a high tropism for mouse muscle tissue (Chumakov *et al.*, 1979). Mouse-adapted strains of HEV71 have been observed to invade many

organs and tissues in infected mice, including the brain, skeletal muscle, cardiac muscle, liver, spleen and lung (Chen *et al.*, 2004; Wang *et al.*, 2004). However, several mouse-adapted strains of HEV71 have been shown to primarily infect skeletal muscle tissue in mice (Arita *et al.*, 2008; Chua *et al.*, 2008; Wang *et al.*, 2011; Wang *et al.*, 2004). Interestingly, two studies have demonstrated that HEV71 is associated with the development of persistent infection in skeletal muscle of both people and mice (Chen *et al.*, 2007a; Douche-Aourik *et al.*, 2003).

We previously identified a non-conservative amino acid substitution in the capsid protein VP2 (K^{149}→I) of CHO-B5 that is able to confer the CHO cell growth-adapted phenotype (Zaini *et al.*, 2012b). As expected, the VP2 (K^{149}→I) mutation identified in CHO-B5 does not confer the mouse virulent phenotype. In our study, viruses expressing the VP1 (K^{244}→E) mutation (CHO-26M-VP1-K244E and CHO-26M-VP1) in addition to VP2 (K^{149}→I) mutation, were virulent in 5 day-old BALB/c mice, with skeletal muscle as the primary site of replication resulting in inflammatory myositis, similar to MP-B5. This indicates that the VP1 (K^{244}→E) change is the critical genetic determinant of mouse-adaptation and virulence. This is consistent with the rapid reversion of the mouse-adapted amino acid residue (E) to the wild-type residue (K) during passage in Vero (primate) cell culture. Another reported genetic determinant of mouse adaptation and virulence has also been identified in the capsid protein VP1 (G^{145}→E) (Arita *et al.*, 2008; Chua *et al.*, 2008). The VP1 (G^{145}→E) mutation was also found to revert rapidly to the wild-type amino acid residue during passage in RD (human) cells (Chua *et al.*, 2008).

It has previously been shown that a synergistic effect of VP2-149 and VP1-145 double mutations in HEV71 enhanced viral infectivity in mouse neuroblastoma (Neuro-2a) cells *in vitro* and in mouse lethality *in vivo* (Huang *et al.*, 2012). In this study, dual capsid protein mutations were found to synergistically enhance HEV71 binding and RNA accumulation in Neuro-2a cells. Thus, dual capsid protein substitutions appear to cooperatively promote viral binding and RNA accumulation of HEV71 in infected cells, thus contributing to enhanced viral infectivity and mouse lethality *in vivo*. Consequently, it is possible that the dual capsid protein substitutions (VP2-149 and VP1-244) identified in MP-B5 also promote HEV71 adaptation in mice through enhanced cell binding activity and RNA accumulation in infected cells. However, the precise mechanism of enhanced cell growth and mouse virulence in MP-B5 remains unclear.

The HEV71 5′ UTR contains a type I IRES and primarily functions in the control of viral protein translation and replication (Andino *et al.*, 1993; Andino *et al.*, 1990; Pilipenko *et al.*, 1989; Pilipenko *et al.*, 1992a). 5′ UTR RNA secondary structures are highly conserved in HEV71 (Thompson & Sarnow, 2003). In our study, two mutations were identified at nucleotide positions 345 and 601 in the 5′ UTR of MP-B5. Both of these mutations are located within the IRES but are not located within 5′ UTR mutation hotspots considered essential for the virulence of HEV71 (Wang *et al.*, 2004). Furthermore, the 5′ UTR nucleotide substitutions identified in MP-B5 are not located adjacent to 5′ UTR position 158, recently identified as a mouse virulence determinant in HEV71 (Yeh *et al.*, 2011). Several 5′ UTR mutations were also identified in a mouse-adapted strain of HEV71 (Arita *et al.*, 2008). However, these workers demonstrated that a single amino acid

change in capsid protein VP1 (G^{145}→E) was solely responsible for the mouse adaptation and virulence in this model. Furthermore, the 5′ UTR region has previously been found not to play a major role in determining the cell culture growth phenotype of HEV71 (Phuektes *et al.*, 2011). Taken together, these findings suggest that mouse adaptation of HEV71 is most frequently associated with capsid protein mutations that alter virus binding and entry into cells, viral RNA synthesis or virion assembly and release. Our finding that a single mutation in the capsid protein VP1 (K^{244}→E) was sufficient to confer the mouse virulence phenotype of HEV71 is consistent with this hypothesis.

Amino acid position VP1-244 is located on the surface-exposed HI loop. Another genetic determinant of mouse-adaptation and virulence, amino acid position VP1-145 (Arita *et al.*, 2008; Chua *et al.*, 2008), is located on the surface-exposed DE loop. By homology modeling, we have further shown that VP1-145 and VP1-244 are located on the virion surface near the fivefold axis of symmetry and are closely adjacent to one another on the three-dimensional structure of the viral particle. Interestingly, VP1-149T was found to be a major determinant of mouse virulence in a mouse-adapted strain of the related enterovirus, coxsackievirus B4 (Caggana *et al.*, 1993). This mutation also maps onto the surface-exposed DE loop, similar to the VP1-145 mouse-adaptation determinant of HEV71.

Previous studies have shown that mutations in the enterovirus VP1 capsid protein are important determinants of host range (Colston & Racaniello, 1995). A three-dimensional structural model of related mouse-adapted polioviruses revealed evidence of changes in the HI loop (residues 244-252) and an extensive

conformational rearrangement in the nearby DE loop (residues 141-153) (Yeates *et al.*, 1991). The simplest explanation for the involvement of surface-exposed portions of the viral capsid in regulating mouse-adaptation is that this phenotype is determined by the ability of the virus to switch receptor usage to molecules expressed on the surface of mouse cells. An alternative explanation is that mouse-adaptation is determined by capsid protein mutations that alter the conformational changes required for cell entry or uncoating in mouse cells subsequent to receptor attachment.

Our mouse model provides an excellent and convenient model for the study of vaccine efficacy through passive protection. Wu *et al.* (2001) showed that immunisation of pregnant mice with inactivated HEV71 protected newborn mice against lethal challenge with mouse-adapted HEV71. More recently, Bek *et al*. (2011) showed that the mouse passive protection model was useful in evaluating the protective efficacy of a formalin-inactivated HEV71 vaccine that has since completed a phase I clinical trial (Li *et al.,* 2012), despite the fact that the main cause of death is due to skeletal muscle myositis. We propose that the mouse-adapted virus reported in this study will primarily be used in the assessment of the protective efficacy of candidate HEV71 vaccines, especially by providing an additional HEV71 sub-genogroup B5, with which to investigate cross-genotype protection.

The mouse-adapted strain that we have selected in this study is the first reported HEV71 strain belonging to sub-genogroup B5 and is associated with a novel lysine (K) to glutamic acid (E) substitution at position 244 in protein VP1.

To date, there has not been a detailed pathologic characterisation of a mouse model of HEV71 infection by a virus strain belonging to this sub-genogroup. This mouse-adapted strain will be useful for the evaluation of cross-protective immunity conferred by candidate vaccines produced from strains belonging to different genetic lineages, an issue that has major implications for vaccine design. Even though HEV71 represents a single serotype, large HEV71 epidemics are often associated with genogroup replacement (Huang *et al.*, 2009b; Wang *et al.*, 2002) and so concern has been raised that a vaccine based on a single viral genogroup will not provide cross-protective immunity against subsequent infection with viruses belonging to a different genogroup (Arita *et al.*, 2007). Several models have provided good evidence of cross-reactive immune responses to HEV71 infection (Bek *et al.*, 2011; Liu *et al.*, 2010; Ong *et al.*, 2010). Although these models have provided good evidence of both cross-reactive immune responses to HEV71 infection (Liu *et al.,* 2010; Ong *et al.,* 2010) and of cross-protection of mice from lethal challenge with viruses belonging to other sub-genogroups (Bek *et al.,* 2011), the development of a sub-genogroup B5 mouse-adapted virus model will allow studies of vaccine-induced cross-protective immunity to be extended to include the most recent genogroup B lineage of HEV71 to evolve in Southeast Asia.

In conclusion, the molecular basis of mouse-adaptation of a sub-genogroup B5 strain of HEV71 was characterised. Only viruses expressing the VP1 ($K^{244}\rightarrow E$) mutation were virulent in 5-day-old BALB/c mice, indicating that the VP1 ($K^{244}\rightarrow E$) change is the critical genetic determinant of mouse adaptation and virulence in this model. The identification of viral genomic regions responsible

for the expanded host range and increased virulence in mice has significantly enhanced our understanding of the molecular biology of HEV71.

6. CHAPTER SIX

A SINGLE MUTATION IN CAPSID PROTEIN VP1 (Q^{145}→E) OF A GENOGROUP C4 STRAIN OF HUMAN ENTEROVIRUS 71 GENERATES A MOUSE VIRULENT PHENOTYPE

6.1. Introduction

We previously isolated a mouse virulent strain of HEV71 belonging to sub-genogroup B3 (HEV71-26M) by serial passage in Chinese hamster ovary (CHO) cells (CHO-26M) and in newborn BALB/c mice (MP-26M) (Chua *et al.*, 2008). Prior CHO-cell adaptation of HEV71 was an essential first step in the adaptation of HEV71 to growth in murine hosts (Chua *et al.*, 2008; Zaini *et al.*, 2012a). We have previously reported that a lysine (K) to isoleucine (I) or methionine (M) change at residue 149 of the VP2 capsid protein is critical for adaptation of HEV71 to CHO cells (Chua *et al.*, 2008; Zaini *et al.*, 2012b), but does not lead to increased virulence in mice. An additional glycine (G) to glutamic acid (E) change at residue 145 of the VP1 capsid protein was found to be necessary to increase viral growth and virulence in mice (Chua *et al.*, 2008). Arita *et al.* (2008) and Huang *et al*. (2012) also demonstrated an identical mutation responsible for adaptation of HEV71 to growth in SCID/NOD and ICR mice, respectively.

From our work in Chapter 4, HEV71 a full length sub-genogroup C4 cDNA clone containing the CHO cell-adaptation marker was not infectious in mice. In this study, we generated a mouse-virulent HEV71 strain representing sub-genogroup C4 by modifying its VP1 capsid protein based on the genetic information derived from our previous mouse-adapted HEV71 (genogroup B3) strain (Chua *et al.,*

2008). Here we demonstrate that introducing a key mutation into the HEV71 VP1 capsid protein is able to generate a mouse virulent HEV71 strain from a different genogroup, as well as providing an alternative strategy for the generation of mouse-virulent HEV71. We also examined the phenotypic characteristics of this mouse-virulent HEV71 strain in mice and in cell culture. This work was recently published (Zaini & McMinn, 2012) and a copy of the manuscript reprint is included in Appendix D.

6.2. Results

6.2.1. Construction of a full-length sub-genogroup C4 infectious cDNA clone containing the VP1 protein mutations identified in MP-26M

Firstly, we compared the complete genome sequence of HEV71-C4 (GenBank ID: JQ965759), determined in Chapter 3, to the available complete genome sequences of HEV71-26M (GenBank ID: EU364841), CHO-26M (GenBank ID: EU376004) and MP-26M (GenBank ID: EU376005). Importantly, we determined the HEV71-C4 capsid protein amino acid residues to be lysine (K) at position 149 in VP2 and to be glutamine (Q) at position 145 in VP1, respectively (Figure 6.1).

We have previously constructed a full-length infectious cDNA clone of HEV71-C4 by RT-PCR assay, restriction enzyme digestion and cloning in two sub-genomic clones using plasmid pMC18 (Chapter 3). We have also constructed a full-length infectious cDNA clone of HEV71-C4 containing the CHO cell-adaptation marker, VP2-K^{149}→I (C4-VP2I) (Chapter 4) (Zaini *et al.*, 2012b). From previous work, we have established that it is not possible to obtain stable CDV populations that contain only the VP1 mouse adaptation mutations and that the CHO cell-

adaptation mutation VP2-K^{149}→I is necessary to increase the stability of the VP1 mouse adaptation mutations (Chua *et al.*, 2008). Consequently, we decided to use the full-length infectious cDNA clone of C4-VP2I as the parental clone for further genetic manipulation.

Firstly, we showed that residue 145 of the HEV71 VP1 capsid protein is highly variable amongst the four strains compared in this study, with the residues glycine (G), glutamic acid (E) or glutamine (Q) identified (Figure 6.1b). As our parental infectious clone, C4-VP2I, contains a glutamine residue at VP1-145, we decided to construct two variants containing either glutamic acid or glycine at this position in order to investigate the effect of these residues on mouse adaptation and virulence. The VP1-Q^{145}→E and VP1-Q^{145}→G mutations were introduced into the C4-VP2I full-length clone by site-directed mutagenesis, generating variants C4-VP2I-VP1E and C4-VP2I-VP1G, respectively (Figure 6.2). The mutagenesis reaction was performed without sub-cloning and a single clone of each mutant was selected and purified plasmid DNA prepared for sequence analysis. VP1 gene RT-PCR and nucleotide sequencing was undertaken to ensure that the site-specific changes were present in the mutated clones.

The infectious cDNA clones of the C4-VP2I-VP1E and C4-VP2I-VP1G variants were transfected into COS-7 cells. We successfully recovered the CDVs from transfected cells at two days post-transfection. The CDVs were passaged once on Vero cells in order to generate high titre working stocks; CDV stocks were found have viral titres of $>10^6$ $TCID_{50}$ mL^{-1}. VP1 gene RT-PCR and nucleotide sequencing was undertaken to ensure that the site-specific change remained

present in the rescued virus populations. Nucleotide sequencing showed that both variants, C4-VP2I-VP1E-CDV and C4-VP2I-VP1G-CDV, retained the introduced VP1-145 mutation at this passage level with no evidence of reversion of the E or G codons to the parental Q codon (Figure 6.3).

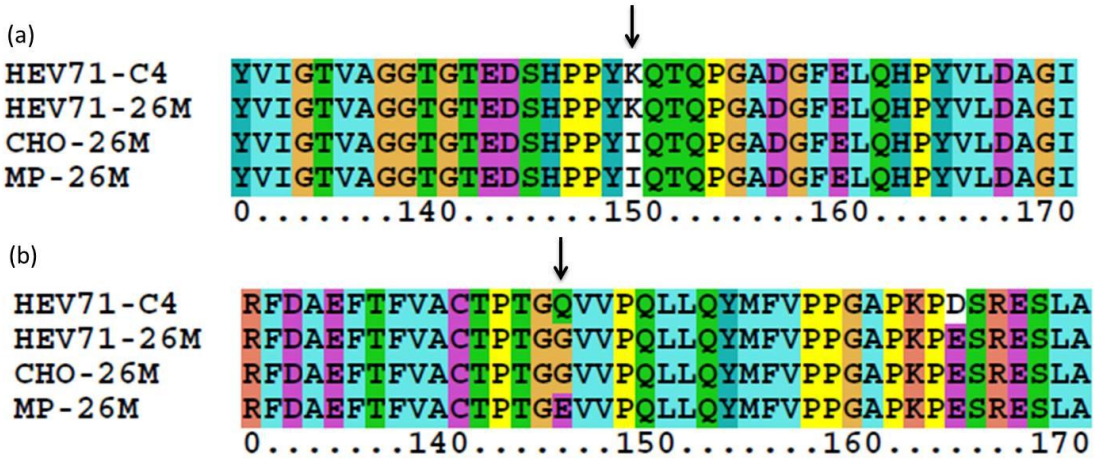

Figure 6.1 Amino acid sequence alignment of the (a) VP2 and (b) VP1 regions of HEV71-C4, HEV71-26M, CHO-26M and MP-26M strains.

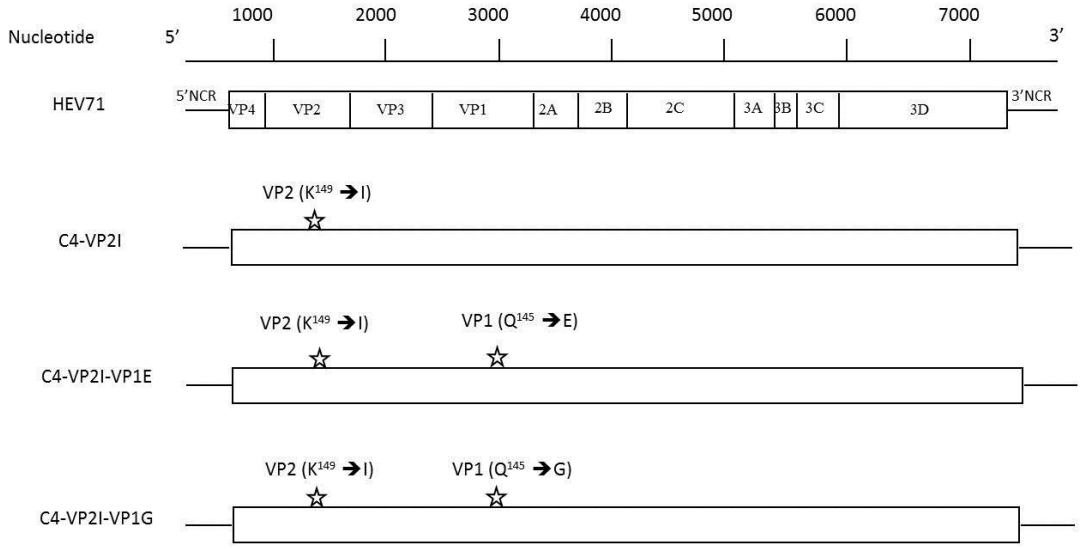

Figure 6.2 Schematic representation of the infectious cDNA clones of C4-VP2I and cDNA clones containing VP1 mutations constructed by site-directed mutagenesis. Genome maps of parental and mutant C4-VP2I are represented as an open box, with individual genes and non-coding regions indicated for HEV71. Amino acid mutations introduced into C4-VP2I-VP1E (VP1, Q^{145}→E) and C4-VP2I-VP1G (VP1, Q^{145}→G) are shown as open stars.

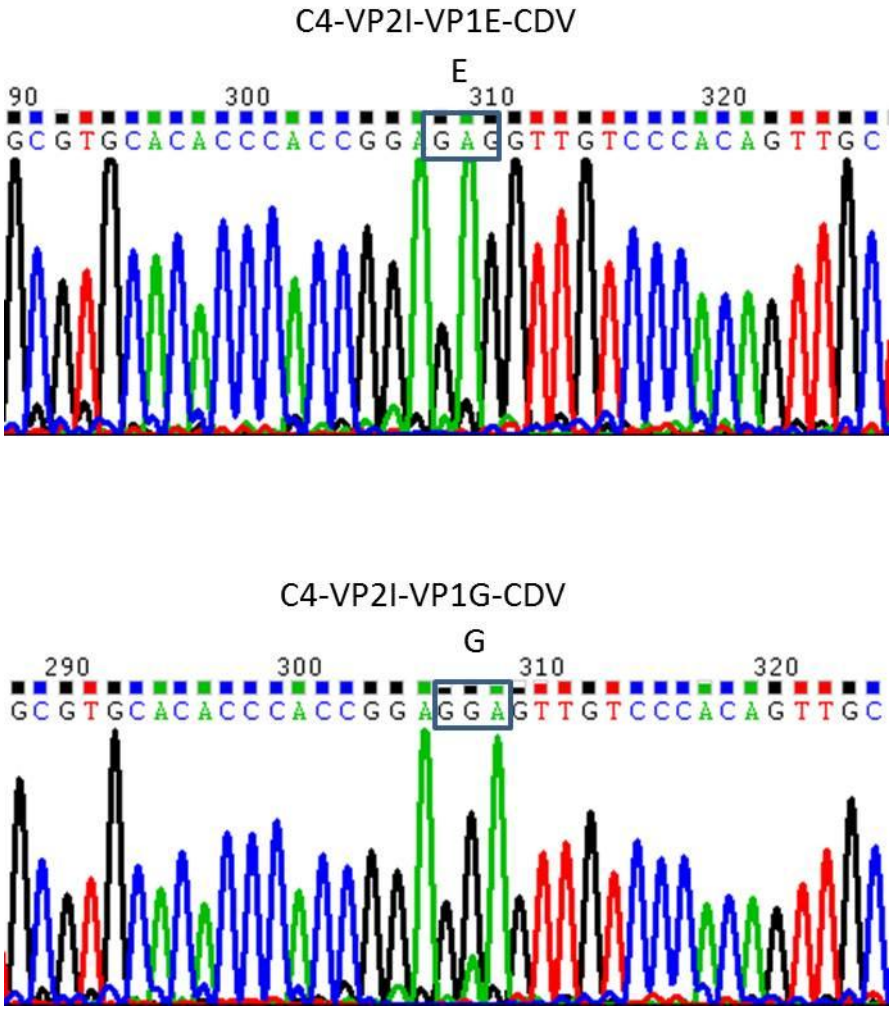

Figure 6.3 Stability of introduced VP1 mutation (a) Q^{145}→E, (b) Q^{145}→G during Vero cell culture passage. CDV populations were passaged once in Vero cells and viral RNA was extracted from culture supernatant collected at passage three. The VP1 genes were amplified by RT-PCR and their nucleotide sequences determined. The open box indicates the nucleotide sequence of the site-specific change and the deduced amino acid residue is indicated above the box.

6.2.2. An amino acid substitution in VP1 (Q^{145}→E) is solely responsible for mouse adaptation and virulence

We next performed mouse virulence assays to compare the survival of BALB/c mice with the parental or mutant CDVs. Similar to our previous mouse experiments, mice were inoculated at five-days-of age via the i.p. route of infection. Groups of six 5 day-old BALB/c mice were infected with approximately 10^4×$TCID_{50}$ of each of the infectious CDV populations. Mice were observed twice daily for clinical signs of illness for 14 days p.i. As expected, the parental C4-VP2I-CDV virus population caused no observable morbidity or mortality in infected mice (Figure 6.4). The C4-VP2I-VP1G-CDV population also exhibited a non-virulent phenotype in mice, with no observable clinical signs of infection or mortality up to 14 days p.i., similar to the parental virus (p>0.05). By contrast, mice infected with the C4-VP2I-VP1E-CDV population showed forelimb and/or hindlimb flaccid paralysis, ruffled fur, weight loss and severe lethargy after three days p.i. A mortality rate of 100% was observed, with death commencing at three days p.i. and reaching 100% by four days p.i. (Figure 6.4). The mean survival time of C4-VP2I-VP1E-CDV-infected mice was calculated to be 3.3 (± 0.5) days.

We next determined the HD_{50} values of the parental and mutant viruses. Groups of six 5-day-old BALB/c mice were infected by i.p. inoculation with 50 μL of ten-fold serial dilutions of the parental or mutant CDVs and observed for 14 days for clinical signs of HEV71 infection. Mice that developed limb paralysis were euthanased. The HD_{50} values of C4-VP2I-VP1E-CDV in 5-day-old BALB/c mice was determined to be 2.1×10^2 $TCID_{50}$ following the method of (Reed & Muench,

1938) (Table 6.1). This demonstrates that a single amino acid substitution, VP1-Q^{145}→E, is able to confer the mouse virulent phenotype upon clone-derived C4-VP2I. By contrast, C4-VP2I-VP1G-CDV-infected mice survived beyond 14 days p.i., with no clinically-apparent disease observed, indicating that the amino acid substitution VP1-Q^{145}→G does not confer the mouse virulent phenotype.

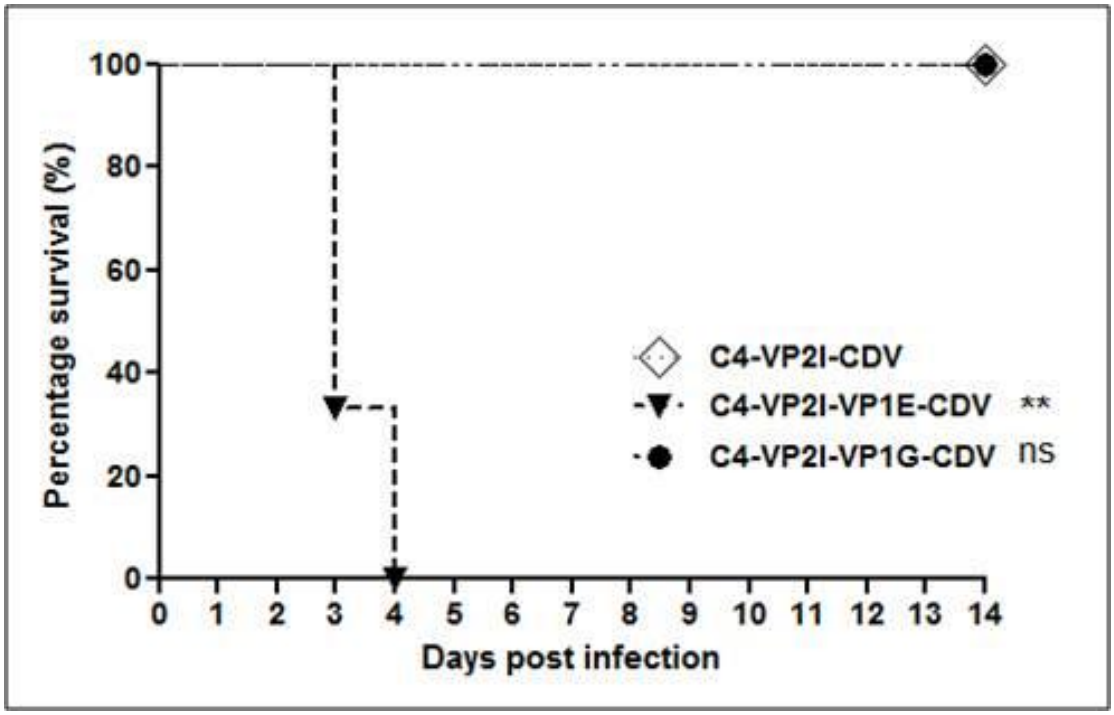

Figure 6.4 Survival of 5-day-old BALB/c mice infected i.p. with parental or mutant strains of HEV71. Kaplan-Meier plots show survival after challenge with C4-VP2I-VP1E-CDV, C4-VP2I-VP1G-CDV or parental C4-VP2I-CDV. The Mantel-Cox Log-rank test was used to compare the survival of mutant virus-infected pups to parental C4-VP2I-CDV-infected pups at 14 days p.i. ** denotes significance value $p<0.01$ and ns denotes significance value $p>0.05$.

Table 6.1 Mortality profile, mean survival time and HD_{50} values after challenge with serial 10-fold dilutions of the parental or mutant viruses

Virus	Mortality (%)	Mean survival time (days ± SEM)	HD_{50} ($TCID_{50}$)*
C4-VP2I-CDV	0	>14	$> 10^4$
C4-VP2I-VP1E-CDV	100	3.3 ± 0.5	2.1×10^2
C4-VP2I-VP1G-CDV	0	>14	$> 10^4$

*HD_{50} values were determined by the method of Reed & Muench (1938)

6.2.3. Phenotypic characterisation of C4-VP2I-VP1E-CDV

In order to investigate the tissue tropism of C4-VP2I-VP1E-CDV, the tissue distribution of mutant virus in infected host tissues was examined. Groups of twelve 5-day-old BALB/c mice were inoculated i.p. with the maximum possible dose ($\sim 10^4 \times TCID_{50}$) of the virulent virus, C4-VP2I-VP1E-CDV. Three infected mice showing clinical grade 3 paralysis (at four days p.i.) (refer to Table 2.16 for clinical grading scale) were sacrificed, perfused, tissues collected and viral titres determined. Virus infectivity was detected in the spleen, liver, heart, skeletal muscle and brain tissue (Figure 6.5). The virus was detected in high titre in skeletal muscle, with a titre $>10^5$ $TCID_{50}$ g^{-1}, indicating that muscle and/or connective tissue is the primary site of C4-VP2I-VP1E-CDV infection in mice. We also recovered viral genomic RNA from the skeletal muscle homogenate, which was amplified by RT-PCR using primers specific for the VP2 and VP1 genes and the amplicons sequenced. We confirmed that the VP2-149I and VP1-145E mutations persisted after passage in BALB/c mice (Figure 6.6).

We next examined the histopathological changes occurring in the tissues of C4-VP2I-VP1E-CDV-infected mice. Groups of twelve 5-day-old BALB/c mice were inoculated i.p. with $\sim 10^4 \times TCID_{50}$ of the C4-VP2I-VP1E-CDV population. Brain, spinal cord and skeletal muscle tissue was collected from three infected mice upon reaching clinical grade 3 paralysis (4-5 days p.i.). The most notable histopathological changes observed in the infected mice were in skeletal muscle tissue sections (Figure 6.7). Neutrophil infiltration and myocyte necrosis, indicating the presence of severe myositis, was observed in all skeletal muscle sections examined. Although myositis was observed in the muscle tissue

surrounding the spinal cord sections, no significant foci of inflammation were observed in the brain and spinal cord sections (cervical and lumbar) of any C4-VP2I-VP1E-CDV-infected mice (data not shown). Furthermore, no histological abnormalities were detected in skeletal muscle sections of mock-infected mice (Figure 6.7).

In order to determine whether more efficient replication contributed to the increased virulence of C4-VP2I-VP1E-CDV in mice, the replication kinetics of C4-VP2I-VP1E-CDV was also examined in Vero cells (MOI = 1) and compared to C4-VP2I-CDV and parental C4-CDV. The replication kinetics and virus yields of C4-VP2I-VP1E-CDV was similar to both C4-VP2I-CDV and C4-CDV in Vero cells (p>0.05), with a lag phase of approximately 4 h p.i. and virus titres increased thereafter (Figure 6.8). C4-VP2I-VP1E-CDV did not appear to replicate more effectively in cell culture and therefore is not a contributing factor to its increased virulence in mice.

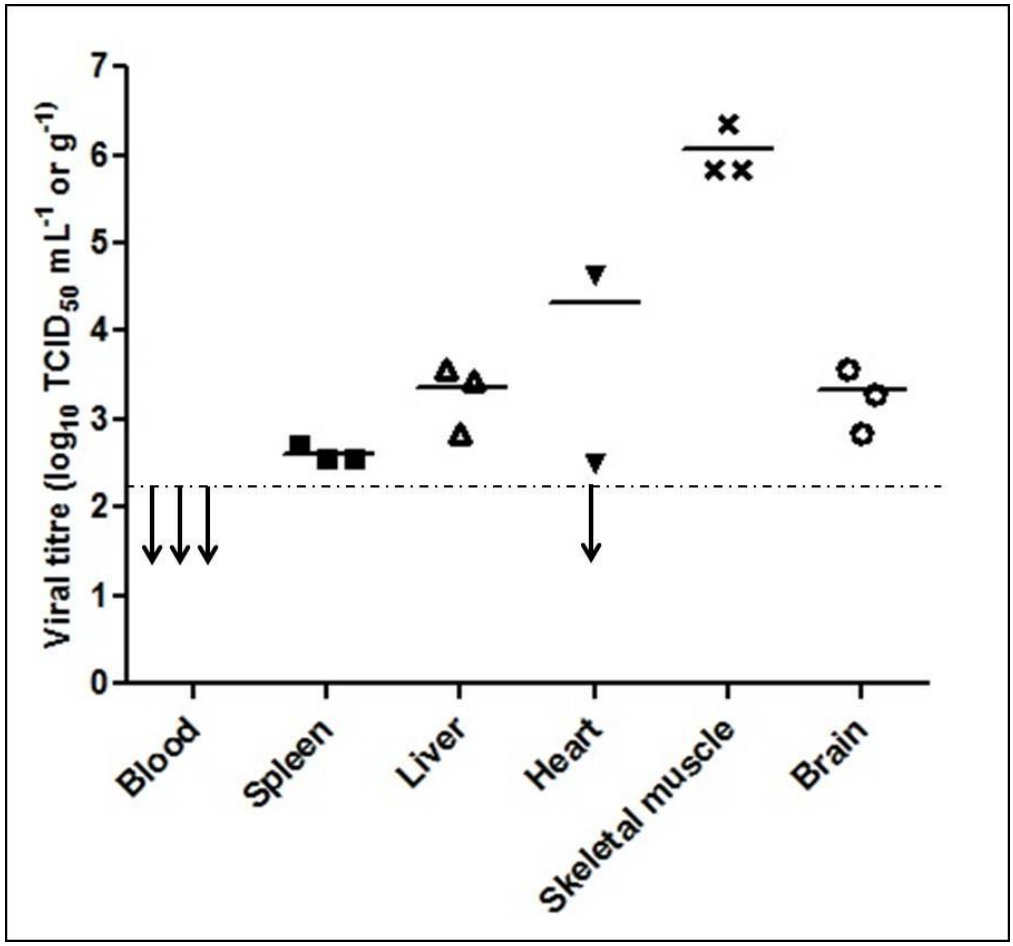

Figure 6.5 Viral loads in selected tissues of 5-day-old BALB/c mice after i.p. challenge with ~10^4×$TCID_{50}$ of C4-VP2I-VP1E-CDV (4 days p.i.). Viral titres in blood were determined as $TCID_{50}$ mL^{-1}. Viral titres in tissue homogenates were determined as $TCID_{50}$ g^{-1}. Dashed line indicates the detection limit of virus titration by $TCID_{50}$ assay (log_{10} 2.2 $TCID_{50}$) and arrows indicates samples with titres below the limit of detection.

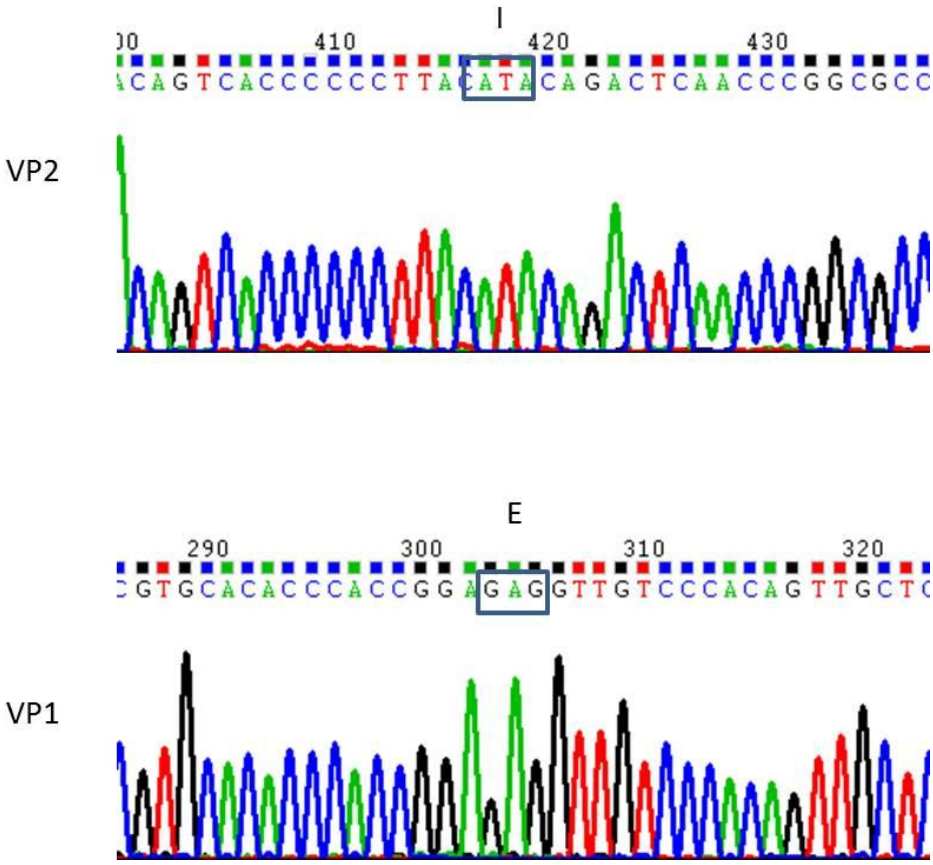

Figure 6.6 Stability of VP2-149I and VP1-145E mutation after passage of C4-VP2I-VP1E-CDV in BALB/c mice. Viral RNA was extracted from skeletal muscle homogenates. The VP2 and VP1 genes were amplified by RT-PCR and their nucleotide sequences determined. The open box indicates the nucleotide sequence of the mutation site and the deduced amino acid residue is indicated above the box.

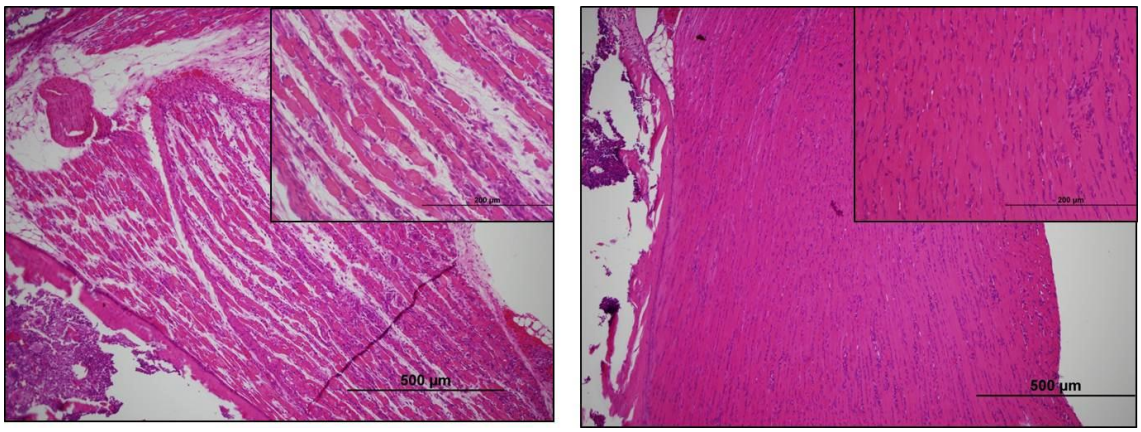

Figure 6.7 Histological analysis of C4-VP2I-VP1E-CDV-infected mice. Severe myositis is present in all C4-VP2I-VP1E-CDV-infected skeletal muscle tissues examined (left). No histological abnormalities were observed in mock-infected skeletal muscle sections (right).

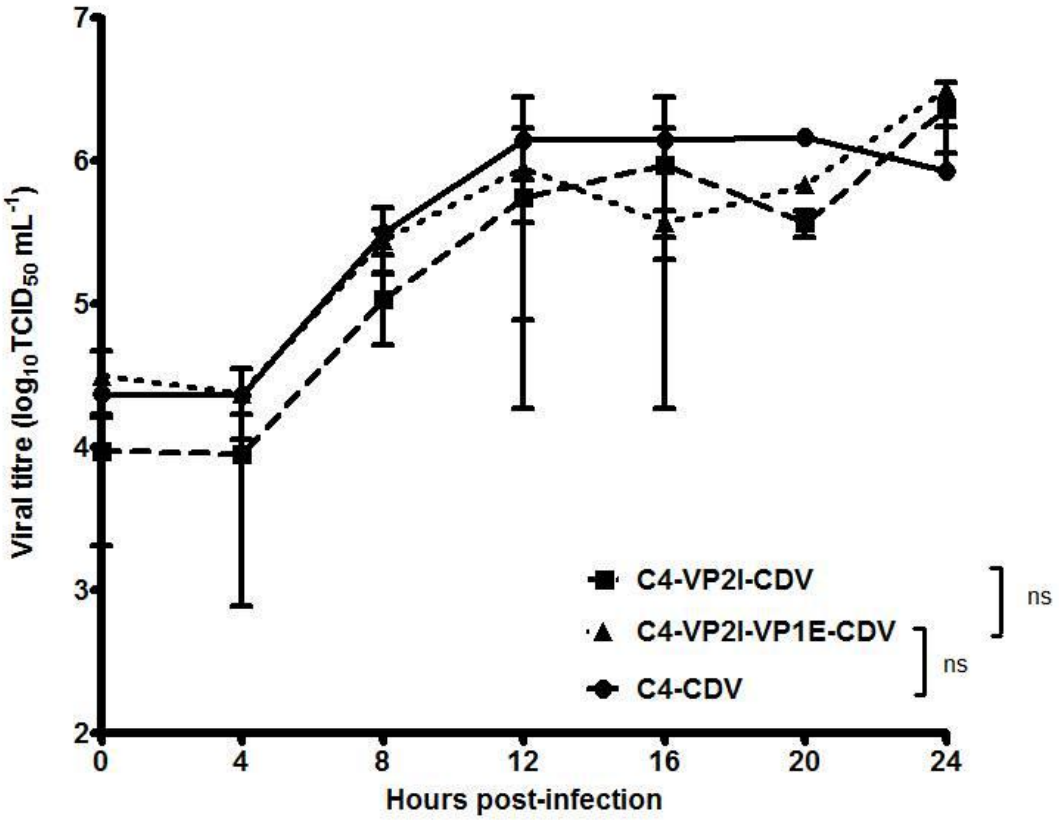

Figure 6.8 Replication kinetics in Vero cells of C4-CDV, C4-VP2I-CDV and C4-VP2I-VP1E-CDV. Cell monolayers were infected at MOI of 1. Cell culture supernatants were then collected at the times indicated. Samples at each time point were freeze-thawed three times and clarified by centrifugation prior to determination of virus titres by $TCID_{50}$ assay. All assays were performed in duplicate. At each time point, the titres are means of two samples; error bars represent SEM. The Mann-Whitney test was used to compare the titres between C4-CDV vs C4-VP2I-VP1E-CDV and C4-VP2I-CDV vs C4-VP2I-VP1E-CDV. ns denotes significance value $p>0.05$.

6.2.4. Homology modeling

In Chapter 5, we demonstrated by homology modeling that the VP1-145 mouse virulence marker is exposed on the DE loop of VP1. In order to demonstrate the different amino acid residues of VP1-145 (Q, E or G) within the VP1 capsid protein, three-dimensional structural models of the VP1 protein containing the three alternative amino acid residues were predicted (Figure 6.9) by homology modeling as describe in section 5.2.9. Figure 6.9b shows the predicted structure of VP1 protein with amino acid residue of polar acidic glutamic acid (E) at position 145, which confers the mouse virulence phenotype.

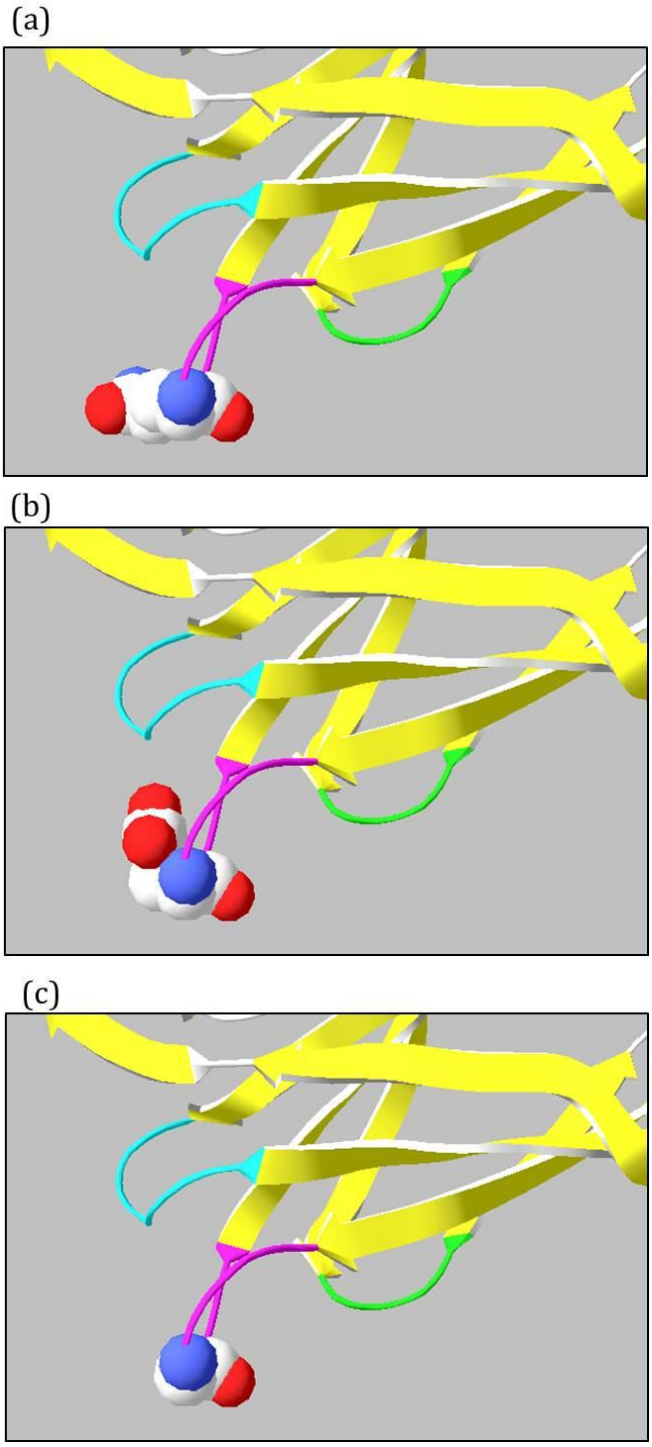

Figure 6.9 Homology models showing the predicted three-dimensional structure of HEV71 VP1 protein with amino acid residue 145 exposed on the DE loop of the VP1 protein. Amino acid residue (a) glutamine (Q); (b) glutamic acid (E); (c) glycine (G) is displayed as a space-fill model.

6.3. Discussion

We have shown that residue VP1-145E is a critical determinant of mouse adaptation and virulence of HEV71 in two different sub-genogroups, B3 and C4. We demonstrated that the genetic changes that enable mouse-adaptation of HEV71 from these two sub-genogroups are identical. Mouse virulence was conferred when the amino acid residue at position VP1-145 is polar acidic glutamic acid (E). Both VP2-149 and VP1-145 are exposed on VP1 external loops, EF and DE, respectively (Chua *et al.*, 2008; Zaini *et al.*, 2012b). These two loops have been shown to project beyond the virion surface in the mature HEV71 particle (Wang *et al.*, 2012c). The CHO-associated VP2 residue 149I appears to stabilise the VP1 residue 145E via an as yet undefined interaction between these two capsid proteins. It has also previously been shown that a synergistic effect of VP2-149 and VP1-145 double mutations in HEV71 enhanced viral infectivity in mouse neuroblastoma (Neuro-2a) cells *in vitro* and in mouse lethality *in vivo* (Huang *et al.*, 2012).

Skeletal muscle is the primary site of C4-VP2I-VP1E-CDV replication in mice. Histological analysis of skeletal muscle showed that infection with this virus induced severe inflammatory myositis. No histological abnormalities were observed in the brain or spinal cords of any C4-VP2I-VP1E-CDV-infected mice. As with our other mouse-adapted viruses (Chua *et al.*, 2008; Zaini *et al.*, 2012a), the presence of myositis in infected mice and a lack of evidence of CNS disease, despite the presence of virus in brain tissue in low titre, suggest that the observed limb paralysis and the cause of death was due primarily to severe inflammatory myositis.

As with our previous mouse models (Chua *et al.*, 2008; Zaini *et al.*, 2012a), this model also provides an excellent and convenient model for the study of vaccine efficacy through passive protection. The sub-genogroup C4 mouse-adapted strain described in this study is the first reported mouse virulent HEV71 strain generated by reverse genetic modification of the capsid protein and without serial passage in mice. Other than its use as a passive protection model, this model will also be useful in the evaluation of cross-protective immunity conferred by candidate vaccines produced from strains belonging to different genetic lineages, an issue that has major implications for vaccine design. The development of a sub-genogroup C4 mouse-adapted virus model will allow studies of vaccine-induced cross-protective immunity to be extended to include the most recent genogroup C lineage of HEV71 to evolve in Southeast Asia. Therefore we propose that the mouse virulent virus generated from this study should be primarily used in the assessment of the protective efficacy of candidate HEV71 vaccines, especially by providing an additional HEV71 sub-genogroup C4, with which to investigate cross-genotype protection.

This work also demonstrates an alternative strategy for the generation of mouse virulent HEV71 without the use of animals during the adaptation process. This approach to the introduction of key mouse adaptation mutations in the capsid proteins will have a large impact on the HEV71 mouse-adaptation protocol in the future, as mouse-virulent HEV71 virus can now be generated by reverse genetic manipulation of the viral genome *in vitro*, thus reducing the requirement for animal use. Furthermore, knowledge gained from this study will assist in

furthering research on the virulence of this increasingly important human pathogen.

7. CHAPTER SEVEN

GENERAL DISCUSSION

The overall purpose of this thesis has been to examine the construction of infectious cDNA clones of HEV71 and the development of mouse models of HEV71 infection (representing different virus genogroups) for studies of vaccine efficacy. In Chapter 3, the complete genomes of three genetically distinct strains of HEV71 isolated from outbreaks of HFMD in Brunei in 2006 (AbuBakar *et al.*, 1999), Sydney in 1998 (Sanders *et al.*, 2006) and southern Vietnam in 2005 (Tu *et al.*, 2007), respectively, were determined and analysed, including an analysis of regions known to form RNA secondary structures.

Infectious cDNA clones of the HEV71-C2 (genogroup C2) and HEV71-C4 (genogroup C4) were successfully constructed. These full-length infectious cDNA clones were generated using an established cDNA clone construction protocol developed by previous members of our research group (Chua *et al.*, 2008; Phuektes *et al.*, 2011). Sub-genomic and full-length cDNA clones of HEV71-C2 and HEV71-C4 were constructed in the low copy-number plasmid pMC18 and using the bacterial host *E. coli* XL10-gold. CDVs of HEV71-C2 and HEV71-C4 were successfully rescued by transfection of plasmid cDNA into COS-7 cells. Analysis of the *in vitro* phenotype of both CDVs illustrates the integrity of the infectious clone system. C2-CDV and C4-CDV were found to display cell culture growth properties indistinguishable from their respective parental viruses. These clones were used as tools to investigate the molecular basis of HEV71 virulence and pathogenesis in mice.

An infectious cDNA clone of the other HEV71 strain, HEV71-B5 (genogroup B5), was not successfully generated using a similar construction strategy. More than 30 clones of HEV71-B5 were generated and screened for the anticipated band size by restriction endonuclease digestion, but we were unable to recover infectious virus upon transfection in COS-7 cells. In order to achieve successful infection, viral transcripts must interact with virally encoded proteins, most particularly with the viral replicase and with host cell components that form the translation machinery; therefore the structure of viral transcripts need to mimic that of virion RNA as closely as possible (Boyer & Haenni, 1994). Several parameters have a dramatic influence on the infectivity of viral transcripts: (1) the heterogeneity of the transcript population, (2) the presence of point mutations , and, (3) the sequence at the 5′ and 3′ ends (number and sequence of non-viral nucleotides, presence of a cap structure at the 5′ end or a poly (A) tail at the 3′ end) (Boyer & Haenni, 1994).

All DNA polymerases make mistakes during DNA synthesis, occasionally inserting an incorrect nucleotide into the growing DNA strand. Most polymerases, however, are able to rectify these errors by reversing over the mistake and resynthesising the correct sequence. This property is referred to as "proofreading function". *Taq* polymerase lacks a proofreading activity and as a result is unable to correct its errors (Tindall & Kunkel, 1988). This means that the DNA synthesised by *Taq* polymerase is not always an accurate copy of the template molecule. Additionally, PCR involves copies being made of copies of copies, so the polymerase-induced errors gradually accumulate, the fragments produced at the end of a PCR containing copies of earlier errors together with

any new errors introduced during the final round of synthesis and overall may potentially affect the activity of the viral transcripts. The non-infectious HEV71-B5 full-length clones were not sequenced to identify the mutation/s that caused the non-infectious phenotype. Therefore, a genetic analysis could not be made on these non-infectious full-length cDNA clones.

Similar to the related PV, HEV71 has a limited host range, with humans the only known natural host. Non-human primate models have long been the most suitable animal models to study the pathogenesis of both PV and HEV71. Since the identification of the cellular receptor for PV, PVR (CD155)-expressing transgenic mice have been developed (Koike *et al.*, 1994; Ren *et al.*, 1990). PVR transgenic mice have largely eliminated the need for primates and have become the definitive small animal model for most experimental procedures, providing new information on PV pathogenesis and serving as a tool for vaccine efficacy testing (Koike *et al.*, 1994; Koike *et al.*, 1991; Ren & Racaniello, 1992). Unfortunately, a transgenic mouse expressing the human receptor for HEV71, SCARB2, has not been reported to date. Nevertheless, IFNRI/II knockout mice have recently been shown to support infection of unadapated strains of HEV71 (Khong *et al.*, 2012). However, the use of immune knockout mice is of limited practical value for vaccine efficacy studies (Bek & McMinn, 2010). Therefore, several mouse-adapted strains have been developed by serial passage in mouse brain or muscle (Arita *et al.*, 2008; Chen *et al.*, 2004; Chua *et al.*, 2008; Ong *et al.*, 2008; Wang *et al.*, 2011; Wang *et al.*, 2004).

A previous study by our group (Chua *et al.*, 2008) established a mouse HEV71 infection model using a mouse-adapted variant of HEV71-26M, which belongs to genogroup B3 (MP-26M). MP-26M was selected by serial passage of HEV71-26M in CHO cells, and CHO cell-adapted virus (CHO-26M) was then serially passaged (×6) by i.c. inoculation in one-day-old BALB/c mice. Despite improved growth in CHO cells, CHO-26M did not cause any clinical signs of infection in newborn BALB/c mice. By contrast, infection of newborn mice with MP-26M resulted in severe disease and death in an age-, dose- and route-of-infection-dependent manner. A non-conservative amino acid substitution in the capsid protein VP2 (K^{149}→I) was identified in the CHO cell-adapted virus. An additional amino acid substitution in the capsid protein VP1 (G^{145}→E) was found necessary to increase viral growth and virulence in mice (Chua *et al*., 2008). These two capsid protein genes VP1 (G^{145}→E) and VP2 (K^{149}→I) were found to act cooperatively to generate a genetically stable mouse-adapted phenotype (Chua *et al.* 2008).

In Chapter 4, we described the adaptation of the three HEV71 strains, HEV71-B5, HEV71-C2 and HEV71-C4, to growth in CHO cell cultures. CHO cell-adapted variants of HEV71-B5 and HEV71-C2, CHO-B5 and CHO-C2, respectively, were selected after serial passage in CHO cells at a high MOI (Zaini *et al.*, 2012b) (manuscript reprint included in Appendix B). However, HEV71-C4 did not successfully adapt to growth in CHO cells after three passages. A non-conservative amino acid substitution in the capsid protein VP2 (K^{149}→I) and VP2 (K^{149}→M) were identified in the CHO cell-adapted virus populations of CHO-B5 and CHO-C2, respectively. Manipulation of the HEV71-C4 genome by site-directed mutagenesis of the amino acid residue VP2-149 enabled the virus to

grow in CHO cells. Both HEV71-C4 CDV containing the CHO cell-adaptation marker, VP2 (K^{149}→I) and VP2 (K^{149}→M) grew efficiently in CHO cells, indicating that amino acid substitutions at amino acid position VP2-149 are solely responsible for the adaptation of virus to growth in CHO cells.

Adaptation has been described as the modification of an organism to make it more fit for existence within a certain environment (Domingo & Holland, 1997; Domingo *et al.*, 1997). RNA virus populations are complex and contain heterogeneous mixtures of related viral genomes called quasispecies (Domingo & Holland, 1997; Domingo *et al.*, 1997). Viral quasispecies evolution is decisively influenced by high mutation rates (rate of nucleotide misincorporation per nucleotide copied) during viral replication and in some cases also by molecular recombination and genome segment reassortment (Domingo *et al.*, 2012). During viral infections, viral quasispecies play a key role in the adaptability of viruses to changing environments and the fate of the population as a whole. Viruses with beneficial mutations are able to survive and adapt to a new environment, thus generating new quasispecies. Adaptability is linked to four closely related parameters: replication rate, viral load, genetic heterogeneity and viral fitness (Domingo *et al.*, 2012). This explains why some strains of HEV71 may rapidly adapt to growth under strong selective pressure of CHO cell passage whereas other strains do not.

In our study, newborn BALB/c mice were used in the development of a mouse model of HEV71 infection. Although random-bred mouse strains more accurately reflect the host genetic background associated with human disease, inbred

mouse strains are more suitable for genetic analysis of the molecular determinants of HEV71 virulence. The sensitivity of Swiss mice (random-bred) and BALB/c mice (inbred) was previously compared by i.c. inoculation of the prototype HEV71-BrCr strain (Chua *et al*., unpublished data). It was found that one-day-old Swiss mice required 100-fold more virus to achieve median humane infection endpoints than BALB/c mice. Nevertheless, similar clinical signs were observed in both strains of mice, with fore and/or hindlimb paralysis, hunched back, wasting and eventual death. Based on the higher sensitivity of inbred mice and the need for genetic analyses of the molecular determinants of virulence of HEV71, we selected BALB/c mice for the development of a small animal model of HEV71 infection.

In Chapter 5, a mouse-adapted strain of HEV71-B5 (MP-B5) was selected by serial passage of CHO-B5 in newborn BALB/c mice via the i.c. route of inoculation. Mice infected with MP-B5 developed severe disease in a dose-dependent manner. Muscle tissue was shown to be the major site of replication and was associated with the development of fore and/or hind limb paralysis; skeletal muscle myositis was the primary cause of death. Mouse adaptation of HEV71-B5 involved two nucleotide substitutions in the 5′ UTR and two amino acid substitutions in the VP1 capsid protein. Since we were not able to construct an infectious cDNA clone of HEV71-B5, the infectious clone of HEV71-26M containing the CHO cell growth marker, VP2-K^{149}→I (CHO-26M) was used to study the molecular basis of MP-B5 virulence. Infectious cDNA clone-derived mutant virus populations of CHO-26M containing the VP1 capsid protein mutations identified in MP-B5 were generated and these CDVs were

characterised in the mouse model. Data obtained from our study clearly demonstrated that the VP1 (K^{244}→E) mutation is the major genetic determinant of mouse adaptation. We determined that the 5′ UTR mutations observed in MP-B5 did not cause alterations in predicted RNA secondary structures and are not located adjacent to 5′ UTR position 158, recently identified as a mouse virulence determinant in HEV71 (Yeh *et al.*, 2011) and therefore were not investigated further.

In Chapter 6, we generated a mouse-virulent HEV71 strain representing genogroup C4 by modifying its VP2 and VP1 capsid protein based on the genetic information derived from our previous genogroup B3 mouse-adapted HEV71 strain, MP-26M (Chua *et al.,* 2008). We initially constructed a full-length infectious cDNA clone of HEV71-C4 containing the CHO-26M adaptation marker, VP2 (K^{149}→I). VP1 (Q^{145}→E) or VP1 (Q^{145}→G) mutations were then additionally introduced into the full-length clone by site-directed mutagenesis and their CDVs further characterised in the mouse model. Mouse virulence was conferred when the amino acid residue at position VP1-145 is the polar acidic glutamic acid (E). Similar to our MP-26M and MP-B5 mouse models, skeletal muscle was the primary site of replication of MP-C4 in mice, resulting in myositis associated with limb paralysis and eventual death.

We have clearly shown that residue VP2-149 is responsible for the CHO cell-adapted phenotype of HEV71. We have also demonstrated that residue VP1-145 is a critical determinant of mouse adaptation and virulence of two HEV71 strains belonging to two different genogroups, B3 and C4. Additionally, residue VP1-244

was shown to be the critical determinant of mouse adaptation and virulence of a HEV71 strain belonging to genogroup B5. Interestingly, an identical mutation in VP1 (G^{145}→E) was identified in a mouse-adapted strain of HEV71 selected by Arita *et al*. (2008). Recently, similar mutations responsible for mouse adaptation of two Taiwanese HEV71 strains (both belonging to genogroup C2) (Chen *et al.*, 2004; Wang *et al.*, 2004) , located in the structural protein genes VP1 (G^{145}→E) and in VP2 (K^{149}→M), have been reported (Huang *et al.*, 2012). The VP1 (K^{244}→E) mutation observed in this study appears to be the first report of this mouse virulence marker in HEV71. Taken together, these findings suggest that mouse virulence determinants of HEV71 are most frequently associated with capsid protein mutations that may alter virus binding and entry into cells.

Our study has shown that it was not possible to obtain a stable CDV population that contained only the mouse virulence markers, VP1 (G^{145}→E) (Chua *et al.,* 2008) or VP1 (K^{244}→E) (Zaini *et al.*, 2012a), due to the reversion of VP1 mutation to that of wild type virus. This suggests capsid protein interactions in which the VP2 (K^{149}→I) mutation may help to stabilise VP1 mutation via an as yet unknown interaction between these two capsid proteins. The CHO cell-adaptation marker VP2-149 is located on the surface-exposed EF loop. The mouse adaptation markers VP1-145 and VP1-244 are located on the surface-exposed DE and HI loops, respectively, of the VP1 protein. The VP2 and VP1 interaction may cooperate to introduce structural change in the virion that allows the recognition of a mouse cell receptor. Alternatively, this interaction may facilitate a receptor-mediated conformational change during cell entry and virus uncoating. The EF, DE, HI and BC loops interact with one another to form part of neutralisation-

antigenic site 1 (Moss & Racaniello, 1991). It has been hypothesised that interactions at this interface play a significant role in the dynamics of capsid-associated receptor attachment and cell entry (Moss & Racaniello, 1991). Thus, the mutations predicted in the EF loop of VP2 and the DE loop or HI loop of VP1 may interact and regulate conformational transition of the virion during receptor attachment and cell entry.

Despite their restriction to infection of mice in the first two weeks of life and the predominance of myositis as the cause of morbidity and mortality, mouse models of HEV71 infection using mouse-adapted strains have proven to be useful in determining the protective efficacy of candidate HEV71 vaccines. Wu *et al.* (2001) developed a passive protection assay based on the immunisation of pregnant female mice and challenge of their offspring within the first week of life. They were able to demonstrate 80% survival of five-day-old pups born to mothers immunised with a heat-inactivated strain of HEV71 and challenged with a lethal dose of virus. This model has been reproduced widely in the assessment of candidate HEV71 vaccine efficacy (Bek *et al.*, 2011; Chung *et al.*, 2008; Ong *et al.*, 2010).

The use of mouse-adapted HEV71 strains in vaccine development has been reported in several publications. Ong *et al.* (2010) developed a formaldehyde inactivated whole virus vaccine from a mouse-adapted strain of a sub-genogroup B3 clinical isolate and showed that active immunisation of infant outbred ICR mice provided complete protection against lethal challenge with the same mouse-adapted strain. Serum from immunised mice was also able to passively

protect infant ICR mice against lethal challenge with mouse-adapted virus and was shown to contain neutralising antibody against HEV71 strains belonging to genotypes B3, B4 and C1-C5 (Ong *et al.*, 2010). A recent study has provided direct evidence of cross-protective immunity induced by immunisation with a formalin-inactivated vaccine (Bek *et al.*, 2011). A commercially produced formalin-inactivated vaccine (Sinovac Biotech Ltd., Beijing, Peoples' Republic of China) based on a sub-genogroup C4 strain of HEV71 isolated in China in 2008 (Zhang *et al.*, 2009), fully protected five-day-old BALB/c mice born to immunised mothers against lethal challenge with mouse-adapted sub-genogroup B3 strain MP-26M (Chua *et al.*, 2008). This candidate HEV71 vaccine has recently completed a phase 1 clinical trial (Li *et al.*, 2012). Nevertheless, the protective efficacy of promising HEV71 vaccine candidates should also be investigated in cynomolgus monkeys (*Macaca fascicularis*) prior to human clinical trials as they are a better model of human disease (Hashimoto & Hagiwara, 1982).

To date, this study has provided the first published pathological characterisation of a mouse model of HEV71 infection by a virus strain belonging to genogroup B5 (Zaini *et al.*, 2012a) (manuscript reprint included in Appendix C). Additionally, the genogroup C4 mouse-virulent strain described in this study is the first reported mouse-virulent HEV71 strain generated by reverse genetic modification of the capsid protein and without serial passage in mice (Zaini & McMinn, 2012) (manuscript reprint included in Appendix D). Both of our mouse-adapted virus models will primarily be used in the assessment of the protective efficacy of candidate HEV71 vaccines, especially by providing additional HEV71 genogroups B5 and C4, with which to investigate cross-genotype protection.

In summary, the reverse genetic systems developed in this study have proven to be valuable tools for the study of the molecular mechanisms of HEV71 replication and virulence. Infectious cDNA clones can be used for further study of the genetic elements that control viral translation and replication processes and their impact upon the virulence phenotype. The identification of viral genomic regions responsible for the expanded host range and increased virulence in mice has significantly enhanced our understanding of the molecular biology of HEV71, and thus can advance research on viral pathogenesis and vaccine development for prevention and control of this important neurotropic virus.

REFERENCES

AbuBakar, S., Chee, H. Y., Al-Kobaisi, M. F., Xiaoshan, J., Chua, K. B. & Lam, S. K. (1999). Identification of enterovirus 71 isolates from an outbreak of hand, foot and mouth disease (HFMD) with fatal cases of encephalomyelitis in Malaysia. *Virus Res* **61**, 1-9.

AbuBakar, S., Sam, I. C., Yusof, J., Lim, M. K., Misbah, S., MatRahim, N. & Hooi, P. S. (2009). Enterovirus 71 outbreak, Brunei. *Emerg Infect Dis* **15**, 79-82.

Andino, R., Rieckhof, G. E., Achacoso, P. L. & Baltimore, D. (1993). Poliovirus RNA synthesis utilizes an RNP complex formed around the 5'-end of viral RNA. *Embo J* **12**, 3587-3598.

Andino, R., Rieckhof, G. E. & Baltimore, D. (1990). A functional ribonucleoprotein complex forms around the 5' end of poliovirus RNA. *Cell* **63**, 369-380.

Arita, M., Ami, Y., Wakita, T. & Shimizu, H. (2008). Cooperative effect of the attenuation determinants derived from poliovirus sabin 1 strain is essential for attenuation of enterovirus 71 in the NOD/SCID mouse infection model. *J Virol* **82**, 1787-1797.

Arita, M., Nagata, N., Iwata, N., Ami, Y., Suzaki, Y., Mizuta, K., Iwasaki, T., Sata, T., Wakita, T. & Shimizu, H. (2007). An attenuated strain of enterovirus 71 belonging to genotype a showed a broad spectrum of antigenicity with attenuated neurovirulence in cynomolgus monkeys. *J Virol* **81**, 9386-9395.

Arita, M., Shimizu, H., Nagata, N., Ami, Y., Suzaki, Y., Sata, T., Iwasaki, T. & Miyamura, T. (2005). Temperature-sensitive mutants of enterovirus 71 show attenuation in cynomolgus monkeys. *J Gen Virol* **86**, 1391-1401.

Bedard, K. M., Daijogo, S. & Semler, B. L. (2007). A nucleo-cytoplasmic SR protein functions in viral IRES-mediated translation initiation. *Embo J* **26**, 459-467.

Bedard, K. M. & Semler, B. L. (2004). Regulation of picornavirus gene expression. *Microb Infect* **6**, 702-713.

Bek, E. J., Hussain, K. M., Phuektes, P., Kok, C. C., Gao, Q., Cai, F., Gao, Z. & McMinn, P. C. (2011). Formalin-inactivated vaccine provokes cross-protective immunity in a mouse model of human enterovirus 71 infection. *Vaccine* **29**, 4829-4838.

Bek, E. J. & McMinn, P. C. (2010). Recent advances in research on human enterovirus 71. *Future Virol* **5**, 453-468.

Bek, E. J. & McMinn, P. C. (2012). The Pathogenesis and Prevention of Encephalitis due to Human Enterovirus 71. *Curr Infect Dis Rep* **14**, 397-407.

Boot, H. J., Dokic, K. & Peeters, B. P. (2001). Comparison of RNA and cDNA transfection methods for rescue of infectious bursal disease virus. *J Virol Methods* **97**, 67-76.

Boot, H. J., ter Huurne, A. A., Peeters, B. P. & Gielkens, A. L. (1999). Efficient rescue of infectious bursal disease virus from cloned cDNA: evidence for involvement of the 3'-terminal sequence in genome replication. *Virology* **265**, 330-341.

Boyer, J. C. & Haenni, A. L. (1994). Infectious transcripts and cDNA clones of RNA viruses. *Virology* **198**, 415-426.

Brown, B. A., Oberste, M. S., Alexander, J. P., Jr., Kennett, M. L. & Pallansch, M. A. (1999). Molecular epidemiology and evolution of enterovirus 71 strains isolated from 1970 to 1998. *J Virol* **73**, 9969-9975.

Brown, B. A. & Pallansch, M. A. (1995). Complete nucleotide sequence of enterovirus 71 is distinct from poliovirus. *Virus Res* **39**, 195-205.

Burke, K. L., Almond, J. W. & Evans, D. J. (1991). Antigen chimeras of poliovirus. *Prog Med Virol* **38**, 56-68.

Caggana, M., Chan, P. & Ramsingh, A. (1993). Identification of a single amino acid residue in the capsid protein VP1 of coxsackievirus B4 that determines the virulent phenotype. *J Virol* **67**, 4797-4803.

Cardosa, M. J., Perera, D., Brown, B. A., Cheon, D., Chan, H. M., Chan, K. P., Cho, H. & McMinn, P. (2003). Molecular epidemiology of human enterovirus 71 strains and recent outbreaks in the Asia-Pacific region: comparative analysis of the VP1 and VP4 genes. *Emerg Infect Dis* **9**, 461-468.

Castro, C., Arnold, J. J. & Cameron, C. E. (2005). Incorporation fidelity of the viral RNA-dependent RNA polymerase: a kinetic, thermodynamic and structural perspective. *Virus Res* **107**, 141-149.

Chan, Y. F. & AbuBakar, S. (2005). Human enterovirus 71 subgenotype B3 lacks coxsackievirus A16-like neurovirulence in mice infection. *Virol J* **2**, 74.

Chan, Y. F., Sam, I. C. & AbuBakar, S. (2010). Phylogenetic designation of enterovirus 71 genotypes and subgenotypes using complete genome sequences. *Infect Genet Evol* **10**, 404-412.

Chang, G. H., Lin, L., Luo, Y. J., Cai, L. J., Wu, X. Y., Xu, H. M. & Zhu, Q. Y. (2010). Sequence analysis of six enterovirus 71 strains with different virulences in humans. *Virus Res* **151**, 66-73.

Chang, L. Y., Chang, I. S., Chen, W. J., Huang, Y. C., Chen, G. W., Shih, S. R., Juang, J. L., Shih, H. M., Hsiung, C. A., Lin, T. Y. & Huang, L. M. (2008). HLA-A33 is associated with susceptibility to enterovirus 71 infection. *Pediatrics* **122**, 1271-1276.

Chang, S. C., Li, W. C., Chen, G. W., Tsao, K. C., Huang, C. G., Huang, Y. C., Chiu, C. H., Kuo, C. Y., Tsai, K. N., Shih, S. R. & Lin, T. Y. (2012). Genetic characterization of enterovirus 71 isolated from patients with severe disease by comparative analysis of complete genomes. *J Med Virol* **84**, 931-939.

Chen, C. S., Yao, Y. C., Lin, S. C., Lee, Y. P., Wang, Y. F., Wang, J. R., Liu, C. C., Lei, H. Y. & Yu, C. K. (2007a). Retrograde axonal transport: a major transmission route of enterovirus 71 in mice. *J Virol* **81**, 8996-9003.

Chen, K. T., Chang, H. L., Wang, S. T., Cheng, Y. T. & Yang, J. Y. (2007b). Epidemiologic features of hand-foot-mouth disease and herpangina caused by enterovirus 71 in Taiwan, 1998-2005. *Pediatrics* **120**, e244-252.

Chen, P., Song, Z., Qi, Y., Feng, X., Xu, N., Sun, Y., Wu, X., Yao, X., Mao, Q., Li, X., Dong, W., Wan, X., Huang, N., Shen, X., Liang, Z. & Li, W. (2012). Molecular Determinants of Enterovirus 71 Viral Entry: CLEFT AROUND GLN-172 ON VP1 PROTEIN INTERACTS WITH VARIABLE REGION ON SCAVENGE RECEPTOR B 2. *J Biol Chem* **287**, 6406-6420.

Chen, T. C., Chang, H. Y., Lin, P. F., Chern, J. H., Hsu, J. T., Chang, C. Y. & Shih, S. R. (2009). Novel antiviral agent DTriP-22 targets RNA-dependent RNA polymerase of enterovirus 71. *Antimicrob Agents Chemother* **53**, 2740-2747.

Chen, X., Zhang, Q., Li, J., Cao, W., Zhang, J. X., Zhang, L., Zhang, W., Shao, Z. J. & Yan, Y. (2010). Analysis of recombination and natural selection in human enterovirus 71. *Virology* **398**, 251-261.

Chen, Y. C., Yu, C. K., Wang, Y. F., Liu, C. C., Su, I. J. & Lei, H. Y. (2004). A murine oral enterovirus 71 infection model with central nervous system involvement. *J Gen Virol* **85**, 69-77.

Chow, K. C., Lee, C. C., Lin, T. Y., Shen, W. C., Wang, J. H. & Peng, C. T. (2000). Congenital enterovirus 71 infection: a case study with virology and immunohistochemistry. *Clin Infect Dis* **31**, 509-512.

Chua, B. H., Phuektes, P., Sanders, S. A., Nicholls, P. K. & McMinn, P. C. (2008). The molecular basis of mouse adaptation by human enterovirus 71. *J Gen Virol* **89**, 1622-1632.

Chua, K. B., Chua, B. H., Lee, C. S., Chem, Y. K., Ismail, N., Kiyu, A. & Kumarasamy, V. (2007). Genetic diversity of enterovirus 71 isolated from cases of hand, foot and mouth disease in the 1997, 2000 and 2005 outbreaks, Peninsular Malaysia. *Malays J Pathol* **29**, 69-78.

Chua, K. B. & Kasri, A. R. (2011). Hand foot and mouth disease due to enterovirus 71 in Malaysia. *Virol Sin* **26**, 221-228.

Chumakov, M., Voroshilova, M., Shindarov, L., Lavrova, I., Gracheva, L., Koroleva, G., Vasilenko, S., Brodvarova, I., Nikolova, M., Gyurova, S., Gacheva, M., Mitov, G., Ninov, N., Tsylka, E., Robinson, I., Frolova, M., Bashkirtsev, V., Martiyanova, L. & Rodin, V. (1979). Enterovirus 71 isolated from cases of epidemic poliomyelitis-like disease in Bulgaria. *Arch Virol* **60**, 329-340.

Chung, P. W., Huang, Y. C., Chang, L. Y., Lin, T. Y. & Ning, H. C. (2001). Duration of enterovirus shedding in stool. *J Microbiol Immunol Infect* **34**, 167-170.

Chung, Y. C., Ho, M. S., Wu, J. C., Chen, W. J., Huang, J. H., Chou, S. T. & Hu, Y. C. (2008). Immunization with virus-like particles of enterovirus 71 elicits potent immune responses and protects mice against lethal challenge. *Vaccine* **26**, 1855-1862.

Colston, E. & Racaniello, V. R. (1994). Soluble receptor-resistant poliovirus mutants identify surface and internal capsid residues that control interaction with the cell receptor. *Embo J* **13**, 5855-5862.

Colston, E. M. & Racaniello, V. R. (1995). Poliovirus variants selected on mutant receptor-expressing cells identify capsid residues that expand receptor recognition. *J Virol* **69**, 4823-4829.

Couderc, T., Delpeyroux, F., Le Blay, H. & Blondel, B. (1996). Mouse adaptation determinants of poliovirus type 1 enhance viral uncoating. *J Virol* **70**, 305-312.

Couderc, T., Hogle, J., Le Blay, H., Horaud, F. & Blondel, B. (1993). Molecular characterization of mouse-virulent poliovirus type 1 Mahoney mutants: involvement of residues of polypeptides VP1 and VP2 located on the inner surface of the capsid protein shell. *J Virol* **67**, 3808-3817.

Davis, J. A. (1999/2000). The Triple A Approach to Ensuring Animal Welfare. In *Animal Welfare Information Center Bulletin*, pp. 3-4.

De, W., Changwen, K., Wei, L., Monagin, C., Jin, Y., Cong, M., Hanri, Z. & Jun, S. (2011). A large outbreak of hand, foot, and mouth disease caused by EV71 and CAV16 in Guangdong, China, 2009. *Arch Virol* **156**, 945-953.

Deshpande, J. M., Nadkarni, S. S. & Francis, P. P. (2003). Enterovirus 71 isolated from a cse of acute flaccid paralysis in India represents a new genotype. *Curr Sci* **84**, 1350-1353.

Domingo, E. & Holland, J. J. (1997). RNA virus mutations and fitness for survival. *Annu Rev Microbiol* **51**, 151-178.

Domingo, E., Menendez-Arias, L. & Holland, J. J. (1997). RNA virus fitness. *Rev Med Virol* **7**, 87-96.

Domingo, E., Sheldon, J. & Perales, C. (2012). Viral quasispecies evolution. *Microbiol Mol Biol Rev* **76**, 159-216.

Douche-Aourik, F., Berlier, W., Feasson, L., Bourlet, T., Harrath, R., Omar, S., Grattard, F., Denis, C. & Pozzetto, B. (2003). Detection of enterovirus in human skeletal muscle from patients with chronic inflammatory muscle disease or fibromyalgia and healthy subjects. *J Med Virol* **71**, 540-547.

Evans, D. M., Dunn, G., Minor, P. D., Schild, G. C., Cann, A. J., Stanway, G., Almond, J. W., Currey, K. & Maizel, J. V., Jr. (1985). Increased neurovirulence associated with a single nucleotide change in a noncoding region of the Sabin type 3 poliovaccine genome. *Nature* **314**, 548-550.

Foltz, C. J. & Ullman-Cullere, M. (1999). Guideline for Assessing the health and Condition of Mice. In *Lab Animal*, pp. 28-31.

Fujimoto, T., Chikahira, M., Yoshida, S., Ebira, H., Hasegawa, A., Totsuka, A. & Nishio, O. (2002). Outbreak of central nervous system disease associated with hand, foot, and mouth disease in Japan during the summer of 2000: detection and molecular epidemiology of enterovirus 71. *Microbiol Immunol* **46**, 621-627.

Ghukasyan, V., Hsu, Y. Y., Kung, S. H. & Kao, F. J. (2007). Application of fluorescence resonance energy transfer resolved by fluorescence lifetime imaging microscopy for the detection of enterovirus 71 infection in cells. *J Biomed Opt* **12**, 024016.

Gilbert, G. L., Dickson, K. E., Waters, M. J., Kennett, M. L., Land, S. A. & Sneddon, M. (1988). Outbreak of enterovirus 71 infection in Victoria, Australia, with a high incidence of neurologic involvement. *Pediatr Infect Dis J* **7**, 484-488.

Goodfellow, I., Chaudhry, Y., Richardson, A., Meredith, J., Almond, J. W., Barclay, W. & Evans, D. J. (2000). Identification of a cis-acting replication element within the poliovirus coding region. *J Virol* **74**, 4590-4600.

Hagiwara, A., Yoneyama, T. & Hashimoto, I. (1982). Isolation of a temperature-sensitive strain of enterovirus 71 with reduced neurovirulence for monkeys. *J Gen Virol* **64**, 499-502.

Hamaguchi, T., Fujisawa, H., Sakai, K., Okino, S., Kurosaki, N., Nishimura, Y., Shimizu, H. & Yamada, M. (2008). Acute encephalitis caused by intrafamilial transmission of enterovirus 71 in adult. *Emerg Infect Dis* **14**, 828-830.

Hashimoto, I. & Hagiwara, A. (1982). Pathogenicity of a poliomyelitis-like disease in monkeys infected orally with enterovirus 71: a model for human infection. *Neuropathol Appl Neurobiol* **8**, 149-156.

Hellen, C. U. & Sarnow, P. (2001). Internal ribosome entry sites in eukaryotic mRNA molecules. *Genes Dev* **15**, 1593-1612.

Herold, J. & Andino, R. (2001). Poliovirus RNA replication requires genome circularization through a protein-protein bridge. *Mol Cell* **7**, 581-591.

Herrero, L. J., Lee, C. S., Hurrelbrink, R. J., Chua, B. H., Chua, K. B. & McMinn, P. C. (2003). Molecular epidemiology of enterovirus 71 in peninsular Malaysia, 1997-2000. *Arch Virol* **148**, 1369-1385.

Ho, H. Y., Cheng, M. L., Weng, S. F., Chang, L., Yeh, T. T., Shih, S. R. & Chiu, D. T. (2008). Glucose-6-phosphate dehydrogenase deficiency enhances enterovirus 71 infection. *J Gen Virol* **89**, 2080-2089.

Hogle, J. M., Chow, M. & Filman, D. J. (1985). Three-dimensional structure of poliovirus at 2.9 A resolution. *Science* **229**, 1358-1365.

Holland, J., Spindler, K., Horodyski, F., Grabau, E., Nichol, S. & VandePol, S. (1982). Rapid evolution of RNA genomes. *Science* **215**, 1577-1585.

Huang, P. N., Lin, J. Y., Locker, N., Kung, Y. A., Hung, C. T., Huang, H. I., Li, M. L. & Shih, S. R. (2011a). Far upstream element binding protein 1 binds the internal ribosomal entry site of enterovirus 71 and enhances viral translation and viral growth. *Nucleic Acids Res* **39**, 9633-9648.

Huang, S. C., Chang, C. L., Wang, P. S., Tsai, Y. & Liu, H. S. (2009a). Enterovirus 71-induced autophagy detected in vitro and in vivo promotes viral replication. *J Med Virol* **81**, 1241-1252.

Huang, S. C., Hsu, Y. W., Wang, H. C., Huang, S. W., Kiang, D., Tsai, H. P., Wang, S. M., Liu, C. C., Lin, K. H., Su, I. J. & Wang, J. R. (2008). Appearance of intratypic recombination of enterovirus 71 in Taiwan from 2002 to 2005. *Virus Res* **131**, 250-259.

Huang, S. W., Hsu, Y. W., Smith, D. J., Kiang, D., Tsai, H. P., Lin, K. H., Wang, S. M., Liu, C. C., Su, I. J. & Wang, J. R. (2009b). Reemergence of enterovirus 71 in 2008 in taiwan: dynamics of genetic and antigenic evolution from 1998 to 2008. *J Clin Microbiol* **47**, 3653-3662.

Huang, S. W., Kiang, D., Smith, D. J. & Wang, J. R. (2011b). Evolution of re-emergent virus and its impact on enterovirus 71 epidemics. *Exp Biol Med (Maywood)* **236**, 899-908.

Huang, S. W., Wang, Y. F., Yu, C. K., Su, I. J. & Wang, J. R. (2012). Mutations in VP2 and VP1 capsid proteins increase infectivity and mouse lethality of enterovirus 71 by virus binding and RNA accumulation enhancement. *Virology* **422**, 132-143.

Huang, Y. P., Lin, T. L., Hsu, L. C., Chen, Y. J., Tseng, Y. H., Hsu, C. C., Fan, W. B., Yang, J. Y., Chang, F. Y. & Wu, H. S. (2010). Genetic diversity and C2-like subgenogroup strains of enterovirus 71, Taiwan, 2008. *Virol J* **7**, 277.

Hunziker, I. P., Cornell, C. T. & Whitton, J. L. (2007). Deletions within the 5'UTR of coxsackievirus B3: consequences for virus translation and replication. *Virology* **360**, 120-128.

Hurrelbrink, R. J., Nestorowicz, A. & McMinn, P. C. (1999). Characterization of infectious Murray Valley encephalitis virus derived from a stably cloned genome-length cDNA. *J Gen Virol* **80 (Pt 12)**, 3115-3125.

Janda, M., French, R. & Ahlquist, P. (1987). High efficiency T7 polymerase synthesis of infectious RNA from cloned brome mosaic virus cdna and effects of 5' extensions on transcript infectivity. *Virology* **158**, 259-262.

Jia, Q., Hogle, J. M., Hashikawa, T. & Nomoto, A. (2001). Molecular genetic analysis of revertants from a poliovirus mutant that is specifically adapted to the mouse spinal cord. *J Virol* **75**, 11766-11772.

Kauder, S., Kan, S. & Racaniello, V. R. (2006). Age-dependent poliovirus replication in the mouse central nervous system is determined by internal ribosome entry site-mediated translation. *J Virol* **80**, 2589-2595.

Kawamura, N., Kohara, M., Abe, S., Komatsu, T., Tago, K., Arita, M. & Nomoto, A. (1989). Determinants in the 5' noncoding region of poliovirus Sabin 1 RNA that influence the attenuation phenotype. *J Virol* **63**, 1302-1309.

Khong, W. X., Yan, B., Yeo, H., Tan, E. L., Lee, J. J., Ng, J. K., Chow, V. T. & Alonso, S. (2012). A Non-Mouse-Adapted Enterovirus 71 (EV71) Strain Exhibits Neurotropism, Causing Neurological Manifestations in a Novel Mouse Model of EV71 Infection. *J Virol* **86**, 2121-2131.

Knowles, N. J., Hovi, T., Hyypiä, T., King, A. M. Q., Lindberg, A. M., Pallansch, M. A., Palmenberg, A. C., Simmonds, P., Skern, T., Stanway, G., Yamashita, T. & Zell, R. (2012). *Picornaviridae. In: Virus Taxonomy: Classification and Nomenclature of Viruses: Ninth Report of the International Committee on Taxonomy of Viruses.*: San Diego: Elsevier.

Koike, S., Taya, C., Aoki, J., Matsuda, Y., Ise, I., Takeda, H., Matsuzaki, T., Amanuma, H., Yonekawa, H. & Nomoto, A. (1994). Characterization of three different transgenic mouse lines that carry human poliovirus receptor gene--influence of the transgene expression on pathogenesis. *Arch Virol* **139**, 351-363.

Koike, S., Taya, C., Kurata, T., Abe, S., Ise, I., Yonekawa, H. & Nomoto, A. (1991). Transgenic mice susceptible to poliovirus. *Proc Natl Acad Sci U S A* **88**, 951-955.

Kok, C. C., Phuektes, P., Bek, E. & McMinn, P. C. (2012). Modification of the untranslated regions of human enterovirus 71 impairs growth in a cell-specific manner. *J Virol* **86**, 542-552.

Komatsu, H., Shimizu, Y., Takeuchi, Y., Ishiko, H. & Takada, H. (1999). Outbreak of severe neurologic involvement associated with Enterovirus 71 infection. *Pediatr Neurol* **20**, 17-23.

Kraus, W., Zimmermann, H., Zimmermann, A., Eggers, H. J. & Nelsen-Salz, B. (1995). Infectious cDNA clones of echovirus 12 and a variant resistant against the uncoating inhibitor rhodanine differ in seven amino acids. *J Virol* **69**, 5853-5858.

Kuo, R. L., Kung, S. H., Hsu, Y. Y. & Liu, W. T. (2002). Infection with enterovirus 71 or expression of its 2A protease induces apoptotic cell death. *J Gen Virol* **83**, 1367-1376.

Lancaster, K.Z. & Pfeiffer, J.K. (2012). Viral population dynamics and virulence thresholds. *Curr Opin Microbiol* **15**, 525-530.

Lai, C. J., Zhao, B. T., Hori, H. & Bray, M. (1991). Infectious RNA transcribed from stably cloned full-length cDNA of dengue type 4 virus. *Proc Natl Acad Sci U S A* **88**, 5139-5143.

Lal, S. K., Kumar, P., Yeo, W. M., Kar-Roy, A. & Chow, V. T. (2006). The VP1 protein of human enterovirus 71 self-associates via an interaction domain spanning amino acids 66-297. *J Med Virol* **78**, 582-590.

Lee, J. J., Seah, J. B., Chow, V. T., Poh, C. L. & Tan, E. L. (2011). Comparative proteome analyses of host protein expression in response to Enterovirus 71 and Coxsackievirus A16 infections. *J Proteomics* **74**, 2018-2024.

Leong, W. F. & Chow, V. T. (2006). Transcriptomic and proteomic analyses of rhabdomyosarcoma cells reveal differential cellular gene expression in response to enterovirus 71 infection. *Cell Microbiol* **8**, 565-580.

Li, M. L., Hsu, T. A., Chen, T. C., Chang, S. C., Lee, J. C., Chen, C. C., Stollar, V. & Shih, S. R. (2002). The 3C protease activity of enterovirus 71 induces human neural cell apoptosis. *Virology* **293**, 386-395.

Li, Y. P., Liang, Z. L., Gao, Q., Huang, L. R., Mao, Q. Y., Wen, S. Q., Liu, Y., Yin, W. D., Li, R. C. & Wang, J. Z. (2012). Safety and immunogenicity of a novel human Enterovirus 71 (EV71) vaccine: A randomized, placebo-controlled, double-blind, Phase I clinical trial. *Vaccine* **30**, 3295-3303.

Lin, J. Y., Chen, T. C., Weng, K. F., Chang, S. C., Chen, L. L. & Shih, S. R. (2009a). Viral and host proteins involved in picornavirus life cycle. *J Biomed Sci* **16**, 103.

Lin, J. Y., Li, M. L., Huang, P. N., Chien, K. Y., Horng, J. T. & Shih, S. R. (2008). Heterogeneous nuclear ribonuclear protein K interacts with the enterovirus 71 5' untranslated region and participates in virus replication. *J Gen Virol* **89**, 2540-2549.

Lin, J. Y., Li, M. L. & Shih, S. R. (2009b). Far upstream element binding protein 2 interacts with enterovirus 71 internal ribosomal entry site and negatively regulates viral translation. *Nucleic Acids Res* **37**, 47-59.

Lin, K. H., Hwang, K. P., Ke, G. M., Wang, C. F., Ke, L. Y., Hsu, Y. T., Tung, Y. C., Chu, P. Y., Chen, B. H., Chen, H. L., Kao, C. L., Wang, J. R., Eng, H. L., Wang, S. Y., Hsu, L. C. & Chen, H. Y. (2006). Evolution of EV71 genogroup in Taiwan from 1998 to 2005: an emerging of subgenogroup C4 of EV71. *J Med Virol* **78**, 254-262.

Lin, Y. W., Lin, H. Y., Tsou, Y. L., Chitra, E., Hsiao, K. N., Shao, H. Y., Liu, C. C., Sia, C., Chong, P. & Chow, Y. H. (2012). Human SCARB2-mediated entry and endocytosis of EV71. *PLoS One* **7**, e30507.

Liu, J. N., Wang, W., Duo, J. Y., Hao, Y., Ma, C. M., Li, W. B., Lin, S. Z., Gao, X. Z., Liu, X. L., Xu, Y. F., Xu, W. B., Qin, C. & Zhang, L. F. (2010). Combined peptides of human enterovirus 71 protect against virus infection in mice. *Vaccine* **28**, 7444-7451.

Lum, L. C., Wong, K. T., Lam, S. K., Chua, K. B. & Goh, A. Y. (1998a). Neurogenic pulmonary oedema and enterovirus 71 encephalomyelitis. *Lancet* **352**, 1391.

Lum, L. C., Wong, K. T., Lam, S. K., Chua, K. B., Goh, A. Y., Lim, W. L., Ong, B. B., Paul, G., AbuBakar, S. & Lambert, M. (1998b). Fatal enterovirus 71 encephalomyelitis. *J Pediatr* **133**, 795-798.

Lyons, T., Murray, K. E., Roberts, A. W. & Barton, D. J. (2001). Poliovirus 5'-terminal cloverleaf RNA is required in cis for VPg uridylylation and the initiation of negative-strand RNA synthesis. *J Virol* **75**, 10696-10708.

Macadam, A. J., Pollard, S. R., Ferguson, G., Dunn, G., Skuce, R., Almond, J. W. & Minor, P. D. (1991). The 5' noncoding region of the type 2 poliovirus vaccine strain contains determinants of attenuation and temperature sensitivity. *Virology* **181**, 451-458.

Mao, L. X., Wu, B., Bao, W. X., Han, F. A., Xu, L., Ge, Q. J., Yang, J., Yuan, Z. H., Miao, C. H., Huang, X. X., Zhang, C. & Xu, H. (2010). Epidemiology of hand, foot, and mouth disease and genotype characterization of Enterovirus 71 in Jiangsu, China. *J Clin Virol* **49**, 100-104.

Martino, T. A., Tellier, R., Petric, M., Irwin, D. M., Afshar, A. & Liu, P. P. (1999). The complete consensus sequence of coxsackievirus B6 and generation of infectious clones by long RT-PCR. *Virus Res* **64**, 77-86.

McMinn, P., Lindsay, K., Perera, D., Chan, H. M., Chan, K. P. & Cardosa, M. J. (2001a). Phylogenetic analysis of enterovirus 71 strains isolated during linked epidemics in Malaysia, Singapore, and Western Australia. *J Virol* **75**, 7732-7738.

McMinn, P., Stratov, I., Nagarajan, L. & Davis, S. (2001b). Neurological manifestations of enterovirus 71 infection in children during an outbreak of hand, foot, and mouth disease in Western Australia. *Clin Infect Dis* **32**, 236-242.

McMinn, P. C. (2002). An overview of the evolution of enterovirus 71 and its clinical and public health significance. *FEMS Microbiol Rev* **26**, 91-107.

McMinn, P. C. (2012). Recent advances in the molecular epidemiology and control of human enterovirus 71 infection. *Curr Opin Virol* **2**, 199-205.

McWilliam Leitch, E. C., Cabrerizo, M., Cardosa, J., Harvala, H., Ivanova, O. E., Koike, S., Kroes, A. C., Lukashev, A., Perera, D., Roivainen, M., Susi, P., Trallero, G., Evans, D. J. & Simmonds, P. (2012). The association of recombination events in the founding and emergence of subgenogroup evolutionary lineages of human enterovirus 71. *J Virol* **86**, 2676-2685.

Mendelsohn, C. L., Wimmer, E. & Racaniello, V. R. (1989). Cellular receptor for poliovirus: molecular cloning, nucleotide sequence, and expression of a new member of the immunoglobulin superfamily. *Cell* **56**, 855-865.

Merkle, I., van Ooij, M. J., van Kuppeveld, F. J., Glaudemans, D. H., Galama, J. M., Henke, A., Zell, R. & Melchers, W. J. (2002). Biological significance of a human enterovirus B-specific RNA element in the 3' nontranslated region. *J Virol* **76**, 9900-9909.

Merovitz, L., Demers, A. M., Newby, D. & McDonald, J. (2000). Enterovirus 71 infections at a Canadian center. *Pediatr Infect Dis J* **19**, 755-757.

Miyamura, K., Nishimura, Y., Abo, M., Wakita, T. & Shimizu, H. (2011). Adaptive mutations in the genomes of enterovirus 71 strains following infection of mouse cells expressing human P-selectin glycoprotein ligand-1. *J Gen Virol* **92**, 287-291.

Mizuta, K., Abiko, C., Murata, T., Matsuzaki, Y., Itagaki, T., Sanjoh, K., Sakamoto, M., Hongo, S., Murayama, S. & Hayasaka, K. (2005). Frequent importation of enterovirus 71 from surrounding countries into the local community of Yamagata, Japan, between 1998 and 2003. *J Clin Microbiol* **43**, 6171-6175.

Moss, E. G. & Racaniello, V. R. (1991). Host range determinants located on the interior of the poliovirus capsid. *Embo J* **10**, 1067-1074.

Munemura, T., Saikusa, M., Kawakami, C., Shimizu, H., Oseto, M., Hagiwara, A., Kimura, H. & Miyamura, T. (2003). Genetic diversity of enterovirus 71 isolated from cases of hand, foot and mouth disease in Yokohama City between 1982 and 2000. *Arch Virol* **148**, 253-263.

Murray, M. G., Bradley, J., Yang, X. F., Wimmer, E., Moss, E. G. & Racaniello, V. R. (1988). Poliovirus host range is determined by a short amino acid sequence in neutralization antigenic site I. *Science* **241**, 213-215.

Nagata, N., Iwasaki, T., Ami, Y., Tano, Y., Harashima, A., Suzaki, Y., Sato, Y., Hasegawa, H., Sata, T., Miyamura, T. & Shimizu, H. (2004). Differential localization of neurons susceptible to enterovirus 71 and poliovirus type 1 in the central nervous system of cynomolgus monkeys after intravenous inoculation. *J Gen Virol* **85**, 2981-2989.

Nagata, N., Shimizu, H., Ami, Y., Tano, Y., Harashima, A., Suzaki, Y., Sato, Y., Miyamura, T., Sata, T. & Iwasaki, T. (2002). Pyramidal and extrapyramidal involvement in experimental infection of cynomolgus monkeys with enterovirus 71. *J Med Virol* **67**, 207-216.

Nishimura, Y., Shimojima, M., Tano, Y., Miyamura, T., Wakita, T. & Shimizu, H. (2009). Human P-selectin glycoprotein ligand-1 is a functional receptor for enterovirus 71. *Nat Med* **15**, 794-797.

Ong, K. C., Badmanathan, M., Devi, S., Leong, K. L., Cardosa, M. J. & Wong, K. T. (2008). Pathologic characterization of a murine model of human enterovirus 71 encephalomyelitis. *J Neuropathol Exp Neurol* **67**, 532-542.

Ong, K. C., Devi, S., Cardosa, M. J. & Wong, K. T. (2010). Formaldehyde-inactivated whole-virus vaccine protects a murine model of enterovirus 71 encephalomyelitis against disease. *J Virol* **84**, 661-665.

Ooi, M. H., Wong, S. C., Podin, Y., Akin, W., del Sel, S., Mohan, A., Chieng, C. H., Perera, D., Clear, D., Wong, D., Blake, E., Cardosa, J. & Solomon, T. (2007). Human enterovirus 71 disease in Sarawak, Malaysia: a prospective clinical, virological, and molecular epidemiological study. *Clin Infect Dis* **44**, 646-656.

Pallansch, M. & Roos, R. (2007). Enteroviruses: polioviruses, coxsackieviruses, echoviruses and newer enteroviruses. In *Fields Virology*, Fifth edn, pp. 840-893. Edited by D. M. Knipe & P. M. Howley: Lippincott Williams and Wilkins.

Patel, K. P. & Bergelson, J. M. (2009). Receptors identified for hand, foot and mouth virus. *Nat Med* **15**, 728-729.

Paul, A. V., Peters, J., Mugavero, J., Yin, J., van Boom, J. H. & Wimmer, E. (2003). Biochemical and genetic studies of the VPg uridylylation reaction catalyzed by the RNA polymerase of poliovirus. *J Virol* **77**, 891-904.

Paul, A. V., Rieder, E., Kim, D. W., van Boom, J. H. & Wimmer, E. (2000). Identification of an RNA hairpin in poliovirus RNA that serves as the primary template in the in vitro uridylylation of VPg. *J Virol* **74**, 10359-10370.

Pfeiffer, J. K. & Kirkegaard, K. (2005). Increased fidelity reduces poliovirus fitness and virulence under selective pressure in mice. *PLoS pathogens* **1**, e11.

Phuektes, P., Chua, B. H., Sanders, S., Bek, E. J., Kok, C. C. & McMinn, P. C. (2011). Mapping genetic determinants of the cell-culture growth phenotype of enterovirus 71. *J Gen Virol* **92**, 1380-1390.

Pilipenko, E. V., Blinov, V. M., Romanova, L. I., Sinyakov, A. N., Maslova, S. V. & Agol, V. I. (1989). Conserved structural domains in the 5'-untranslated region of picornaviral genomes: an analysis of the segment controlling translation and neurovirulence. *Virology* **168**, 201-209.

Pilipenko, E. V., Gmyl, A. P., Maslova, S. V., Svitkin, Y. V., Sinyakov, A. N. & Agol, V. I. (1992a). Prokaryotic-like cis elements in the cap-independent internal initiation of translation on picornavirus RNA. *Cell* **68**, 119-131.

Pilipenko, E. V., Maslova, S. V., Sinyakov, A. N. & Agol, V. I. (1992b). Towards identification of cis-acting elements involved in the replication of enterovirus and rhinovirus RNAs: a proposal for the existence of tRNA-like terminal structures. *Nucleic Acids Res* **20**, 1739-1745.

Plevka, P., Perera, R., Cardosa, J., Kuhn, R. J. & Rossmann, M. G. (2012). Crystal structure of human enterovirus 71. *Science* **336**, 1274.

Poyry, T., Hyypia, T., Horsnell, C., Kinnunen, L., Hovi, T. & Stanway, G. (1994). Molecular analysis of coxsackievirus A16 reveals a new genetic group of enteroviruses. *Virology* **202**, 982-987.

Puenpa, J., Theamboonlers, A., Korkong, S., Linsuwanon, P., Thongmee, C., Chatproedprai, S. & Poovorawan, Y. (2011). Molecular characterization and complete genome analysis of human enterovirus 71 and coxsackievirus A16 from children with hand, foot and mouth disease in Thailand during 2008-2011. *Arch Virol* **156**, 2007-2013.

Racaniello, V. R. (2007). Picornaviridae: the viruses and their replication. In *Fields Virology*, Fifith Edition edn, pp. 795-838. Edited by D. M. Knipe & P. M. Howley: Lippincott Williams & Wilkins.

Racaniello, V. R. & Baltimore, D. (1981). Cloned poliovirus complementary DNA is infectious in mammalian cells. *Science* **214**, 916-919.

Reed, L. J. & Muench, H. (1938). A simple method of estimating fifty percent endpoints. *Am J Hyg* **27**, 493-497.

Ren, R. & Racaniello, V. R. (1992). Human poliovirus receptor gene expression and poliovirus tissue tropism in transgenic mice. *J Virol* **66**, 296-304.

Ren, R. B., Costantini, F., Gorgacz, E. J., Lee, J. J. & Racaniello, V. R. (1990). Transgenic mice expressing a human poliovirus receptor: a new model for poliomyelitis. *Cell* **63**, 353-362.

Roberts, G. B. & Boyd, J. F. (1987). The histopathology of enterovirus infections of new-born mice. *J Infect* **15**, 45-56.

Sanders, S. A., Herrero, L. J., McPhie, K., Chow, S. S., Craig, M. E., Dwyer, D. E., Rawlinson, W. & McMinn, P. C. (2006). Molecular epidemiology of enterovirus 71 over two decades in an Australian urban community. *Arch Virol* **151**, 1003-1013.

Schmidt, N. J., Lennette, E. H. & Ho, H. H. (1974). An apparently new enterovirus isolated from patients with disease of the central nervous system. *J Infect Dis* **129**, 304-309.

Schuffenecker, I., Mirand, A., Antona, D., Henquell, C., Chomel, J. J., Archimbaud, C., Billaud, G., Peigue-Lafeuille, H., Lina, B. & Bailly, J. L. (2011). Epidemiology of human enterovirus 71 infections in France, 2000-2009. *J Clin Virol* **50**, 50-56.

Shafren, D. R., Dorahy, D. J., Greive, S. J., Burns, G. F. & Barry, R. D. (1997). Mouse cells expressing human intercellular adhesion molecule-1 are susceptible to infection by coxsackievirus A21. *J Virol* **71**, 785-789.

Shekhar, K., Lye, M. S., Norlijah, O., Ong, F., Looi, L. M., Khuzaiah, R., Marzuki, I., Hussein, I., Wong, S. L., Mohan, J., Sinniah, M. & Abu Bakar, S. (2005). Deaths in children during an outbreak of hand, foot and mouth disease in Peninsular Malaysia--clinical and pathological characteristics. *Med J Malaysia* **60**, 297-304.

Shih, S. R., Ho, M. S., Lin, K. H., Wu, S. L., Chen, Y. T., Wu, C. N., Lin, T. Y., Chang, L. Y., Tsao, K. C., Ning, H. C., Chang, P. Y., Jung, S. M., Hsueh, C. & Chang, K. S. (2000). Genetic analysis of enterovirus 71 isolated from fatal and non-fatal cases of hand, foot and mouth disease during an epidemic in Taiwan, 1998. *Virus Res* **68**, 127-136.

Shih, S. R., Stollar, V. & Li, M. L. (2011). Host factors in enterovirus 71 replication. *J Virol* **85**, 9658-9666.

Shih, S. R., Weng, K. F., Stollar, V. & Li, M. L. (2008). Viral protein synthesis is required for Enterovirus 71 to induce apoptosis in human glioblastoma cells. *J Neurovirol* **14**, 53-61.

Shimizu, H., Utama, A., Onnimala, N., Li, C., Li-Bi, Z., Yu-Jie, M., Pongsuwanna, Y. & Miyamura, T. (2004). Molecular epidemiology of enterovirus 71 infection in the Western Pacific Region. *Pediatr Int* **46**, 231-235.

Shimizu, H., Utama, A., Yoshii, K., Yoshida, H., Yoneyama, T., Sinniah, M., Yusof, M. A., Okuno, Y., Okabe, N., Shih, S. R., Chen, H. Y., Wang, G. R., Kao, C. L., Chang, K. S., Miyamura, T. & Hagiwara, A. (1999). Enterovirus 71 from fatal and nonfatal cases of hand, foot and mouth disease epidemics in Malaysia, Japan and Taiwan in 1997-1998. *Jpn J Infect Dis* **52**, 12-15.

Siguret, V., Ribba, A. S., Cherel, G., Meyer, D. & Pietu, G. (1994). Effect of plasmid size on transformation efficiency by electroporation of Escherichia coli DH5 alpha. *BioTechniques* **16**, 422-426.

Silvestri, L. S., Parilla, J. M., Morasco, B. J., Ogram, S. A. & Flanegan, J. B. (2006). Relationship between poliovirus negative-strand RNA synthesis and the length of the 3' poly(A) tail. *Virology* **345**, 509-519.

Singh, S., Poh, C. L. & Chow, V. T. (2002). Complete sequence analyses of enterovirus 71 strains from fatal and non-fatal cases of the hand, foot and mouth disease outbreak in Singapore (2000). *Microbiol Immunol* **46**, 801-808.

Solomon, T., Lewthwaite, P., Perera, D., Cardosa, M. J., McMinn, P. & Ooi, M. H. (2010). Virology, epidemiology, pathogenesis, and control of enterovirus 71. *Lancet Infect Dis* **10**, 778-790.

Solomon, T. & Willison, H. (2003). Infectious causes of acute flaccid paralysis. *Curr Opin Infect Dis* **16**, 375-381.

Steil, B. P. & Barton, D. J. (2009). Cis-active RNA elements (CREs) and picornavirus RNA replication. *Virus Res* **139**, 240-252.

Tai, W. C., Hsieh, H. J. & Wu, M. T. (2009). Hand, foot and mouth disease in a healthy adult caused by intrafamilial transmission of enterovirus 71. *Br J Dermatol* **160**, 890-892.

Tamura, K., Peterson, D., Peterson, N., Stecher, G., Nei, M. & Kumar, S. (2011). MEGA5: molecular evolutionary genetics analysis using maximum likelihood, evolutionary distance, and maximum parsimony methods. *Mol Biol Evol* **28**, 2731-2739.

Tao, Z., Wang, H. & Xu, A. (2012). Identification of a c2 subgenogroup strain of enterovirus 71 in a retrospective study in shandong province, china, from 1990 to 2010. *J Clin Microbiol* **50**, 1823-1824.

Tee, K. K., Lam, T. T., Chan, Y. F., Bible, J. M., Kamarulzaman, A., Tong, C. Y., Takebe, Y. & Pybus, O. G. (2010). Evolutionary genetics of human enterovirus 71: origin, population dynamics, natural selection, and seasonal periodicity of the VP1 gene. *J Virol* **84**, 3339-3350.

Thompson, J. D., Gibson, T. J., Plewniak, F., Jeanmougin, F. & Higgins, D. G. (1997). The CLUSTAL_X windows interface: flexible strategies for multiple sequence alignment aided by quality analysis tools. *Nucleic Acids Res* **25**, 4876-4882.

Thompson, S. R. & Sarnow, P. (2003). Enterovirus 71 contains a type I IRES element that functions when eukaryotic initiation factor eIF4G is cleaved. *Virology* **315**, 259-266.

Tindall, K.R. & Kunkel, T.A. (1988). Fidelity of DNA synthesis by the Thermus aquaticus DNA polymerase. *Biochemistry* **27**, 6008-6013.

Tong, C. Y., Bible, J. M. & Platt, C. (2011). A fatal case of enterovirus 71 infection with a single nucleotide variation in domain V of the 5' untranslated region. *Pediatr Infect Dis J* **30**, 1013-1014.

Tsai, H. P., Kuo, P. H., Liu, C. C. & Wang, J. R. (2001). Respiratory viral infections among pediatric inpatients and outpatients in Taiwan from 1997 to 1999. *J Clin Microbiol* **39**, 111-118.

Tu, P. V., Thao, N. T., Perera, D., Huu, T. K., Tien, N. T., Thuong, T. C., How, O. M., Cardosa, M. J. & McMinn, P. C. (2007). Epidemiologic and virologic investigation of hand, foot, and mouth disease, southern Vietnam, 2005. *Emerg Infect Dis* **13**, 1733-1741.

Tung, W. H., Hsieh, H. L. & Yang, C. M. (2010). Enterovirus 71 induces COX-2 expression via MAPKs, NF-kappaB, and AP-1 in SK-N-SH cells: Role of PGE(2) in viral replication. *Cel Signal* **22**, 234-246.

van der Sanden, S., Koopmans, M., Uslu, G. & van der Avoort, H. (2009). Epidemiology of enterovirus 71 in the Netherlands, 1963 to 2008. *J Clin Microbiol* **47**, 2826-2833.

van der Sanden, S., van Eek, J., Martin, D. P., van der Avoort, H., Vennema, H. & Koopmans, M. (2011). Detection of recombination breakpoints in the genomes of human enterovirus 71 strains isolated in the Netherlands in epidemic and non-epidemic years, 1963-2010. *Infect Genet Evol* **11**, 886-894.

van Ooij, M. J., Vogt, D. A., Paul, A., Castro, C., Kuijpers, J., van Kuppeveld, F. J., Cameron, C. E., Wimmer, E., Andino, R. & Melchers, W. J. (2006). Structural and functional characterization of the coxsackievirus B3 CRE(2C): role of CRE(2C) in negative- and positive-strand RNA synthesis. *J Gen Virol* **87**, 103-113.

Wang, J., Wu, Z. & Jin, Q. (2012a). COPI Is Required for Enterovirus 71 Replication. *PLoS One* **7**, e38035.

Wang, J. R., Tuan, Y. C., Tsai, H. P., Yan, J. J., Liu, C. C. & Su, I. J. (2002). Change of major genotype of enterovirus 71 in outbreaks of hand-foot-and-mouth disease in Taiwan between 1998 and 2000. *J Clin Microbiol* **40**, 10-15.

Wang, S. M., Ho, T. S., Lin, H. C., Lei, H. Y., Wang, J. R. & Liu, C. C. (2012b). Reemerging of enterovirus 71 in Taiwan: the age impact on disease severity. *Eur J Clin Microbiol Infect Dis* **31**, 1219-1224.

Wang, S. M., Lei, H. Y., Huang, K. J., Wu, J. M., Wang, J. R., Yu, C. K., Su, I. J. & Liu, C. C. (2003). Pathogenesis of enterovirus 71 brainstem encephalitis in pediatric patients: roles of cytokines and cellular immune activation in patients with pulmonary edema. *J Infect Dis* **188**, 564-570.

Wang, W., Duo, J., Liu, J., Ma, C., Zhang, L., Wei, Q. & Qin, C. (2011). A mouse muscle-adapted enterovirus 71 strain with increased virulence in mice. *Microb Infect* **13**, 862-870.

Wang, X., Peng, W., Ren, J., Hu, Z., Xu, J., Lou, Z., Li, X., Yin, W., Shen, X., Porta, C., Walter, T. S., Evans, G., Axford, D., Owen, R., Rowlands, D. J., Wang, J., Stuart, D. I., Fry, E. E. & Rao, Z. (2012c). A sensor-adaptor mechanism for enterovirus uncoating from structures of EV71. *Nat Struct Mol Biol* **19**, 424-429.

Wang, X., Zhu, C., Bao, W., Zhao, K., Niu, J., Yu, X. F. & Zhang, W. (2012d). Characterization of full-length enterovirus 71 strains from severe and mild disease patients in northeastern China. *PLoS One* **7**, e32405.

Wang, Y. F., Chou, C. T., Lei, H. Y., Liu, C. C., Wang, S. M., Yan, J. J., Su, I. J., Wang, J. R., Yeh, T. M., Chen, S. H. & Yu, C. K. (2004). A mouse-adapted enterovirus 71 strain causes neurological disease in mice after oral infection. *J Virol* **78**, 7916-7924.

Weng, K. F., Chen, L. L., Huang, P. N. & Shih, S. R. (2010). Neural pathogenesis of enterovirus 71 infection. *Microb Infect* **12**, 505-510.

Weng, K. F., Li, M. L., Hung, C. T. & Shih, S. R. (2009). Enterovirus 71 3C protease cleaves a novel target CstF-64 and inhibits cellular polyadenylation. *PLoS pathogens* **5**, e1000593.

Wong, K. T., Munisamy, B., Ong, K. C., Kojima, H., Noriyo, N., Chua, K. B., Ong, B. B. & Nagashima, K. (2008). The distribution of inflammation and virus in human enterovirus 71 encephalomyelitis suggests possible viral spread by neural pathways. *J Neuropathol Exp Neurol* **67**, 162-169.

Wright, A. J. & Phillpotts, R. J. (1998). Humane endpoints are an objective measure of morbidity in Venezuelan encephalomyelitis virus infection of mice. *Arch Virol* **143**, 1155-1162.

Wu, C. N., Lin, Y. C., Fann, C., Liao, N. S., Shih, S. R. & Ho, M. S. (2001). Protection against lethal enterovirus 71 infection in newborn mice by passive immunization with subunit VP1 vaccines and inactivated virus. *Vaccine* **20**, 895-904.

Xie, J., Jiao, Y., Qiu, Z., Li, Q. & Li, T. (2010). Significant elevation of B cells at the acute stage in enterovirus 71-infected children with central nervous system involvement. *Scand J Infect Dis* **42**, 931-935.

Yamayoshi, S., Iizuka, S., Yamashita, T., Minagawa, H., Mizuta, K., Okamoto, M., Nishimura, H., Sanjoh, K., Katsushima, N., Itagaki, T., Nagai, Y., Fujii, K. & Koike, S. (2012). Human SCARB2-dependent infection by coxsackievirus A7, A14, and A16 and enterovirus 71. *J Virol* **86**, 5686-5696.

Yamayoshi, S. & Koike, S. (2011). Identification of a human SCARB2 region that is important for enterovirus 71 binding and infection. *J Virol* **85**, 4937-4946.

Yamayoshi, S., Yamashita, Y., Li, J., Hanagata, N., Minowa, T., Takemura, T. & Koike, S. (2009). Scavenger receptor B2 is a cellular receptor for enterovirus 71. *Nat Med* **15**, 798-801.

Yang, K. D., Yang, M. Y., Li, C. C., Lin, S. F., Chong, M. C., Wang, C. L., Chen, R. F. & Lin, T. Y. (2001). Altered cellular but not humoral reactions in children with complicated enterovirus 71 infections in Taiwan. *J Infect Dis* **183**, 850-856.

Yeates, T. O., Jacobson, D. H., Martin, A., Wychowski, C., Girard, M., Filman, D. J. & Hogle, J. M. (1991). Three-dimensional structure of a mouse-adapted type 2/type 1 poliovirus chimera. *Embo J* **10**, 2331-2341.

Yeh, M. T., Wang, S. W., Yu, C. K., Lin, K. H., Lei, H. Y., Su, I. J. & Wang, J. R. (2011). A single nucleotide in stem loop II of 5'-untranslated region contributes to virulence of enterovirus 71 in mice. *PLoS One* **6**, e27082.

Yi, L., Lu, J., Kung, H. F. & He, M. L. (2011). The virology and developments toward control of human enterovirus 71. *Crit Rev Microbiol* **37**, 313-327.

Yip, C. C., Lau, S. K., Zhou, B., Zhang, M. X., Tsoi, H. W., Chan, K. H., Chen, X. C., Woo, P. C. & Yuen, K. Y. (2010). Emergence of enterovirus 71 "double-recombinant" strains belonging to a novel genotype D originating from southern China: first evidence for combination of intratypic and intertypic recombination events in EV71. *Arch Virol* **155**, 1413-1424.

Yoke-Fun, C. & AbuBakar, S. (2006). Phylogenetic evidence for inter-typic recombination in the emergence of human enterovirus 71 subgenotypes. *BMC Microbiol* **6**, 74.

Yu, H., Chen, W., Chang, H., Tang, R., Zhao, J., Gan, L., Liu, B., Chen, J. & Wang, M. (2010). Genetic analysis of the VP1 region of enterovirus 71 reveals the emergence of genotype A in central China in 2008. *Virus Genes* **41**, 1-4.

Yun, S. I., Kim, S. Y., Rice, C. M. & Lee, Y. M. (2003). Development and application of a reverse genetics system for Japanese encephalitis virus. *J Virol* **77**, 6450-6465.

Zaini, Z. & McMinn, P. (2012). A single mutation in capsid protein VP1 (Q145E) of a genogroup C4 strain of human enterovirus 71 generates a mouse virulent phenotype. *J Gen Virol* **93**, 1935-1940.

Zaini, Z., Phuektes, P. & McMinn, P. (2012a). Mouse adaptation of a sub-genogroup B5 strain of human enterovirus 71 is associated with a novel lysine to glutamic acid substitution at position 244 in protein VP1. *Virus Res* **167**, 86-96.

Zaini, Z., Phuektes, P. & McMinn, P. (2012b). A reverse genetic study of the adaptation of human enterovirus 71 to growth in Chinese hamster ovary cell cultures. *Virus Res* **165**, 151-156.

Zhang, Y., Cui, W., Liu, L., Wang, J., Zhao, H., Liao, Y., Na, R., Dong, C., Wang, L., Xie, Z., Gao, J., Cui, P., Zhang, X. & Li, Q. (2011a). Pathogenesis study of enterovirus 71 infection in rhesus monkeys. *Lab Invest* **91**, 1337-1350.

Zhang, Y., Tan, X. J., Wang, H. Y., Yan, D. M., Zhu, S. L., Wang, D. Y., Ji, F., Wang, X. J., Gao, Y. J., Chen, L., An, H. Q., Li, D. X., Wang, S. W., Xu, A. Q., Wang, Z. J. & Xu, W. B. (2009). An outbreak of hand, foot, and mouth disease associated with subgenotype C4 of human enterovirus 71 in Shandong, China. *J Clin Virol* **44**, 262-267.

Zhang, Y., Wang, J., Guo, W., Wang, H., Zhu, S., Wang, D., Bai, R., Li, X., Yan, D., Zhu, Z., Tan, X., An, H., Xu, A. & Xu, W. (2011b). Emergence and transmission pathways of rapidly evolving evolutionary branch C4a strains of human enterovirus 71 in the Central Plain of China. *PLoS One* **6**, e27895.

Zuker, M. (2003). Mfold web server for nucleic acid folding and hybridization prediction. *Nucleic Acids Res* **31**, 3406-3415.

APPENDICES